



Department of Geosciences

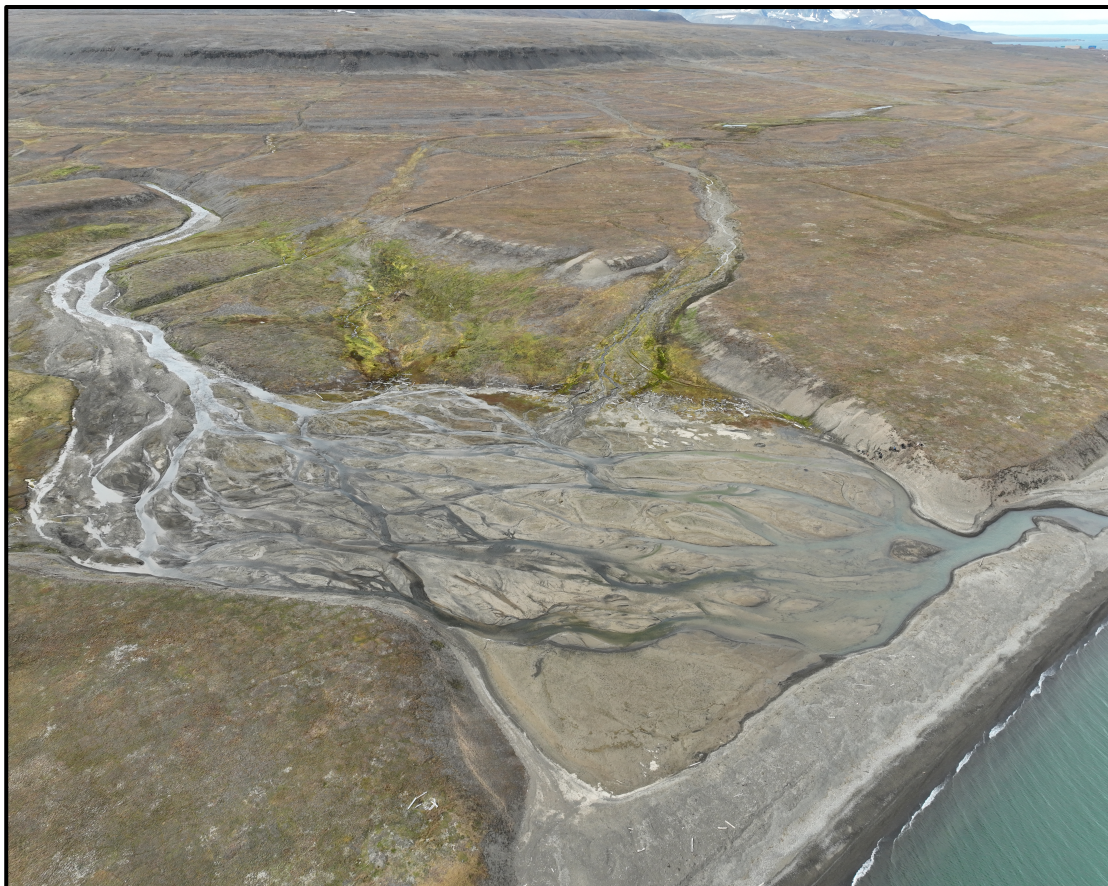
**A sedimentary insight into the coastal and environmental  
evolution of Hollendarbukta, Isfjorden: Early Holocene to present**

Luke Simmons

Master's thesis in Geology, GEO-3900, May 2024

Supervisors: Anders Schomacker and Mark Furze

Co-supervisors: Sofia Kjellman and Katrine Husum



## **Acknowledgements**

The process of working on my project and completing this thesis has been a true pleasure and a memorable academic adventure.

I owe thanks to the Research Council of Norway for funding the fieldwork through the Arctic Field Grant, which primarily made this project possible. On that note, a successful field campaign would not have been possible without the unwavering support from everyone in the UNIS Logistics Department. Amelie, you earned your brownies and more are on the way!

Days in the field were fruitful and for that I thank the tenacious field team: Mathilde, Magnus, David, Håvard, Simon and Miriam for your time, enthusiasm, and laughter along the way. Further thanks are in order to the laboratory and administrative staff at both UiT and UNIS for guidance and assistance over the course of the project.

My utmost gratitude and thanks go to the team of supervisors that I had the delight of working alongside over the past year. As well as countless opportunities, you presented me with the gift of autonomy that has undoubtedly shaped my academic development. You are all figures to look up to and I sincerely hope it is not goodbye but until next time!

# Table of Contents

<b>ACKNOWLEDGEMENTS.....</b>	<b>2</b>
<b>ABSTRACT .....</b>	<b>6</b>
<b>1 INTRODUCTION .....</b>	<b>8</b>
<b>1.1 Aims and objectives .....</b>	<b>10</b>
<b>1.2 Study area.....</b>	<b>11</b>
1.2.1 High Arctic setting of Svalbard.....	11
1.2.2 Oceanography and circulation systems .....	12
1.2.3 Modern climate.....	15
1.2.4 Local geology .....	16
1.2.5 Local study site .....	18
<b>2 BACKGROUND .....</b>	<b>20</b>
<b>2.1 Late Weichselian: Svalbard-Barents Sea Ice Sheet (SBIS).....</b>	<b>20</b>
2.1.1 Last Glacial Maximum .....	20
2.1.2 Deglaciation.....	23
2.1.3 Post-glacial emergence.....	24
<b>2.2 Holocene climatic developments.....</b>	<b>26</b>
2.2.1 Early Holocene .....	26
2.2.2 Holocene Thermal Maximum.....	27
<b>2.3 Previous work.....</b>	<b>28</b>
<b>3 METHODOLOGY AND MATERIALS .....</b>	<b>31</b>
<b>3.1 Field campaign.....</b>	<b>31</b>
3.1.1 Field techniques.....	33
3.1.2 Sedimentology.....	35
<b>3.2 Geomorphic mapping .....</b>	<b>39</b>
3.2.1 Desk-based mapping .....	39
<b>3.3 Laboratory work .....</b>	<b>42</b>
3.3.1 Weighing and wet sieving .....	43

3.3.2	Microscope analysis.....	43
3.3.3	Laser Diffraction Particle Size Analyser.....	43
<b>3.4</b>	<b>Software and online data resources.....</b>	<b>47</b>
3.4.1	GRADISTAT v8.0.....	47
3.4.2	Inkscape.....	50
3.4.3	QGIS.....	50
3.4.4	SeKlima.....	50
3.4.5	Copernicus Data Space Ecosystem Hub.....	50
<b>4</b>	<b>RESULTS AND INTERPRETATION.....</b>	<b>51</b>
<b>4.1</b>	<b>Geomorphic map.....</b>	<b>52</b>
<b>4.2</b>	<b>Hollendardalen.....</b>	<b>53</b>
4.2.1	Overview.....	53
4.2.2	Stratigraphy.....	55
4.2.3	Environmental synthesis.....	75
<b>4.3</b>	<b>Bogebekken: Mya truncata Section.....</b>	<b>76</b>
4.3.1	Overview.....	76
4.3.2	Stratigraphy.....	77
4.3.3	Environmental synthesis.....	85
<b>4.4</b>	<b>Bogebekken: Arctica islandica Section.....</b>	<b>86</b>
4.4.1	Overview.....	86
4.4.2	Stratigraphy.....	87
4.4.3	Environmental synthesis.....	103
<b>4.5</b>	<b>Modern environment.....</b>	<b>104</b>
4.5.1	Characteristics of Hollendarelva fluvial system.....	104
4.5.2	Characteristics of Bogebekken shoreline.....	110
<b>5</b>	<b>DISCUSSION.....</b>	<b>112</b>
<b>5.1</b>	<b>Assigning a relative sea level curve.....</b>	<b>112</b>
<b>5.2</b>	<b>Constraining ages of undated sections.....</b>	<b>114</b>
<b>5.3</b>	<b>Coastal evolution.....</b>	<b>115</b>
5.3.1	Deglaciation.....	115
5.3.2	Early Holocene.....	116

5.3.3	Early Middle Holocene.....	122
5.3.4	Late Middle Holocene to present.....	123
<b>5.4</b>	<b>Assessment of grain size analysis.....</b>	<b>124</b>
<b>5.5</b>	<b>Absence of foraminifera .....</b>	<b>125</b>
<b>6</b>	<b>CONCLUSIONS .....</b>	<b>127</b>
<b>7</b>	<b>FUTURE WORK.....</b>	<b>130</b>
<b>8</b>	<b>APPENDIX.....</b>	<b>132</b>
<b>8.1</b>	<b>Hollendardalen: (HDS3/4).....</b>	<b>132</b>
8.1.1	Grain size analysis (Prodelta).....	132
8.1.2	Grain size analysis (Lower delta slope) .....	136
8.1.3	Grain size analysis (Upper delta slope).....	141
<b>8.2</b>	<b>Bogebekken: Mya truncata Telegraph Section (BKS2) .....</b>	<b>145</b>
8.2.1	Grain size analysis .....	145
<b>8.3</b>	<b>Bogebekken: Arctica islandica Section (BKS1).....</b>	<b>150</b>
8.3.1	Grain size analysis .....	150
	<b>REFERENCES.....</b>	<b>152</b>

## Abstract

Dramatic physical and biological shifts are occurring in the Arctic in response to rising surface air temperatures. Sedimentary coastal environments are particularly sensitive to these changes as they form at the interface between the terrestrial and shallow marine realm. The need to investigate sedimentary archives from coastal environments is crucial, to understand how they have responded during periods of abrupt climate change and elucidate how they may evolve in the future. This study investigates the raised marine sediments exposed within Hollendarbukta, Isfjorden, to document sedimentological and geomorphic evidence for the coastal and environmental evolution of the study site from the Early Holocene to present.

The data collected from four outcrops along Hollendardalen and Bogebeekken is compiled to propose a three-phase evolutionary model of the coastal environment. The initial stage of development (*c.* 11.0-9.4 cal. ka BP) is recorded at Hollendardalen by the progradation of an embayed fjord side delta. The coarsening upwards sequence of sediments contains five sub-environments that progressively shallow and include: prodelta, lower delta slope, upper delta slope, delta front beach and backshore deposits. In a distal shoreline setting of the embayed fjord side delta, a glacimarine bottomset outcrops along the raised marine terrace in Bogebeekken. Hypopycnal sediment plumes, surge-type turbidity currents and periods of ice-rafting governed sedimentation during this phase of delta progradation. The results align with a rapidly falling relative sea level during the Early Holocene acting as a governing regime control, alongside a strongly seasonal climate and dominant fluvial regime modulating a high sediment influx of fines and freshwater to the shallow marine realm.

The second stage of evolution occurred between *c.* 9.4-7.9 cal. ka BP. High sedimentation during the Early Holocene promoted rapid filling of the coastal basin and caused the transition from an embayed fjord side environment to a higher energy, linear coastline. This corresponds with the Holocene Thermal Maximum where thermophilous *Arctica islandica* molluscs in the marine terrace at Bogebeekken, indicate that the shallow marine environment was subject to warmer than present Atlantic Water intrusion. This study suggests that shallowing of the coastal basin during shoreline progradation, was concurrent with a transition to a higher energy linear shoreline, that promoted favourable conditions for Atlantic Water intrusion into the shallow marine environment at the study site. Whilst warmer and improved environmental conditions allowed *Arctica islandica* to thrive, the shoreline was likely too high energy and too shallow for foraminifera to inhabit the area.

The final stage of coastal evolution occurred from *c.* 7.9 cal. ka BP to present. Progradation of the beachface and backshore continued and approached the present-day shoreline at Hollendarbukta. In conjunction with slowing glacio-isostatic uplift during the Middle to Late Holocene, the braided fluvial system of Hollendarelva and Bogebecken migrated throughout the entire valley. Uplift was significant enough for the braided river to cannibalise the raised marine sediment and incise *c.* 8-13 m marine terraces within Hollendarbukta. Ultimately, resulting in the present-day system characterised by an extensive braidplain that feeds into the wave dominated, micro-tidal and coarse-grained shoreline at Hollendarbukta.

# 1 Introduction

The Arctic region is experiencing pronounced climatic changes as temperatures rise at twice the rate of the Northern Hemisphere and with respects to the archipelago of Svalbard, up to seven times the global average (Hanssen-Bauer et al., 2019; Nordli et al., 2020). Rising air temperatures are accompanied by an increase in precipitation, which is forecast to increase over the course of the century, as a result of enhanced polar moisture transport and increased evaporation from warmer and ice-free Arctic Seas (Zhang et al., 2013; Bintanja & Selten, 2014; Kopec et al., 2016). Concurrent with increased meridional heat and moisture transport is an increase in extreme winter cyclone events in the Arctic, as data from Ny-Ålesund indicates an increased trend of six events/decade over 1979-2015 (Rinke et al., 2017). Furthermore, studies have demonstrated that increased storm frequencies and increased heat content of Atlantic Water are together driving additional sea ice loss within the Eurasian Basin (Onarheim et al., 2014; Polyakov et al., 2017; Rinke et al., 2017; Duarte et al., 2020).

In response to rising air temperatures, increased precipitation and increased storm frequencies in the Arctic, dramatic physical and biological shifts are occurring in the terrestrial, freshwater, cryospheric, coastal and ocean ecosystems (Lee et al., 2023). Environments that are highly sensitive to such changes are Arctic sedimentary coastlines (Lantuit et al., 2012). Controls that govern high latitude coastline evolution include sediment supply, relative sea level, glacier state, permafrost regime, snow cover and sea ice conditions (Sessford et al., 2015). These controls are directly impacted by the effects of a warming Arctic, such as glaciers losing mass, major river discharge increasing, sea ice retreating and ultimately nutrient pathways in the near-shore zones changing (Lantuit et al., 2012; Lee et al., 2023).

Considering this, the need to investigate sedimentary archives from coastal environments is essential, to understand how they have responded during times of abrupt climatic change to elucidate how they may evolve under climatic projections. A key time period to conduct such investigations is the Early Holocene that spans 11.7-8.2 cal. ka BP (Cohen et al., 2013; Walker et al., 2014). Within this period is the warmer than present interval around Svalbard 11-9 cal. ka BP that is denoted as the Holocene Thermal Maximum (Salvigsen et al., 1992; Rasmussen et al., 2012; van der Bilt et al., 2019). Thermophilous molluscs (*Zirfaea crispata*, *Arctica islandica*, *Mytilus edulis* and *Modiolus modiolus*) within glacio-isostatically uplifted coastal deposits indicate that warm waters were present along the shorelines of Svalbard's fjords during this period (Feyling-Hanssen, 1955; Salvigsen et al., 1992; Mangerud &



Svendsen, 2018). These thermophilous molluscs have been used to suggest shallow water temperatures at least 6 °C warmer than present during the time interval 10-9.2 cal. ka BP (Beierlein et al., 2015; Mangerud & Svendsen, 2018). Ensuing this marine thermal maximum was a glacial minimum that certainly occurred after 10-9.2 cal. ka BP, most likely during the Middle Holocene between 8.0-6.0 cal. ka BP (Farnsworth et al., 2020). The characteristics and occurrence of the above, render the Early to Middle Holocene a fascinating time to investigate coastal and environmental evolution in response to a marine thermal maximum and glacial minimum within a High Arctic setting. However, it is imperative to recognise that the Early Holocene was a period of dramatic relative sea level fall at high latitudes in response to deglaciation and glacio-isostatic uplift (Forman et al., 2004), which largely governed environmental evolution alongside climatic and oceanographic perturbations.

This study provides a sedimentary insight into the evolution of the shallow marine realm of a High Arctic side entry fjord system throughout the Early Holocene to present. Shedding light on the depositional processes that governed sedimentation and presenting the characteristics of the resulting products, will lead to a greater understanding of how the shallow marine environment evolved from the Early Holocene to its present system state. The findings will be summarised with a conceptual model that captures aspects of the highly dynamic and rapidly changing coastlines at high latitudes in response to changes in sediment supply, relative sea level, glacial state and extended open water seasons.

## **1.1 Aims and objectives**

The initial purpose of this investigation was to sample the raised marine terraces within Hollendarbukta, Isfjorden, Western Svalbard, in the hope that they would contain foraminifera to use as a biogenic proxy for a palaeoenvironmental reconstruction of the shallow marine environment during the Early Holocene. Unfortunately, after an extensive and thorough laboratory investigation, all sediment samples were found to be devoid of foraminifera. This led to a realignment of the project's aims, objectives, and research questions.

The purpose of this study is thus to conduct a sedimentological and geomorphic investigation of the raised marine terraces that are present within the fjord side environment of Hollendarbukta.

Research questions that this project will address are:

- What sedimentary environments do the raised marine terraces record and what sedimentary processes governed their deposition?
- To what extent did climate, sediment supply, sea level and glacial state influence the evolution of the valley throughout the Holocene?
- How can the absence of foraminifera be explained in relation to the sedimentary environments described?

Through answering these questions, the ultimate goal of the investigation is to provide an environmental synthesis of the study area, constructing an evolutionary model of the coastal environment from the Early Holocene to present.

## 1.2 Study area

This chapter presents an overview of the study area. Firstly, an overview of the regional setting of Svalbard is described and thereafter the oceanography and large-scale circulation systems. The local physiographic setting of Isfjorden is then presented followed by the modern climate, site-specific geology, and local study site.

### 1.2.1 High Arctic setting of Svalbard

The Svalbard archipelago lies at the gateway to the Arctic Ocean, on the north-western margin of the Barents Shelf, approximately 900 km north of the Norwegian mainland (Figure 1). The archipelago includes the far-reaching extent of Bjørnøya, Hopen and Kong Karl's Land, thus its latitudinal range extends from 74 to 81 °N and longitudinally from 10 to 35 °E. Presently, 57% of the archipelago is covered by ice sheets, ice caps and glaciers, with 68% of this glaciated area draining through tide water glaciers that have a combined terminus width of ~740 km (Nuth et al., 2013). The largest island of the archipelago is Spitsbergen, which covers an area of 37 503 km<sup>2</sup>, amounting to over 60% of Svalbard's landmass (Dallmann, 2015). The topography and landscapes expressed across Spitsbergen have been shaped over the millennia by tectonic activity and more recently Pleistocene glaciations. During periods of glaciation, erosion dominates, and the valley sides and fjord floors are etched and scoured as glaciers and ice sheets expand. As the ice masses retreat during interstadial and interglacial periods, sediment accumulates and fills fjord valleys and the unsupported valley sides undergo the process of paraglacial landscape readjustment, resulting in a blanket of mass wasting material covering the terrain (Church & Ryder, 1972). Large fjord systems across Spitsbergen dissect the present coastline and during deglaciation of the Late Weichselian Svalbard-Barents Sea Ice Sheet, acted as major drainage channels for fast flowing ice streams (Landvik et al., 1998; Landvik et al., 2005; Ottesen et al., 2005). With respect to Western Spitsbergen, Isfjorden is the most expansive as it branches far inland, reaching Central Spitsbergen where it terminates at its head with Nordfjorden, Ekmanfjorden, Dicksonfjorden, Billefjorden, Sassenfjorden and Tempelfjorden. The coastal lowlands of the west coast of Spitsbergen are characterised by coastal plains and strandflats that represent the nearshore marine environment of interglacial periods (Figure 4). Subsequent uplift due to regional glacio-isostatic rebound exposes these sedimentary archives of the shallow marine environments above present sea level, providing the opportunity to gain insight into their evolution.

## 1.2.2 Oceanography and circulation systems

Three main water masses are responsible for influencing the oceanographic system surrounding Svalbard, Atlantic Water, Arctic Water and Coastal Waters (Figure 1).

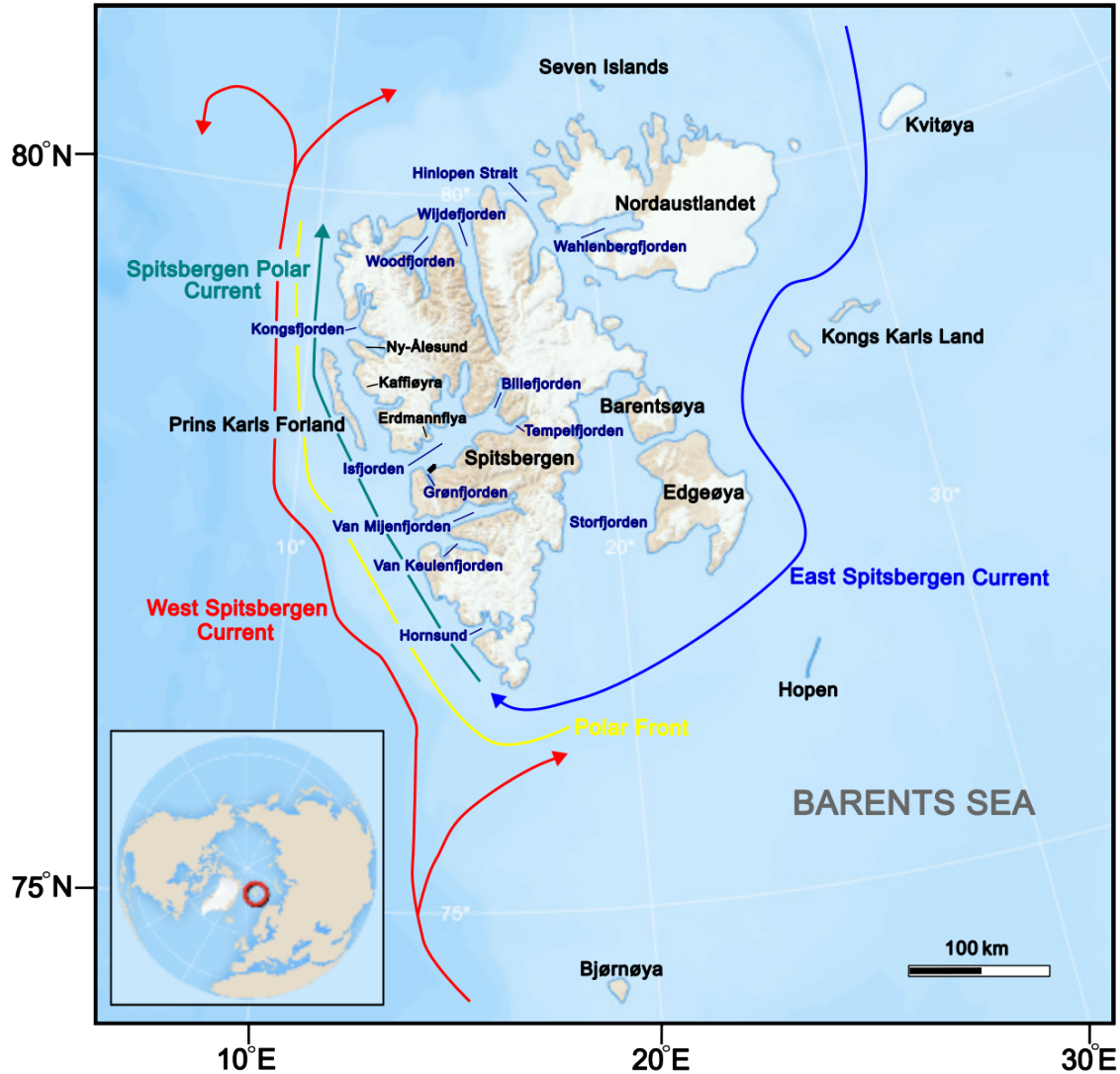


Figure 1: Oceanographic map of Svalbard. Source of basemap: Norwegian Polar Institute (NPI).

Atlantic Water, sourced in the North Atlantic Ocean, enters the Nordic Seas through a main inflow in the Faroese Channel (Hopkins, 1991). It is transported northwards by the Norwegian-Atlantic Current as surface waters which are dynamically constrained to the eastern side of the Nordic Seas (Aagaard et al., 1987; Hopkins, 1991). As the North Atlantic Current reaches the tip of Norway, it bifurcates, and the eastern branch of Atlantic Water enters the Barents Sea through the Barents Sea Opening as part of the North Cape Current (NCC) (Ingvaldsen et al., 2004).

The main core of the Atlantic Water moves northwards as the West Spitsbergen Current, transporting Atlantic Water along the continental margin of the Barents Sea and Svalbard towards the Arctic Ocean (Hopkins, 1991). The properties of the warm and saline Atlantic Water transported by the West Spitsbergen Current is defined by a temperature  $>3$  °C and a practical salinity of 34.9-35.2 (psu) (Fraser et al., 2018). However, along its northward trajectory, the Atlantic Water within the West Spitsbergen Current cools by  $\sim 0.2$  °C per 100 km (Kolås & Fer, 2018). In addition to the West Spitsbergen Current transporting Atlantic Water northwards, the Spitsbergen Trough Current circulates Atlantic Water into the fjord troughs along the West Spitsbergen Shelf and represents a longer and slower route of Atlantic Water towards the Arctic Ocean (Nilsen et al., 2016).

Arctic Water enters the Barents Sea from the north as the East Spitsbergen Current. At the southern tip of Svalbard, the warm and saline Atlantic Water meets the colder and fresher Arctic Water transported by the East Spitsbergen Current (Saloranta & Svendsen, 2001; Skogseth et al., 2005). The Spitsbergen Polar Current then transports the cold and fresh Arctic Water northwards along the West Spitsbergen Shelf in the surface layer that is influenced by freshwater discharge from the fjords along the Spitsbergen Coast (Nilsen et al., 2016). The boundary between the Atlantic Water and the Arctic Water on the West Spitsbergen Shelf marks the position of the Arctic Front (Svendsen et al., 2002). Changes in the proximity of the Arctic Front to the coast of Svalbard can result in Atlantic Water moving further up the shelf (Swift, 1986).

Coastal Waters around Svalbard and within the fjords are largely influenced by freshwater input from various sources. Freshwater is supplied at the surface through melt water from glaciers and fast ice, as well as at deeper levels through the calving of icebergs from glaciers (Svendsen et al., 2002). Additionally, the terrestrial input from fluvial systems will contribute towards this. Due to its low salinity and corresponding low density, the Coastal Water forms a layer of water that is well isolated from underlying water (Dallmann, 2015). The salinity stratified surface layer is influenced by surface processes such as wind forcing, heat exchange with the atmosphere and solar heating through radiation, which in turn results in a large variability in its temperature and salinity properties (Saloranta & Svendsen, 2001).

### **1.2.2.1 Local physiographic setting: Isfjorden**

Isfjorden system is the most extensive fjord system of Spitsbergen, measuring *c.* 108 km in length, *c.* 70 km in width and up to 425 m in depth. The fjord mouth is wide and without a sill, which holds significance as it facilitates the topographic steering and intrusion of AW into the fjord (Ślubowska-Woldengen et al., 2007; Nilsen et al., 2008). Associated with the main part of Isfjorden is 13 tributary fjords and bays, nine of which include tidewater terminating glaciers. The drainage basin feeding into the fjord system is 7309 km<sup>2</sup>, making it the second largest on Spitsbergen (Hagen et al., 1993). Despite the eight tidewater glaciers, total glacier coverage within the fjord system is ~40%, considerably less than the 57% average across the archipelago (Forwick & Vorren, 2009; Nuth et al., 2013).

### **1.2.2.2 Fjord-shelf exchange and local hydrography: Isfjorden**

Hydrographically, Isfjorden is characterised by the presence of water masses that are both internal and external in their origin (Nilsen et al., 2008). Internal water masses can be subdivided into Surface Waters, Local Waters, and Winter-Cooled Waters. Surface Waters are relatively fresh and usually replenished during the late spring and summer as a result of glacial melt, fluvial runoff and precipitation (Nilsen et al., 2008). The nine tidewater glaciers that terminate within the fjord and its tributaries will largely be contributing towards the formation of these Surface Waters (Rasmussen et al., 2012). Conversely, over the winter in December/January, the tributary fjords of inner Isfjorden are covered with seasonal fast ice, while the outer part of the fjord is ice free (Rasmussen et al., 2012). The sea ice extent and coverage can vary inter-annually (Węśławski et al., 1995; Svendsen et al., 2002; Nilsen et al., 2008) and it is largely controlled by interactions between the ocean and atmosphere (Cottier et al., 2007). Despite this, the presence of Surface Waters is likely less prominent during the winter compared to the late spring and summer months.

By comparison, Local Water and Winter Cooled Water have an increased salinity caused by brine generation during the formation of sea ice in the winter (Forwick & Vorren, 2009). Due to its cold temperature and enrichment with salt, Winter Cooled Water can sometimes reach a high enough density to mix with and cool underlying Atlantic Water (Rasmussen et al., 2012). The intensity of its formation, may further influence the exchange of water masses between the fjord and adjacent shelf, with a strong formation of Winter Cooled Water leading to a stronger inflow of Atlantic Water during the summer (Nilsen et al., 2008; Rasmussen et al., 2012).

External water masses that intrude into Isfjorden through the mouth of the fjord include Atlantic Water from the West Spitsbergen Current and Arctic-type Water that is heavily modified from the East Spitsbergen Current (Nilsen et al., 2008). The Atlantic Water circulates into the fjord from the shelf, entering through the southern part, and exiting through the northern part (Nilsen et al., 2008). The inflow of Atlantic Water exhibits a seasonality with more warm and saline properties over the summer months and colder and less saline properties during the winter months (Svendsen et al., 2002). In addition to the seasonality of this intrusion, the volume of inflow varies inter-annually (Svendsen et al., 2002). Vertical mixing between the Arctic-type Surface Water and the underlying AW results in the formation of Transformed Atlantic Water (TAW) that is slightly colder and slightly fresher ( $T > 1\text{ }^{\circ}\text{C}$ , salinity  $>34.7$  psu) than its counterpart in the West Spitsbergen Current (Svendsen et al., 2002; Cottier et al., 2005; Nilsen et al., 2008).

Bottom water temperatures within Isfjorden fluctuates between  $-2\text{ }^{\circ}\text{C}$  in the winter and  $>2\text{ }^{\circ}\text{C}$  in the summer (Nilsen et al., 2008). In contrast to this  $4\text{ }^{\circ}\text{C}$  seasonal temperature range, salinity changes in the bottom water masses are negligible ( $< 0.2$ ) exhibiting far less seasonality (Cottier et al., 2005; Nilsen et al., 2008).

### **1.2.3 Modern climate**

The present-day climate in Svalbard is highly sensitive, due to its geographic placement at the intersection of the North Atlantic Drift (West Spitsbergen Current) and the southern border of Arctic sea-ice extent (Aagaard et al., 1987; Rogers et al., 2005). Svalbard's climate can broadly be classified as a dry, High Arctic climate, exhibiting periglacial conditions, extreme low temperatures, and continuous permafrost (Christiansen et al., 2010; French, 2017). Despite this classification, Svalbard and the adjacent oceanic areas experience a milder, wetter and cloudier climate than average for corresponding latitudes (Hanssen-Bauer et al., 2019). A significant contributor towards this milder climate is the West Spitsbergen Current, which releases heat and moisture to the region as well as affecting the concentration of sea ice (Walczowski & Piechura, 2011). Highlighting the influence of the West Spitsbergen Current on the heat and precipitation variability of Svalbard is the annual temperature and precipitation maps of Svalbard for the period 1971-2000 in Figure 2. Over this period, mean annual air temperature at Svalbard Airport was  $-5.9\text{ }^{\circ}\text{C}$  and mean annual precipitation was 196 mm (Hanssen-Bauer et al., 2019).

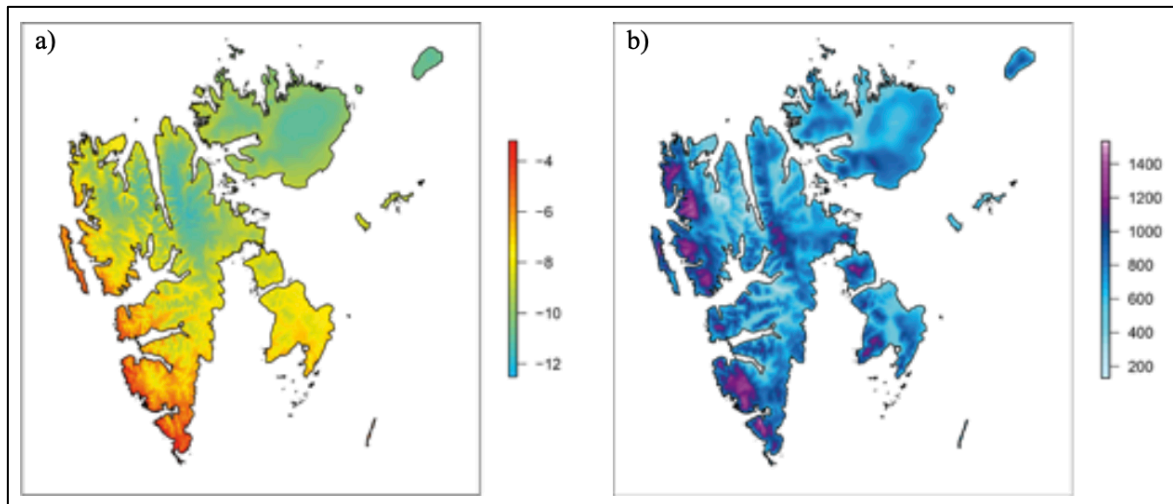


Figure 2: Maps of Svalbard indicating mean annual air temperature ( $^{\circ}\text{C}$ ) (A) and mean annual precipitation (mm) (B) data for the archipelago from the Sval-Imp dataset (Østby et al., 2017). Source of figure: Hanssen-Bauer et al. (2019).

Regionally, two large atmospheric circulation systems influence the climate system around Svalbard, the Icelandic low-pressure and the Siberian high-pressure system (Hanssen-Bauer et al., 2019). Interactions between these two circulation systems, cause high temperatures to be driven northward over Svalbard by the main North Atlantic cyclone track (Hanssen-Bauer, 1990). Regional precipitation over Svalbard is closely linked with the North Atlantic Oscillation (Dickson et al., 2000).

#### 1.2.4 Local geology

The dominant bedrock geology within Isfjorden consists of partially deformed sedimentary rocks that are Devonian to Paleogene in age (Figure 3) (Dallmann, 2002). Highly deformed sedimentary and metamorphic rocks that are Palaeoproterozoic to Mesoproterozoic in age are found in the western part of the fjord system, whereas in the east and north-eastern parts there are small areas of volcanic and metamorphic rocks (Dallmann, 2002). With respects to the study area in this project, the site specific bedrock geology includes Paleogene sedimentary basin deposits (Dallmann, 2015). The clastic sedimentary succession included within this basin consists of sandstones, siltstones, shales and to a lesser extent coals and conglomerates (Dallmann, 2015). Draped over this bedrock within the surrounding valleys and strandflats are unconsolidated Quaternary marine and fluvial sediments that form the focus of this investigation.





Figure 3: Base map indicating the bedrock geology of Svalbard. Paleogene geology of the study area highlighted by the red square (Elvevold et al., 2007). Source of figure: Norwegian Polar Institute, 2002 (<https://www.npolar.no/tema/geologi-svalbard/>).

### 1.2.5 Local study site

The sites that are the focus of this investigation are located within Hollendarbukta, a small bay on the southern shore of Isfjorden, Western Spitsbergen, *c.* 20 km east of the mouth of the fjord (Figure 9). Hollendardalen is the main valley that is associated with Hollendarbukta, and within this valley are two fluvial systems that are used to describe the relative position of the field localities. The main braided system is Hollendarelva, and *c.* 500 m to the west of Hollendarelva is the minor stream of Bogebecken. The catchment area for Hollendarelva is 87.78 km<sup>2</sup> (NVE, 2024) and includes numerous tributaries and five valley glaciers: Paxbreen, Häggbreen, Irabreen, Stolleybreen and Passfjellbreen (Figure 4).

The coastal area adjacent to Hollendarbukta is characterised by low relief strand plains and a series of beach ridges that run in a shoreline parallel direction. The raised marine sediments are also present up-valley in Hollendardalen and are prominent in N-S trending, *c.* 2.5 km stretch of fluvially incised terrace that separates Hollendarelva in the east and Bogebecken in the west (Figure 4). The raised marine sediments studied in this investigation, outcrop alongside Bogebecken (BKS1 and BKS2) and Hollendarelva (HDS3 and HDS4) (Figure 4).

Having described the local study site, it is fitting to outline the reasoning behind selecting it as a suitable area to conduct this investigation at. Firstly, its position *c.* 20 km east of the mouth of Isfjorden means it is situated in a location that makes it susceptible to oceanographic perturbations occurring between the West Spitsbergen Shelf and Isfjorden. Secondly, remotely conducted reconnaissance surveys revealed that the raised marine terraces stretch *c.* 2.5 km inland, in one continuous terrace that is exposed on both sides Hollendarelva and Bogebecken, resulting in an array of outcrop potentialities to investigate environmental changes up-valley. Lastly, whilst three previous studies had been conducted by Sharin et al. (2014); Bakken (2021) and Christman (2022) on the thermophilous molluscs within one outcrop in Hollendarbukta, the rest of the valley remained relatively understudied and underrepresented within the literature, particularly with respects to sedimentological and geomorphic investigations.

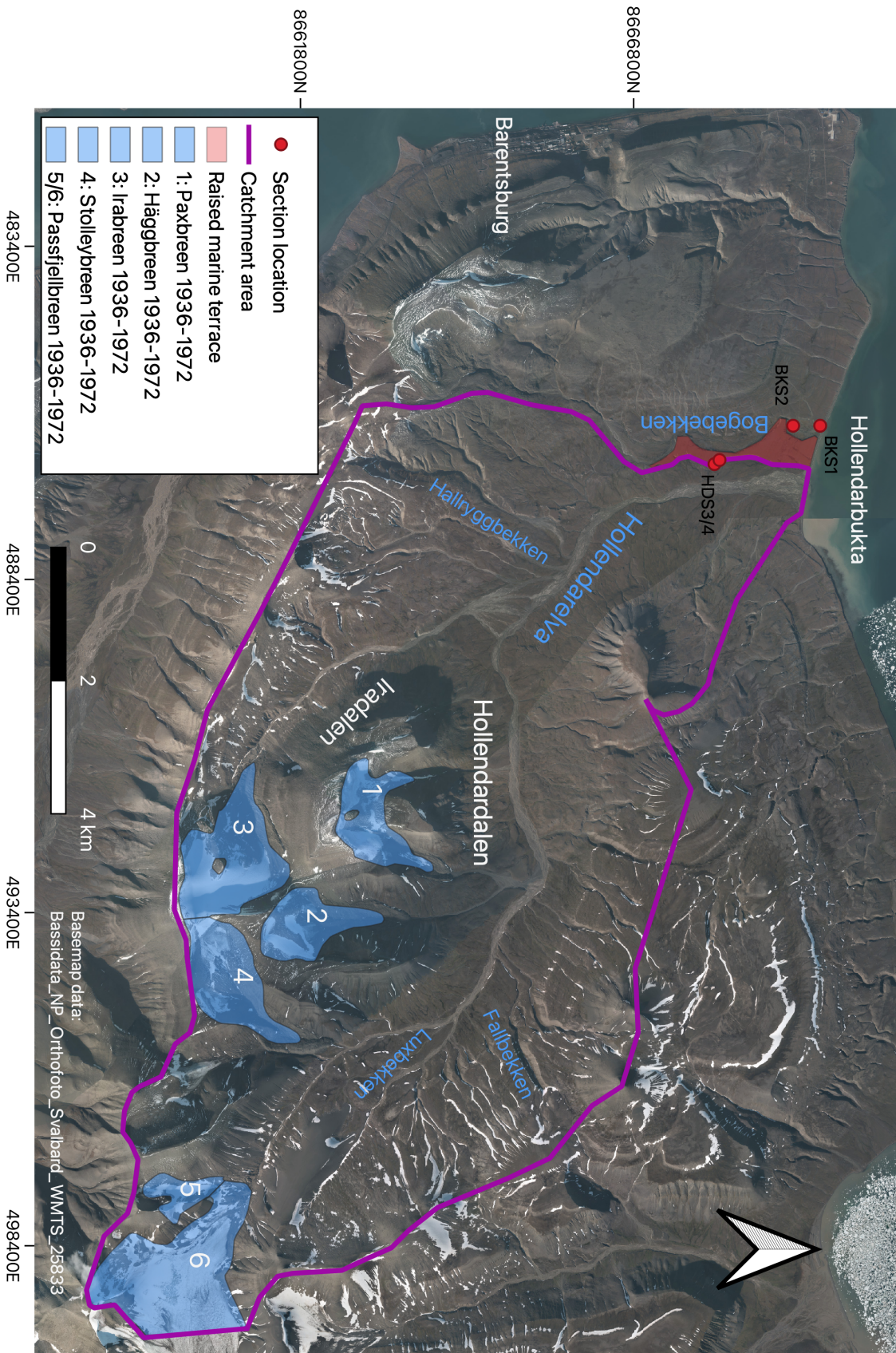


Figure 4: Map of the catchment area of the study site including names of minor and major tributaries and valley glaciers. Source of watershed catchment area boundary: The Norwegian Water Resources and Energy Directorate (NVE) (<https://temakart.nve.no/tema/faresoner>). Maximum glacier extent during the 1936-1972 provided by The Norwegian Polar Institute (NPI): <https://geokart.npolar.no/Html5Viewer/index.html?viewer=Svalbardkartet>.

## 2 Background

### 2.1 Late Weichselian: Svalbard-Barents Sea Ice Sheet (SBIS)

#### 2.1.1 Last Glacial Maximum

During the Late Weichselian glaciation (25-15 ka), the interconnected complex of ice sheets within Northern Eurasia were composed of various sectors that covered Scandinavia, Greenland, Iceland, Svalbard, the Barents Sea, the Kara Sea and the British-Irish Sea (Figure 5) (Svendsen et al., 2004; Sejrup et al., 2005; Funder et al., 2011; Patton et al., 2017). These ice sheets are collectively grouped as the Eurasian Ice Sheet complex (EurIS; Hughes et al., 2016). Within this complex, the largest ice sheet was the predominantly terrestrially based Scandinavian Ice Sheet (SIS), and to the north of this was the marine based Svalbard-Barents Ice Sheet (SBIS) (Svendsen et al., 2004; Mangerud et al., 2008; Hughes et al., 2016).

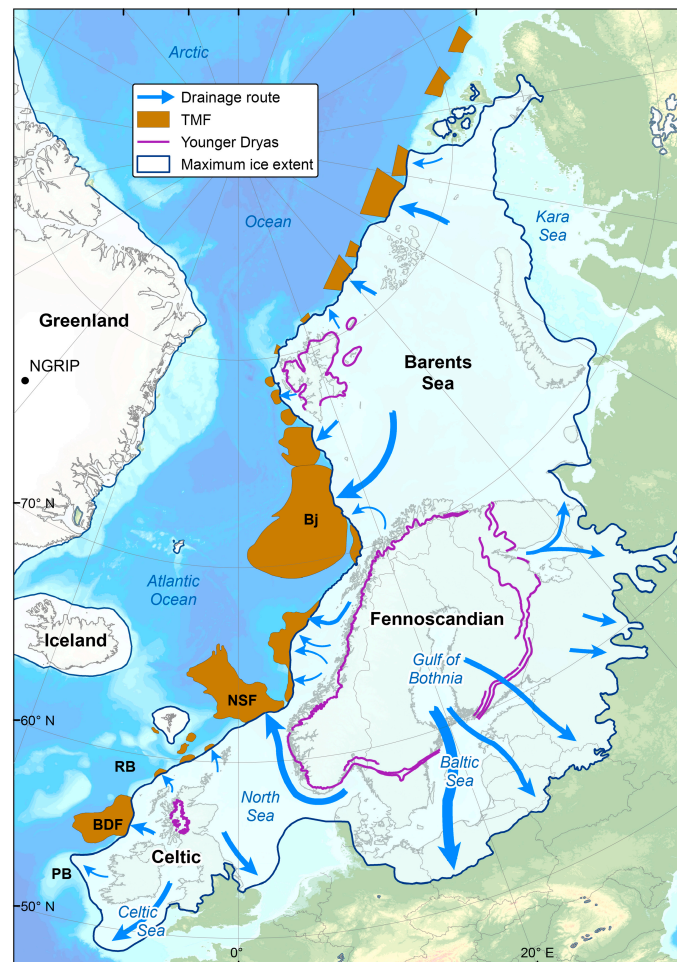


Figure 5: The Eurasian Ice Sheet Complex (EurIS) adapted from Ottesen et al. (2005) and Clark et al. (2012) and sourced from Patton et al. (2017). Glacial limits are from Ehlers and Gibbard (2007), Patton et al. (2015) and Stroeven et al. (2016). Trough mouth fans (TMF) are in brown and adapted from Dahlgren et al. (2005) and Batchelor and Dowdeswell (2014). PB: Porcupine Bank; BDF: Barra and Donegal Fans; RB: Rosemary Bank; NSF: North Sea Fan; BJ: Bjørnøyrenna Fan.

In the build-up to the Late Weichselian glaciation, the EurIS began to grow at *c.* 40 ka BP, however, the maximum extent of the different sectors of the ice sheet complex varied spatially and temporally (Svendsen et al., 2004; Böse et al., 2012; Clark et al., 2012; Hughes et al., 2016). First order thermomechanical modelling confirms this asynchronous growth during the build-up to the LGM, where the maximum stand was short lived as the North Sea and Atlantic margins were already in retreat as the eastern margins were advancing until *c.* 20 ka BP (Patton et al., 2016). As a result, the Last Glacial Maximum (LGM), can be defined by the most recent peak in global ice volume which dates to 23-21 ka BP (Clark et al., 2009). This corresponds with the maximum ice coverage of  $5.5 \times 10^6 \text{ km}^2$  at *c.* 22.7 ka BP as established by Patton et al. (2016). Furthermore, this is in accordance with the chronology and time slice reconstruction conducted by Hughes et al. (2016), who established the EurIS complex as a whole attained its maximum extent at *c.* 21 ka.

Detailed marine studies have demonstrated through the occurrence of till overlain by glaciomarine sediment, that the Svalbard Barents Sea Ice Sheet (SBIS) extended across the Barents Sea and beyond the coastline onto the shelf of Western Svalbard during the LGM (Mangerud et al., 1992; Landvik et al., 1998). This is further supported by glacial debris flows found at the mouth of Bjørnøya and Isfjorden trough mouth fans (TMF) (Landvik et al., 1998; Batchelor & Dowdeswell, 2014). The Late Weichselian SBIS dynamics were initially proposed to result from the interplay of a multi-domed ice sheet with numerous accumulation areas, where the high relief valleys and fjords had a substantial influence on ice flow (Landvik & Salvigsen, 1985; Forman, 1989; Mangerud et al., 1992; Landvik et al., 1998). Indeed, later work confirmed a complex and time-transgressive multi-ice-dome history with sub-marine geophysical evidence supporting former ice-stream flows (Ottesen et al., 2007; Ottesen & Dowdeswell, 2009; Dowdeswell et al., 2010). Furthermore, terrestrial data including cosmogenic radionuclide dating of glacially scoured bed rock and erratic boulders in Nordaustlandet presented by Hormes et al. (2011) indicates that actively erosive ice streams scoured coastal and fjord bathymetry during the Late Weichselian. These findings are compatible with the sub-marine evidence from Dowdeswell et al. (2010), suggesting local cold-based ice domes over Nordaustlandet during the Late Weichselian were potentially confluent with the ice dome over Eastern Spitsbergen (Figure 6). These findings are in accordance with the recent view that the SBIS was multi-domed and highly dynamic in its configuration (Hogan et al., 2017).

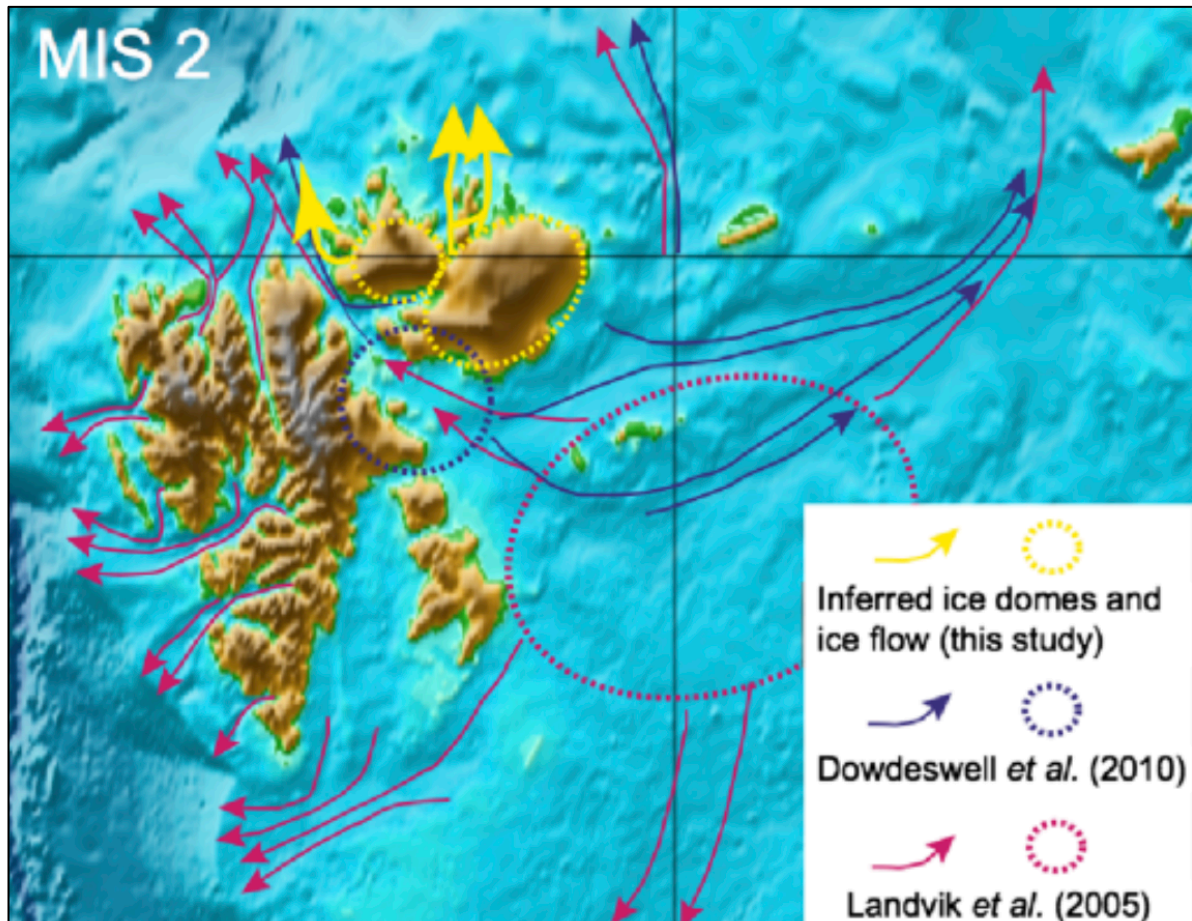


Figure 6: Reconstruction of ice-domes and ice flows of the SBIS during the Late Weichselian from Hormes et al. (2011) in yellow, Dowdeswell et al. (2010) in blue and Landvik et al. (2005) in red. Figure sourced from Hormes et al. (2011).

Early work using isobase maps revealed a centre of post-glacial uplift in the northern-central Barents Sea and together with glaciological and isostatic modelling, suggested the ice sheet was 2-3 km thick in this area (Landvik et al., 1998). This supported modelling by Lambeck (1996) that indicated the ice sheet was >800 m thick on the western coast of Spitsbergen. More recently, modelling conducted by Sejrup et al. (2022) aligns with a 2-3 km thickness in the northern-central Barents Sea between 19-18 ka. Despite this, peak glaciation of the SBIS is proposed to have been a short lived event, c. 3-5 cal. ka (Landvik et al., 1998).

### 2.1.2 Deglaciation

Deglaciation of the SBIS that occurred in a step-wise fashion, with maximum retreat during warm phases and halts or readvances during colder phases (Figure 7) (Svendsen et al., 1996; Landvik et al., 1998; Hogan et al., 2017; Nielsen & Rasmussen, 2018). Retreat from the shelf edge along the western Barents Sea margin is first noted in Storfjorden Trough at 20 ka (Rasmussen et al., 2007). In the northern Barents Sea between 19-16.5 ka major calving and dynamic thinning throughout shelf troughs was accompanied by considerable inland ice-sheet-thinning as a result of ice drawdown (Hogan et al., 2017). The pattern of retreat in the Eastern Barents Sea is poorly identified, although there are some indications of late-stage ice flow from an ice centre close to the central bank of the Barents Sea (Bjarnadóttir et al., 2014; Hughes et al., 2016).

A period with significant melt water delivery predominantly associated with the collapse of the SBIS occurred between 16-14 ka, where stratification and a strong contrast between warm bottom water and cold surface waters has been highlighted in the western Barents Sea (El bani Altuna et al., 2021; Rasmussen & Thomsen, 2021). Recent modelling suggests that across the Barents Sea, delayed heating of the subsurface waters strengthened by a gradual decrease in precipitation related to cooling of the surface waters, coincides with an accelerated retreat of the SBIS at 16-15 ka (Sejrup et al., 2022). This timing is consistent the findings of Landvik et al. (1998) who propose the onset of deglaciation of the SBIS along the western Spitsbergen continental margin to have begun at 15 ka, where it was significantly influenced by large-scale calving over deep troughs along the shelves (Landvik et al., 1998). Furthermore, Svendsen et al. (1996) proposed that the ice front retracted from the shelf at 14.8 ka, where a dramatic influx of fine-grained glaciomarine sediments at 13 ka is believed to reflect enhanced melting and/or current activity associated with climatic warming. By 12.3 ka, the outer part of Isfjorden became rapidly deglaciated (Mangerud et al., 1992; Elverhøi et al., 1995; Svendsen et al., 1996; Mangerud et al., 1998). The final retreat of the icefront to the tributary heads and coastal areas of Isfjorden had occurred by 10 ka in response to Holocene warming (Svendsen et al., 1996; Landvik et al., 1998; Lønne, 2005). Modelling efforts made by Sejrup et al. (2022) highlight that similarly to the build-up to the LGM, disintegration of the EurIS was far from homogeneous, and deglaciation of the marine sectors was mainly driven by temperature forced mass balance in the south and oceanic conditions in the north.

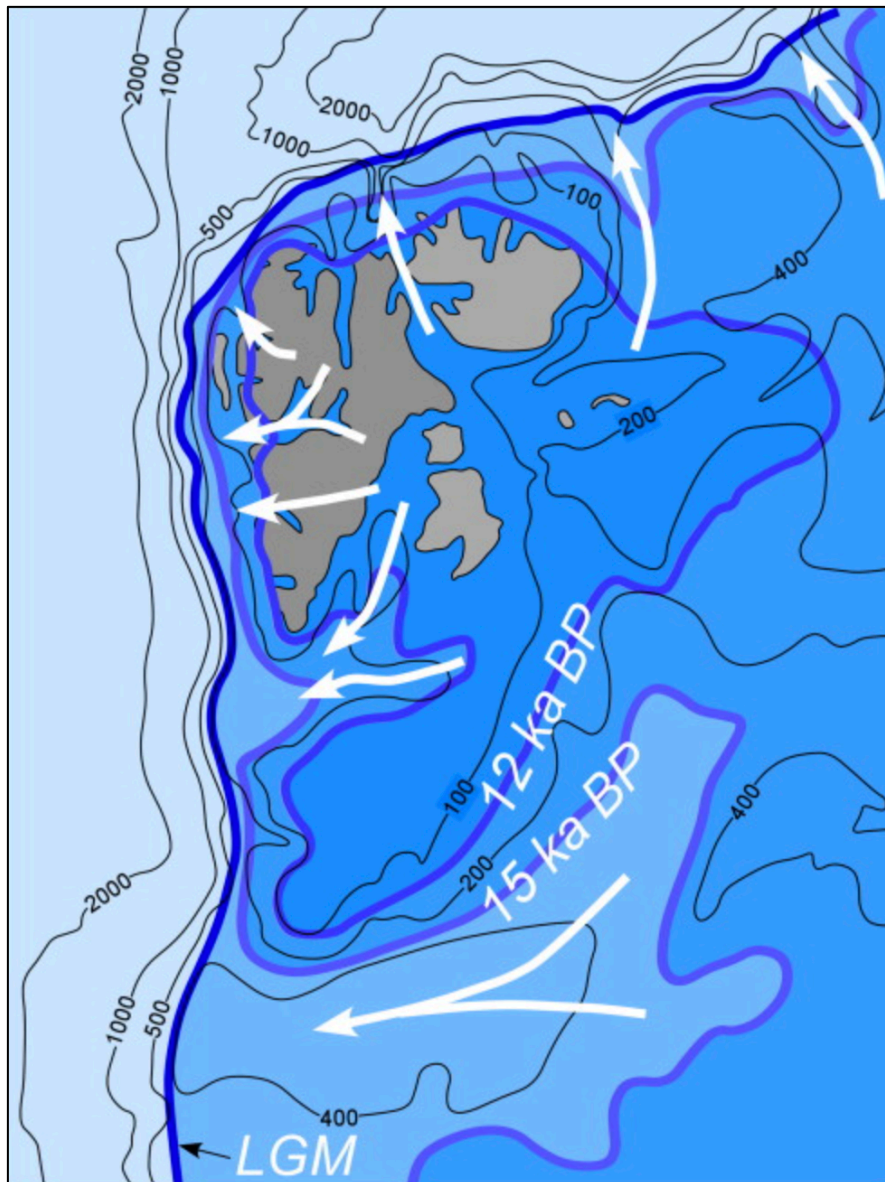


Figure 7: Reconstruction of the Late Weichselian SBIS extent at the LGM and subsequent stages of deglaciation at 15-12 cal. ka BP (Landvik et al., 1998). Figure source from and modified by: Ingólfsson and Landvik (2013).

### 2.1.3 Post-glacial emergence

In response to the unloading of ice from the land during deglaciation, glacio-isostatic uplift becomes a dominant force acting on the architecture of the landscape. As the land rises and relative sea level falls, successions of raised beaches coat the coastal environment, providing an insight into the position of previous shorelines whilst recording the pattern of deglacial history (Forman et al., 1987; Bondevik et al., 1995). Demonstrated by Figure 8, is the considerable variability in the regional uplift experienced across Svalbard, which results from ice cover thickness, duration, timing of deglaciation, and in some cases, ice expansion (Forman et al., 2004; Ingólfsson & Landvik, 2013; Farnsworth et al., 2020).



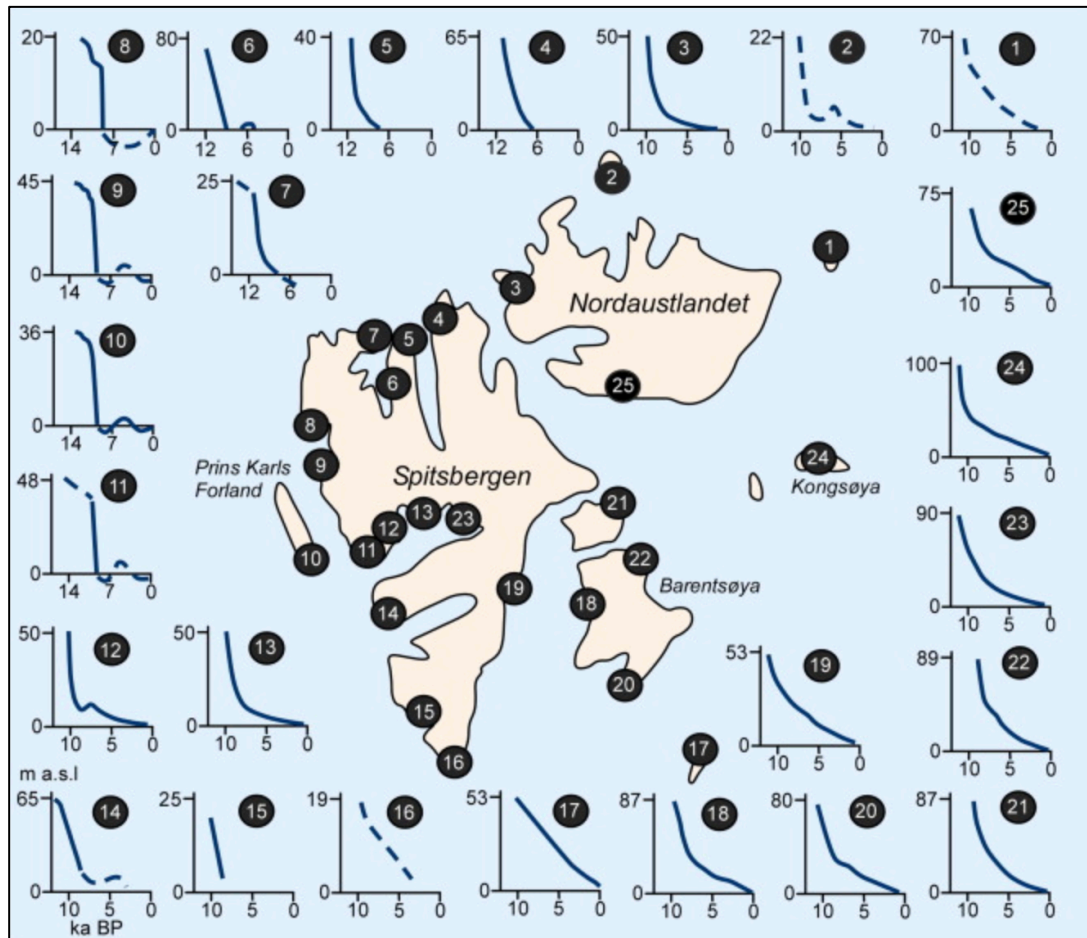


Figure 8: Comparative figure of the identified marine limits (ML) and relative sea level curves across Svalbard in relation to the last deglaciation (Forman, 1990; Forman et al., 2004). Figure sourced from and modified by: Ingólfsson and Landvik (2013).

In addition to the pattern of deglaciation, the raised shorelines hold the key to constraining the magnitude and distribution of past-ice loads through their altitude compared to present sea level (Forman et al., 2004). Since the late 1950's numerous quantitative studies have focussed on defining and refining post-glacial emergence and the timing of deglaciation around Svalbard (Olsson & Feyling-Hanssen, 1959; Blake, 1961; Salvigsen, 1978, 1981; Forman et al., 1987; Landvik et al., 1987; Salvigsen et al., 1990; Bondevik et al., 1995; Brückner et al., 2002; Schomacker et al., 2019). As mentioned above, models of the thickness of the SBIS varied between 2000-3000 m at the centre of the icesheet, to >800 m on the west coast of Spitsbergen (Lambeck, 1996; Landvik et al., 1998). Locations in close proximity to maximum loading exhibit the highest marine limits e.g. Kongsøya at 94-98 m and Svenskøya at 120 m (Salvigsen & Nydal, 1981; Ingólfsson et al., 1995), in comparison to sites on the west coast that record a marine limit often half of that (Figure 8) (Salvigsen et al., 1990; Forman et al., 2004). Highly spatial variability of emergence across the Barents Sea suggests that Western and Northern Spitsbergen were situated near the reactive ice margin and

sustained a brief ice coverage (*c.* 2-6 ka), whereas Central and Eastern Svalbard and Franz Josef Land, were beneath a considerable ice load for a longer period (Forman et al., 2004).

The occurrence of organic material such as shells, driftwood and whalebones within the raised beaches provide the opportunity to radiocarbon date the past shorelines to determine the rate of isostatic uplift (Salvigsen et al., 1990; Forman et al., 2004; Sessford et al., 2015; Schomacker et al., 2019). Despite spatial variability, the radiocarbon dates from raised beaches and the established relative sea level curves generally support that the greatest rate of glacio-isostatic uplift of the past 11.7 cal. ka BP were experienced during the Early Holocene (10-25 m/ka) (Salvigsen, 1981; Salvigsen & Österholm, 1982; Salvigsen et al., 1990; Forman et al., 2004; Farnsworth et al., 2020). Throughout the Middle Holocene, glacio-isostatic uplift rates decrease to *c.* 5 m/ka, with a continued decrease throughout the Late Holocene, where relative sea level is believed to continue to have been regressive (Bondevik et al., 1995; Forman et al., 2004; Sessford et al., 2015; Farnsworth et al., 2020)

## **2.2 Holocene climatic developments**

### **2.2.1 Early Holocene**

The onset of the Holocene period (11.7 cal. ka BP) marked the end of the Pleistocene and the transition to warmer interglacial conditions (Dansgaard et al., 1993; Cohen et al., 2013). The Early Holocene was characterised by warmer than present climatic conditions and strong seasonality that has been closely linked with the insolation signal, *i.e.*, a higher insolation signal resulting in warmer climatic conditions (Berger & Loutre, 1991; Harrison et al., 1992; Renssen et al., 2012; Zhang et al., 2016).

Similarly to present day climate warming, Early Holocene warming disproportionately affected higher latitudes compared to lower latitudes (Kaufman et al., 2004; Kaplan & Wolfe, 2006; Miller et al., 2010). This phenomena of ‘Arctic Amplification’ results in surface air temperatures changes in the Arctic largely exceeding those of the Northern Hemisphere as a whole (Miller et al., 2010). Alongside warmer surface air temperatures, oceanic conditions also experienced warming in comparison to deglaciation. In fact, at *c.* 11 cal. ka BP marine geological archives from across the Barents Sea-Svalbard region suggest warmer oceanographic conditions, that are considered to be tied to the northward flow of relatively warm and saline Atlantic water from the south (Rasmussen et al., 2007; Aagaard-Sørensen et al., 2010; Skirbekk et al., 2010; Kristensen et al., 2013). This enhanced northward ocean heat

flow was particularly distinguished along the western margin of Svalbard, where transfer functions based on benthic foraminifera suggest some of the highest bottom water temperatures of the Holocene occurring between 11.5 to 8.2 cal. ka BP (Rasmussen et al., 2014).

### **2.2.2 Holocene Thermal Maximum**

Within the Early Holocene was a warmer than present climatic interval termed the Holocene Thermal Maximum (HTM). Globally this occurred between *c.* 10 to 6 ka BP and a significant driving force was orbital forcing that resulted in higher than present summer insolation values resulting in warmer air and ocean temperatures during this period (Jakobsson et al., 2010). To elaborate on this, Pieńkowski et al. (2021) present data from Berger (1978) that shows at 80 °N, mean insolation increased by 5 W m<sup>-2</sup> annually and *c.* 50 W m<sup>-2</sup> in June compared to present, highlighting the significance of the increased insolation signal experienced at high latitudes during this time interval. This increased insolation signal and enhanced presence of Atlantic Water, had a cascade of physical and biological implication around the Svalbard region both in the terrestrial and marine realm. On the Western Spitsbergen continental margin, the HTM is proposed to have occurred between *c.* 10.0 to 8.8 cal. ka BP (Birks, 1991; Salvigsen et al., 1992; Sarnthein et al., 2003; Hald et al., 2004; Rasmussen et al., 2007).

Terrestrial data across Svalbard provide evidence for higher air temperatures than present during the HTM. This includes glacial lake records indicating glaciers having a smaller extent (Svendsen & Mangerud, 1997; van der Bilt et al., 2015), plant macrofossils indicating July temperatures 2 °C higher than today on the west coast (Birks, 1991) and alkenone temperature reconstructions suggesting temperatures up to 7 °C warmer than present in Northern Svalbard during peak Early Holocene warmth (van der Bilt et al., 2019). Despite this, recent modelling of relative sea level histories conducted by Fjeldskaar et al. (2018) suggests glaciers on the Nordaustlandet and Eastern Spitsbergen survived the HTM. When considering the shallow marine realm, the occurrence of thermophilous marine molluscs (e.g., *Arctica islandica* (Linnaeus, 1767), *Zirfaea crispata* (Linné, 1758), *Mytilus edulis* (Linné, 1758) and *Modiolus modiolus* (Linné, 1758)) within glacio-isostatically uplifted coastal deposits indicate that warm waters were present along the shorelines of Svalbard's fjords during the HTM (Feyling-Hanssen, 1955; Salvigsen et al., 1992; Hjort et al., 1995; Salvigsen, 2002; Hansen et al., 2011; Mangerud & Svendsen, 2018). Out of these

thermophilous marine molluscs, *Zirfaea crispata* and *Arctica islandica* are the most warmth demanding species and their presence in the raised marine record of Svalbard occurs only between 10-9.2 cal. ka BP (Mangerud & Svendsen, 2018). This indicates that maximum ocean temperatures occurred shortly after the onset of the Early Holocene and before the peak in summer solar insolation (Mangerud & Svendsen, 2018). A study conducted on the *Arctica islandica* shells from Dicksonfjorden, North Isfjorden, used  $\delta^{18}\text{O}$  profiles to calculate that water temperatures at *c.* 30 m water depth were 6 °C warmer than present around 10 cal. ka BP (Beierlein et al., 2015).

The suite of terrestrial and marine evidence provided above firmly demonstrates that the HTM around the Barents Sea-Svalbard region was a period that holds potential to further investigate and understand environmental evolutions during warmer-than-present conditions.

### **2.3 Previous work**

Established literature concerning the study site at Bogebecken within Hollendarbukta is scarce and primarily limited to a paper published in Cyrillic by Sharin et al. (2014), a master's thesis conducted by Bakken (2021) and an unpublished bachelors thesis by Christman (2022). Despite these three studies, the sedimentology and geomorphology of the study site is poorly documented. Initially, Sharin et al. (2014) investigated a section on the western side of the terrace at the mouth of Bogebecken and divided the stratigraphy into three members (top to bottom): grey sand and gravel; brown sandy silt with mollusc shells; and a black silt. Aside from the stratigraphical description of the section, Sharin et al. (2014) conducted radiocarbon dating on 5 mollusc shells (*Mya truncata* and *Arctica islandica*) that were situated in the “5 m” thick ‘brown sandy silt’ member. The dates from the sampled mollusc shells led Sharin et al. (2014) to publish that the 5 m thick sandy silt member at Bogebecken was deposited between 10.5 and 9.4 cal. ka BP. In addition to dating the section, Sharin et al. (2014) identified the marine limit within Bogebecken to be 70 m a.s.l.

Bogebecken was later visited by Bakken (2021) during a master's thesis field campaign, investigating the distribution of molluscs at sites around Isfjorden. In the quest to validate the work conducted by Sharin et al. (2014), a section in close proximity along the western edge of the marine terrace at the mouth of Bogebecken was investigated by Bakken (2021). Stratigraphically, Bakken (2021) divided the section into three units, similarly to Sharin et al. (2014). The investigations conducted by Sharin et al. (2014) and Bakken (2021) yielded a

total of 11 radiocarbon dates that are used in this investigation to constrain the age of the *Arctica islandica* Section at Bogebecken (Table 1). The raw  $^{14}\text{C}$  ages have been recalibrated with the Marine20 calibration curve (Heaton et al., 2020) using the online calibration programme Calib 8.20 (<http://calib.org/calib/calib.html>) provided by Stuiver and Reimer (1993). Additionally, the revised regional marine reservoir correction age ( $\Delta R_R$ ) of  $-61 \pm 37$   $^{14}\text{C}$  for mollusc shells dated from within the oceanographic setting of western Svalbard has been applied during calibration (Pieńkowski et al., 2022). The median recalibrated ages (cal. ka BP) are determined with 95.4% probability ( $\sigma_2$ ).

The recalibrated dates show a poor stratigraphic age zonation, with the dates from Bakken (2021) being generally younger than those from Sharin et al. (2014) (Table 1). The section is constrained by the oldest date at the base of the section (1 m a.s.l.) is c. 9.4 cal. ka BP and the youngest date towards the top of the section (4 m a.s.l.) is c. 7.9 cal. ka BP.

Table 1: Radiocarbon dates from Sharin et al. (2014) and Bakken (2021) for the *Arctica islandica* Section at Bogebecken. Raw  $^{14}\text{C}$  ages have been recalibrated with the Marine20 calibration curve (Heaton et al., 2020) using the online calibration programme Calib 8.20 (<http://calib.org/calib/calib.html>) provided by (Stuiver & Reimer, 1993) with a  $\Delta R$  correction age of  $-61 \pm 37$   $^{14}\text{C}$  applied (Pieńkowski et al., 2022). Calibrated ages are presented with a 95.5% probability ( $\sigma_2$ ).

Radiocarbon dates from the <i>Arctica islandica</i> Section at Bogebecken (BKS1)								
Field sample number	Elevation (m a.s.l.)	Raw $^{14}\text{C}$ age	$\pm$	Cal. ka BP: 95.4% probability ( $\sigma_2$ )			Dated material	References
				Median	From	To		
BB-20-S-04-02	4.0 - 4.1	8450	150	8923	8500	9349	<i>Arctica islandica</i>	Bakken (2021)
BB-20-S-04-01a	4.0 - 4.1	7530	120	7878	7595	8160	<i>Arctica islandica</i>	Bakken (2021)
BB-20-S-03-01	2.7 – 2.85	8440	150	8902	8478	9326	<i>Arctica islandica</i>	Bakken (2021)
LU-6992 (Lab ID)	2.5	8700	120	9222	8908	9535	<i>Arctica islandica</i>	Sharin et al. (2014)
BB-20-S-02-2a	1.9 – 2.2	8480	140	8961	8556	9365	<i>Arctica islandica</i>	Bakken (2021)

BB-20-S-02-01	1.9 – 2.2	8750	200	9294	8729	9858	<i>Arctica islandica</i>	Bakken (2021)
BB-20-S-01-04	1.0 – 1.3	8640	180	9103	8623	9583	<i>Arctica islandica</i>	Bakken (2021)
BB-20-S-01-03	1.0 – 1.3	8240	160	8680	8253	9106	<i>Arctica islandica</i>	Bakken (2021)
BB-20-S-01-02a	1.0 – 1.3	8280	140	8720	8339	9100	<i>Arctica islandica</i>	Bakken (2021)
BB-20-S-01-01a	1.0 – 1.3	8840	160	9431	8984	9878	<i>Arctica islandica</i>	Bakken (2021)
GIN-14735 (Lab ID)	1	8700	50	9234	9436	9031	<i>Arctica islandica</i>	Sharin et al. (2014)

### **3 Methodology and materials**

This chapter presents an overview of the field campaign that formed the basis for this investigation. Field techniques and sampling protocols are described, detailing the instruments used and procedures behind sediment analysis and the geomorphic mapping. Laboratory work that followed the field campaign is outlined with a detailed and reproducible workflow that was applied during the grain size analysis aspect of the investigation. Finally, an overview of the softwares and digital resources used in this project is presented.

#### **3.1 Field campaign**

The field work campaign at Bogebecken within Hollendardalen was conducted between the 27<sup>th</sup> and 29<sup>th</sup> of July 2023. Daily transport to and from the field was made by PolarCirkel boats that departed from the boat harbour in Longyearbyen.

Initially, the field team conducted a morning of reconnaissance hiking up valley along the stretch of raised marine terraces that progress inland from the present-day shoreline. The objective was to identify potential workable sections that could be exposed and cleaned prior to sedimentological logging and sediment sampling. Having identified four promising sections (Figure 9), the remaining two and a half days were spent conducting sedimentological and geomorphological analysis of the valley with the techniques that are described and documented below.



Figure 9: Location of the broad study area within Hollandarbukta, Isfjorden marked with a red square on the inset map. Position of the section locations within this investigation at Bogebekken and Hollendardalen are marked with a red dot. Section locations from previous studies in the area conducted by Bakken (2021) are marked with a blue triangle, and by Sharin et al. (2014) with a green diamond.



### **3.1.1 Field techniques**

#### **3.1.1.1 Location positioning**

Location positioning whilst in the field was essential for marking the base of sections, elevation baseline data and other points of interest. It was therefore carried out using two types of systems. The first being a handheld Garmin Map 66i Global Positioning System (GPS) and the other a Leica CS20 Global Navigation Satellite Service (GNSS) system coupled with a GS16 antenna. Through collecting location positioning with two different devices, the degree of accuracy between the coordinates could be determined when plotted onto a topographic base map. Whilst the handheld Garmin device determines its GPS position from triangulation with satellites orbiting the Earth, the Leica GNSS is a Differential Global Positioning System (DGPS) that determines its position with reference to a nearby base station (in this case in Longyearbyen) that has exact known coordinates. Through connection with this base station, location positioning with a DGPS system can be referred to as 'Real-Time-Kinematics' (RTK). This reduces the error of a measured location considerably, resulting in centimetre precision when recording location positions. The coordinate system used throughout the project is the Universal Transverse Mercator (UTM). This is a projected coordinate system that divides the world into 60 north-south zones that are 6 ° in longitude wide. With respects to Western Spitsbergen and the study area of interest, the designated zone is 33X.

#### **3.1.1.2 Elevation data**

Recording the elevation of the base of sections and dated material within, is imperative to construct a relative sea level curve and constrain a relative sea level history for the locality. Elevation data is commonly expressed as meters above present sea level (m a.s.l.). Prior to an explanation of how elevation data was measured and collected in the field, it is necessary to outline the process behind establishing the benchmark of '0 meters' that was used during the field campaign.

#### **3.1.1.3 Establishing a benchmark**

Relative sea level is the average measure of the sea surface in relation to the shoreline at a given location over a particular time. Whereas the water level at a specific site varies in relation to tides and meteorological conditions such as air pressure and wind. To establish a

measurable baseline in the field, a point of ‘best known’ elevation is required to act as a benchmark to determine the relative elevation of features with respect to this point.

The study site is affected by semi-diurnal tides meaning there are two high and two low tides each day. The high tide mark therefore provides a point of reference that can be corrected to a height above relative sea level by accounting for water level variations. The Norwegian Mapping Authority (2014) has 24 permanent tidal gauges, the closest of which to the study site is at Ny-Ålesund (Figure 1). Data provided by The Norwegian Mapping Authority (2014) indicates the water and tide level height in centimetres with reference to a historic vertical chart datum (1996-2014) that acts as a mean relative sea level. The high tide mark measured on the beachface at Bogebecken on the 26<sup>th</sup> of July, provided the ‘0 meters’ benchmark throughout the field campaign, and the elevation of the base of sections above this point were recorded. They were later corrected to m a.s.l. using water level and high tide data as well as mean sea level observations for Ny-Ålesund between the reference period of 1996-2014.

#### 3.1.1.4 Optical sighting levelling

With a benchmark established on the shoreline, the elevation of the base of the *Arctica islandica* Section at Bogebecken (BKS1) could be established through an optical sighting level survey (Figure 10). This technique is used to determine distance and elevation between two points, in this case the high tide benchmark and the base the of BKS1.



Figure 10: Mathilde and David conducting an optical sighting survey on the shoreline of Bogebecken to establish the elevation of the base of BKS1 in relation to the high tide mark on the 26th of July 2023. Optical sighting scope on the left, operated by Mathilde and measuring pole on the right, held by David. Photo: Mark Furze.

The process involves one person operating the sighting scope (Figure 10, left) and the other holding the measuring pole vertically (Figure 10, right). By aligning the numbering on the measuring pole within the cross hairs of the scope during the first ‘backsight’ reading, the height above the benchmark is established. The measuring pole can then be moved past the scope and towards the end destination to similarly conduct a ‘foresight’ reading. Once a backsight and fore-sight reading have been recorded, the person operating the scope can move past the new position of the measuring stick, again towards the end destination. Only one person will move at a single time. This process is repeated until a closing foresight reading is made at the final point of interest. The same procedure is then carried out in a reverse order back towards the benchmark. This is to identify if incorrect measurements have been made along the transect.

#### **3.1.1.5 Digital Barometer Altimeter**

To determine the elevation above the high tide benchmark of Sections 2, 3 and 4 (Figure 9), a Handheld Digital Barometer Altimeter (Nova Lynx 230-M202) was used. The device accurately measures atmospheric pressure to within 0.015” Hg which equates to a precision of approximately half a meter when measuring altitude (Mark Furze pers. com). At the beginning of each day, a reading was made at the high tide benchmark and the coordinates, time and altitude were recorded. At each subsequently visited location, additional readings were taken, at a minimum, on arrival and before departure. This procedure allows for relative altitude differences between two points to be determined. Before departure from the field, a final reading was taken at the same benchmark. This allows for air pressure changes to be tracked throughout the day. This established elevation was then combined with the difference between the high tide benchmark and the mean sea level (1996-2014) to provide the presented m a.s.l. for each section.

#### **3.1.2 Sedimentology**

The sedimentary investigation was conducted on the raised marine terraces within Hollendarbukta. Four outcrops were investigated, two are on the western edge of the terrace at Bogebecken and two are on the western edge of the terrace at Hollendarelva. Fluvial incision has exposed the terraces however, each section required cleaning prior to analysis. This involved removing slumped superficial material with spades and creating stepped ‘windows’ measuring 1-2 m wide and up to 1.5 m high progressively up the section. Trowels

were used to further define the windows and create a flat and workable surface, and, in some cases, sedimentary structures were enhanced through spraying with water.

### **3.1.2.1 Sedimentary logging**

A detailed sedimentary log was constructed for each section following a procedure similar to the one outline by Krüger and Kjær (1999) for the description of glacial diamicts and associated sediments. However, minor adjustments were made to best fit the description of the sediments within the study site and so the procedure followed is outline below.

Firstly, the base of the section was established and marked with a rock to cement its position and allow for a distinguishable position for elevation data to be measured from. Wooden rulers were used to measure the height from this base mark to the top of the section. The logging scales adopted were 1:20 (Section 1) or 1:10 (Section 2-4). When describing the sediments a series of classification schemes were adopted to standardise the procedure and enable comparisons with other published literature (Figure 11).

The grain size classification used was after Udden (1914) and Wentworth (1922) and the degree of sediment sorting followed a visual representation of the statistical parameters established by Folk (1980) (Figure 11). Grain roundness was estimated using a hand lens to examine the sediment in the field using the classification of Powers (1953) as a reference point (Figure 11). Additionally, grain shape was approximately determined in the field in line with the classification of classification of Zingg (1935) to establish whether clasts were disc, blade, rod or spherical in shape. It is stressed that a detailed analysis of clast fabric or morphology was not performed during this investigation, and so reference to grain shape, sorting and rounding in the results section is based solely on qualitative field observations.

As well as grain size trends, sedimentary structures, unit boundaries, bedding inclinations, sampling heights and shell positions were recorded. Pictures were taken of each section and specific sedimentary structures and features to allow for a post field work review and the creation of annotated figures. Additionally, the mobile phone app '3D Scanner' enabled orthomosaics of the sections to be constructed almost immediately in the field and these are presented in the sections below.

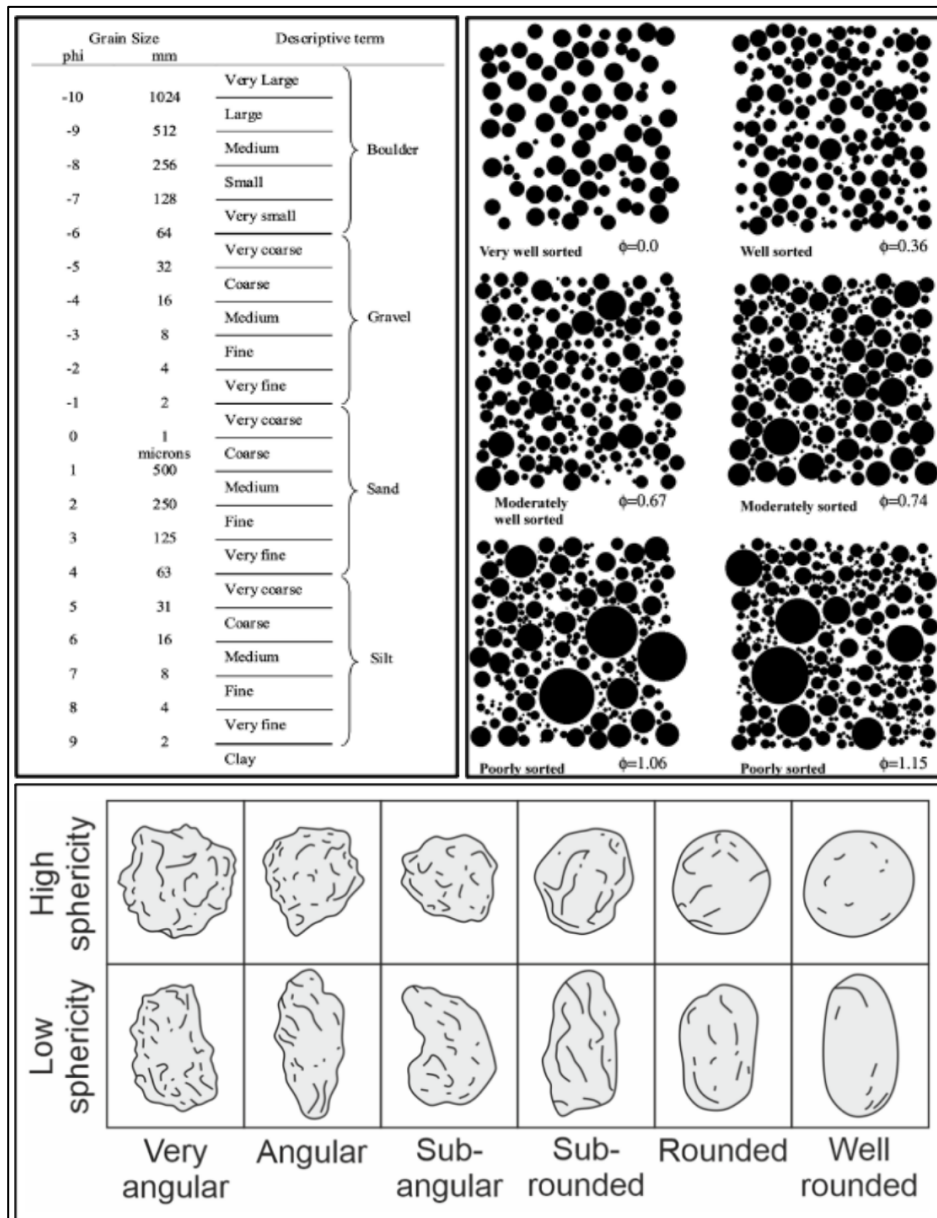


Figure 11: (Top left) Grain size classification table used during sedimentary logging after Udden (1914) and Wentworth (1922), adapted by Blott and Pye (2001). (Top right) Visual representation of sediment sorting classification used in the field based on Folk (1980) textural classification. Diagram sourced from: Jerram (2001). (Bottom) Grain roundness classification used in sedimentary logging based on the classification established by Powers (1953). Diagram sourced from: Russell et al. (2023).

### 3.1.2.2 Sampling procedure

The primary objective with sediment sampling was to target fine grained sediment that may contain foraminifera. To constrain a narrow time interval of the sampled section, 1-2 cm horizons were sampled and approximately 150 – 200 g of sediment was collected. Sediment beds were marked with a knife and the sediment was excavated into a plastic zip-lock bag labelled with the section number and the sampling height. As well as sediment samples, molluscs were sampled, and their degree of preservation noted in case of their use in radiocarbon dating.

### **3.1.2.3 Defining lithofacies**

In this investigation, the lithofacies are defined and delineated in accordance with Lee (2018) by establishing: (1) their lithology and sedimentary structure; and (2) their geometry and relation to adjacent lithofacies. Key field descriptions such as sediment texture, bedding thickness and nature of contacts are all combined to distinguish individual lithofacies. Where possible, these physical descriptors are supplemented with data obtained through detailed grain size analysis retrieved with a Laser Particle Size Analyser as outlined in the methodology section below.

This detailed grain size analysis enabled fine grain size fractions to be distinguished and this led to a comprehensive separation of fine grained lithofacies based primarily on grain size using the laboratory derived data. One option when defining lithofacies is to divide texturally similar lithofacies into 'sub lithofacies' e.g. Alexanderson and Bernhardson (2019). In this investigation, texturally similar fine grained lithofacies are broadly grouped according to the Folk (1954) classification e.g. 'sandy silt'. However, given the availability of detailed grain size analysis data, these texturally similar fine grained lithofacies are defined in further detail in lithofacies tables that highlights nuanced distinctions between them. Having established the sedimentological character of the lithofacies, an interpretation can be made about the depositional process that led to its formation. Texturally similar lithofacies are then divided into separate lithofacies associations based on their stratigraphic position and relation to other lithofacies, which is used to separate them into different depositional environments.

### **3.1.2.4 Defining lithofacies associations**

Lithofacies associations are established by combining two or more lithofacies to represent a depositional palaeo-environment. Combining lithofacies into lithofacies associations, enables a sequence of palaeo-environments to be constructed indicating a larger depositional system. In a coastal setting that has been subject to regional glacio-isostatic uplift throughout the Holocene, a large part of identifying palaeo-environments is based on their stratigraphic position up sequence. Therefore, when establishing the lithofacies associations presented in the results of this investigation, their stratigraphic position, the lithofacies character and correlation of the deposits with other published literature is used to strengthen the suggested palaeo-depositional environment.

## 3.2 Geomorphic mapping

Reconnaissance and sedimentological investigation of the raised marine terraces during the field campaign provided a broad overview of character of the sediments within the study area. However, detailed geomorphic mapping has been conducted remotely using a combination of aerial orthophotos, satellite imagery and topographic base maps.

### 3.2.1 Desk-based mapping


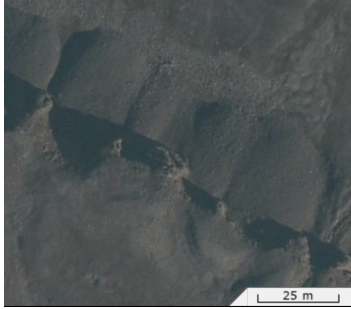
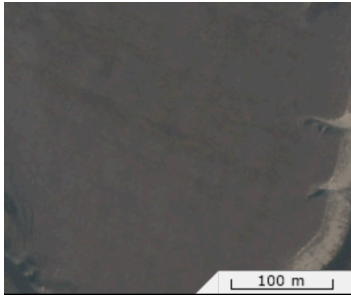
The construction of the geomorphic map presented for the study area in Figure 13 was produced using the Geographic Information System QGIS version 3.22. The data used in the remote geomorphic mapping phase of the project is presented in Table 2. The map colours and symbology used are in accordance with the Norwegian SOSI Standard (Coordinated Scheme for Location Information) for Quaternary geological maps. This scheme utilises a standardised legend determined from the genetic classification of the deposit (Bergstrøm et al., 2001; Rubensdotter et al., 2018).

*Table 2: Information on the data set used for remote geomorphic mapping including data type, data ID, projection, year, and a reference to the data source.*

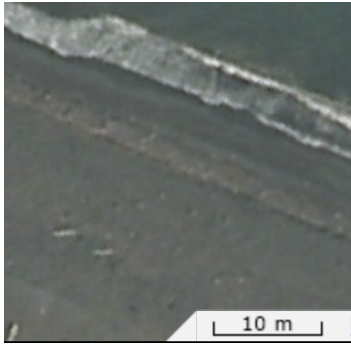
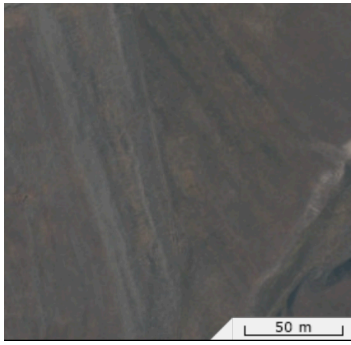
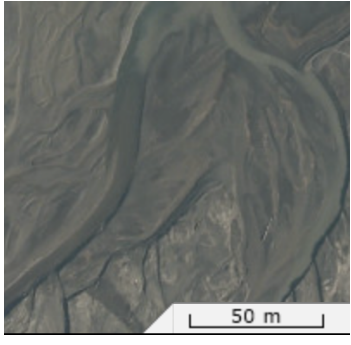

Data type	Data ID	Projection	Year	Data source
Topographic map	NP_Basiskart_Svalbard_WMTS_25833	WGS 84 UTM zone 33 N (EPSG:25833)	2009	Norwegian Polar Institute (2009a)
Orthophoto	NP_Ortofoto_Svalbard_WMTS_25833	ETRS 89 UTM zone 33 N (EPSG:25833)	2009	Norwegian Polar Institute (2009b)
Satellite imagery	NP_Satellitt_Svalbard_WMTS_25833	ETRS 89 UTM zone 33 N (EPSG:25833)	2009	Norwegian Polar Institute / USGS Landsat (2009)
Digital Elevation Model	S0_DTM5_2010_13836_33	ETRS 89 UTM zone 33 N (EPSG:25833)	2010	Norwegian Polar Institute (2014)
Digital Elevation Model	S0_DTM5_2011_25162_33	ETRS 89 UTM zone 33 N (EPSG:25833)	2011	Norwegian Polar Institute (2014)


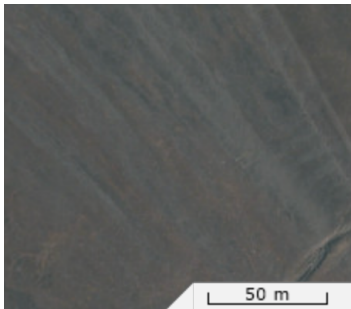
When constructing the geomorphic map, the criteria for assigning land surfaces to different classifications was based on field observations of sediment character, thickness, and extent at the various outcrop localities. This approach was extrapolated during the remote mapping phase and so it is necessary to present descriptions and visual cues of the key deposits and features in Table 3 that are interpreted in the Quaternary geomorphic map (Figure 13).

Table 3: Visual criteria and descriptions used to classify key Quaternary lithologies and features during the geomorphic mapping phase of the study site at Hollendarbukta. Symbols and codes are in accordance with SOSI Standard (see above). Visual representation is provided by in the form of an orthophoto sourced from Norwegian Polar Institute (2009b)

Visual representation	Lithology	Description	Symbol/ code
	Weathered bedrock	Exposed bare rock with sparse vegetation cover, composing fjell areas the highest elevations of the study site. Uneven and rouged surface expression.	071
	Colluvium	Coarse, blocky debris deposited at the base of a bedrock scarp forming steep, cone and tounge shape deposits.	080
	Marine fine-grained deposit	Thick (>3 m) and continuous raised marine sediment capped with beach ridges. Outcrops presented in this investigation.	041



	<p>Marine beach, present</p>	<p>Active sand and gravel beach face affected by wave and tide processes.</p>	<p>042</p>
	<p>Marine beach deposit, raised</p>	<p>Thin (&lt;3 m) cover of raised marine beach deposits overlying bedrock.</p>	<p>043</p>
	<p>Fluvial deposit, recent</p>	<p>Fluvial sediment consisting of cobbles, pebbles, sand, and gravel deposited by active channels. Minimal vegetation cover.</p>	<p>050</p>
	<p>Fluvial deposit, pre-recent</p>	<p>Fluvial sediment consisting of pebbles, gravel and sand with inactive channels and considerable vegetation cover.</p>	<p>051</p>

	<p>Beach ridges</p>	<p>Low amplitude (&lt;75 cm), parallel, aggregational feature. Capping thick and continuous marine fine-grained deposits.</p>	<p>201 /////</p>
	<p>Shoreline in unconsolidated sediment</p>	<p>Moderate amplitude (c. 1-1.5 m, parallel and erosional feature. Associated with thin raised marine beach deposits that are draped over bedrock.</p>	<p>202 §§§§</p>

### 3.3 Laboratory work

Preliminary laboratory work was conducted in the Arctic Geology Laboratory at the University Centre in Svalbard. This including weighing and wet sieving the sediment to prepare the samples for microscope analysis which was later conducted at the Norwegian Polar Institute in Tromsø. Unfortunately, an initial analysis of the 100 µm size fraction showed the samples were devoid of foraminifera. Regardless of this, a brief overview of the methodology of preparing the foraminiferal samples (wet sieving) is presented as these samples were used to investigate the organic and inorganic content of their coarse >500 µm grain size fraction.

As foraminifera were absent within the sediment samples, it was decided to obtain detailed grain size data. This analysis was carried out using a Laser Particle Size Analyser (LPSA). This procedure was deemed more appropriate for conducting grain size analysis compared to wet sieving, as the sediment samples were predominantly composed of fine-grained material that was rich in clay and silt particles. Through performing this method of analysis, a larger, and higher resolution dataset could be generated in comparison to the results generated from wet sieving these sized particles.

### **3.3.1 Weighing and wet sieving**

Approximately 50 g of wet bulk sediment was measured using a Sartorius CP 64 digital weighing scale that measured the weight of the sample to a precision of 4 decimal places. Wet sieving involved flushing the sample through sieves with mesh sizes 500  $\mu\text{m}$ , 100  $\mu\text{m}$  and <63  $\mu\text{m}$  that were pre decided to control the resolution of the study based on previous work that has been conducted. A moderate flow of tap water (<50°C) was used to wash the sediment through the sieves. The process of sieving allows the sediment to be separated into different size fractions allowing for grain size analysis and sedimentological observations of grains of certain sizes to be conducted. The residue from each size fraction was collected in a glass funnel with a filter paper pocket that was labelled with the section number, sample depth and size fraction. The filter paper containing the residue from the size fractions was then oven dried at 30°C overnight. The samples were then collected in accordingly labelled dram glasses. As the decision to conduct a grain size analysis on the sediment samples using the LPSA had been made, weighing the individual grain size fractions post sieving and drying was not performed. One reason behind this is that grain size distributions generated through wet sieving are calculated as a percentage of the total mass of the sample, whereas results generated through LPSA are calculated as a percentage of the sample volume. As a result, the two datasets would not be directly comparable.

### **3.3.2 Microscope analysis**

Microscope analysis of the >500  $\mu\text{m}$  size fraction was conducted using a Leica MZ10 stereomicroscope with a zoom of 0-11x. A recorded fraction of the sample was spread over a metal counting tray and grain characters such as shape and roundness were observed. Additionally, shell fragments and other biogenic material were described.

### **3.3.3 Laser Diffraction Particle Size Analyser**

Grain size analysis was carried out in the Department of Geoscience Laboratory at UiT The Arctic University of Norway using the Beckman Coulter (LS 13320) Laser Particle Size Analyser. The theory behind how Laser Diffraction Particle Size Analysers measure particle size is as followed. The technique involves shining a laser beam through a chamber containing sediment in suspension. The angle of diffraction when the laser hits the suspended grains is in accordance with the size of the particle. Through applying the Fraunhofer and

Mie theories of light scattering, the instrument can calculate the percentage volume of grains between 0.04 – 2000 microns.

### **3.3.3.1 Sample preparation**

Initially the wet sediment samples were freeze dried. In preparation for freeze drying, a representative 50 g of wet sediment was placed in a labelled ziplock bag and frozen for 24 hours in a conventional freezer. Once fully frozen, freeze drying of the sediments was undertaken using a Christ Alpha 1-4 LSC Freeze Dryer and the process took approximately 24 hours (Figure 12, A).

The sediment samples in bags were placed on the trays in the freeze dryer and the bags were left open to allow the vapor to escape before condensing on a collection plate at the bottom of the freeze dryer. The principle underlying freeze drying is sublimation, where a solid shifts directly to a gas, essentially skipping the liquid phase. Through controlling the temperature and reducing the pressure by creating a vacuum, the process of sublimation speeds up, making it a useful deliberate drying technique (Shukla, 2011). Freeze-dried materials have the tendency to be drier in comparison to their conventionally dried counterparts due to a higher surface area to volume ratio (Ward & Matejschuk, 2021). With respects to this purpose, it makes the samples easier to desiccate when agitated by hand, forming a fine powder. This increased the probability that 2 g of sediment was representative of the sample.

### **3.3.3.2 Chemical treatment**

Chemical treatment is a two-stage process that ensures the removal of calcium carbonate and organic matter from within the sediment sample and means the grain size results solely reflect the lithological content of the sediment. Firstly, hydrochloric acid (HCl) is added to remove calcium carbonate within the sediment. Secondly, hydrogen peroxide (H<sub>2</sub>O<sub>2</sub>) is added to remove any organic matter. Hydrogen peroxide is a commonly used reagent to remove organic matter from soil and sediment samples (Mikutta et al., 2005; Gray et al., 2010). However, various treatment methods conducted on riverine and marine sediments indicate observable differences in grain size distributions obtained while applying different pre-treatment methods (Allen & Thornley, 2004; Gray et al., 2010). Therefore, the methodology used in this study is based on a standardised test procedure for the addition of hydrogen peroxide to marine samples, established at the laboratory of the Department of Geosciences, UiT The Arctic University of Norway by Sternal et al. (2017).

### **3.3.3.3 Hydrochloric acid procedure**

Firstly, 20 mL of diluted (20 %) hydrochloric acid was combined with the sediment in the test tubes (Figure 12, B). Samples were left for 12 hours to give the acid sufficient time to react with the calcium carbonate ( $\text{CaCO}_3$ ). To rinse acid residue out of the sediment sample, 200 mL of distilled water was added to each test tube. The test tubes were then placed in an Eppendorf Centrifuge 5702 and spun at 4000 RPM for 4 minutes (Figure 12, C). This step was repeated three times.

### **3.3.3.4 Hydrogen peroxide procedure**

Next, 20 mL of 20% hydrogen peroxide was added to each of the test tubes. The test tubes were incubated for 2 hours at 80 °C in a VWR 18 L thermal bath to speed up the reaction (Figure 12, D). After two hours, the test tubes were removed, and the samples were washed with distilled water in the same fashion as described above.

### **3.3.3.5 Post chemical treatment preparation**

With the calcium carbonate and organic matter removed from the sediment sample, the content of the test tube was flushed into capped plastic beakers. The beakers were labelled with the sample ID before being dried in the oven dryer at 25 °C for 48 hours. Using the Sartorius CP 64 digital weighing scale, a representative 0.15 – 0.2 g of dried sediment was weighed back into the plastic beaker. 20 mL of cold tap water was then added to each sample before placing them onto the Edmund Bühler GmbH SM-30 shaker for 48 hours. This step ensures dispersion of any dried clumps and promotes the sediment being suspended prior to analysis in the Particle Size Analyser.

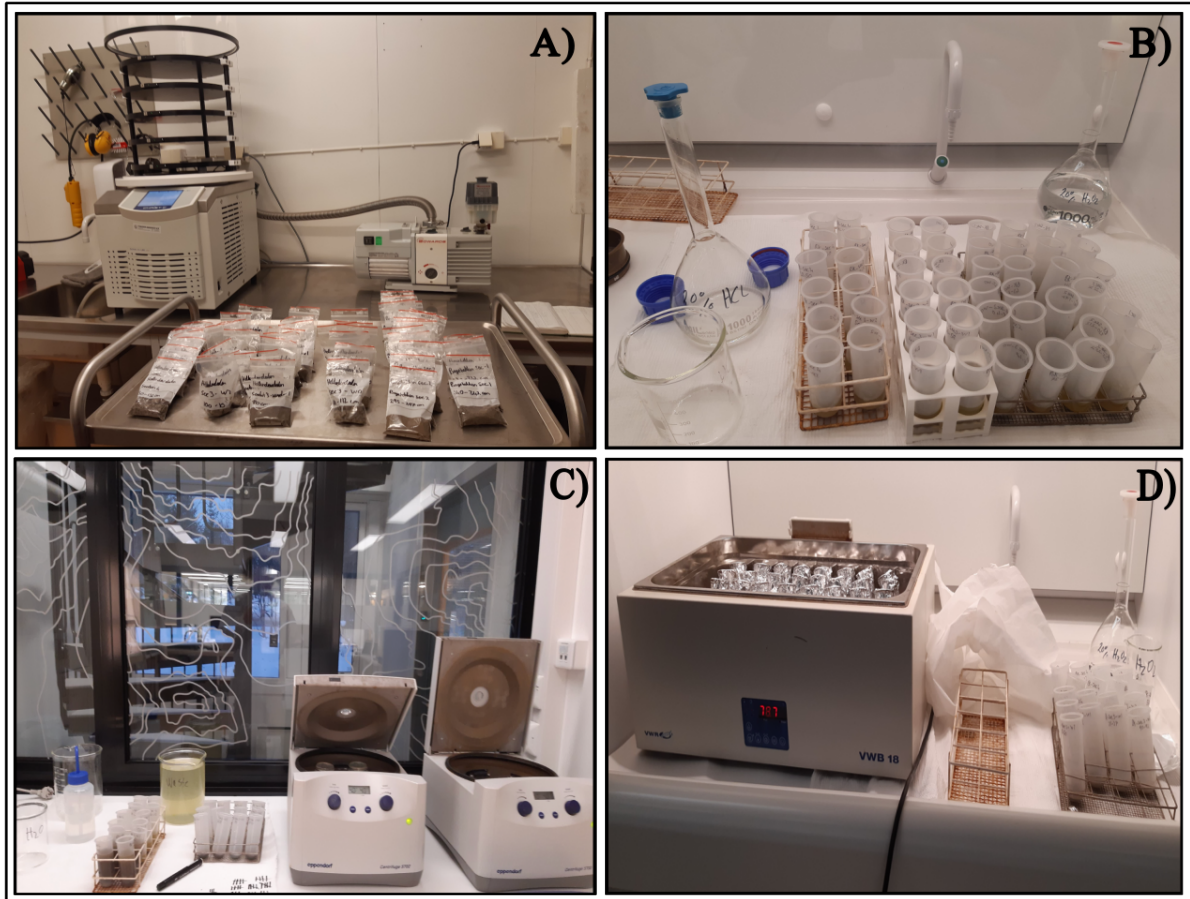


Figure 12: Pictures indicating the different stages of sample preparation for grain size analysis. Wet sediment samples prior to freeze-drying (A). The addition of 20 mL of dilute hydrochloric acid to the samples (B). Rinsing hydrochloric acid residue from the samples using distilled water and the centrifuges (C). Incubating the samples in a water bath during hydrogen peroxide treatment (D).

### 3.3.3.6 Laser Diffraction Particle Size Analyser procedure

Immediately before analysis in the Laser Particle Size Analyser, a few drops of Calgon water softener were added to the test tube containing the sample and it was placed in an ultrasonic bath for five minutes. This step ensures the disintegration of flocculated particles. The sample was then added to the solution chamber in the instrument. Each sample was analysed three times to improve the reliability of the results.

### **3.4 Software and online data resources**

#### **3.4.1 GRADISTAT v8.0**

Grain size distribution results generated through the LPSA were processed with GRADISTAT v8.0, a statistics package developed by Blott and Pye (2001), that allows for the analysis of unconsolidated sediments obtained through sieving or laser diffraction granulometry. The following section is described in accordance with their work. The program is provided in a Microsoft Excel format which allows for both spreadsheet and graphical output of calculated statistics.

As stated above, each sample was analysed three times to increase the validity of the results. The three sets of results were then combined and divided by three to get an average of the grain sizes for each size fraction. This average of the percentage of sediment grains detected in each 'bin' of the LPSA were entered into matching columns of the spreadsheet. The program calculated the statistics using the Method of Moments in Microsoft Visual Basic programming language: mean, mode (s), sorting (standard deviation), skewness, kurtosis,  $D_{10}$ ,  $D_{50}$ ,  $D_{90}/D_{10}$ ,  $D_{75}/D_{25}$  and  $D_{75}-D_{25}$ . Grain size parameters were calculated both arithmetically and geometrically (in microns) as well as logarithmically (in the phi scale) in accordance with Krumbein and Pettijohn (1938). Linear interpolation was additionally used to calculate statistical parameters by Folk and Ward (1957) graphical method and obtain physical descriptions (e.g. "coarse silt" and "poorly sorted") (Table 5).

Furthermore, the program provides a physical description of the textural group for each sediment sample and a sediment name (e.g. "fine sand coarse silt") after Folk (1954), which is plotted onto a textural triangle identifying the percentage of sand, silt and clay. A table providing the percentage of grains falling into each size fraction, modified from Udden (1914) and Wentworth (1922) is presented. The graphical output of data from the program used in this project is in the form of grain size distributions in both metric and phi units.

Table 4: Statistical formulae used to calculate grain size parameters and the associated descriptive terminology. Abbreviations used are:  $f$  is the frequency in percent;  $m$  is the mid-point of each class interval in the metric ( $m_m$ ) or phi ( $m_\phi$ ) units;  $P_x$  and  $\phi_x$  are the grain size diameters in metric and phi units at the cumulative percentile value of  $x$ . (Blott & Pye, 2001).

(a) Arithmetic Method of Moments					
Mean		Standard Deviation		Skewness	
$\bar{x}_a = \frac{\sum f m_m}{100}$		$\sigma_a = \sqrt{\frac{\sum f (m_m - \bar{x}_a)^2}{100}}$		$Sk_a = \frac{\sum f (m_m - \bar{x}_a)^3}{100\sigma_a^3}$	
				Kurtosis	
				$K_a = \frac{\sum f (m_m - \bar{x}_a)^4}{100\sigma_a^4}$	
(b) Geometric Method of Moments					
Mean		Standard Deviation		Skewness	
$\bar{x}_g = \exp \frac{\sum f \ln m_m}{100}$		$\sigma_g = \exp \sqrt{\frac{\sum f (\ln m_m - \ln \bar{x}_g)^2}{100}}$		$Sk_g = \frac{\sum f (\ln m_m - \ln \bar{x}_g)^3}{100 \ln \sigma_g^3}$	
				Kurtosis	
				$K_g = \frac{\sum f (\ln m_m - \ln \bar{x}_g)^4}{100 \ln \sigma_g^4}$	
Sorting ( $\sigma_g$ )		Skewness ( $Sk_g$ )		Kurtosis ( $K_g$ )	
Very well sorted	< 1.27	Very fine skewed	< -1.30	Very platykurtic	< 1.70
Well sorted	1.27 – 1.41	Fine skewed	-1.30 – -0.43	Platykurtic	1.70 – 2.55
Moderately well sorted	1.41 – 1.62	Symmetrical	-0.43 – +0.43	Mesokurtic	2.55 – 3.70
Moderately sorted	1.62 – 2.00	Coarse skewed	+0.43 – +1.30	Leptokurtic	3.70 – 7.40
Poorly sorted	2.00 – 4.00	Very coarse skewed	> +1.30	Very leptokurtic	> 7.40
Very poorly sorted	4.00 – 16.00				
Extremely poorly sorted	> 16.00				
(c) Logarithmic Method of Moments					
Mean		Standard Deviation		Skewness	
$\bar{x}_\phi = \frac{\sum f m_\phi}{100}$		$\sigma_\phi = \sqrt{\frac{\sum f (m_\phi - \bar{x}_\phi)^2}{100}}$		$Sk_\phi = \frac{\sum f (m_\phi - \bar{x}_\phi)^3}{100\sigma_\phi^3}$	
				Kurtosis	
				$K_\phi = \frac{\sum f (m_\phi - \bar{x}_\phi)^4}{100\sigma_\phi^4}$	
Sorting ( $\sigma_\phi$ )		Skewness ( $Sk_\phi$ )		Kurtosis ( $K_\phi$ )	
Very well sorted	< 0.35	Very fine skewed	> +1.30	Very platykurtic	< 1.70
Well sorted	0.35 – 0.50	Fine skewed	+0.43 – +1.30	Platykurtic	1.70 – 2.55
Moderately well sorted	0.50 – 0.70	Symmetrical	-0.43 – +0.43	Mesokurtic	2.55 – 3.70
Moderately sorted	0.70 – 1.00	Coarse skewed	-0.43 – -1.30	Leptokurtic	3.70 – 7.40
Poorly sorted	1.00 – 2.00	Very coarse skewed	< -1.30	Very leptokurtic	> 7.40
Very poorly sorted	2.00 – 4.00				
Extremely poorly sorted	> 4.00				



Table 5: Statistical formulae used to calculate grain size parameters and the associated descriptive terminology. Abbreviations used are:  $f$  is the frequency in percent;  $m$  is the mid-point of each class interval in the metric (mm) or phi ( $m_\phi$ ) units;  $P_x$  and  $\phi_x$  (Blott & Pye, 2001)

(d) Logarithmic (Original) Folk and Ward (1957) Graphical Measures					
Mean		Standard Deviation		Skewness	
$M_z = \frac{\phi_{16} + \phi_{50} + \phi_{84}}{3}$		$\sigma_I = \frac{\phi_{84} - \phi_{16}}{4} + \frac{\phi_{95} - \phi_5}{6.6}$		$Sk_I = \frac{\phi_{16} + \phi_{84} - 2\phi_{50}}{2(\phi_{84} - \phi_{16})} + \frac{\phi_5 + \phi_{95} - 2\phi_{50}}{2(\phi_{95} - \phi_5)}$	
				$K_G = \frac{\phi_{95} - \phi_5}{2.44(\phi_{75} - \phi_{25})}$	
Sorting ( $\sigma_I$ )		Skewness ( $Sk_I$ )		Kurtosis ( $K_G$ )	
Very well sorted	< 0.35	Very fine skewed	+0.3 to +1.0	Very platykurtic	< 0.67
Well sorted	0.35 – 0.50	Fine skewed	+0.1 to +0.3	Platykurtic	0.67 – 0.90
Moderately well sorted	0.50 – 0.70	Symmetrical	+0.1 to 0.1	Mesokurtic	0.90 – 1.11
Moderately sorted	0.70 – 1.00	Coarse skewed	0.1 to 0.3	Leptokurtic	1.11 – 1.50
Poorly sorted	1.00 – 2.00	Very coarse skewed	0.3 to 1.0	Very leptokurtic	1.50 – 3.00
Very poorly sorted	2.00 – 4.00			Extremely leptokurtic	> 3.00
Extremely poorly sorted	> 4.00				
(e) Geometric Folk and Ward (1957) Graphical Measures					
Mean			Standard Deviation		
$M_G = \exp \frac{\ln P_{16} + \ln P_{50} + \ln P_{84}}{3}$			$\sigma_G = \exp \left( \frac{\ln P_{16} - \ln P_{84}}{4} + \frac{\ln P_5 - \ln P_{95}}{6.6} \right)$		
Skewness			Kurtosis		
$Sk_G = \frac{\ln P_{16} + \ln P_{84} - 2(\ln P_{50})}{2(\ln P_{84} - \ln P_{16})} + \frac{\ln P_5 + \ln P_{95} - 2(\ln P_{50})}{2(\ln P_{95} - \ln P_5)}$			$K_G = \frac{\ln P_5 - \ln P_{95}}{2.44(\ln P_{25} - \ln P_{75})}$		
Sorting ( $\sigma_G$ )		Skewness ( $Sk_G$ )		Kurtosis ( $K_G$ )	
Very well sorted	< 1.27	Very fine skewed	0.3 to 1.0	Very platykurtic	< 0.67
Well sorted	1.27 – 1.41	Fine skewed	0.1 to 0.3	Platykurtic	0.67 – 0.90
Moderately well sorted	1.41 – 1.62	Symmetrical	0.1 to +0.1	Mesokurtic	0.90 – 1.11
Moderately sorted	1.62 – 2.00	Coarse skewed	+0.1 to +0.3	Leptokurtic	1.11 – 1.50
Poorly sorted	2.00 – 4.00	Very coarse skewed	+0.3 to +1.0	Very leptokurtic	1.50 – 3.00
Very poorly sorted	4.00 – 16.00			Extremely leptokurtic	> 3.00
Extremely poorly sorted	> 16.00				

### **3.4.2 Inkscape**

Inkscape is an open-source vector graphics editor that has been used throughout the project to create figures and draw sedimentological logs. The version used is 1.3.2.

### **3.4.3 QGIS**

The open-source Geographical Information System QGIS version 3.22 was used throughout this project, primarily to construct a geomorphic map of the study area. Satellite and drone images were also georeferenced and annotated using the software.

### **3.4.4 SeKlima**

Modern climate data collected by the Norwegian Centre for Climate services (2023) has been accessed through their website and is used in the modern environment section of this investigation. The Norwegian Meteorological Institute provides a search engine where different weather elements at registered weather stations can be investigated over certain time periods. Monthly precipitation values for the meteorological station Isfjord radio at were used. The period for the monthly precipitation values covers 2015-2023 and this is rationalised in the modern environment section that follows.

### **3.4.5 Copernicus Data Space Ecosystem Hub**

Satellite imagery of the study area has been sourced through Copernicus Data Space Ecosystem Hub (2023), previously known as Sentinels Scientific Data Hub. The interactive web portal provided the Earth observation data from Sentinel 2-L1C satellites with a resolution of <60 m and in true colour, which allowed for the investigation of the coastal area and sedimentation processes. Once the study area was identified, the time parameters were set to correspond with climate data sourced from SeKlima. The period of interest covered July and August 2023 as these were the months when the field campaign was conducted and two months where there was a large disparity in monthly precipitation values. To ensure the satellite imagery was fit for purpose, with the study area being visible, the cloud coverage was set to <20 %. Days of the month where there was less than 20 % cloud coverage were then downloaded. Spatial analysis of the sedimentation processes resulting from fluvial input into the fjord was then conducted using both the Copernicus Data Space Ecosystem Hub and QGIS to produce annotated maps comparing images from the two months.

## 4 Results and interpretation

This section presents the results of the project. Where an interpretation is made, this will be clearly separated with a subsection heading.

The section outline is as follows:

- Geomorphic map visualising the Quaternary geology and geomorphology of the study area.
- A paleo-sedimentary investigation conducted through sedimentary logs, annotated photographs, and grain size data.
- A modern environmental synthesis of the study area presented through annotated aerial images, climate data, and satellite imagery.

Specifically, a detailed overview of each of the four sections selected for a sedimentological investigation is depicted through overview figures. A detailed sedimentary analysis is presented in the form of sedimentary logs. This is followed by a description of the lithofacies identified within the sections that are presented in a lithofacies table.

As stated in the methodology, the lithofacies are defined and delineated by establishing: (1) their lithology and sedimentary structure; and (2) their geometry and relation to adjacent lithofacies (Lee, 2018). Key field descriptions such as sediment texture, bedding thickness and nature of contacts are all combined together with detailed and laboratory derived grain size data.

This forms the basis for an interpretation of the processes that may have led to their formation. The established lithofacies are then grouped into lithofacies associations as described in the methodology to suggest a depositional environment. To link the observations and interpretations, an environmental synthesis of the conditions active over the period of deposition of the section is proposed.

Lastly, a modern environmental overview is presented. The results of this section highlight characteristics of the active system as well as climate data and satellite imagery. The purpose behind this is to investigate links between the past and present depositional environments. In this way, a greater insight into the sedimentary evolution of the study area can be discussed.

## 4.1 Geomorphic map

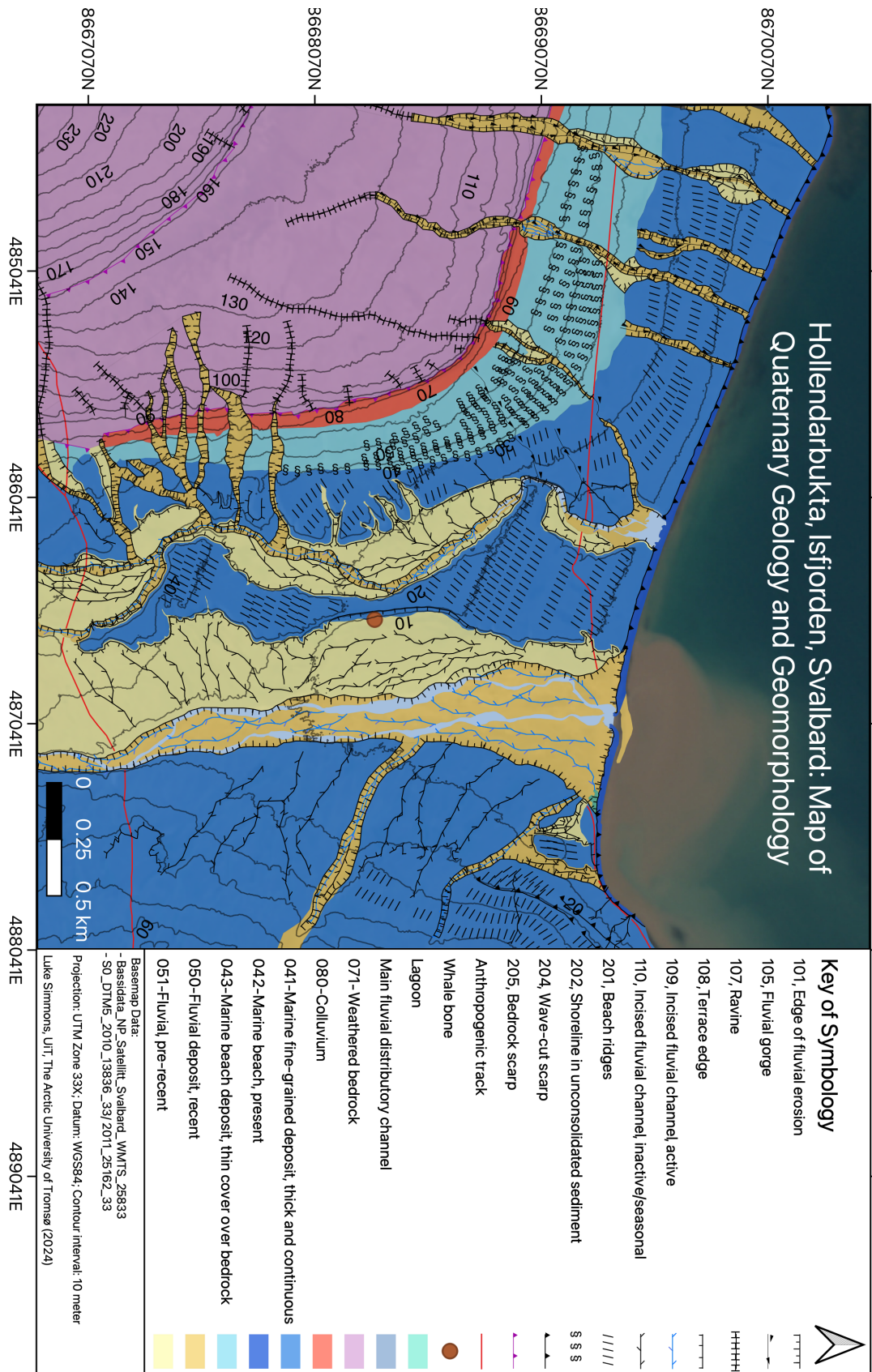


Figure 13: Map of the Quaternary geology and geomorphology at the study site of Hollendarbukta, Isfjorden.

## 4.2 Hollendardalen

### 4.2.1 Overview

Two studied outcrops are on the Hollendardalen (eastern) side of the marine terraces within the valley. The two sections are termed Hollendardalen Section 3 (HDS3) and Hollendardalen Section 4 (HDS4), and they are positioned *c.* 1.5 km from the present shoreline (Figure 9). The largest section comprising the entire terrace is HS3 (Figure 14). The coordinates for the base of the section are 33X E486604 N8668084 and the elevation 18.5 m a.s.l. The height of the section is 12 m, and the width of the investigated section is 15 m.

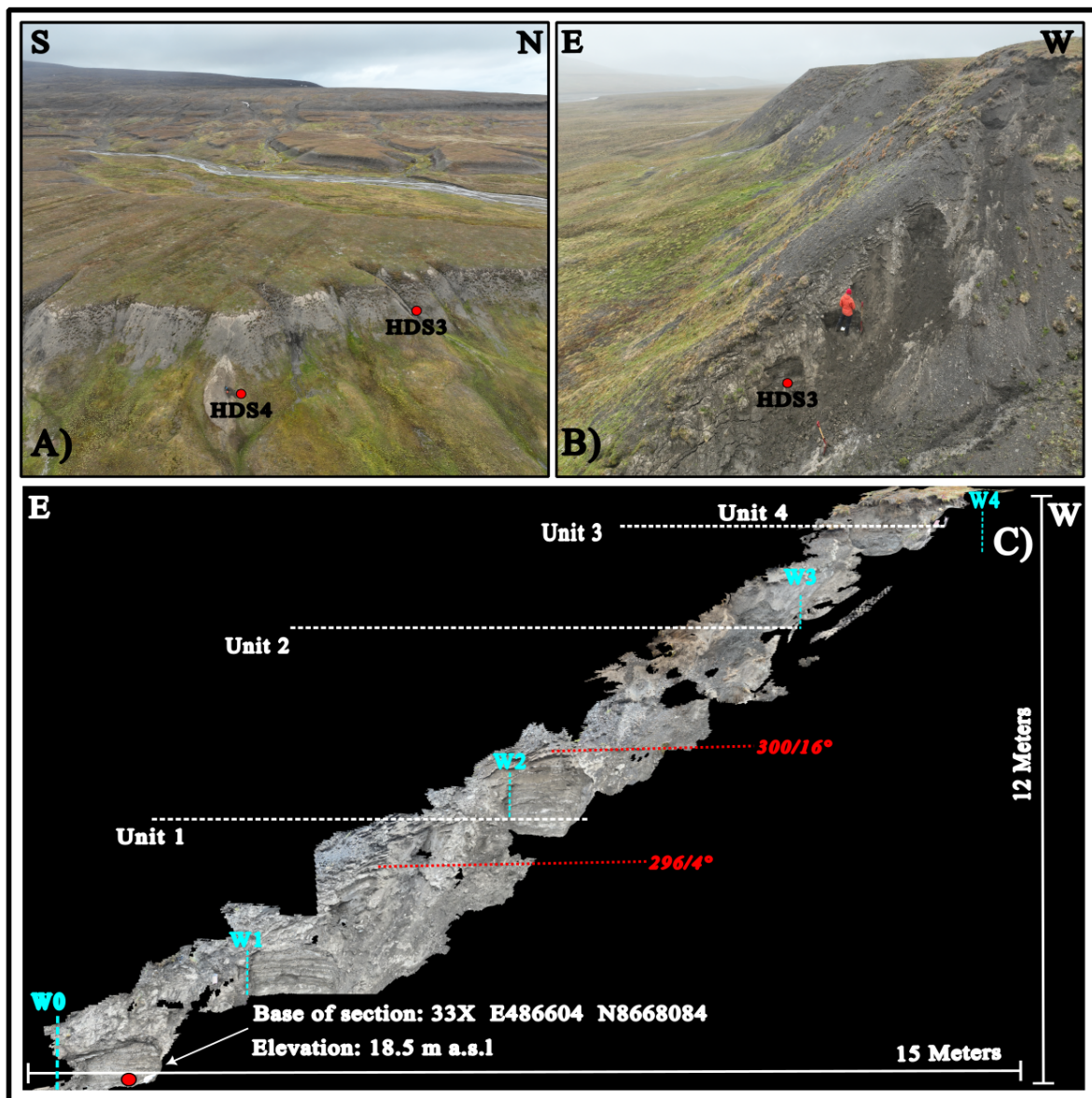


Figure 14: Overview information of Section 3 at Hollendardalen (HDS3). A and B indicate the position of the section on the western edge of the marine terrace at Hollendardalen. C shows a 3D model constructed in the field using the 3D Scanner mobile app. The model is annotated with the coordinates for the base of the section, the elevation in m a.s.l., the dimensions of the outcrop, strike, and dip of the bedding (red) and the position of the windows exposed in the section (blue).

Given the height of the section, and the short time available, the entire section was not cleaned and exposed. Instead, 5 ‘windows’ (W0, W1, W2, W3 and W4) measuring c. 1 m wide and c. 1-1.5 m high were exposed to give an insight into the internal structure of the section at key points (Figure 14, C). HDS3 has been divided into four stratigraphic units that are described and interpreted below in the stratigraphy section.

The smallest of the sections within Hollendardalen, HDS4 (Figure 15). It is positioned stratigraphically below HDS3 and c. 100 m up valley (Figure 14, A). The coordinates for the base of the section at HDS4 are 33X E486660 N8668013 and this position is elevated at 16.5 m a.s.l. The height of the section that was cleaned and investigated was c. 1.3 m (Figure 19). Given the small scale of the outcrop, a sedimentological log was not constructed, but the lithofacies identified are indicated in Table 6, and an annotated picture is included in the lithofacies association section below. The section is described to provide an understanding of the stratigraphically lowest sediment studied in Hollendardalen and further contextualise the depositional environment.

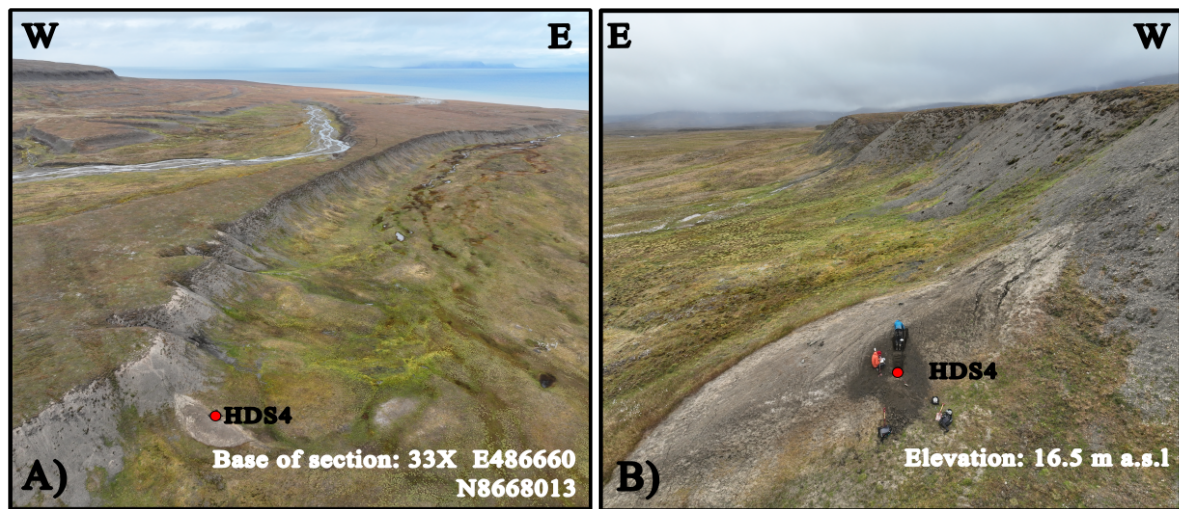


Figure 15: Overview information of Section 4 at Hollendardalen (HDS4). A indicates the coordinates for the base of the section (33X E486660 N8668013). B indicates the base of the section elevated at 16.5 m a.s.l.

## 4.2.2 Stratigraphy

This section presents the stratigraphy of Section 3 and 4 within Hollendardalen.

Sedimentological observations from are illustrated in the sedimentary log (Figures 16/17) alongside process interpretations and the lithofacies associations into interpreted sub-environments.

### 4.2.2.1 Sedimentary log

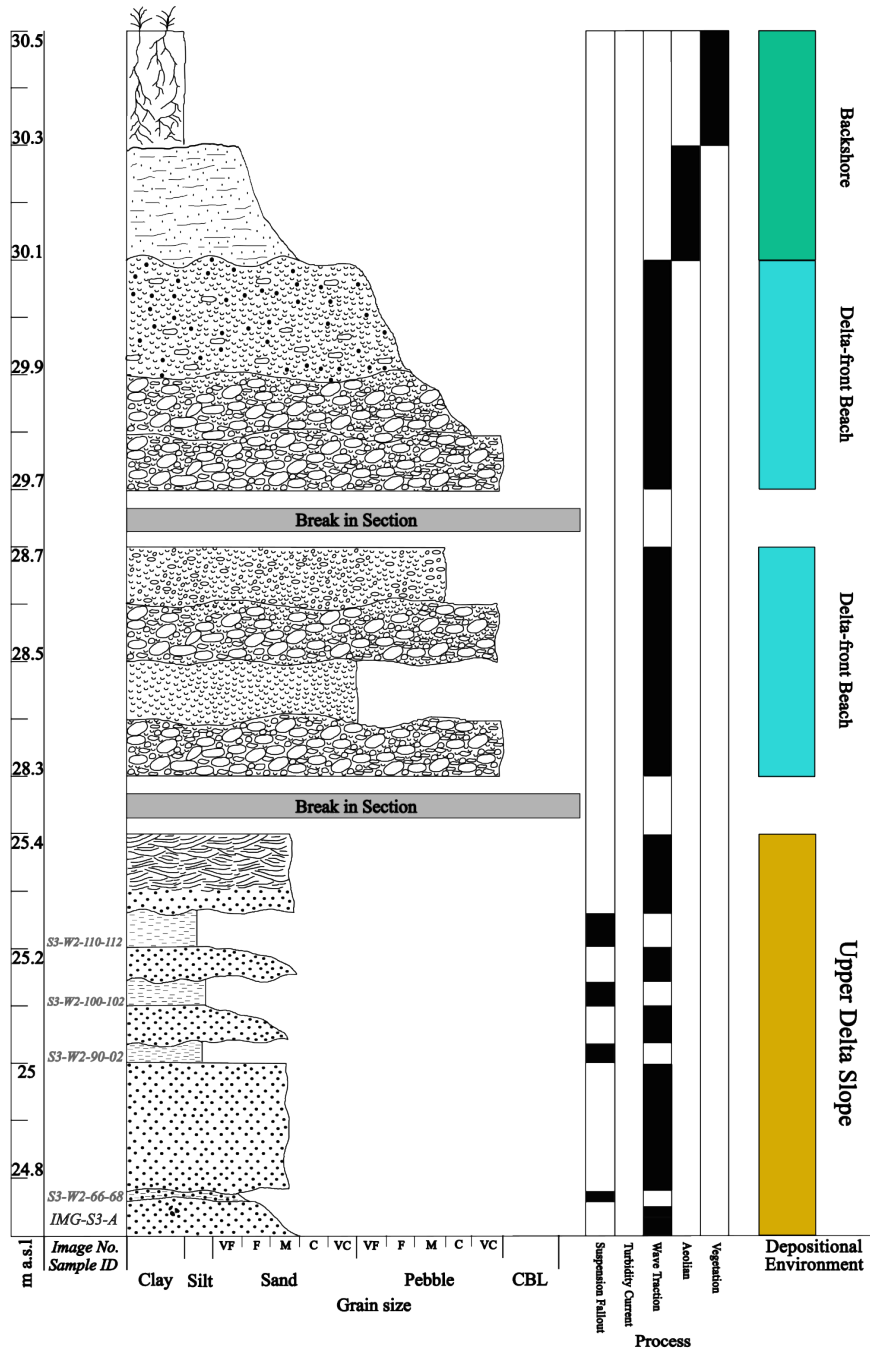


Figure 16: Sedimentary log (1/2) of Section 3 at Hollendardalen (HDS3).

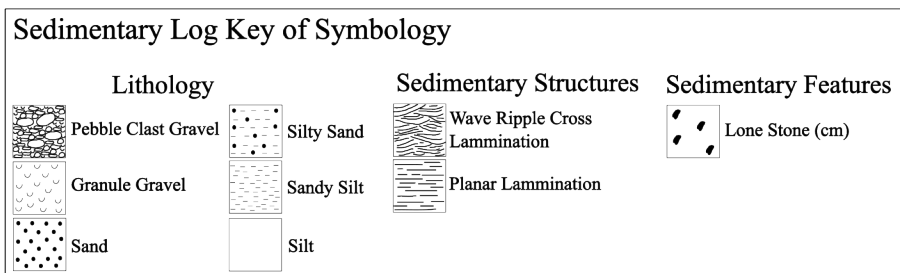
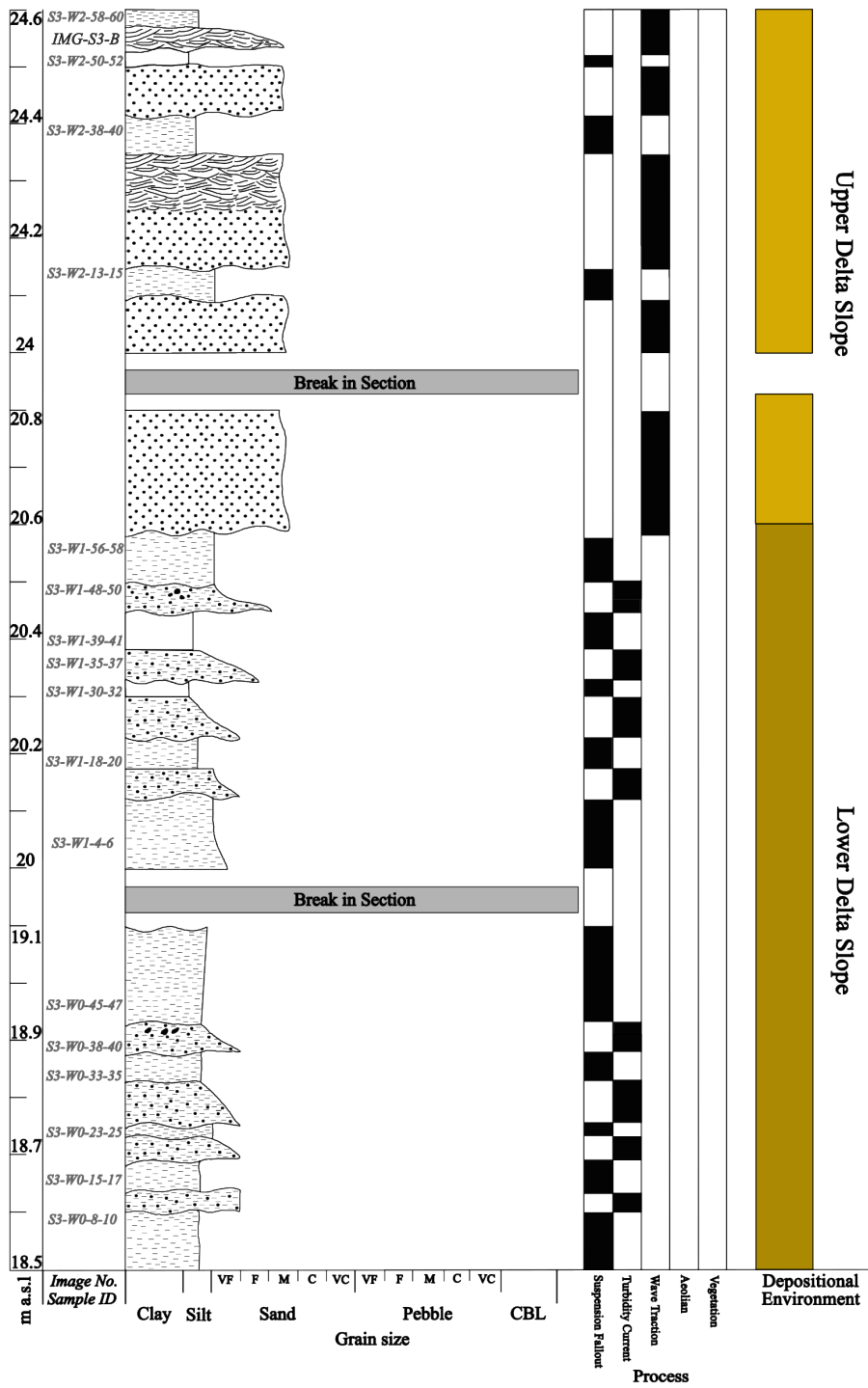


Figure 17: Sedimentary log (2/2) and key of symbology for Section 3 at Hollendardalen (HDS3).



#### 4.2.2.2 Lithofacies description

A comprehensive description of the 13 lithofacies identified within HDS3 and HDS4 is provided below in Table 6. The lithofacies are grouped into five sub-environments and interpreted with respects to their depositional process.

Table 6: Lithofacies descriptions of five sub-environments within Hollendardalen (HDS3 and HDS4).

Lithofacies description	Height up section	Textural, clast and statistical description	Bed and contact geometry	Structures/ mollusc content	Process interpretation	Environment interpretation
Laminated fine to very coarse silt	HDS4: 17-17.8	<ul style="list-style-type: none"> <li>- Mean grain size: 8-9 <math>\mu\text{m}</math> (medium silt)</li> <li>- Geometric (<math>\mu\text{m}</math>) value of sorting (<math>\sigma</math>): 4.7 to 5.4</li> <li>- Verbal classification: very poorly sorted</li> <li>- Skewness: symmetrical or fine skewed</li> <li>- Textural classification: silt</li> </ul>	<ul style="list-style-type: none"> <li>- Bed thickness: 10-30 cm</li> <li>- Contacts: sharp and regular</li> </ul>	- Laminated	Marine suspension fallout	Prodelta
Massive very fine sandy, fine to very coarse silt	HDS4: 16.8-17.6	<ul style="list-style-type: none"> <li>- Mean grain size: 11-13 <math>\mu\text{m}</math> (medium silt)</li> <li>- Geometric (<math>\mu\text{m}</math>) value of sorting (<math>\sigma</math>): 4.7 to 5.4</li> <li>- Verbal classification: very poorly sorted</li> <li>- Skewness: symmetrical, very fine and fine skewed</li> <li>- Textural classification: sandy silt</li> </ul>	<ul style="list-style-type: none"> <li>- Bed thickness: 2-10 cm</li> <li>- Contacts: sharp and regular</li> </ul>	- Massive	Turbidity current	
Massive fine sandy, fine silt	HDS4: 16.6	<ul style="list-style-type: none"> <li>- Mean grain size: 10.5 <math>\mu\text{m}</math> (medium silt)</li> <li>- Geometric (<math>\mu\text{m}</math>) value of sorting (<math>\sigma</math>): 6.7</li> <li>- Verbal classification: very poorly sorted</li> <li>- Skewness: coarse skewed</li> <li>- Textural classification: sandy silt</li> </ul>	<ul style="list-style-type: none"> <li>- Bed thickness: 2 cm</li> <li>- Contacts: sharp and irregular</li> </ul>	- Massive	Turbidity current	

Finning upwards silty, fine to very fine sand	HDS3: 18.6-20.5	<ul style="list-style-type: none"> <li>- Moderately to poorly sorted</li> <li>- Sand grains are well-rounded and spherical</li> <li>- Outsized, sub rounded, clasts (cm scale), observed in W0-40 cm and W1-50 cm</li> </ul>	<ul style="list-style-type: none"> <li>- Bed thickness: 3-10 cm</li> <li>- Contacts: sharp and irregular</li> </ul>	<ul style="list-style-type: none"> <li>- Normal grading</li> <li>- Outsized clasts</li> </ul>	Turbidity current	Lower-delta slope	
Laminated, very fine sandy, fine to very coarse silt	HDS3: 18.5-25.3	<ul style="list-style-type: none"> <li>- Mean grain size: 8.8 <math>\mu\text{m}</math> (medium silt) - 20.3 <math>\mu\text{m}</math> (coarse silt)</li> <li>- Geometric (<math>\mu\text{m}</math>) value of sorting (<math>\sigma</math>): 4.7 to 7.7</li> <li>- Verbal classification: very poorly sorted</li> <li>- Skewness: symmetrical and fine skewed</li> <li>- Textural classification: sandy silt</li> </ul>	<ul style="list-style-type: none"> <li>- Bed thickness: 2-15 cm</li> <li>- Contacts: sharp and irregular</li> </ul>	<ul style="list-style-type: none"> <li>- Lamination supported by the fissile texture</li> </ul>	Marine suspension fallout	Lower and upper-delta slope	Lower and upper-delta slope
Laminated fine to medium silts	HDS3: 20.3-25.5	<ul style="list-style-type: none"> <li>- Mean grain size: 7.9 – 9.8 <math>\mu\text{m}</math> (medium silt)</li> <li>- Geometric (<math>\mu\text{m}</math>) value of sorting (<math>\sigma</math>): 4.6 to 4.8</li> <li>- Verbal classification: very poorly sorted</li> <li>- Skewness: symmetrical and fine skewed</li> <li>- Textural classification: silt</li> </ul>	<ul style="list-style-type: none"> <li>- Bed thickness: 3-7 cm</li> <li>- Contacts: sharp and regular</li> </ul>	<ul style="list-style-type: none"> <li>- Lamination supported by the fissile texture</li> </ul>	Marine suspension fallout		
Massive and/or fining upwards and fine to medium sand	HDS3: 20.6-25.3	<ul style="list-style-type: none"> <li>- Beds are poorly to moderately sorted</li> <li>- Sand grains are rounded to well-rounded</li> <li>- Coarse grains/granule gravels are sub angular to rounded</li> <li>- Outsized, sand/siltstone lone stones. Lone stones and clasts are sub-angular to sub-rounded (cm scale)</li> </ul>	<ul style="list-style-type: none"> <li>- Bed thickness: 5-20 cm</li> <li>- Contacts: lower contact is sharp and irregular. Upper contact is sharp and planar or gradational</li> </ul>	<ul style="list-style-type: none"> <li>- Normal grading</li> <li>- Massive deposits, appear structureless</li> </ul>	Wave traction	Upper-delta slope	
Medium sand with wave ripple cross lamination	HDS3: 24.25-25.4	<ul style="list-style-type: none"> <li>- Beds are moderately to well-sorted</li> <li>- Sand grains are rounded to well rounded</li> <li>- Sand grains are spherical in shape</li> </ul>	<ul style="list-style-type: none"> <li>- Bed thickness: 5-10 cm</li> <li>- Contacts: sharp and irregular or gradational</li> </ul>	<ul style="list-style-type: none"> <li>- Wave ripple cross lamination</li> </ul>	Wave traction		

Massive clast supported coarse pebble gravel	HDS3: 28.3-29.9	<ul style="list-style-type: none"> <li>- Poorly to moderately sorted beds</li> <li>- Majority clast supported, outsized coarse pebble</li> <li>- Pore space filled with granule gravel matrix</li> <li>- Clasts are rounded to well-rounded/rounded</li> </ul>	<ul style="list-style-type: none"> <li>- Bed thickness: 10 cm</li> <li>- Contacts: sharp and irregular</li> </ul>	<ul style="list-style-type: none"> <li>- Mostly massive but one exception at 29.8-29.9 m a.s.l. which is normally graded</li> </ul>	Wave traction	Delta-front beach
Massive very fine to medium granule gravel	HDS3: 28.4-28.7	<ul style="list-style-type: none"> <li>- Moderately to well-sorted beds</li> <li>- Sub-angular to sub-rounded gravel grains. Generally horizontally aligned disc, blade, and oval shape</li> <li>- Occasional rounded disc shaped clasts (20-30 mm in length)</li> </ul>	<ul style="list-style-type: none"> <li>- Bed thickness: 10 cm</li> <li>- Contacts: sharp and irregular</li> </ul>	<ul style="list-style-type: none"> <li>- Massive</li> </ul>	Wave traction	
Fining upwards granule gravel to very coarse sand with outsized clasts	HDS3: 29.9-30.1	<ul style="list-style-type: none"> <li>- Poorly to moderately sorted beds</li> <li>- Sub-rounded to rounded gravels: discoidal, blade and oval shape</li> <li>- Outsized, disc and rod-shaped clasts that are rounded and generally horizontally aligned</li> </ul>	<ul style="list-style-type: none"> <li>- Bed thickness: 20 cm</li> <li>- Contacts: sharp and irregular</li> </ul>	<ul style="list-style-type: none"> <li>- Normal grading</li> </ul>	Wave traction	
Fining upwards and planar laminated sand	HDS3: 30.1-30.3	<ul style="list-style-type: none"> <li>- Moderately to well-sorted beds</li> <li>- Sub-rounded sand grains that are spherical in shape</li> </ul>	<ul style="list-style-type: none"> <li>- Bed thickness: 20 cm</li> <li>- Contacts: sharp and irregular</li> </ul>	<ul style="list-style-type: none"> <li>- Normal grading</li> <li>- Weak planar lamination</li> </ul>	Aeolian	Backshore
Vegetated sand/silt with rootlets	HDS3: 30.3-30.5	<ul style="list-style-type: none"> <li>- Moderately to well-sorted beds</li> <li>- Well-rounded to sub-rounded grains</li> </ul>	<ul style="list-style-type: none"> <li>- Bed thickness: 20 cm</li> <li>- Contacts: sharp and irregular or gradational</li> </ul>	<ul style="list-style-type: none"> <li>- Rootlets</li> </ul>	<ul style="list-style-type: none"> <li>Aeolian</li> <li>Vegetation</li> </ul>	

### 4.2.2.3 Lithofacies association

#### 4.2.2.3.1 Prodelta lithofacies (HDS4)

##### Description

Three lithofacies are associated with this depositional environment (Table 6). They include laminated fine to very coarse silt, massive, very fine sandy, fine to very coarse silt and fine sandy, fine silt. Texturally, the lithofacies are described as ‘silt’ and sandy silt’ on the textural triangle (Figure 18)

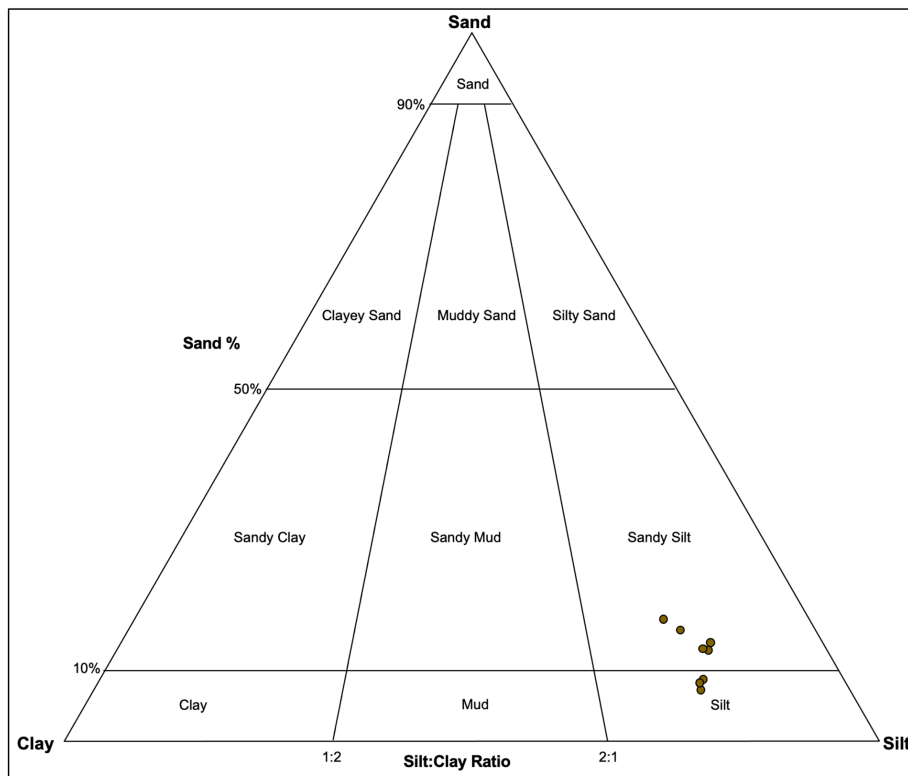


Figure 18: Grain size textural triangle for 8 sediment samples from the prodelta lithofacies at Hollendardalen Section 4 (HDS4) at Hollendardalen. Generated with GRADISTAT v8 (Blott, 2010).

The three lithofacies are interbedded, with the fine to very coarse silts present in 10-30 cm bed thicknesses, in comparison to the 2-10 cm thickness of the sandy silts (Figure 19). Bed contacts between the lithofacies are sharp and regular. The strike of the beds is parallel to the present shoreline orientated at 300° and the dip is either zero or <5°. Associated with the lithofacies of the prodelta environment, is a high salt content within the sediment. This is indicated in Figure 20 where a thin veneer of reprecipitated salt covers the outcrop.

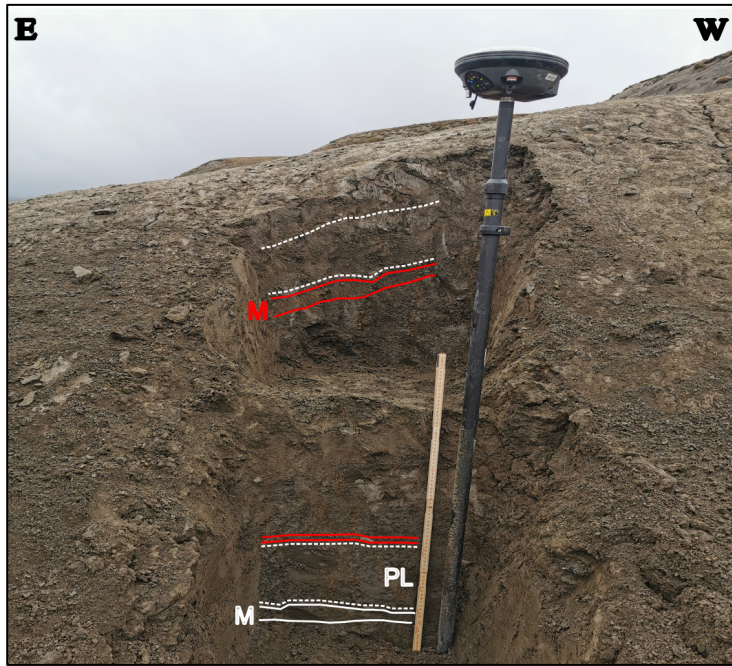


Figure 19: Annotated picture of the three lithofacies associations of the pro-deltaic sub-environment (HDS4). The base of the unit is the massive fine sandy, fine silt highlighted with a solid white line. The planar laminated fine to very coarse silt is highlighted with a dashed white line and the massive very fine sandy, silt is highlighted with a red solid line. The ruler is extended to 80 cm.

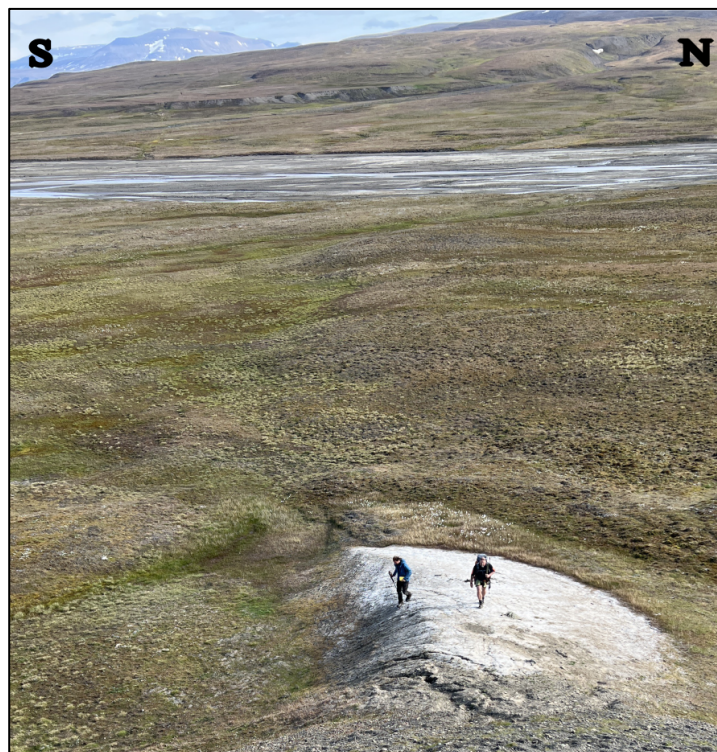


Figure 20: Picture of Section 4 at Hollendardalen (HDS4) highlighting the thin veneer of reprecipitated salt covering the outcrop. Photo: Mathilde Lyford-Jahnsen.

## Interpretation

The three lithofacies are attributed to two depositional processes: marine suspension fallout and turbidity currents.

The suspension fallout facies include the laminated fine to very coarse silts that make up most of the unit as they are 10-30 cm thick. The supply of these sediments to the prodelta likely results from the input of a buoyant, freshwater, and sediment-laden plume supplied by the fluvial feeder system. Hypopycnal flows are common in marine littoral deltas and form when the freshwater discharge and the sediment it is transporting in suspension, is less dense than the water in the basin (Bates, 1953). Generally, suspended sediment concentrations accompanying the fluvial inflow into present-day Arctic fjords are several orders of magnitude less than is needed to overcome the buoyant effect of saline water (Gilbert, 1983). As a result, the freshwater and suspended sediment (silt) are transported in a buoyant plume, than can extend for *c.* 7 km from the coastline (Figure 46) before subsequent collapse results in deposition from suspension of the fine grained material within the coastal environment (Zavala, 2020b).

The degree of mixing between the sediment-laden plume and the pycnocline is an important factor in controlling collapse of the plume from suspension, as salinity values of 3-4 ‰ are effective in promoting the flocculation of fine particles, which in turn controls the extent of sedimentation (Hoskin & Burrell, 1972; Kranck, 1973; Gilbert, 1983). Grain size analysis reveals a mean grain size of 8-13  $\mu\text{m}$  (medium silt) which holds significance as it provides an insight into the settling time of the particles. According to Stoke's Law a particle 14  $\mu\text{m}$  in diameter, will settle from a 100 m salt water column of water at 0 °C within 14 days, in comparison to a particle of 4  $\mu\text{m}$  that will take 146 days (Gilbert, 1983). The range of 8-13  $\mu\text{m}$  of the facies attributed to marine suspension fallout therefore indicates a relatively fast settling time that would be further enhanced by flocculation induced by mixing with saline water.

The sandy silt and silt lithofacies associated with the prodelta environment, generally contain a higher percentage of silt than the sandy silt and silt lithofacies associated with the lower delta slope (Figures 18 and 21). These findings are in accordance with the general assumption that deeper parts of fjord environments have the lowest energy which in turn favours the settling from suspension of finer grained particles (Syvitski & Farrow, 1989). Furthermore, a

longer transport distance from the coast and into the fjord would expectedly result in a higher percentage of the finer silts (Faust et al., 2017). Together these observations support these lithofacies being associated with a deeper and more distal environment, than those of the lower delta slope, hence their association with a prodelta environment.

The massive, sandy silt lithofacies are those interpreted to result from low density turbidity currents. The sharp contacts separating the suspension fallout and turbidity current facies support an abrupt transition in the transport mechanism energy and sediment supply. The shift in transport mechanism energy may be the result of a transition from a buoyant hypopycnal overflow to a more dense hyperpycnal underflow current where the river effluent is more dense than the water within the basin (Bates, 1953). The thin nature of the beds indicates that these events are short-lived and may simply relate to a period of higher fluvial discharge, capable of transporting coarser grains down the delta slope towards the prodelta environment. Alternatively, it may result from a minor shift in sediment supply from alternate delta distributaries (Kneller & Buckee, 2000).

The thin veneer of salt covering HDS4 and associated with the prodelta lithofacies indicates that deposition of these lithofacies is in strong association with a brackish marine environment.

#### 4.2.2.3.2 Lower delta slope facies (Unit 1: HDS3)

##### Description

Three lithofacies are associated with the lower delta slope (Table 6). They predominantly consist of laminated very fine sandy, fine to very coarse silts and laminated fine to medium silts. Textural classification of these sediments defines them as ‘sandy silt’ and ‘silt’ (Figure 21). Interbedded with these sandy silts and silts are fining upwards, silty fine to very fine sand lithofacies.

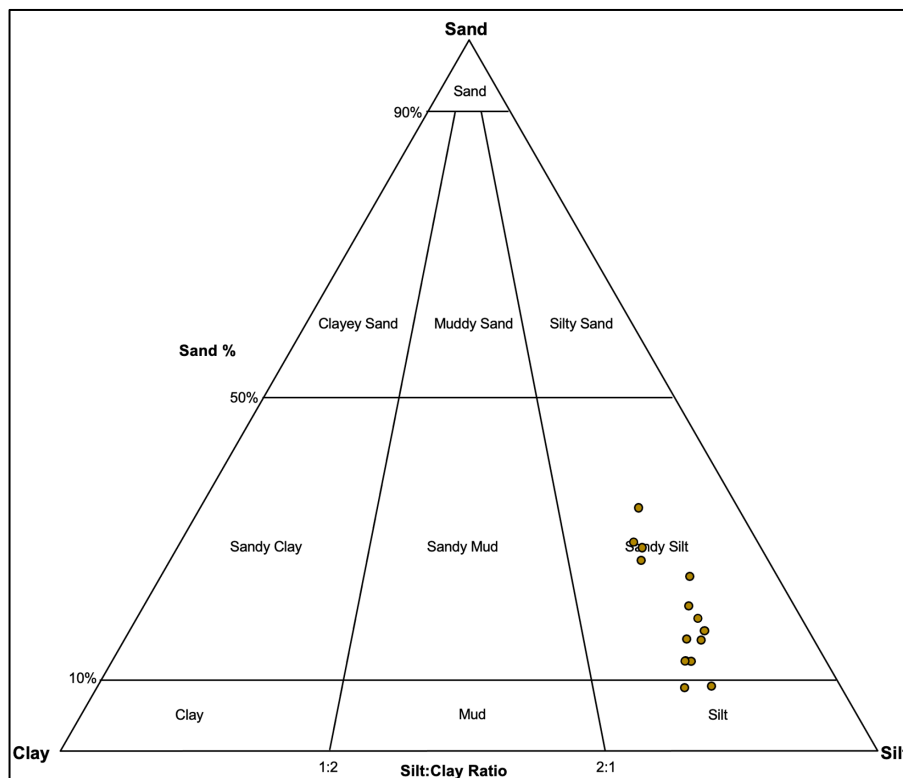
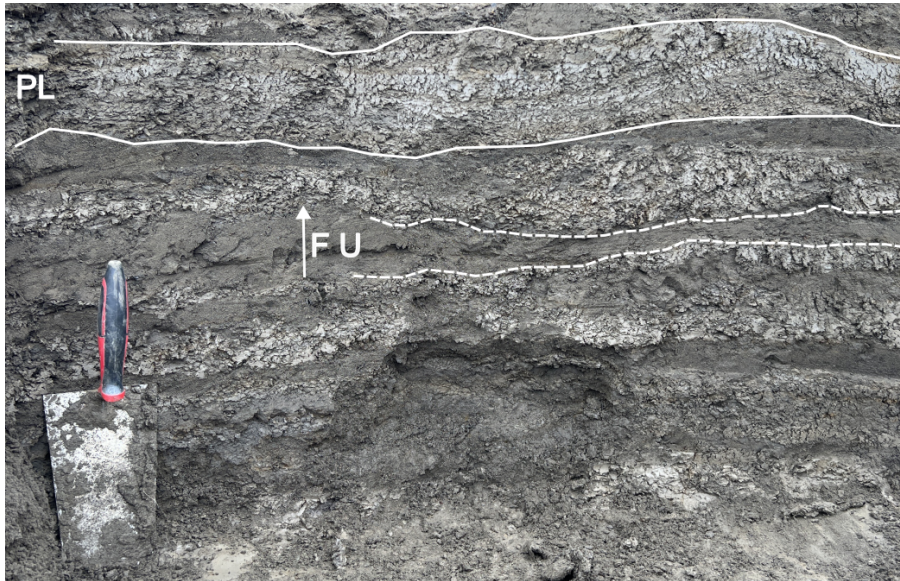


Figure 21: Grain size textural triangle for 14 sediment samples (HD-S3-W0-8-11 to HD-S3-W1-80) from the lower delta slope deposits in Section 3 at Hollendardalen. Generated with GRADISTAT v8 (Blott, 2010).

The sandy silts and silts are dominant, exhibiting bed thicknesses of 10-15 cm, in comparison to the coarser silty sand and sand beds <10 cm. Despite the disparity in thickness, the interbedded lithofacies show a rhythmic cyclicity in their occurrence. The alternating facies are separated by sharp, irregular, and planar contacts.





*Figure 22: Annotated picture of lower delta slope lithofacies. Planar laminated sandy silts and silts highlighted with white solid line. Fining upwards silty sand highlighted with white dashed line. Trowel handle is c. 15 cm.*

### **Interpretation**

The three lithofacies that are associated with the lower delta slope, are interpreted to result from suspension fallout and turbidity currents, similarly to the prodeltaic deposits.

The thicker beds of sandy silt and silt indicate dominance of a sustained and steady mechanism behind their deposition. The fine grain size and planar lamination inferred through the fissility of the beds (Figure 22), indicates these lithofacies are deposited as a result of suspension fallout (Mackiewicz et al., 1984). The fine to medium silts observed are interpreted to represent the ambient, low background energy of the depositional environment, where the finest grained particles can settle out from within the water column. As described above, the interconnectedness of these deposits with varying fluvial discharge may result in the variations in grain size that are observed.

Attributing the interbedded nature of the deposits to seasonal variability, can be explained as followed. The sandy silts and silts represent quiescent periods of deposition such as the autumn and winter when fluvial discharge is low and the river supplying the delta is frozen (Eilertsen et al., 2005). Similar fine grained lithofacies have been observed confining silty sand packages in the lower delta slope of the Målselv Valley in Northern Norway (Eilertsen et al., 2011). Deposition of genetically similar deposits from a similarly interpreted coarse grain deltaic environment within the Arctic makes this an equally viable depositional process relating to the formation of the sandy silt and silt beds observed within unit 1 in HDS3.

Furthermore, Hill et al. (2001) measured suspended sediment concentrations of 3-12 mg L<sup>-1</sup> across the delta slope of the fine grained high latitude Mackenzie Delta, Canada during the winter months. This was in addition to current speeds below the minimal critical velocity needed to transport fine sand grains (Kauppaymuthoo, 1997). Suspended sediment concentrations in Arctic nival and glacial melt water outflows are normally less than 2 g L<sup>-1</sup>, although values of 10-39 g L<sup>-1</sup> have been reported (Church & Gilbert, 1975), of course, with extremes related to high melt rates or annual extremes (Powell, 1981). The findings from Hill et al. (2001) of minimal sediment transport during the winter months, is in accordance with the sandy silt and silt lithofacies accumulating during the autumn and winter period, when a reduced supply of sediment would facilitate particles of this grain size settling from suspension and accumulating on the basin floor. This is strengthened by the explanation provided above in the prodelta interpretation regarding the settling time of particles from suspension within this grain size diameter range. A period of between 14-146 days (Gilbert, 1983) to settle from suspension under the outlined water column and depth properties would easily be accounted for in the long winter periods that are experienced in the High Arctic setting of the study area.

Conversely, the fining upward silty sands lithofacies that are interpreted to have been deposited by turbidity currents, would indeed be induced during the late spring and early summer season. During this period, enhanced fluvial discharge and sediment supply would result in instabilities along the upper delta slope, and potentially even a mouth bar collapse, which would provide the mechanism and source for a low-density turbidity current, depositing such lithofacies at the lower delta slope (Syvitski & Shaw, 1995). Similar, sharp based sand deposits interbedded within suspension fallout facies are described from a deltaic environment in Eastern Greenland by Hansen (2004) and attributed to surge type turbidity currents. In this case, the fining upward nature of the lithofacies may reflect waning of the current in response to variations in fluvial discharge (Kneller, 1995).

#### 4.2.2.3.3 Upper delta slope facies (Unit 2: HDS3)

##### Description

Four lithofacies are associated with the upper delta slope (Table 6). Similarly to the lower delta slope, the laminated very fine sandy, fine to very coarse silts and fine to medium silt are present. Their textural similarity is highlighted in their textural classification, where they are placed as sandy silts and silts (Figure 23). Despite their textural similarity, these lithofacies have *c.* 10-15 % less sand content when compared with the lower delta slope lithofacies (Figure 21).

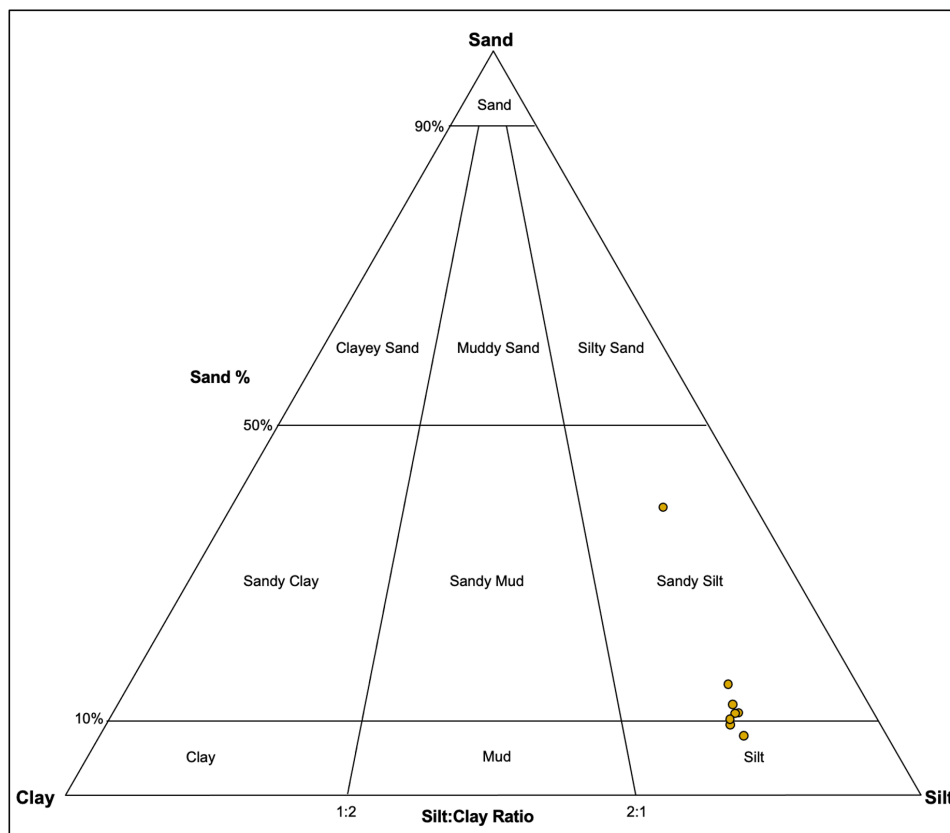


Figure 23: Grain size textural triangle for eight sediment samples from the upper delta slope deposits in Section 3 at Hollendardalen. Generated with GRADISTAT v8 (Blott, 2010).

Interbedded with the sandy silts and silts are massive or fining upwards fine to medium sands and the medium sands with wave ripple cross laminations (Figure 24, B). Occasional sub-rounded to sub-angular outsized clasts/lone stones are observed for example at 24.75 m a.s.l. (Figure 24, A).

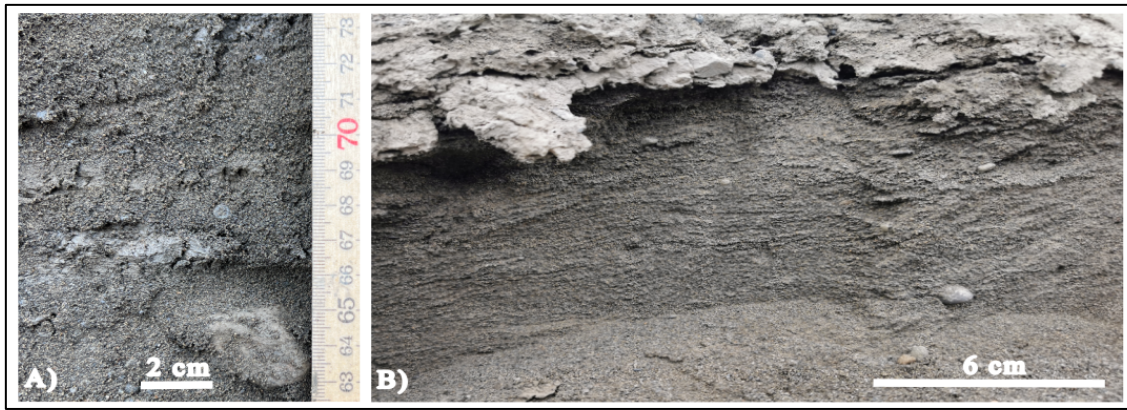


Figure 24: Picture of 2 cm, sub-rounded to sub-angular silt stone lone stone observed at 24.75 m a.s.l. (A). Wave ripple cross laminations observed within a fine sand bed of the upper delta slope (B).

In contrast to the lower delta slope, the upper delta slope is marked by a dominance of the coarser grained beds, that are *c.* 20 cm bed thick, whereas the finer grained sandy silts and silts beds are <10 cm thick. Accompanying the increased grain size up sequence, and transition to a dominance of coarser sands over fine sandy silts and silts, is the occurrence of wave ripple cross lamination (Figure 25).

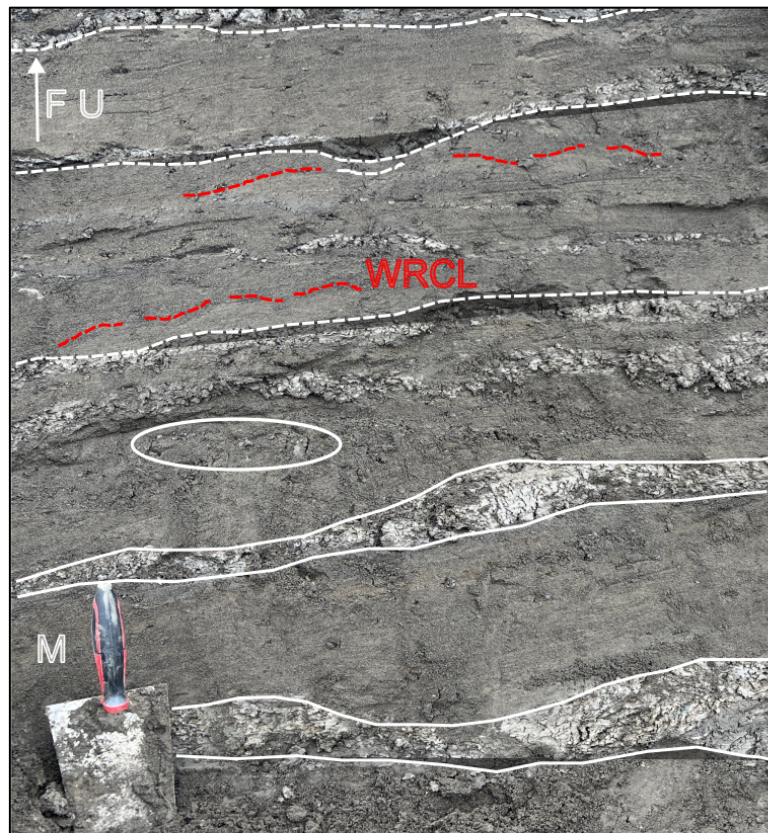


Figure 25: Annotated picture of the upper delta slope lithofacies. Sandy silt and silts are highlighted with a white solid line. Massive and fining upwards fine to medium sands are highlighted in a white dashed line. The upper bounding surface of Wave ripple cross lamination (WRCL) is highlighted with a red dashed line. Lone stones and gravel grains are circled in white. Trowel handle is *c.* 15 cm.

## **Interpretation**

The upper delta slope is characterised by suspension fallout and wave traction facies, similarly to the lower delta slope deposits. However, the transition to a dominance of wave traction facies over suspension fallout facies as well as a coarsening upwards sequence is indicative of a shallowing water depth. Hence, the deduction of a transition from the lower to upper delta slope is made.

Textural similarity in both the field and laboratory analysis of the sandy silt and silts leads to the interpretation that these lithofacies were similarly deposited by suspension fallout. Interestingly, there is *c.* 10-20 % less sand observed within the sandy silts in comparison to the lower delta slope deposits. This finding is in disagreement with the typical sediment distribution pattern within fjord environments, where coarser and heavier sediment components are usually deposited in a proximal position to the shore and river estuary, and grain size decreases with depth (Holtedahl, 1975; Skei, 1983; Faust et al., 2017). In this case, the sandy silt and silt lithofacies exhibit a finer grained signature, up-sequence within a shallowing environment, where distance to the shore and river inflow would be more proximal. A possible explanation for this could relate to reduced fluvial discharge, in response to changes in precipitation and meltwater runoff. To some extent, this finding is in accordance with a decreasing fluvial influence on sedimentation corresponding with an increased influence of basin processes such as wave action modulating sedimentation on the upper delta slope.

The transition to an increased thickness of coarser grained sands over the sandy silt and silts indicates that there is a shallowing of water depth within the depositional environment. The massive and fining upwards sands with and without wave ripple cross lamination further support this shallowing of the depositional environment. The presence of wave ripple cross lamination indicates that these beds were deposited in an environment that is above the wave base, where the oscillatory motion of waves results in the migration of sand grains producing cross laminations (De Raaf et al., 1977). Whilst the occurrence of ripples within the sand deposits may be argued as reflecting the Bouma Sequence stage 'C', this is dismissed as the ripples here are identified as symmetrical, indicating an oscillatory wave motion as opposed to asymmetrical ripples formed by a unidirectional current flow (Bouma, 1964).

The sub-rounded to sub-angular 2 cm lone stone is interesting as its angularity and shape suggest prior transport before deposition which may have resulted within the fluvial or littoral

zone. It is well understood that sea ice is an active depositional agent in the sedimentology of Arctic coastal environments (Barnes et al., 1982). One mechanism to supply gravels from the littoral zone is that gravel may freeze to the base of sea ice and upon break-up of the ice be transported into deeper marine environments (Rosen, 1979). Alternatively, sand and gravels may be washed onto ice by waves, freeze in place and as the sediment accumulates, it promotes sinking, where then the sediment laden ice is transported again into deeper marine environments (Gilbert, 1983). The occurrence of the lone stone, accompanied by a lens of gravel grains (Figure 24, A) favours this mechanism of transport and sedimentation. It is also reported by Hill et al. (2001), that freezing of the fluvial system in Arctic deltas can result in 'ice-jamming', where breakup of the ice during the spring thaw can entrain fluvial sediment and transport it out onto the delta slope. Despite these proposed mechanisms, iceberg rafting depositing coarse-grained material within the shallow marine is a completely viable mechanism as will later be discussed.

The above processes provide mechanisms to support the presence of littoral and fluvially derived lone stones in the shallow marine environment due to sedimentation related to ice transport within the upper delta slope. They further highlight the significance of seasonality at the time of deposition and lead to the environmental interpretation that sea ice was seasonally present within the fjord side environment.

#### 4.2.2.3.4 Delta-front beach facies (Unit 3: HDS3)

##### Description

Three lithofacies are associated with the delta-front beach (Table 6): a massive clast supported coarse pebble gravel; massive, fine to medium granule gravel; and fining upward granule gravel to coarse sand with outsized clasts. These lithofacies represent a major jump in grain size from the underlying silt, sandy silts and sands that comprise the delta slope facies. The lithofacies exposed within W3 and W4 of the section are separated from the upper delta slope facies by a sharp and erosive boundary and overlie the delta slope facies in a sub-horizontal manner.



*Figure 26: Annotated picture of two lithofacies present within the delta front beach. The basal coarse pebble gravel is highlighted with a dashed white line and is overlain by the massive granule gravel. Clast alignment within the granule gravel is highlighted with a red dashed line. Trowel handle is ~15 cm.*

At the base of W3, massive and the coarse pebble gravel is interbedded with the granule gravels on a decimetre scale (Figure 26). The pebble gravel is moderately sorted whereas the granule gravel is poorly sorted and the two lithofacies are separated by a sharp and regular boundary. The pebble clasts in the pebble gravel contain several rod and disc shaped clasts that are horizontally aligned and supported in a granule gravel matrix (Figure 26). In the massive beds in the lower section of the facies, granule gravels dominate with a distinct lack of sandy matrix.

Up sequence a transition to fining upward beds occurs and the granule gravel matrix begins to include coarse sand that is not evident in the lowermost lithofacies. The outsized clasts in the upper most granule gravel and coarse sand transition from spherical and rod shape to oval disc and blade shape.

### **Interpretation**

These deposits are interpreted to construct a sequence of gravel beach, that is prograding at the front of the deltaic system. The observations collated to deduce this interpretation are elaborated on below.

Firstly, the top of HDS3, similarly to the rest of the raised marine terraces is capped with low amplitude, undulating and shoreline parallel morphological features that are classified as beach ridges. This implies that underlying stratigraphy is related to this morphological feature. The increase in grain size of this facies association and sharp boundary separating it from the underlying delta slope facies indicates that it was erosionally emplaced. Under a falling relative sea level, the progradation of the shoreline is expected and during this process erosion of underlying strata would occur. Finally, the pebbles and gravels lithofacies bear some resemblance with those observed within similar, coarse-grained shorelines and therefore provide an insight into periods of beachface construction and destruction relating to the depositional energy of the system.

The clast supported pebble gravel at the base of W3, show a degree of horizontal layering alongside well-rounded rod and spherical shaped clasts, which is indicative of size and shape sorting that is associated with beach deposits during constructive and destructive phase (Bluck, 1998). The visual assessment in the field of their roundness and the shape of the clasts suggests that they have been subject to substantial erosion, which may be the result of swash and backwash processes along the beachface. The absence of a sandy matrix within the pebble gravel may result from destruction of the beachface through sustained and longer lasting backwash processes, where the porous clasts act as a sieve for the finer particles to be combed through (Postma & Nemeč, 1990). Alternatively, during a sustained period of moderate energy, rod and spherical shaped clasts within gravel beaches have the tendency to roll and avalanche down the beachface, accumulating at the toe of the slope as the undertow decelerates (De Giorgio et al., 2023). Given this lithofacies stratigraphic position below the granule gravels above, this mode of transport and deposition seems probable and can be linked with a period of beachface destruction.



On the contrary, the granule gravels containing some horizontally aligned discoidal and blade shaped clasts that are present up-sequence are interpreted to indicate a period of beach front construction. The disc shape clasts have likely been entrained within breaking waves during storm events and transported higher up the beachface in comparison to their spherical counterparts (Bluck, 1967). Their alignment along a strike parallel with the shoreline further supports this. During this period of construction of the delta beach front, the transportation of material up the beachface may have resulted in berms and ridge like structures. These would in turn contribute towards the beach ridge morphology that is prominent along the top of terrace at HDS3.

#### 4.2.2.3.5 Backshore facies (Unit 4: HDS3)

##### Description

Two lithofacies are associated with the backshore environment (Table 6). They include moderately to well sorted fining upward sands and vegetated sands with rootlets. The grains are sub-well rounded, and their shape is mainly spherical. The two lithofacies are separated by a sharp and irregular contact. These lithofacies represent a final fining upwards of the sedimentary succession recorded within HDS3.

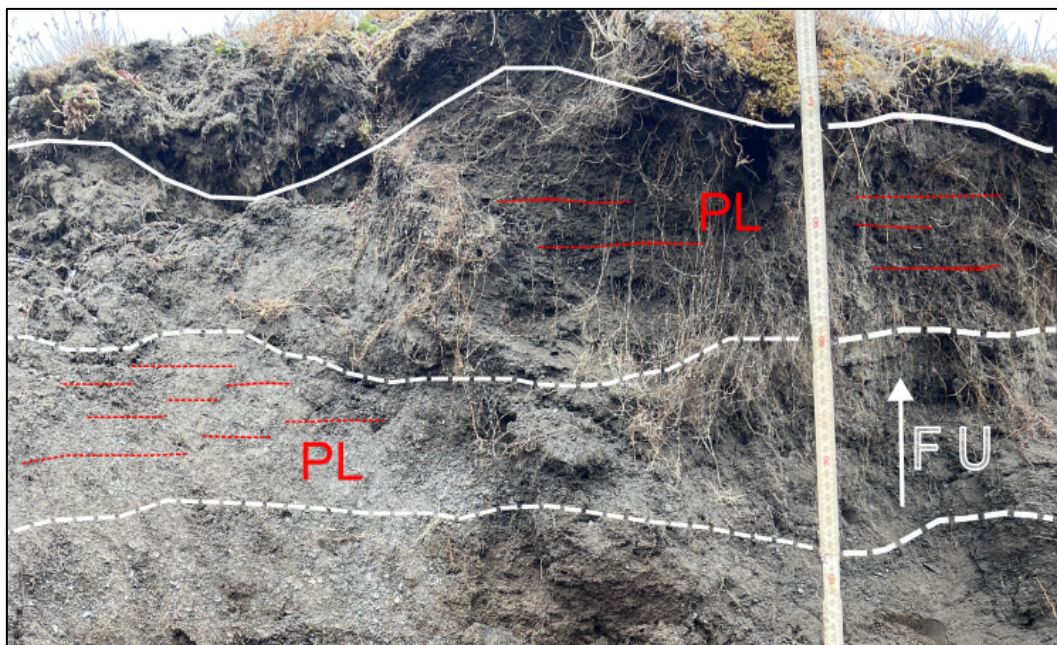


Figure 27: Annotated picture of the two backshore lithofacies within HDS3. The fining upward and weakly planar laminated sands highlighted with a white dashed line and the overlying planar laminated sands with rootlets highlighted with a white solid line.

## **Interpretation**

The fining upward and planar laminated coarse to fine sand lithofacies are interpreted to result from the transportation of grains through saltation by aeolian processes. The grain shape and degree of rounding support this mechanism of transport. In line with relative sea level fall, delta beachfront facies will be progressively becoming exposed and sub-aerial, subjecting them to land-based processes.

The morphology of the valley provides the potential for local katabatic winds to be funnelled along its transect seaward, providing the mechanism for transporting the finer grained material. Indeed, Maxwell (1980) recorded wind velocities in excess of  $150 \text{ km h}^{-1}$  being funnelled between the long and narrow fjord valley sides within the Canadian Arctic during the winter. Assuming wind velocities of even a fraction of this, which could be expected given Svalbard's frequently windy climate, the critical velocity for the transportation of the grains observed within the lithofacies would be likely. Further attributing the transport and deposition of the lithofacies to katabatic winds, would infer that the provenance of the sediment was up valley from within the frozen surface of a braided delta plain. In which case, transport through this mechanism would be more likely during the late autumn to early winter as opposed to the summer when the braid plain surface likely be wetted due to higher fluvial discharges (Gilbert, 1983). Recent studies have identified the continued development of loess deposits within Adventdalen, Isfjorden, throughout the Late Holocene, with a short period of reworking or non-deposition during the Little Ice Age (Rasmussen et al., 2023). Together these findings strengthen the interpretation of the depositional mechanism through correlation with similarly formed deposits in regionally similar environments.

The rootlets are linked with present day vegetation as they could be traced upwards to the surface and were connected to vegetation on the terrace surface (Figure 27).

### 4.2.3 Environmental synthesis

Hollendaralen sections record a coarsening upwards sequence that includes five sub-environments: a prodelta, lower-delta slope, upper-delta slope, delta front beach and backshore. This type of sequence indicates a shallowing of water depth that records the systems response to changing regime controls of relative sea-level fall and reduced accommodation space as the shallow marine is supplied with fine grained material.

The prodelta and lower-delta slope sediments are deposited in a shoreline distal setting, inferred through the high salt content of the sediment that indicates deposition under marine/brackish water conditions, as well as the finest grain lithofacies. This aligns with the typical sediment distribution pattern in modern fjord environments where the finest grains are transported further from the source at the head of the fjord (Holtedahl, 1975; Skei, 1983; Faust et al., 2017). Sediments character suggests deposition by suspension fallout from buoyant hypopycnal sediment plumes and surge-type turbidity currents (Bates, 1953; Gilbert, 1983; Mackiewicz et al., 1984; Kneller, 1995; Zavala, 2020b). The interbedded sediments and associated depositional mechanisms reflect a seasonal sediment influx, largely modulated by a highly seasonal fluvial regime. The upper-delta slope deposits were deposited by suspension fallout and wave traction which is consistent with a shallowing environment (De Raaf et al., 1977; Mackiewicz et al., 1984). A coarsening of grains and occurrence of wave ripple cross lamination indicates deposition above the wave base (De Raaf et al., 1977). As a result, record deposition in a proximal position to the shoreline. Outsized lone stones indicate that sea ice acts to some extent as a transport mechanism of coarse grains to the shallow marine at the time of deposition (Barnes et al., 1982; Gilbert, 1983; Hill et al., 2001). Seasonality continues to be exhibited in the sediments up sequence although the shallowing of the environment results in a transition of modulating regime influences from fluvially dominated to wave dominated. Delta front beach sediments capped with backshore deposits represent the final stage of shallowing and transition from sub-littoral deposition where wave traction dominates (Bluck, 1967; Postma & Nemec, 1990; De Giorgio et al., 2023) to sub-aerial deposition controlled by aeolian processes (Maxwell, 1980; Gilbert, 1983; Rasmussen et al., 2023). These sedimentological interpretations correlated with the geomorphic data in Figure 13, that identifies higher elevation beach ridges orientated perpendicular to the present-day shoreline. Together the data indicates that the early stage of coastal evolution of Hollendarbukta occurred through the progradation of an embayed deltaic system.

### 4.3 Bogebekken: *Mya truncata* Section

#### 4.3.1 Overview

Section 2 at Bogebekken (BKS2) is located on the western side of Bogebekken, *c.* 350 m south of the present shoreline (Figure 9). The outcrop is within a 3.7 m high fluviially incised terrace that is *c.* 20 m south of the E-W trending Russian telegraph pole line. The coordinates for the base of the section are 33X E486125 N8669237 and is elevated at 3.5 m a.s.l.

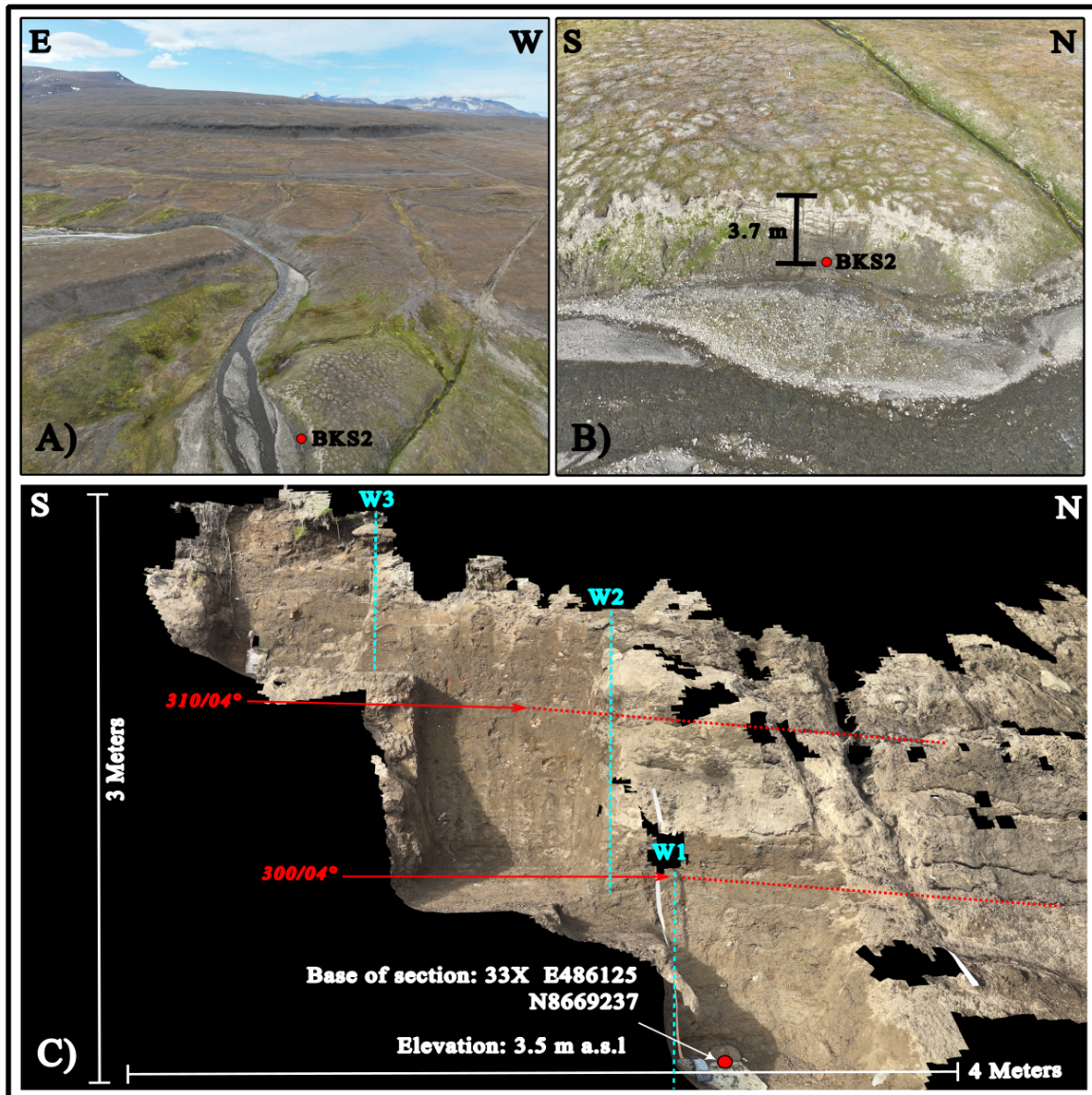


Figure 28: Overview information of the *Mya truncata* Section at Bogebekken (BKS2). A and B indicate the position of the outcrop on the western edge of the terrace at Bogebekken. C is a 3D model constructed in the field using the 3D Scanner mobile app. The 3D model is annotated to indicate the coordinates at the base of the section, the elevation in m a.s.l., the dimensions of the outcrop, strike, and dip of bedding and the position of the exposed windows.

### 4.3.2 Stratigraphy

#### 4.3.2.1 Sedimentary log

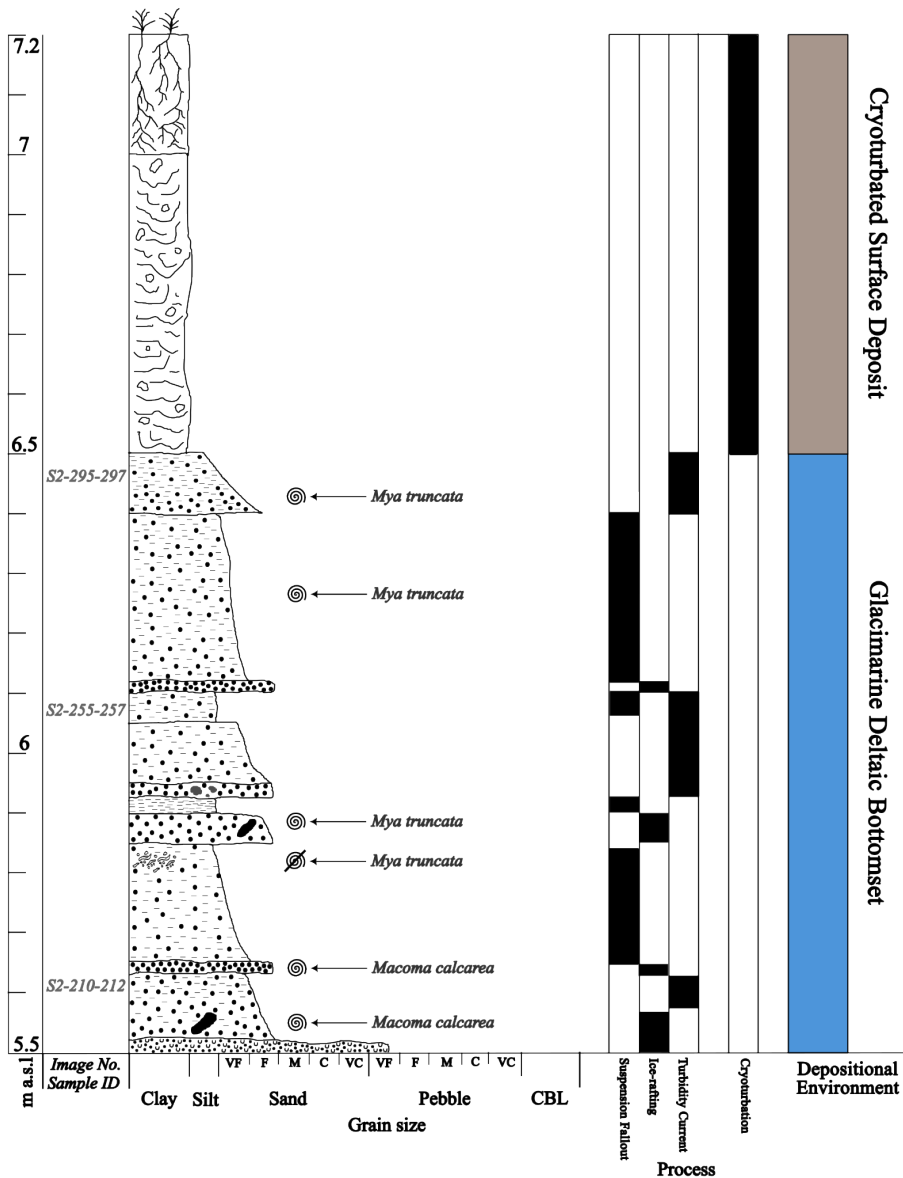
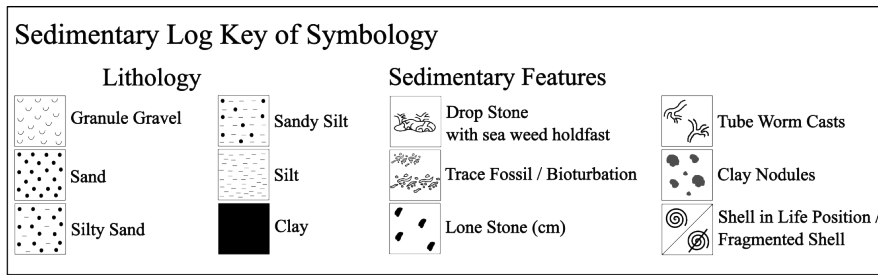


Figure 29: Sedimentary log (1/2) and key of symbology of the *Mya truncata* Section at Bogebecken.

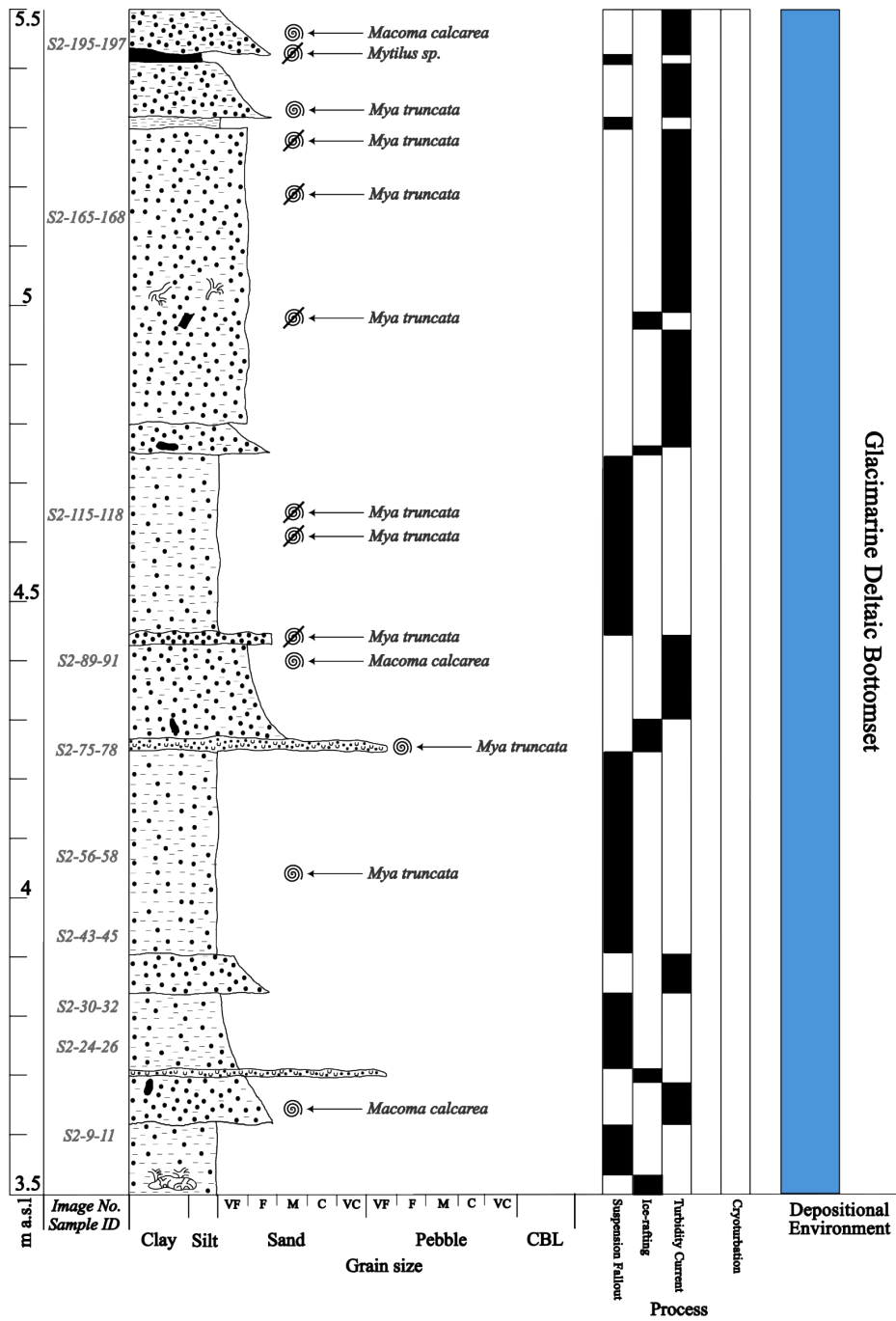


Figure 30: Sedimentary log (2/2) of the *Mya truncata* Section at Bogebekken.

### 4.3.2.2 Lithofacies description

A total of 7 lithofacies are described and the interpreted depositional processes that led to their formation are presented in Table 7. This is alongside their facies association within their sub-environment.

Table 7: Lithofacies description of the sediments composing the glaciomarine deltaic bottom set facies association within the *Mya truncata* Section in Bogebecken.

Lithofacies description	m a.s.l.	Textural, clast and statistical description	Bed and contact geometry	Structures/ mollusc content	Process interpretation	Environment interpretation
Massive very fine sandy, medium to very coarse silt	3.5-6.1	<ul style="list-style-type: none"> <li>- Mean grain size: 11-23 <math>\mu\text{m}</math> (medium to coarse silt)</li> <li>- Geometric (<math>\mu\text{m}</math>) value of sorting (<math>\sigma</math>): 4-5</li> <li>- Verbal classification: very poorly sorted</li> <li>- Skewness: very fine to fine skewed</li> <li>- Textural classification: sandy silt</li> <li>- Lone stone (10x12 cm) is sandstone lithology and contains seaweed holdfast remnants (Figure 32, A)</li> </ul>	<ul style="list-style-type: none"> <li>- Bed thickness: 10-35 cm</li> <li>- Contacts: Irregular</li> </ul>	<ul style="list-style-type: none"> <li>- <i>Mya truncata</i> in life position 4.05 m a.s.l.</li> <li>- <i>Mya truncata</i> in death position 4.6 m a.s.l.</li> </ul>	Marine suspension fallout	Glaciomarine deltaic bottomset
Fining upwards, silty, fine to very fine sand with lone stones	3.6-5.5	<ul style="list-style-type: none"> <li>- Very poorly sorted silty sand with rounded to well-rounded sand grains</li> <li>- Lone stones (cm scale) are angular to sub-angular and occasionally well rounded</li> <li>- Lone stones are both vertically and horizontally emplaced</li> </ul>	<ul style="list-style-type: none"> <li>- Bed thickness: 5-10 cm</li> <li>- Contacts: sharp, planar, and irregular</li> </ul>	<ul style="list-style-type: none"> <li>- <i>Macoma calcarea</i> in life position at 3.65 m a.s.l.</li> <li>- <i>Mya truncata</i> in life position at 5.3 m a.s.l. (submitted for radiocarbon dating). Individual was well preserved, intact with both shells and most of the periostracum preserved as well as its siphon out in a feeding position.</li> </ul>	Turbidity current	
Medium to coarse sands with granule gravel	3.7-5.75	<ul style="list-style-type: none"> <li>- Very poorly sorted</li> <li>- Gravels are angular to sub-angular</li> </ul>	<ul style="list-style-type: none"> <li>- Bed thickness: 2-3 cm</li> <li>- Contacts: sharp and irregular</li> </ul>	<ul style="list-style-type: none"> <li>- <i>Mya truncata</i> in life position at 4.25 m a.s.l.</li> </ul>	Ice-rafting	

<p>Fining upwards, fine to very fine sandy silt with bioturbations and lone stones</p>	<p>3.6-6.6</p>	<ul style="list-style-type: none"> <li>- Mean grain size: 15-29 <math>\mu\text{m}</math> (medium to coarse silt)</li> <li>- Geometric (<math>\mu\text{m}</math>) value of sorting (<math>\sigma</math>): 4-5</li> <li>- Verbal classification: very poorly sorted</li> <li>- Skewness: symmetrical, very fine and fine skewed</li> <li>- Textural classification: sandy silt</li> <li>- Lone stones are angular to sub-angular and mudstone and sandstone lithology. Generally, they are vertically emplaced</li> </ul>	<ul style="list-style-type: none"> <li>- Bed thickness: 5-20 cm</li> <li>- Contacts: sharp, regular, and irregular</li> </ul>	<ul style="list-style-type: none"> <li>- <i>Macoma calcarea</i> and <i>Mya truncata</i> are common in life position</li> <li>- <i>Macoma calcarea</i> are often thin shelled (&lt;1 mm) and likely juveniles. <i>Mya truncata</i> shells are up to 5 cm in length and &gt;2 mm thick, inferred as adults</li> <li>- Spherical, and pellet shaped bioturbations (cm scale) are observed at 5.8 m a.s.l.</li> <li>- Disarticulated <i>Mytilus sp.</i> valve at 5.45 m a.s.l.</li> </ul>	<p>Turbidity current</p> <p>Ice-rafting</p>	<p>Glacimarine deltaic bottomset</p>	
<p>Fine sand with clay nodules and lone stones</p>	<p>4.4-7</p>	<ul style="list-style-type: none"> <li>- Moderately sorted</li> <li>- Rounded sand grains</li> <li>- Spherical and elongate clay nodules (cm scale)</li> <li>- Sub-angular to angular lone stones that are vertically emplaced and consist of a mud and siltstone lithology (cm scale)</li> </ul>	<ul style="list-style-type: none"> <li>- Bed thickness: 2-5 cm</li> <li>- Contacts: sharp, irregular, and planar</li> </ul>	<ul style="list-style-type: none"> <li>- <i>Mya truncata</i> at 5.85 m a.s.l. and <i>Macoma calcarea</i> at 5.65 m a.s.l. are both in life position.</li> <li>- <i>Mya truncata</i> at 4.42 m a.s.l. is in death position</li> </ul>	<p>Turbidity current</p>		
<p>Laminated silt and clay</p>	<p>4.3-6.7</p>	<ul style="list-style-type: none"> <li>- Moderately to poorly sorted</li> </ul>	<ul style="list-style-type: none"> <li>- Bed thickness: &lt;5 cm</li> <li>- Contacts: sharp and planar</li> </ul>	<ul style="list-style-type: none"> <li>- Laminated</li> </ul>	<p>Marine suspension fallout</p>		
<p>Cryoturbated silty sand with outsized pebble clasts</p>	<p>6.5-7.2</p>	<ul style="list-style-type: none"> <li>- Very poorly sorted</li> <li>- Clasts exhibit a wide range of angularities from sub rounded to angular</li> <li>- Upper part of the deposit is capped with vegetation</li> </ul>	<ul style="list-style-type: none"> <li>Thickness: 70 cm</li> <li>- Contact gradational</li> </ul>	<ul style="list-style-type: none"> <li>- Slumping and cryoturbation</li> </ul>	<p>Cryo-turbation</p>		



### 4.3.2.3 Lithofacies association

#### 4.3.2.3.1 Glacimarine deltaic-bottomset facies

##### Description

The 13 sediment samples analysed from this outcrop are classified as ‘sandy silt’ on the textural triangle and exhibit a *c.* 10-20 % variation in their sand content (Figure 31). The silt grains vary between fine to very coarse in size. The lithofacies are present in 10-50 cm thick, massive, and fining upward beds that are bound by both sharp and gradational contacts.

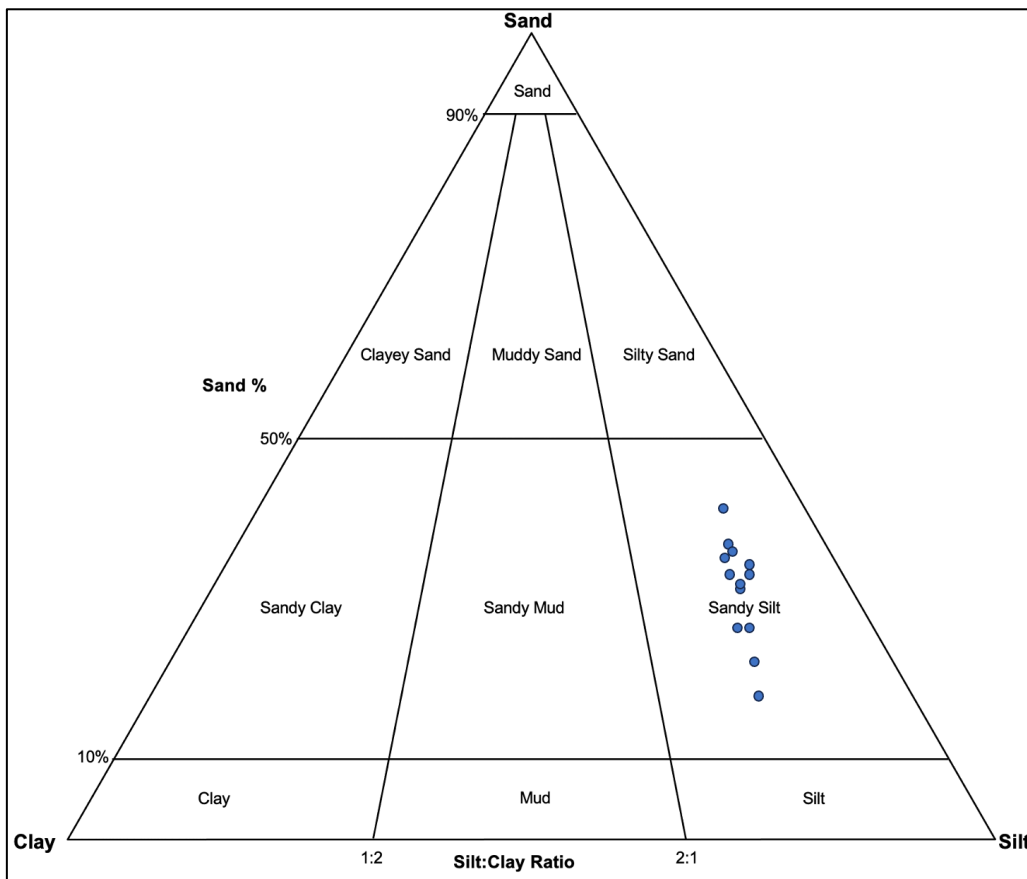


Figure 31: Grain size textural triangle for sediment samples from the glacimarine bottomset in the *Mya truncata* Section at Bøgebekken. Generated with GRADISTAT v8 (Blott, 2010).

Interbedded with the sandy silts and present to a lesser extent are medium to coarse sands with granule gravels, massive and fining upward silty sands, silts, and clay beds. Outsized clasts, including gravels and lone stones that are sub-angular to well-rounded are frequently observed and often positioned upright (Figure 32, B). Clay nodules (cm scale) with concentric rings as part of their internal structuring were revealed during the sieving process. The outcrop is capped by a cryoturbated deposit containing outsized clasts and evidence of slumping.

No foraminifera were found in any of the 13 sediment samples that were taken. The facies are rich with molluscs albeit exhibiting a low species diversity. *Mya truncata* dominate and to a lesser extent *Macoma calcarea*. The *Mya truncata* are commonly >5 cm in length and >2 mm thick (Figure 32, D) with varying degrees of the periostracum preserved. A disarticulated and fragmented *Mytilus* sp. was found during sieving of the sediment sample at 5.45 m a.s.l. Many of the *Mya truncata* are observed in a life position with their feeding siphon out and intact. Tube worm casts are sporadically present within the facies (Figure 32, B) and strikingly an organic branching structure that exhibits similarities to seaweed holdfast was observed on a 10x12 cm lone stone at the base of the outcrop (Figure 32, A). This is in addition to trace fossils and bioturbation.

Sedimentary structures observed in the glaciomarine facies include load structures, where fine grain sand beds overlie sandy silt and sunken, lobate, and irregular bed contacts form between the two deposits (Figure 32, C).

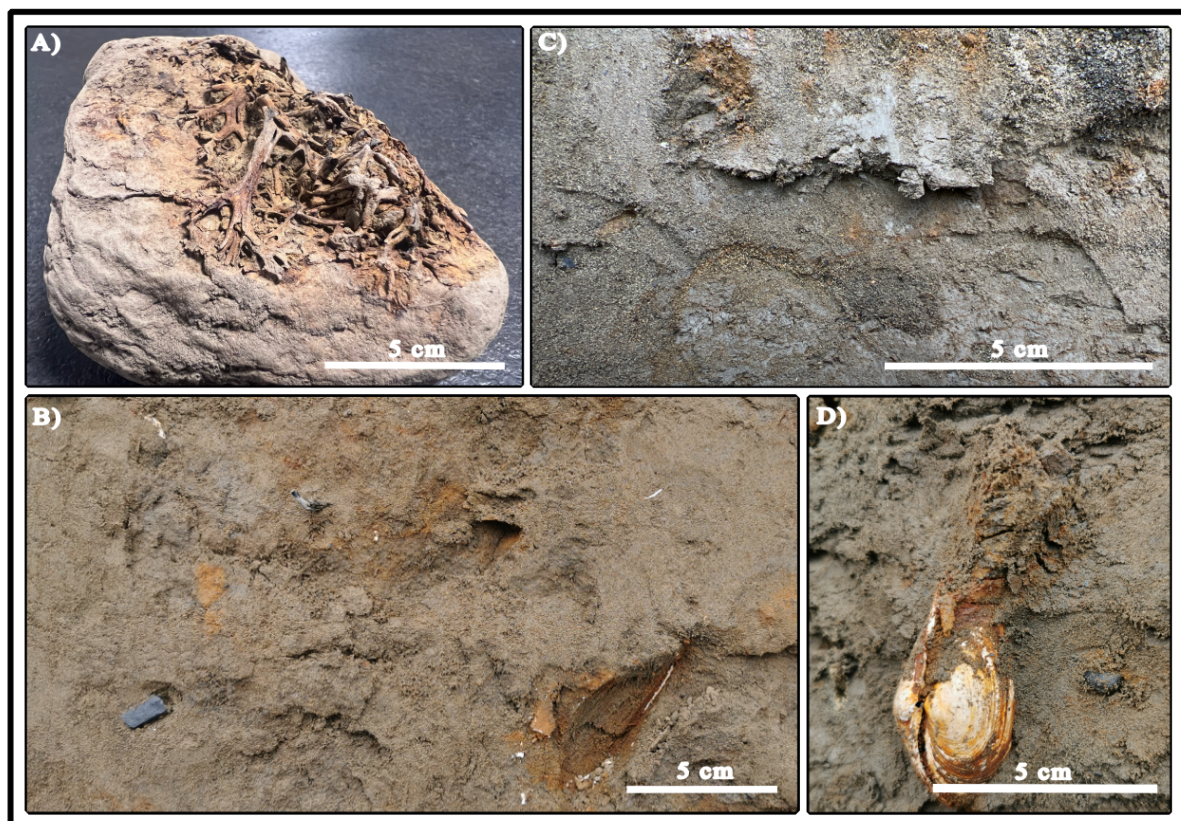


Figure 32: A 10x12 cm sandstone lone stone with branching organic matter, likely seaweed holdfast attached to its upper surface (A). Isolated and near upright angular to sub-angular lone stones (cm scale) and an isolated tube worm cast protruding from the sediment (B). A sunken and lobate load structure evident in the fine sand lens overlying the sandy silt bed below (C). A *Mya truncata* shell (5 cm long and 2 mm thick) in a life position with its feeding siphon out (5.33 m a.s.l.). Additionally, a <1 cm well rounded lone stone is present next to the shell (D).

## Interpretation

The interpreted depositional environment for the *Mya truncata* Section at Bogebecken is a glacial marine deltaic bottomset. No absolute age can be determined for the outcrop as radiocarbon dates have not been returned from the laboratory in time. A tentative age of <11.0-10.8 cal. ka BP is interpreted based on the presence of the *Mytilus* sp. shell and this will be assessed in the discussion.

Depositional processes associated with the lithofacies include marine suspension fallout from hypopycnal flows, turbidity currents and periods of ice-rafting. The massive and laminated beds of sandy silt and silt are predominantly interpreted to be the result of suspension fallout where delivery of the sediment was provided through buoyant sediment-laden hypopycnal plumes (Bates, 1953; Gilbert, 1983; Mackiewicz et al., 1984; Zavala, 2020a). On the contrary, the silty sand and sand lithofacies that fine upwards and are defined by a sharp, undulating and erosive lower contact are interpreted to result from turbidity currents (Mackiewicz et al., 1984; Powell, 1984; Powell & Molnia, 1989). The interbedded lithofacies indicate abrupt transitions in energy within the depositional environment, supporting a highly dynamic depositional system.

Coarse sand beds that include granule gravels (angular to sub-angular) as well as oversized lone and drop stone material (Figures 32, B/D) indicate that the environment was subject to periods of ice rafting. Furthermore, lone stones deposited in a near upright position (Figure 32, B) clearly indicate deposition from floating ice (Lønne, 2005). To attribute the ice rafted material to transport by icebergs or sea ice is to some extent controversial, and so concepts of both will be entertained with respects to the size and shape of the material found within this outcrop. In shore-distal settings, larger particles are generally believed to have been deposited by icebergs (Gilbert, 1990; Knies et al., 2001). In line with this association, the larger cm scale, vertically emplaced lone stone in Figure 32, B, is likely to have been transported by iceberg rafting. Interpretation of the sediment forming within a glacial marine deltaic bottomset environment aligns with deposition in a shoreline-distal setting, strengthening iceberg rafting as a depositional mechanism.

Additionally, the predominant angular/sub-angular shape of grains within this outcrop, are in accordance with deposition by iceberg-rafting, as iceberg-rafted material has been documented as being angular to rounded compared to more rounded sea ice-rafted material

(Gilbert, 1990; Goldschmidt et al., 1992; Lisitzin, 2002). An exception to this is a well-rounded cm scale lone stone is present which due to its roundness falls in line with sea ice-rafting (Figure 32, D). Complicating this deduction is the findings that sea-ice rafted material in High Arctic settings can also be more angular (Gilbert, 1990 and references therein). A study conducted by Forwick and Vorren (2009) in Central Isfjorden, infers that during the period between *c.* 10.2 and 8.8 cal. ka BP, warm surface waters within the fjord would have suppressed the formation of sea ice. This period falls in line with the tentative age of deposition of this unit, and so provides a degree of evidence supporting iceberg-rafting over sea ice-rafting leading to the deposition of the ice rafted material observed within the section. Additionally, sightings of icebergs off the coast of Bjørndalen, Isfjorden (2005) confirms that at present, deposition of larger and more angular iceberg-rafted debris in Isfjorden is possible (Anders Schomacker pers. comm). Despite this, the controversy surrounding the distinction between sea-ice rafted and iceberg rafted means grains observed within this outcrop study are simply referred to as ‘ice-rafted’ in origin.

The low species diversity dominated by *Mya truncata* and to a lesser extent *Macoma calcarea*, that are frequently found buried in a life position, suggests considerable sedimentation rates and reduced salinities that contribute towards an inhospitable environment (Jensen, 1942; Syvitski & Farrow, 1989; Hansen, 2004; Lønne, 2005). The sediment character, content of ice-rafted material and presence of *Mya truncata* buried in growth position exhibits similarities with distal deltaic deposits described by Lønne (2005) from Bolterdalen, Isfjorden and Hansen (2004) from Jameson Land, Eastern Greenland. This strengthens the interpretation of the lithofacies association of the *Mya truncata* Section in Bogebecken to a glacial marine deltaic bottomset depositional environment.

### 4.3.3 Environmental synthesis

The *Mya truncata* Section at Bogebecken (BKS2) contains six lithofacies that have been deposited by suspension fallout from buoyant sediment-laden hypopycnal plumes (Bates, 1953; Gilbert, 1983; Mackiewicz et al., 1984; Zavala, 2020b), turbidity currents (Mackiewicz et al., 1984; Powell, 1984; Powell & Molnia, 1989) and periods of ice-rafting (Gilbert, 1990; Knies et al., 2001; Forwick & Vorren, 2009). The interbedded relationship of the lithofacies and depositional mechanisms influencing sedimentation suggest a highly dynamic depositional environment, that is modulated by high sedimentation rates and to some extent glacier state within Isfjorden.

The suspension fallout and turbidity current lithofacies exhibit a similar sediment character to the prodelta, and lower delta slope deposits described in the Hollendardalen Sections above. This contributed towards the interpretation that this outcrop is similarly deposited in a shoreline distal setting. Furthermore, the deposits are similarly in fitting with the typical sediment distribution pattern in modern fjord environments where the finest grains are transported furthest from the source at the head of the fjord (Holtedahl, 1975; Skei, 1983; Faust et al., 2017). Unfortunately, the lack of overlying strata at the outcrop inhibits correlation to a shallowing sequence and so the lithofacies are broadly defined as representing a deltaic bottomset sub-environment.

There is a strong signal of ice-rafting influencing sedimentation within the outcrop as depicted by the presence of vertically emplaced lone stones and coarse sand and granule gravel beds at various height up sequence (Figures 29 and 30). This supports glacier state within Isfjorden and within the fjord side embayment to some extent acting as an influential regime control at the time of deposition. Therefore, characterisation of the depositional environment as a glacimarine deltaic bottomset is fitting. The dominance of *Mya truncata* buried in growth position with their siphons out and preserved indicates that another significant regime control was sediment supply, which is evidently high enough to outpace the upward migration of the molluscs.

## 4.4 Bogebekken: *Arctica islandica* Section

### 4.4.1 Overview

The *Arctica islandica* Section at Bogebekken (BKS1) is positioned on the western side of Bogebekken and excavated in the marine terrace c. 100 m south of the present shoreline (Figure 9). The coordinates for the base of the section are 33X E486103 N8669589 and this is elevated at 1 m a.s.l. The section is 7.4 m high, 10 m wide, and divided into six units.

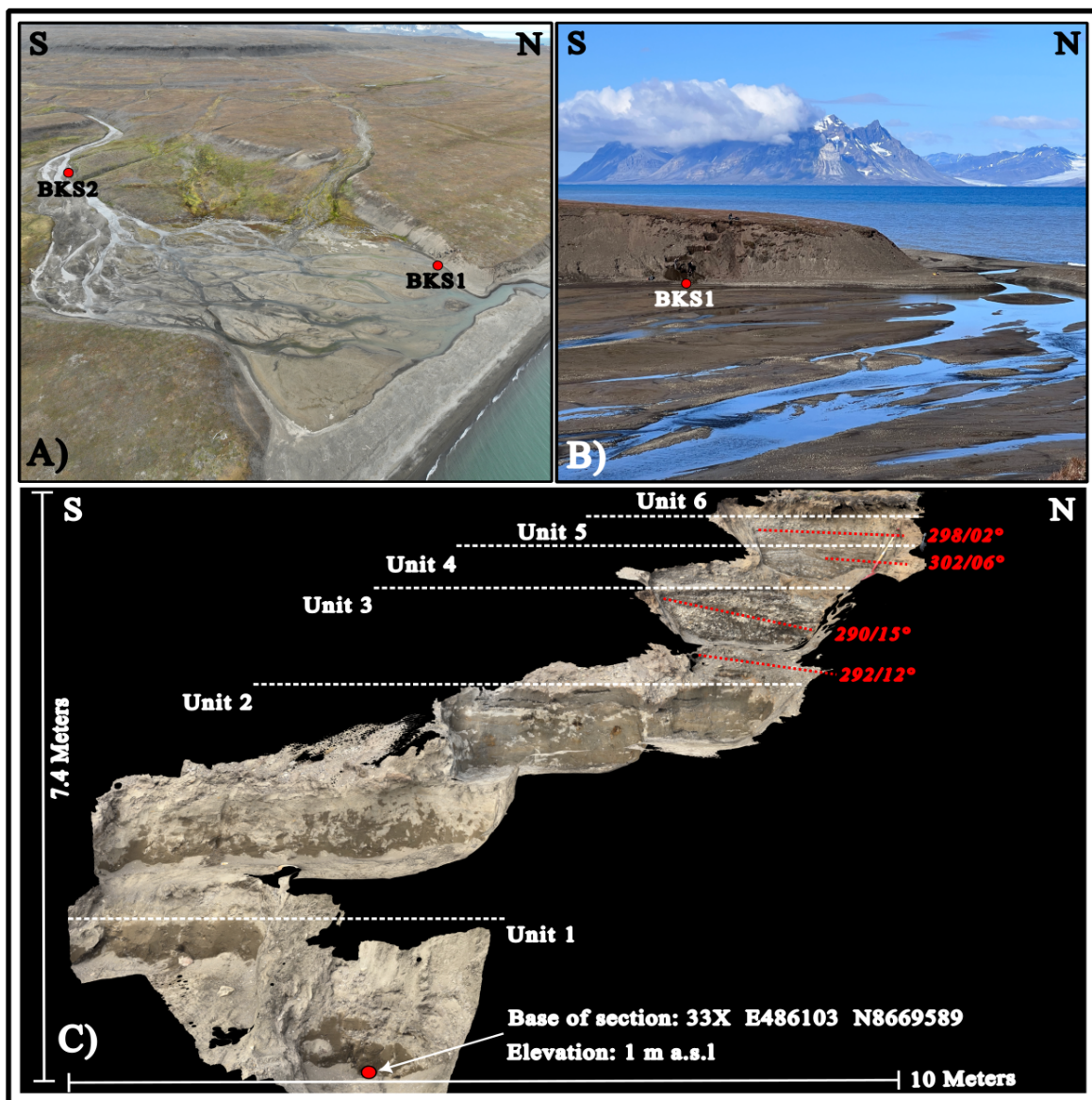


Figure 33: Overview information of the *Arctica islandica* Section at Bogebekken. A and B Indicate the position of the outcrop along the western edge of the raised marine terrace at Bogebekken. C is a 3D model of the BKS1 produced in the field using with the 3D Scanner mobile app with UNIS Bachelor student Magnus Weijers, who published the model on Sketchfab (<https://sketchfab.com/3d-models/hollandardalen-outcrop-005475bdcd544682b3e54ea7a4c2c34d>). The model has been annotated for this investigation to include the coordinates for the base of the section, the elevation in m a.s.l., the dimensions of the outcrop, the strike and dip of bedding and the division of the six units.

## 4.4.2 Stratigraphy

### 4.4.2.1 Sedimentary log

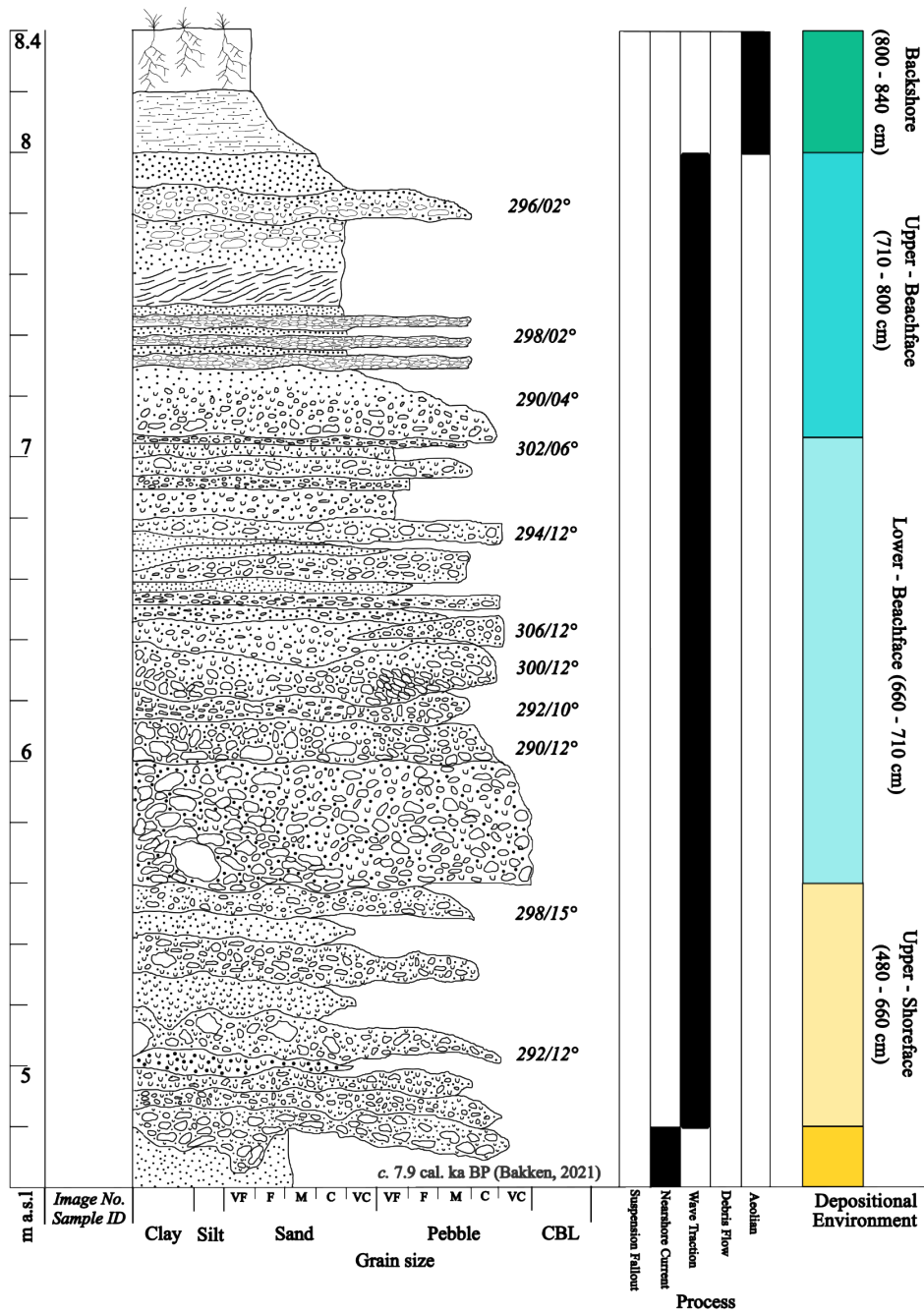


Figure 34: Sedimentary log (1/2) of the Arctica islandica Section at Bogebekken.

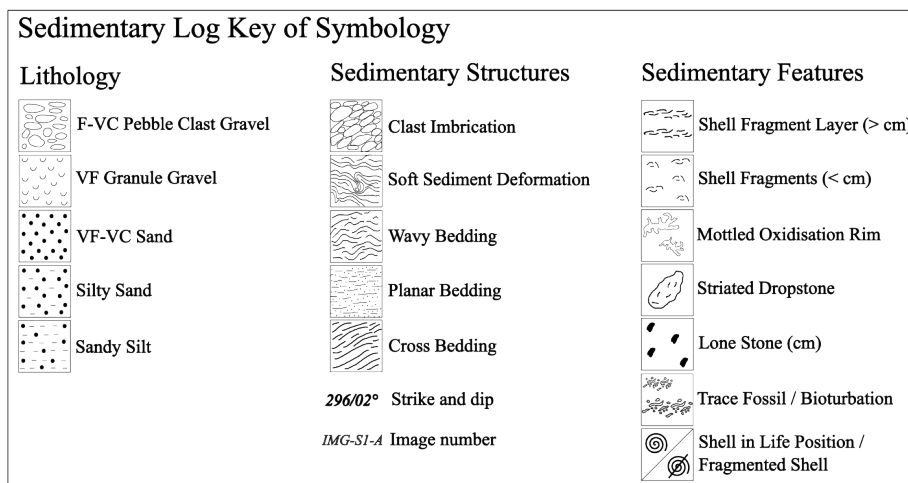
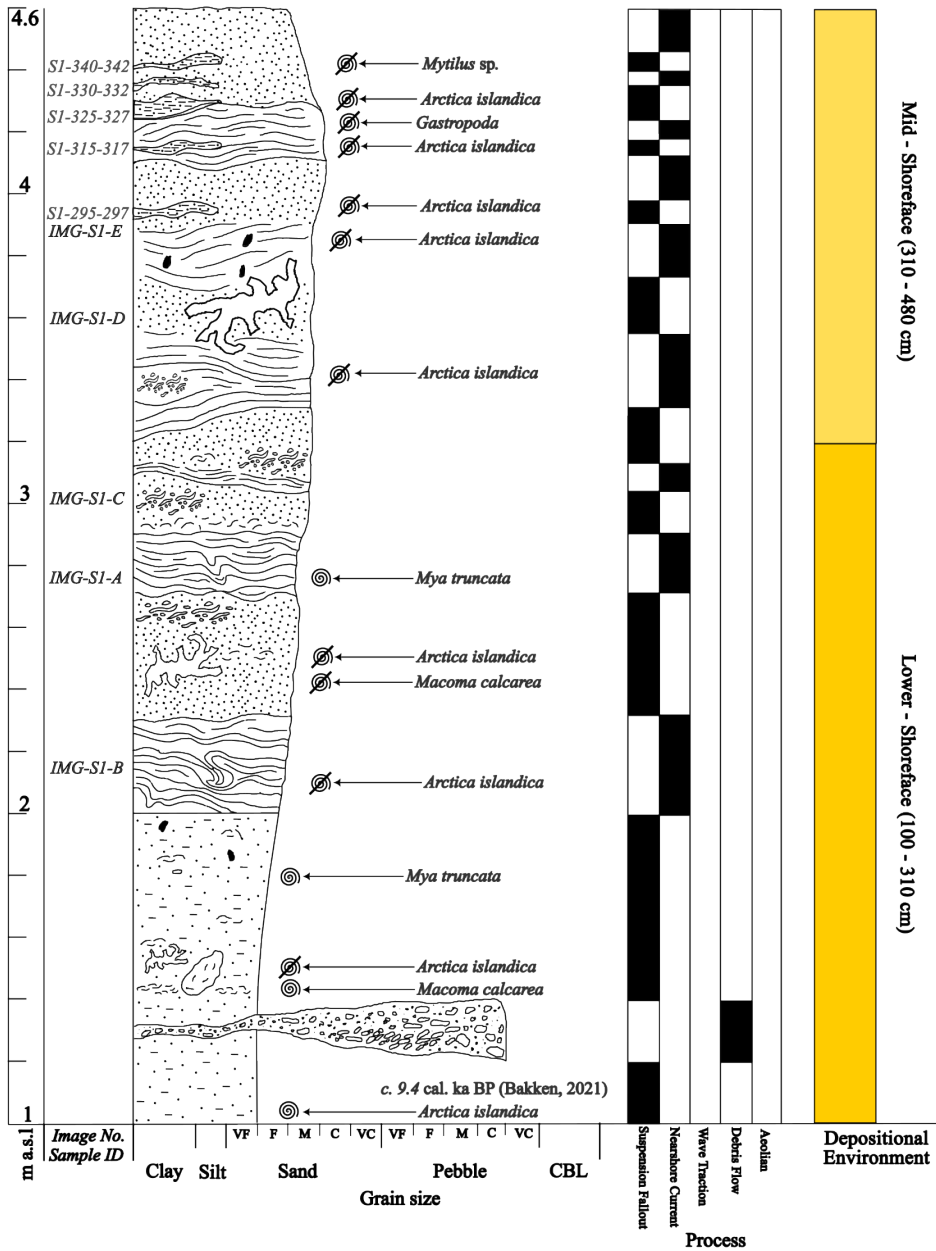


Figure 35: Sedimentary log (2/2) and key of symbology for the Arctica islandica Section at Bogebecken.



#### 4.4.2.2 Lithofacies description

A detailed description of the 15 lithofacies identified within BKS1 is provided below in lithofacies Table 8. The lithofacies are grouped alongside their interpreted sub-environment and attributed depositional process.

Table 8: Lithofacies descriptions of the 15 lithofacies identified within the six sub-environments within the *Arctica islandica* Section at Bøgebekken (BKS1).

Lithofacies description	m a.s.l.	Textural, clast and statistical description	Bed and contact geometry	Structures/ mollusc content	Process interpretation	Environment interpretation
Massive silty, very fine sand	1-2	<ul style="list-style-type: none"> <li>- Moderately sorted beds</li> <li>- Rounded to well-rounded sand grains</li> <li>- Striated dropstone (12x5 cm) at 1.4 m a.s.l.</li> <li>Sandstone lithology and sub-rounded to sub-angular</li> <li>- Several angular-sub-rounded lone stones (2-4 cm)</li> </ul>	<ul style="list-style-type: none"> <li>- Bed thickness: 30-70 cm</li> <li>- Contacts: gradational</li> </ul>	<ul style="list-style-type: none"> <li>- Gradual coarsening up-sequence from very fine to fine sand</li> <li>- <i>Arctica islandica</i> shells, well preserved with periostracum intact in both life and death position</li> <li>- <i>Macoma calcarea</i> shells in both life and death position</li> <li>- <i>Mya truncata</i> in life position with siphon out</li> <li>- Mottled patches (&lt;10 cm), dark brown to orange colour</li> </ul>	Marine suspension fallout	Lower shoreface
Laminated silty fine sand with soft sediment deformation	2-2.9	<ul style="list-style-type: none"> <li>- Moderately well-sorted</li> <li>- Rounded to well-rounded sand grains</li> </ul>	<ul style="list-style-type: none"> <li>- Bed thickness: 20-30 cm</li> <li>- Contact: sharp and irregular</li> </ul>	<ul style="list-style-type: none"> <li>- Laminations are discontinuous, irregular, and vaguely sigmoidal in shape</li> <li>- Soft sediment deformation exhibits a sunken, hook shape geometry</li> <li>- <i>Arctica islandica</i> (&gt;10 cm in length) in death position but well-preserved with periostracum intact</li> <li>- <i>Mya truncata</i> (&gt;5 cm) in life position</li> </ul>	Marine suspension fallout  Nearshore current	

Coarsening upwards, silty fine to medium sand	2.3-5.1	<ul style="list-style-type: none"> <li>- Moderately well-sorted</li> <li>- Rounded to well-rounded sand grains</li> </ul>	<ul style="list-style-type: none"> <li>- Bed thickness: 10-50 cm</li> </ul>	<ul style="list-style-type: none"> <li>- Elongate, pellet shaped bioturbations (cm scale)</li> <li>- <i>Arctica islandica</i> and <i>Macoma calcarea</i> are disarticulated and fragmented. <i>Mytilus</i> sp. at 4.5 m a.s.l.</li> </ul>	<ul style="list-style-type: none"> <li>Marine suspension fallout</li> <li>Nearshore current</li> </ul>	Lower shoreface
Coarse pebble gravel with a sand matrix	1.2-1.3	<ul style="list-style-type: none"> <li>- Poorly to very poorly sorted and sub-rounded to rounded clasts that are rod and spherical shape</li> <li>- Clasts are mostly supported in a sandy matrix apart from the weak imbrication</li> </ul>	<ul style="list-style-type: none"> <li>- Bed thickness: 10 cm</li> <li>- Contacts: sharp and irregular</li> </ul>	<ul style="list-style-type: none"> <li>- Slight imbrication of some clasts</li> </ul>	<ul style="list-style-type: none"> <li>Debris flow</li> </ul>	
Fine to medium sand with wavy bedding	3.2-4.1	<ul style="list-style-type: none"> <li>- Moderately well-sorted</li> <li>- Rounded to well-rounded sand grains</li> <li>- Vertically emplaced lone stone (cm scale). Sandstone lithology and sub-angular to sub-rounded</li> </ul>	<ul style="list-style-type: none"> <li>- Bed thickness: 20-40 cm</li> <li>- Contacts: both sharp and gradational</li> </ul>	<ul style="list-style-type: none"> <li>- Wavy bedding (low angle <math>&gt;5^\circ</math> foresets) emphasised by slight grain size increase to medium sands defining geometry</li> <li>- Isolated pockets of pellet shaped bioturbations (cm scale) at 3.4 m a.s.l.</li> <li>- <i>Arctica islandica</i> are the dominant fauna although all shells are fragmented and in a death position</li> </ul>	<ul style="list-style-type: none"> <li>Marine suspension fallout</li> <li>Nearshore current</li> </ul>	Middle shoreface
Lenticular fine sandy, fine to medium silt	3.95-4.45	<ul style="list-style-type: none"> <li>- Mean grain size: 18-41<math>\mu</math>m (coarse to very coarse silt)</li> <li>- Geometric value (<math>\mu</math>m) for the sorting (<math>\sigma</math>): 7-8</li> <li>- Verbal classification: very poorly sorted</li> <li>- Skewness: symmetrical, very fine, fine, and coarse skewed</li> <li>- "sandy silt"</li> </ul>	<ul style="list-style-type: none"> <li>- Bed thickness: 2-5 cm</li> <li>- Contacts: sharp and irregular</li> <li>- Beds are thin, discontinuous, and lenticular in shape</li> </ul>	<ul style="list-style-type: none"> <li>- Laminated</li> </ul>	<ul style="list-style-type: none"> <li>Marine suspension fallout</li> <li>Nearshore current</li> </ul>	

Matrix supported, fining upward very coarse to coarse pebble gravel	4.8-6.1	<ul style="list-style-type: none"> <li>- Poorly to very poorly sorted</li> <li>- Sub-angular to rounded clasts</li> <li>- Variable clast shape including both spherical rod shapes</li> <li>- Some rod-shaped clasts show a horizontal clast alignment</li> <li>- Sandy matrix with granule gravels</li> </ul>	<ul style="list-style-type: none"> <li>- Bed thickness: 10-40 cm</li> <li>- Contacts: sharp, irregular, and gradational</li> <li>- Bedding inclined at 10-15°</li> </ul>	<ul style="list-style-type: none"> <li>- Weak normal grading</li> <li>- Imbricated clasts dip in a landward direction</li> </ul>	Wave traction	Upper shoreface
Massive coarse to very coarse sand with granule gravel	5-5.5	<ul style="list-style-type: none"> <li>- Moderately to well-sorted</li> <li>- Rounded to well-rounded sand and gravel</li> </ul>	<ul style="list-style-type: none"> <li>- Bed thickness: 5-10 cm</li> <li>- Contacts: sharp and irregular</li> </ul>	<ul style="list-style-type: none"> <li>- Weak normal grading</li> </ul>	Wave traction	
Medium to coarse pebble gravel	6.2-7	<ul style="list-style-type: none"> <li>- Moderately to poorly sorted</li> <li>- Sub-angular to sub-rounded pebble clasts</li> <li>- Predominantly rod-shape</li> <li>- Horizontal alignment with long axis parallel to bedding strike</li> <li>- Supported in a sandy matrix</li> </ul>	<ul style="list-style-type: none"> <li>- Bed thickness: 5-20 cm</li> <li>- Contacts: sharp and irregular</li> <li>- Wedge shape bed geometry</li> <li>- Bedding inclined at 10-12°</li> </ul>	<ul style="list-style-type: none"> <li>- Imbrication of rod-shape clasts that dip seaward.</li> </ul>	Wave traction	Lower beachface
Planar laminated coarse and very coarse sands	6.5-6.8	<ul style="list-style-type: none"> <li>- Moderately to well-sorted</li> <li>- Rounded to well-rounded</li> </ul>	<ul style="list-style-type: none"> <li>- Bed thickness: 5cm</li> <li>- Contacts: sharp and regular</li> <li>- Beds pinch out in a seaward direction</li> </ul>	<ul style="list-style-type: none"> <li>- Planar lamination</li> </ul>	Wave traction	
Fining upwards coarse pebbly sand	7-7.3	<ul style="list-style-type: none"> <li>- Moderately sorted</li> <li>- Rounded to sub-rounded rod-shape clasts</li> </ul>	<ul style="list-style-type: none"> <li>- Bed thickness: 30 cm</li> <li>- Contacts: sharp and regular</li> <li>- Bedding inclined at 6° in a</li> </ul>	<ul style="list-style-type: none"> <li>- Normal grading of rod-shape pebbles to coarse sand</li> </ul>	Wave traction	Upper beachface
Clast supported medium pebble gravel	7.3-7.5	<ul style="list-style-type: none"> <li>- Well-sorted bed</li> <li>- Well-sorted, rounded disc and blade shape pebbles</li> </ul>	<ul style="list-style-type: none"> <li>- Bed thickness: &lt;5 cm</li> <li>- Contacts: sharp</li> <li>- Bedding inclined at 2°</li> </ul>	N/A	Wave traction	

Massive coarse sand	7.35-7.55	- Well-sorted and well-rounded sands	- Bed thickness: <5 cm beds	- Feint planar laminations	Wave traction	Upper beachface
Cross bedded coarse sand	7.55-7.7	- Well-sorted and well-rounded sands	- Bed thickness: 10-20 cm - Contacts: sharp and gradational	- Low angle tabular cross bedding that gradually fades up-sequence	Wave traction	
Fining upwards pebbly coarse sand	7.7-8	- Moderately to well-sorted and rounded to well-rounded sands - Rounded to sub-rounded outsized pebbles that are disc-shaped	- Bed thickness: 10 cm - Contacts: sharp and regular	N/A	Wave traction	
Planar laminated medium to very fine sand	8-8.4	- Well rounded and well sorted sands	- Bed thickness: 20 cm - Contacts: sharp and gradational	- Planar laminated - Rootlets	Aeolian	Backshore

### 4.4.2.3 Lithofacies association

#### 4.4.2.3.1 Lower shoreface lithofacies

##### Description

Four lithofacies are associated with the lower-shoreface (Table 8). They predominantly consist of massive or coarsening upwards silty sand as well as laminated silty sands with sediment deformation (Figure 36, B). At 1.2 m a.s.l., a wedge of coarse pebble gravel with rod and spherical shape clasts pinches out in a shoreward direction. The imbricated clasts show a slight degree of horizontal alignment at the base of the bed which transitions to a more vertical alignment and steepening up sequence (Figure 35). The thin (10 cm) bed has sharp upper and lower contacts and is isolated and irregular compared to the other lithofacies.

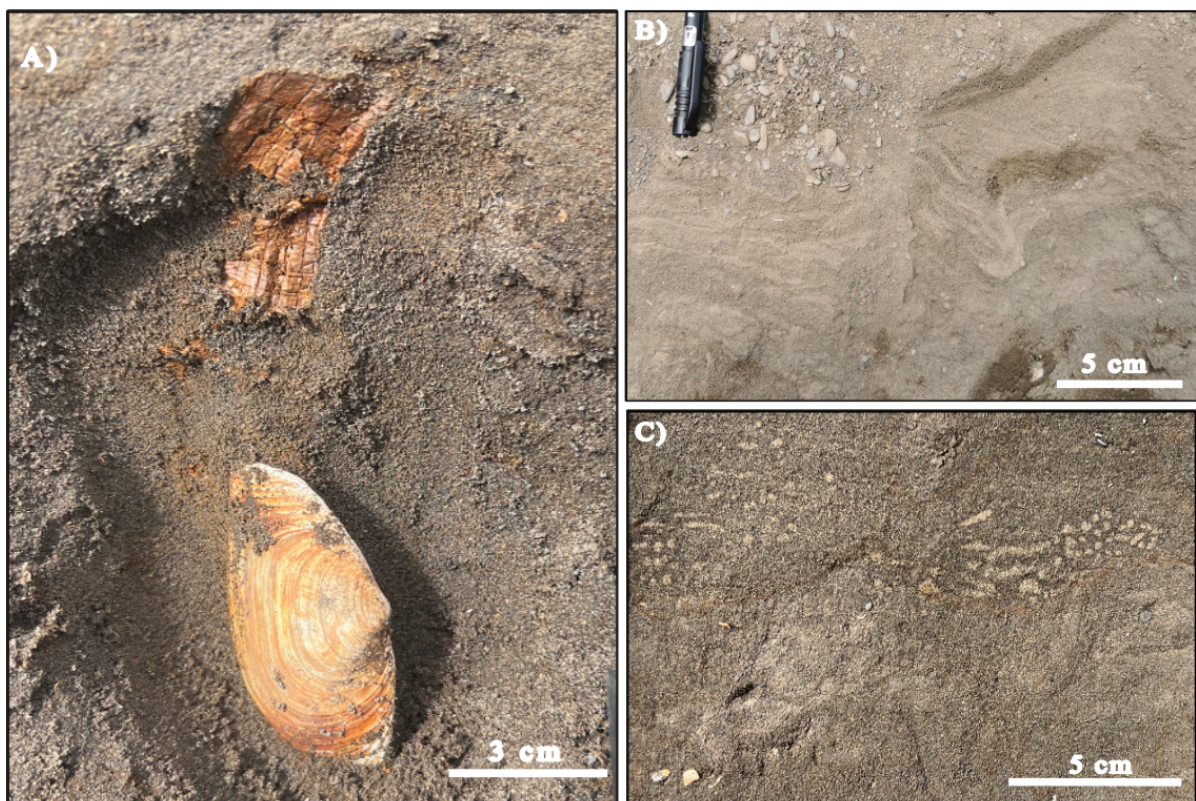


Figure 36: Pictures of sedimentary structures and features within the lower-shoreface environment of the *Arctica islandica* Section at Bogebecken. *Mya truncata* in growth position (A). Soft sediment deformation (B). Clusters of pellet-shaped bioturbations (C).

Sedimentary features include a striated dropstone (10x12 cm) at 1.4 m a.s.l., as well as numerous other angular to sub-rounded lone stones that are only a few cm in size and sub-vertically emplaced. Clusters of pellet-shaped bioturbations are evident at 2.6-3.2 m a.s.l. (Figure 36, C). Additionally, the environment is dominated by a relatively rich diversity of

molluscs including *Arctica islandica*, *Mya truncata* and *Macoma calcarea*. The *Mya truncata* are often in a growth position with their feeding siphon out (Figure 36, A), whereas the *Arctica islandica* are in a death position, albeit well preserved with their periostracum intact.

### **Interpretation**

The main depositional processes acting within this environment are marine suspension fallout and nearshore currents. Secondary to these processes are periods of ice-rafting with an infrequent and irregular debris flow deposit.

The laminations of silt and sand indicate episodic deposition, which may reflect periods where sediments from higher up the shoreface are mobilised by nearshore currents or wave traction, and redeposited lower down the shoreface periodically in lull energy conditions. Periods of calmer energies are supported by the clusters of pellet-shaped bioturbations that indicate seasonally-ice free and open water, with a potentially reduced sediment supply, allowing for organisms to rework and burrow into the sediment (Lønne, 2005).

The presence of the soft sediment deformation (Figure 36, B) is fitting with other sediment characteristics of the lower-shoreface. Soft sediment deformation is commonly found within a silt to fine sand fabric which correlates with the grain size of this lithofacies and its formation indicates a high depositional rate, low permeability and low shear strength of grains within the sediment range (Mills, 1983). A high rate of sedimentation is clearly demonstrated through the burial of *Mya truncata* shells with their siphon out in a feeding position (Figure 36, A). The soft sediment deformation exhibits similar characteristics to convoluted laminations, described by Kuenen (1953) with sharp synclines and low amplitude anticlines that decrease in amplitude at the upper and lower contacts. The occurrence of similar soft sediment deformation has been described by Brenchley and Newall (1977) in shallow marine deposits where their occurrence was proposed to result from shearing within the sediment, during the lateral migration of shoreface sands over muddy sediment during storm events. These findings support the soft sediment deformation being linked with a lower shoreface environment, although a slight difference in the depositional process is noted. Attributing their deposition to the migration of sands during storm events, would further explain and provide a transport mechanism for the fragmented *Arctica islandica* shells that are also present. Together, these interpretations of the sedimentary structures and inferences made from the molluscs, point towards the deposition of this unit in a relatively high energy

shoreface, subject to fluctuating energies induced by storms, nearshore currents and lull periods allowing for suspension settling to occur.

Further supporting a varying energy flux relating to storm events on the shorelines is the outlier lithofacies composed of an isolated wedge-shaped coarse pebble gravel at 1.2-1.3 m a.s.l. The sharp contacts and significant increase in grain size, indicates erosional emplacement, potentially by a debris flow. This may have resulted from wave induced destabilisation of the beachface during a storm, where eroded beachface material is then transported down the steep faced gravel beach by undertow or backwash drawn down to the lower shoreface environment (Massari, 1984; Nemeč, 1990; Lønne & Nemeč, 2004). The slight upward steepening of clasts may result from frictional freezing of the sediment post shearing resulting in a more vertical alignment of the clasts along their a-axis (Nemeč, 1990).

#### **4.4.2.3.1 Middle shoreface lithofacies**

##### **Description**

Two lithofacies characterise the middle shoreface and include coarsening upward fine to medium sands with wavy bedding that are interbedded with lenticular silty sands (Table 8). The composition of the silty sand is shown in the textural triangle below in Figure 37. The middle shoreface succession exhibits a coarsening upwards trend with both sharp and gradational contacts. The silty sands that are present as lenticular and irregular bed geometries are separated from the wavy sand beds by sharp boundaries. Similarly to the sands, the silty sands exhibit a coarsening upward trend (Figure 37).

The mollusc shells are mostly *Arctica islandica* and all are found in a death position but well preserved alongside fragmented *Mya truncata*, *Mytilus* sp. and a gastropod shell. There are large patches (>10 cm) of rusty orange and brown discolouration within the sediment (Figure 38, D) as well as vertically emplaced lone stones (2-4 cm) (Figure 38, E).

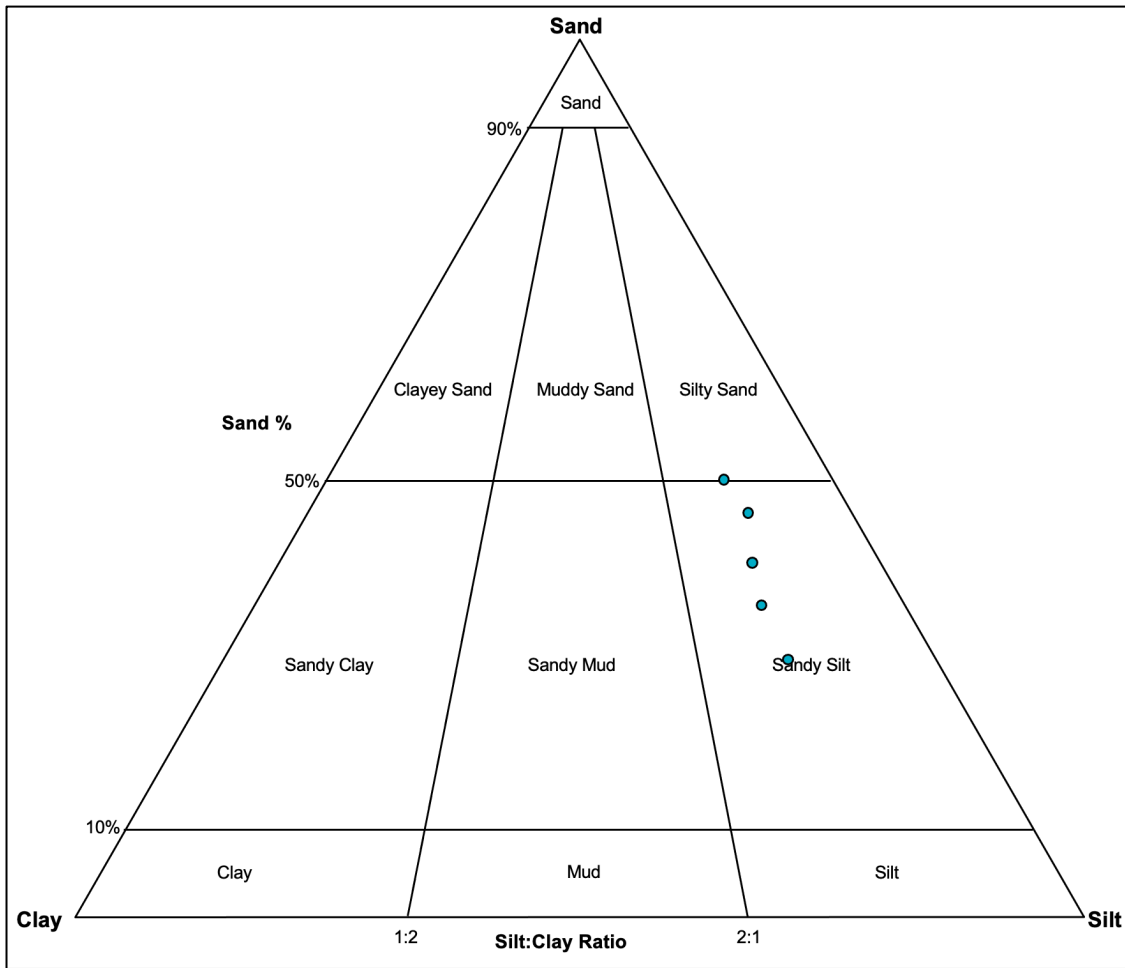


Figure 37: Grain size textural triangle for sediment samples from the middle shoreface at the Arctica islandica Section at Bogebecken. Generated with GRADISTAT v8 (Blott, 2010).

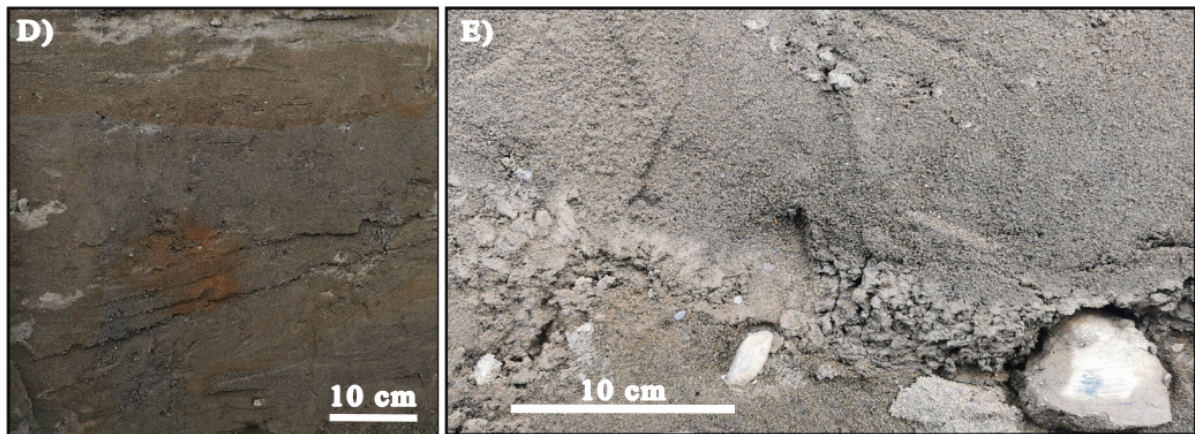


Figure 38: Pictures of sediment character within the middle shoreface sub-environment of the Arctica islandica Section at Bogebecken. Mottled rusty orange discolouration within the sediment (D). Lenticular sandy silt with an upright lone stone and an Arctica islandica shell (E).



## Interpretation

The coarsening upward fine to medium sands that contain wavy bedding are interpreted to result from the migration of sands due to nearshore currents. This could also result from the migration of the sand by wave traction during periods when storm events are affecting the shoreline, and the wave base is deepened. No clear cross stratification was observed, and so deposition is believed to be below the fair-weather wave base, although the low angle undulations in bedding surfaces indicate that mobilisation and migration to some extent was occurring at the depth of deposition. The fragmented and disarticulated *Arctica islandica* shells and shell beds further indicate that there are high energy conditions mobilising and redistributing sediment and material along the middle shoreface. These same mechanisms may have produced the wavy bedding present.

On the contrary, the lenticular sandy silt beds that are present are interpreted to result from suspension fallout during period of quiescent energy (Mackiewicz et al., 1984). The inclusion of upright lone stones (Figure 38, E) indicate that the environment was subject to periods of ice-rafting, and therefore, one explanation of the quieter energy period may result from a winter period in which ice was covering an area of the shallow marine environment. Similar deposits have been described within raised marine sediments from Bolterdalen, Isfjorden where similarly they were proposed to have been deposited under an ice-capped fjord. Temperature reconstructions conducted by Christman (2022) on the *Arctica islandica* within this deposit reveal minimum winter sea surface temperatures below 0 °C which supports conditions in the shallow marine environment capable of supporting sea ice formation. Whilst deposition of the lithofacies during the winter period under potentially ice-capped fjord seems plausible, a lower energy environment is debatable. Challenging this is the fine skewed and bimodal/trimodal grain size distributions of the sediment samples taken from within these lithofacies (Figure 37). These characteristics reflect a dominant sandy signature to the silt beds. The grain size analysis also reveals a very poorly sorted texture (Figure 38, E). The higher percentage of sand present within the sandy silt lithofacies may result from turbidity induced by storm waves over the winter period which caused winnowing from the upper shoreface and sediment redistribution downslope (Faust et al., 2017). The lenticular, irregular and discontinuous nature of the sediment beds supports deposition in a turbid environment that was caused by storms affecting the high energy shoreface. The mottled, rusty orange patches that are laterally extensive are interpreted to result from post depositional breakdown and oxidisation of organic matter, likely mollusc tissue, within the sediment.

#### 4.4.2.3.2 Upper shoreface lithofacies

##### Description

Two interbedded lithofacies are observed in the upper shoreface; a matrix-supported, fining upwards very coarse to coarse pebble gravel and a massive, coarse to very coarse sand with granule gravel (Table 8). Field analysis revealed a variety of clast shapes within the matrix supported pebble gravel and a degree of imbrication at 6.6-7 m a.s.l. (Figure 39). Sharp and irregular contacts separate the two lithofacies. The sand that contains beach gravels are texturally similar to the matrix that supports the pebble gravel. The beds are inclined at 10-15° and dip in a towards the present shoreline (Figure 39).

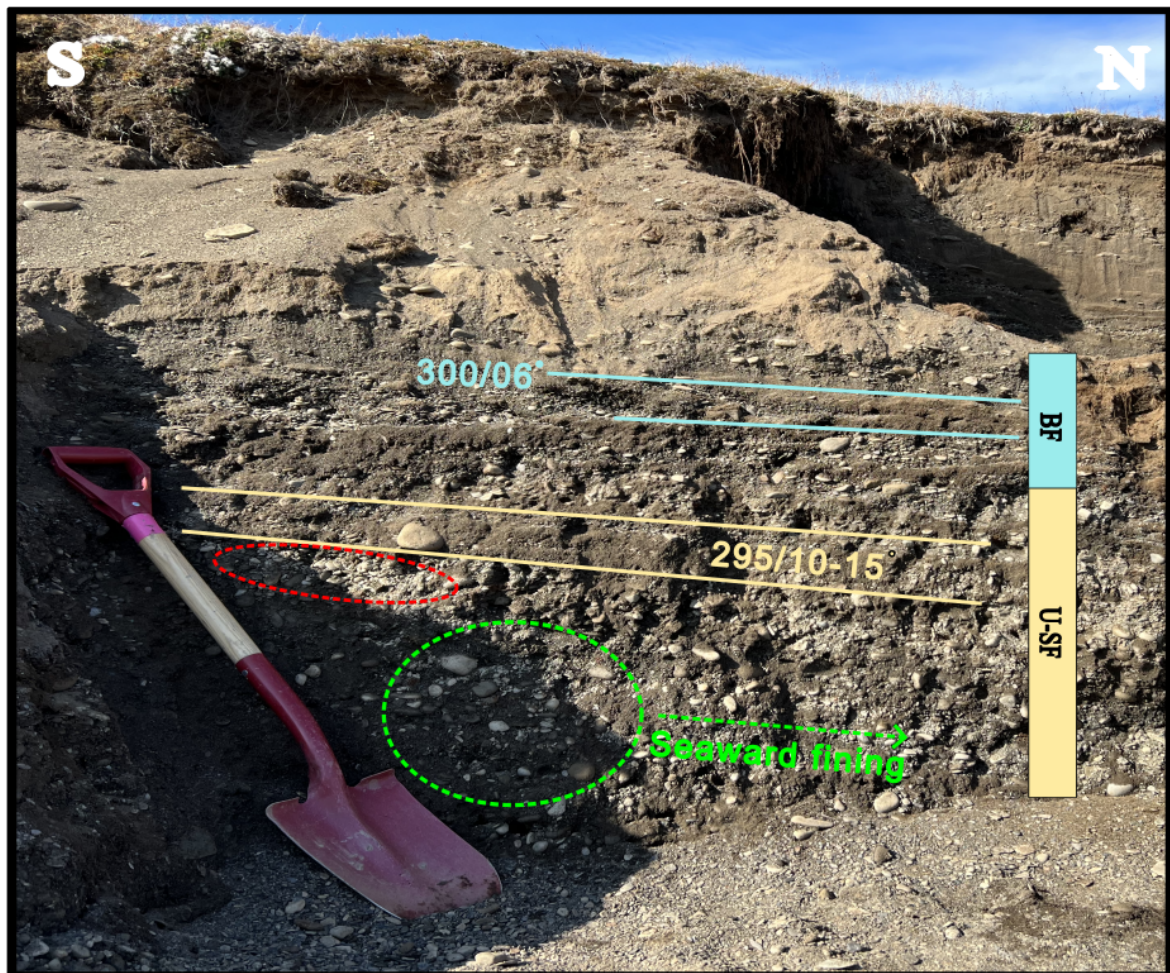


Figure 39: Annotated picture of the upper shoreface (U-SF) facies overlain by the beachface (BF) facies at the Arctica islandica Section at Bogebecken. Strike and dip of the bedding is indicated. Picture highlights the concentration of coarse pebbles accumulating at the base of the gravel plunge (dashed green line). Slight imbrication of clasts circled with a dashed red line. Shovel for scale.

## **Interpretation**

The depositional process acting on the upper shoreface is wave traction. The sharp and irregular boundary and significant increase in grain size indicates that the deposits were erosively emplaced over the middle shoreface deposits.

The coarse sand reflects deposition during fair weather energy conditions. During this period, shoaling waves cause sand to migrate up the shoreface whereas breaking waves mobilise sediment and transport it down the shoreface by backwash and undertow. In comparison, the coarse pebble gravels reflect deposition under higher energies, capable of mobilising and transporting larger material. This occurs when the beachface is eroded during storm events. Supporting deposition under higher energies such as storm events, is the weak normal grading, that could reflect the decrease in environmental energy as the storm wanes and passes. The interbedded nature and character of the two lithofacies is in accordance with the findings of Koster and Steel (1984) who state upper shoreface beach gravels are generally influenced by transport from onshore, offshore, and longshore mechanisms that produce clast-supported and sheet like conglomerates that exhibit normal grading.

The stacking of pebbles in Figure 39 reflects accumulation of clasts at the base of a morphological depression as spherical and rod-shaped clasts avalanche and topple down the steep shoreface slope (10-15 °). A common morphological feature in coarse-grained beach systems is a morphological step called a 'plunge', that occurs at the transition of the beachface to shoreface (Wright & Short, 1984; Hart & Plint, 1989; Aagaard et al., 2013). The steep inclination of the beds, their position at the base of the lower shoreface and its common occurrence on other coarse-grained beach systems supports deposition of these sediments in relation to the gravel plunge. The section of clast supported deposits with weak imbrication dipping in a seaward direction (Figure 39) likely reflects a period of beachface destruction, where offshore transport is dominating and the shoreface is building seaward. This may result from periods of high energy conditions causing rod shape clasts to roll and avalanche down the shoreface before their acceleration decreases and they stack against each other (De Giorgio et al., 2023). Lithofacies exhibiting similar seaward imbrication in coarse-grained beach systems, albeit with a more defined imbrication and segregation of clasts have been attributed to wave tractional processes, which largely supports the depositional mechanism and environment classification of the deposits within the upper shoreface (Bluck, 1967; Orford, 1977; Bluck, 2011).

#### 4.4.2.3.3 Beachface lithofacies

##### Description

Seven lithofacies are identified in the beachface sub-environment and they contain a higher percentage of sand to clasts compared to the upper shoreface deposits. There is a distinct change in the angle of dip of the bedding up sequence from 10-12 ° at the base to 2-6 ° at the top of the beachface. The beachface lithofacies contain clasts that are predominantly disc and blade shaped and a sharp, steeply dipping truncation dissects planar and often clast supported beach gravels (Figure 40). Overlying these beach gravels are cross bedded sands that dip in a landward direction (Figure 40). A fining upwards pebbly sand with isolated and outsized discoidal clasts caps the beachface deposits.

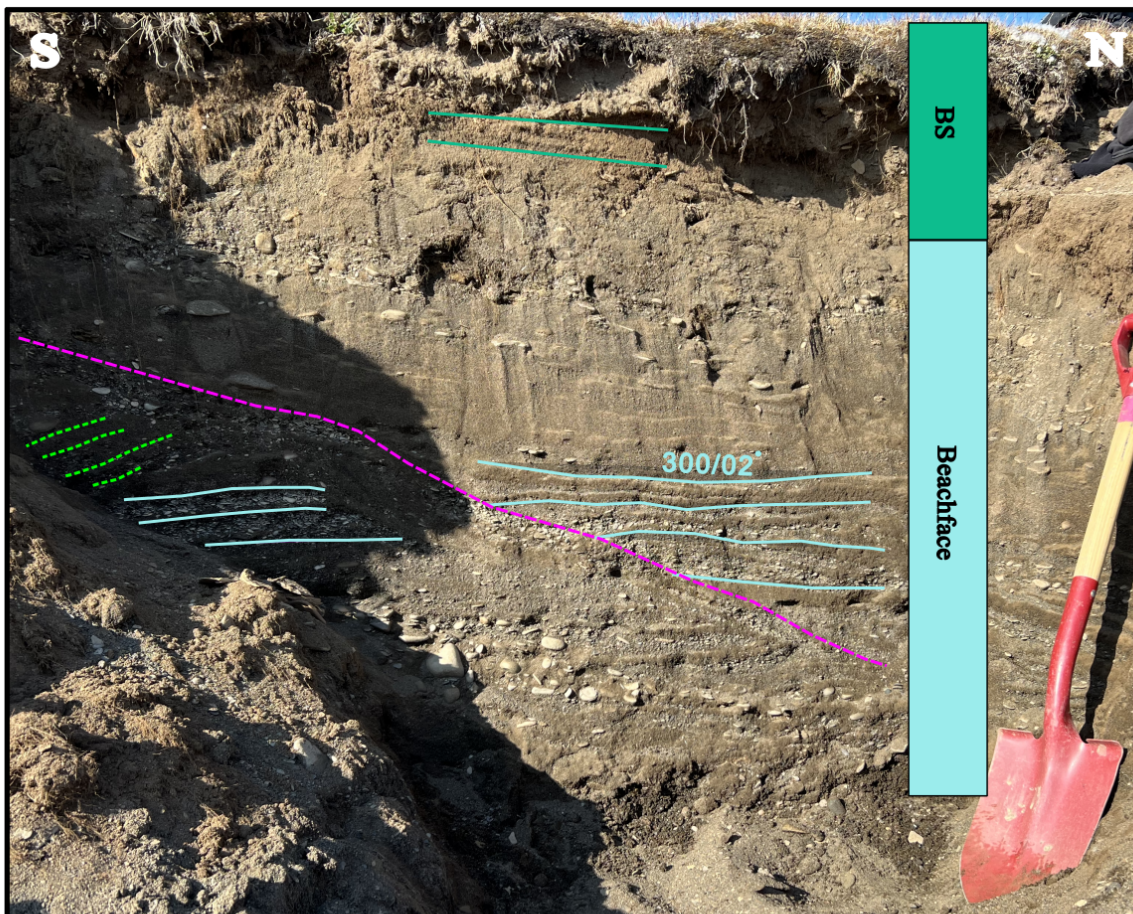


Figure 40: Annotated picture of the beachface (BF) and backshore (BS) sub-environments at the Arctica islandica Section at Bogebecken. Near planar, beach gravels highlighted with a solid light blue line. Landward dipping cross bedding highlighted with a dashed light green line. Steeply dipping truncation surface in dashed purple line. Near planar laminations of the BS highlighted with a dark green line.

## **Interpretation**

The beachface deposits result exclusively from wave traction processes. In coarse-grained gravel shorelines, the beachface is often steep and extends significantly below the water depth of a foreshore environment and so the terminology of ‘lower beachface’ (sub-tidal zone) and ‘upper beachface’ (intertidal zone) is commonly used in their classification (Bourgeois & Leithold, 1984; Massari & Parea, 1988; Postma & Nemec, 1990). Whilst this separation is followed in the sedimentary log and lithofacies descriptions, the interpretations of the lithofacies have been grouped into ‘beachface’ for simplicity.

Well sorted and well-rounded beach gravel and sands with planar laminations, likely reflect swash and backwash processes that are acting on the beachface under fair weather conditions and influencing the sorting of beach material (Bluck, 1967). The gravel and sands beds that are inclined at 4-6 ° with planar lamination are interpreted to reflect beachface aggradation in response to wave swash up the beachface. The coarse-grained character of the planar laminated deposits infers that they were deposited by upper-flow regime conditions that would occur due to wave swash. Deposits that are similar in texture and structure to these lithofacies are identified in Mid-Pleistocene microtidal, wave dominated gravel beach deposits from Southern Italy described by De Giorgio et al. (2023), where they are linked with the lower to upper beachface environment. Additionally, Bluck (1967) identified comparable sediments in South Wales and attributed the deposits to a “sand run” within the coarse grained beach environment. Correlation with these findings supports the depositional processes and attributed sub-environment of the gravel and sand deposits.

Morphological features that are common on sand and gravel beaches and are observed on the modern beach at Bogebecken are high tide and storm berms (Figure 47). During construction of these ridges, sediment is aggraded in a landward direction. This is reflected in the sediments at 7.55-7.6 m a.s.l. where the sand and gravels onlap planar laminated beach gravels and the cross beddings dips in a landward direction (Figure 40). These observations indicate that this section of the sequence reflects the construction of a beach berm as observed in the present-day beach at Bogebecken. The steep truncation surface that cuts through the sediment indicates a period of erosion where a storm events or high spring tides have caused the reworking of the beach berm. Subsequent return to fair weather conditions results in aggradation of beach gravels and sands against the truncation surface.

Progressing up section, the inclination of bedding within the beachface lithofacies decreases from 10-12 ° in the lower beachface to 2-6 ° in the upper beachface (Figure 34). This trend is similarly observed in the Holocene gravelly beach deposits in Crete that have been described by Postma and Nemeč (1990), which validates segregation of the lower and upper beachface deposits described in this sequence.

The transition from spherical and rod-shape clasts in the lower shoreface to disc and blade shaped clasts in the beachface reflects common grain shape segregation in coarse-grained beach systems (Bluck, 1967; Orford, 1978; Caldwell & Williams, 1985; Bluck, 2011). Outsized disc and blade-shaped clasts present within sandy deposits e.g. 7.6-7.8 m a.s.l., may result from emplacement of the clasts higher up the beachface during fair to moderate weather conditions, as the shape and surface area to weight ratio means moderate energy wave can throw them higher up the beachface (Bluck, 1967; Williams & Caldwell, 1988).

#### **4.4.2.3.4 Backshore lithofacies**

##### **Description**

One lithofacies is associated with the backshore environment (Table 8). The fining upwards medium to very fine sands that cap the sequence exhibit planar laminations. Occasionally, coarser grains are evident within, but these are exceptions. Rootlets penetrating through from the overlying vegetation are common.

##### **Interpretation**

The lithofacies is texturally comparable to the backshore lithofacies described at the Hollendardalen localities. It is similarly attributed to result from aeolian processes, where high velocity katabatic winds have transported finer grained sands down the valley, capping the beach sediments (Maxwell, 1980; Gilbert, 1983; Rasmussen et al., 2023). Progradational beaches have the tendency to coarsen upwards through the beachface lithofacies before a gradual fining takes place in the backshore beds (Maejima, 1982). Observation of this end to the sequence, capping both the backshore successions at Bogebeekken and Hollendardalen strengthens the interpretations that the planar laminated sands are indeed representative of a backshore environment.

### 4.4.3 Environmental synthesis

The *Arctica islandica* Section at Bogebeekken records a complete coarsening upwards sequence that includes six sub-environments: a lower, middle, and upper shoreface, lower and upper beachface and backshore. Similarly to Hollendardalen sections, this type of sequence indicates a shallowing of the marine environment in response to the governing regime controls of relative sea level fall, reduced accommodation space and infilling of the shallow marine environment with fine grained material as the shoreline prograded.

The lower to middle shoreface sediments are dated to *c.* 9.4-7.9 cal. ka BP (Sharin et al., 2014; Bakken, 2021). Over this time suspension fallout, nearshore currents and to a lesser extent, periods of ice-rafting contributed towards a high sedimentation rate and result in soft sediment deformation, wavy bedding, and lone stones (Brenchley & Newall, 1977; Mills, 1983; Mackiewicz et al., 1984; Lønne, 2005). The molluscan fauna is diverse with *Arctica islandica*, *Mya truncata*, *Macoma calcarea*, *Mytilus* sp. all present.

Significant indicator species are the thermophilous *Arctica islandica* and *Mytilus* sp. which provide insights into the water depth and water temperature of the shallow marine environment. *Arctica islandica* live in water 15-260 m deep, however, they are most commonly found at 30-60 m (Dahlgren et al., 2000). *Mytilus* sp., on the other hand, have a tighter constraint on their preferred water depth ranging from intertidal to 10 m (Peacock, 1993). The presence of both species within the lower and middle shoreface is recorded in this study and by Sharin et al. (2014) and Bakken (2021). Together, these observations indicate that the water depth in the lower and middle shoreface was likely around the upper limit for *Mytilus* sp. (*c.* 10 m) and the lower limit for the *Arctica islandica* (*c.* 15 m). Presently, the temperature limit for *Arctica islandica* is identified as 8.5 °C (Mangerud & Svendsen, 2018).  $\delta^{18}\text{O}$  profiles measured on *Arctica islandica* shells from Dicksonfjorden, Isfjorden, that date to *c.* 10.0 cal. ka BP indicate that water temperature at *c.* 30 m water depth was 6 °C warmer than present (Beierlein et al., 2015). Furthermore, temperature reconstructions conducted on *Arctica islandica* from the shoreface deposits at Bogebeekken, indicate warmer than present sea surface temperatures with a greater seasonality than present ranging from 6-10 °C (Christman, 2022). *Mytilus* sp., is also a thermophilous mollusc however, its recent re-immigration to Svalbard in 2004 (Berge et al., 2005) means it will not be discussed with

respects to “warmer than present” sea surface temperatures at Bogebecken and instead exclusively be used to constrain water depth.

The upper shoreface and beachface was dominated by wave traction and exhibits similar characteristics in grain shape, sorting and bed geometries to modern coarse-grained gravel beach systems (Bluck, 1967; Koster & Steel, 1984; Williams & Caldwell, 1988; De Giorgio et al., 2023). Capping the coarsening upwards and shallowing sequence are backshore deposits that gradually fine and indicate subaerial exposure (Maxwell, 1980; Maejima, 1982; Gilbert, 1983). The close proximity of the section to the present shoreline and the sedimentological observations above infers deposition in a shallowing, high energy and increasingly wave dominated coastal setting where water depth was *c.* 10-25 m with water temperatures warmer than present (Peacock, 1993; Dahlgren et al., 2000; Mangerud & Svendsen, 2018; Christman, 2022).

## **4.5 Modern environment**

The modern fluvial and beach system at Hollendardalen and Bogebecken includes numerous features that hold potential to provide an insight into the environmental and coastal evolution of Hollendarbukta from the Early Holocene to present day. Depositional processes and morphological features of both environments are analysed to assess the extent to which they may be sedimentary analogues for the Early Holocene environment.

### **4.5.1 Characteristics of Hollendarelva fluvial system**

Hollendarelva is a braided fluvial system that runs for *c.* 16 km from its source at the toe of Passfjellbreen to its mouth at Isfjorden. The catchment area for Hollendarelva is 87.78 km<sup>2</sup> and includes five valley glaciers and numerous tributaries that feed into the system (Figure 4) contributing to a combined inflow of *c.* 45.69 million m<sup>3</sup> per year (NVE, 2024).

At its widest point, the active braidplain extends *c.* 400-500 m and contains a main distributary channel that has transverse gravel bars along its edge and longitudinal gravel bars within the channel (Figure 41). Additionally, a secondary distributary channel is positioned to the west, as well as numerous tertiary channels. Skirting the margins of the active braidplain is an inactive braidplain that is identified through the presence of vegetated bars and inactive fluvial channels.



The active and inactive braidplain of Hollendarelva are separated by a *c.* 1-2 m erosional bank, cut by the active channel (Figure 41). Furthermore, separating Hollendarelva in the east and Bogebebben in the west is the main marine terrace that has formed the basis for this investigation that measures *c.* 8-13 m in elevation from the inactive braidplain.

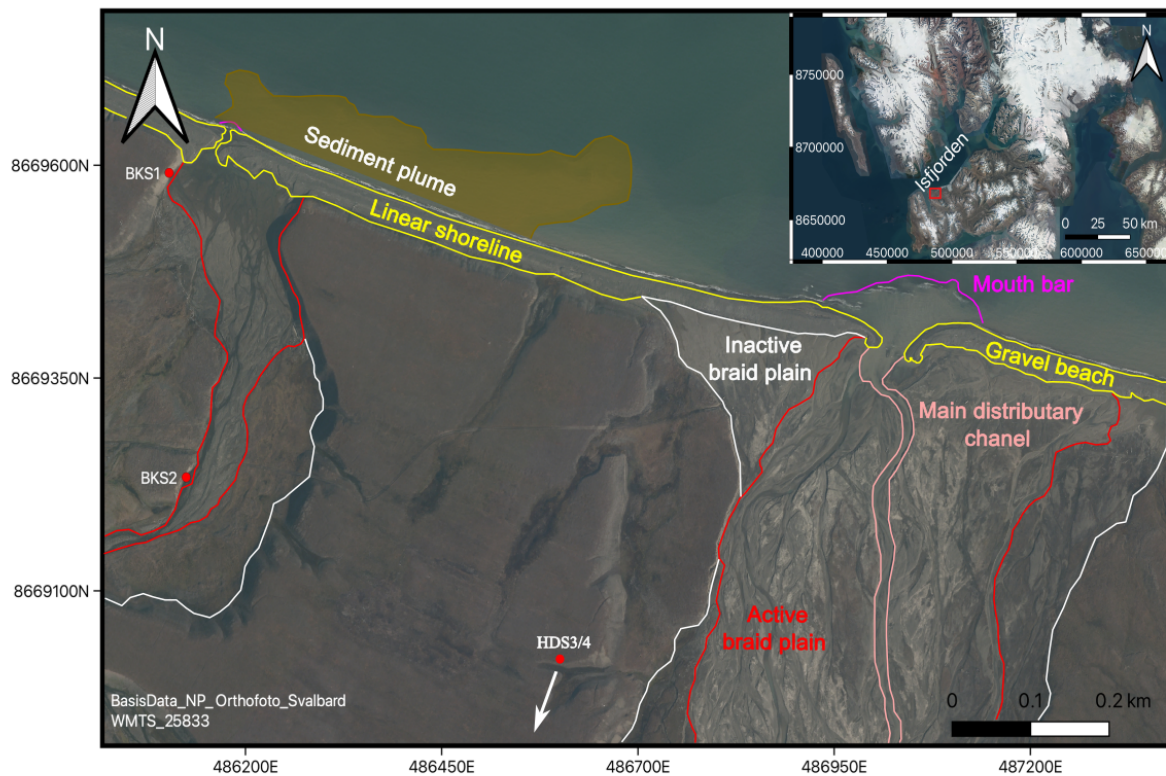


Figure 41: Annotated map showing the characteristics of the modern fluvial systems of Hollendarelva and Bogebebben as well as the present-day shoreline at Hollendarbukta.

Where Hollendarelva discharges into Isfjorden through its main distributary channel, a *c.* 200 m wide mouth bar is present. Evident within Hollendarbukta is a buoyant plume of suspended sediment sourced from Bogebebben and Hollendarelva (Figure 41). The expanse of the sediment plume will have a close relationship with river discharge, which over the summer months is primarily controlled by precipitation falling within the catchment area of Hollendarelva. Through assessing the extent of the plume over a period of high versus low precipitation presents an opportunity to investigate the extent to which the process contributes towards sedimentation in the shallow marine environment. In turn, this can contribute towards an enhanced understanding of sedimentation during the Early Holocene within the deltaic environment of Hollendarbukta. To quantitatively assess these processes, the analysis of precipitation data and satellite imagery is presented in the following section.

#### 4.5.1.1 Climate Data

The closest meteorological station to the study site is Isfjord Radio, which is located at Kapp Linné on the southern shore of Isfjorden, *c.* 20 km west of the study site. This proximity and open access of monthly precipitation values through the Norwegian Centre for Climate services (2023) enables quantification of the monthly precipitation values for July and August 2023. It is assumed that the precipitation values observed at Isfjord Radio are reliable to those received in the catchment at Hollendarelva.

The reference period of 2015-2023 was selected instead of the last normal period 1991-2020, firstly, as there was an absence of precipitation data from June 1967 to July 2015 for the station. Data from Svalbard Airport could have been used although this is 30 km further to the east and so the precipitation values were deemed less likely to be representative of those received in the catchment area of Hollendarelva. Additionally, the eight-year reference period is long enough to highlight that there is a great disparity in the monthly precipitation values for July (3 mm) and August (45.9 mm) in 2023 (Norwegian Centre for Climate services, 2023) (Figure 42). It also highlights the monthly precipitation values over these months have a <5-year return period (Figure 42) which means that the influence they have on fluvial discharge and thus the extent of the sediment plume can be considered relatively common.

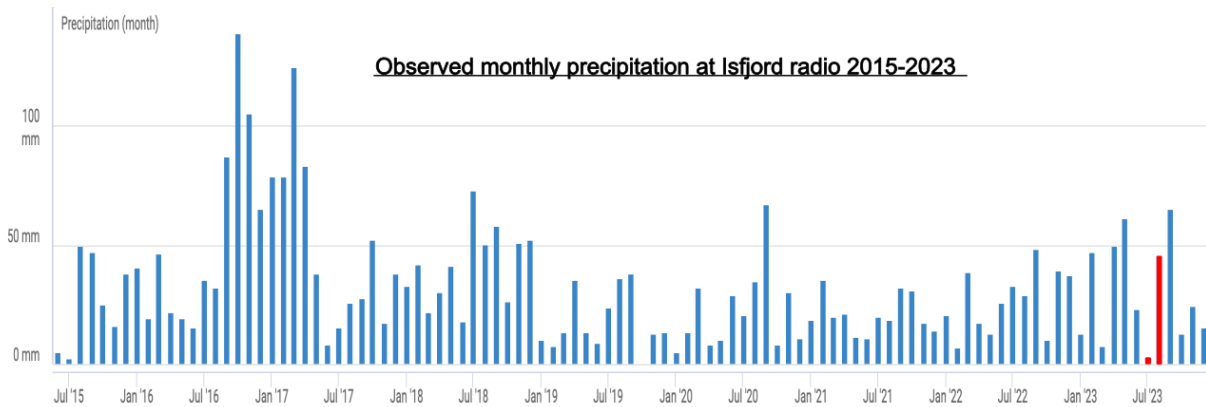


Figure 42: Observed monthly precipitation data collected at Isfjord Radio station for the period of 2015-2023. Monthly precipitation for July and August 2023 is highlighted with red bars. Data provided by: Norwegian Centre for Climate services (2023).

## 4.5.1.2 Satellite imagery

### 4.5.1.2.1 July 2023

On the 17<sup>th</sup> of July 2023, in a month where only 3 mm of precipitation fell, the sediment plume extended a maximum of *c.* 4.3 km north and covered an area *c.* 11.5 km<sup>2</sup> (Figure 43). The plume was concentrated in a shoreline proximal position (<1 km) where it was initially transported west. Further out into Isfjorden, the diluted distal extent of the plume drifted east.



Figure 43: Sentinel 2 satellite imagery of study site at Bøgebekken and Hollendardalen, collected on the 17/07/2023. Source of Copernicus Ecosystem Data Access Hub (<https://dataspace.copernicus.eu/browser>).

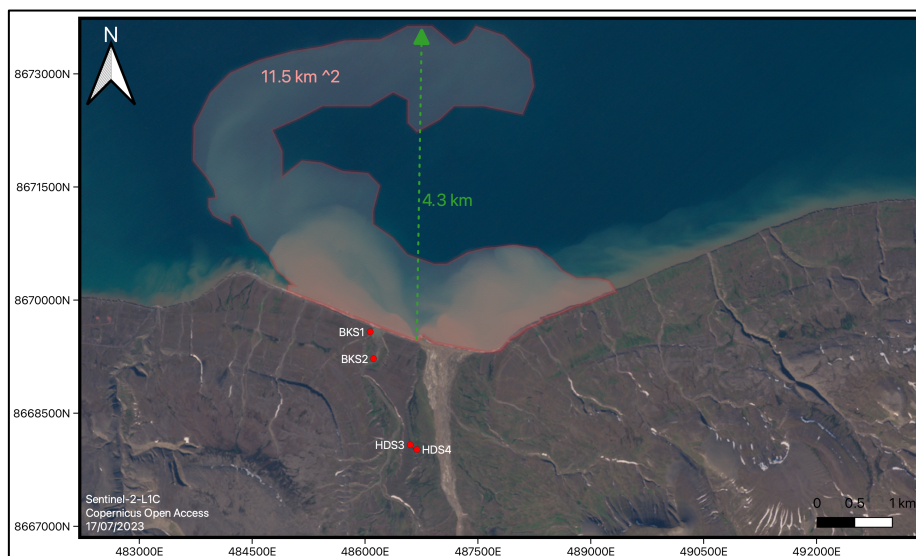


Figure 44: Annotated Sentinel 2 satellite imagery of study site at Bøgebekken and Hollendardalen, collected on the 17/07/2023. Source of data: Copernicus Ecosystem Data Access Hub (<https://dataspace.copernicus.eu/browser>).

#### 4.5.1.2.2 August 2023

In comparison, on the 8<sup>th</sup> of August 2023, in a month when 45.9 mm of precipitation fell, the sediment plume covered an area of *c.* 7 km<sup>2</sup> and extended a maximum of 7 km in an easterly direction along the coastline of Hollendarbukta (Figure 46). At the time the image was taken, the sediment plume was less expansive, but more concentrated, and extended almost twice as far from the coast than on the 17<sup>th</sup> of July.

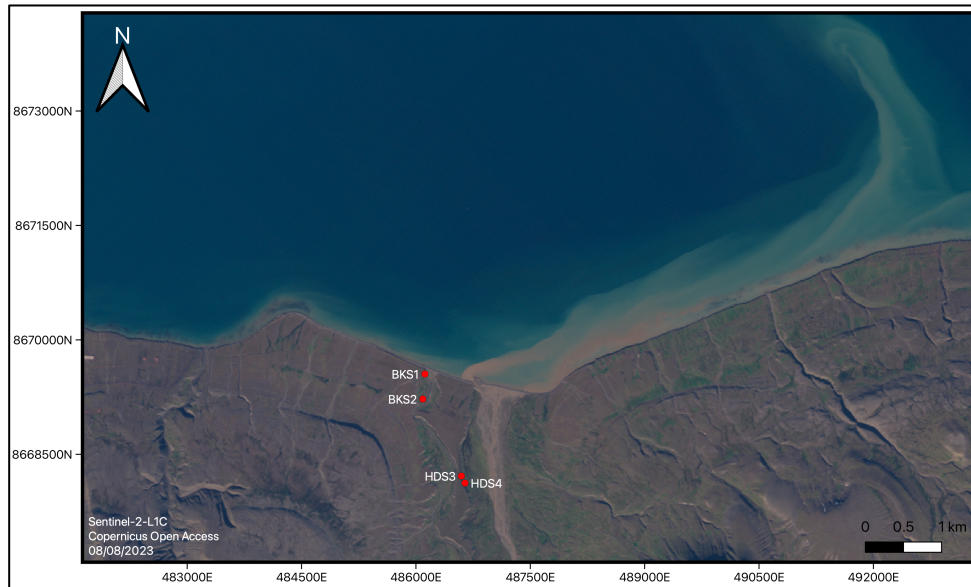


Figure 45: Sentinel 2 satellite imagery of study site at Bogebekken and Hollendardalen, collected on the 08/08/2023. Source of data: Copernicus Ecosystem Data Access Hub (<https://dataspace.copernicus.eu/browser>).

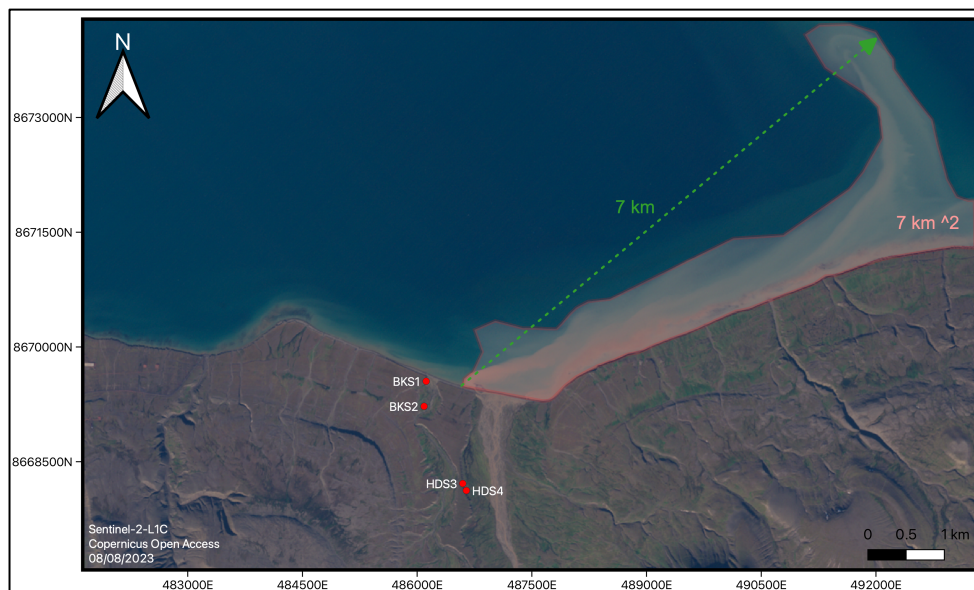


Figure 46: Annotated Sentinel 2 satellite imagery of study site at Bogebekken and Hollendardalen, collected on the 08/08/2023. Source of data: Copernicus Ecosystem Data Access Hub (<https://dataspace.copernicus.eu/browser>).

#### 4.5.1.3 Interpretation of satellite imagery

The precipitation data and satellite imagery highlight that Hollendarelva and Bogebeekken are capable of transporting sediment via a buoyant sediment plume up to 7 km from the river mouth, during months with high values >40 mm of precipitation. Even in months where precipitation is low (<5 mm), the sediment plume covers an area of 11 km<sup>2</sup>. This data supports the hypothesis that the fluvial systems entering Hollendarbukta contribute to sedimentation in the shallow marine environment to a considerable extent.

The investigated months are over the summer period when the rivers are fully open and there is a minimal snow cover, therefore river discharge is likely lower than the time following the spring snow melt. The results identify a positive correlation between the maximum extent and concentration of the sediment plume and higher monthly precipitation values. As precipitation volume directly correlates with river discharge, it seems reasonable to assume that following the spring snow melt, sediment influx to Hollendarbukta from both Bogebeekken and Hollendarelva would be considerably higher. In which case, these observations of the extent and expanse of sedimentation into the shallow marine are conservative over an annual period. This further strengthens the statement that the present-day fluvial systems of Hollendarelva and Bogebeekken influence sedimentation of the shallow marine environment of Hollendarbukta to a considerable extent. It is significant to highlight, that these observations do not include the influence of temperature during the investigated period. With five glaciers within the catchment area of Hollendarelva (Figure 4), a warm and sunny day over the summertime would undoubtedly influence the degree of melt water generated and supplied to the fluvial system, especially from the largest of the valley glaciers Passfjellbreen. In which case, it cannot be commented on to what extent this has influenced the extent and concentration of the sediment plume on the selected days although it is noted that this is an uncertainty in the investigation.

Despite the uncertainties, this data strengthens the interpretations that sedimentation in the Early Holocene embayed deltaic environment of the study site, was largely influenced by deposition from suspended sediment plumes entering the shallow marine environment, likely from a well-established, braided fluvial system. In which case, the present-day braided fluvial system can to some extent be considered as a modern analogue to the Early Holocene braided deltaic system, that supplied the embayed coastline with fine grained sediment during the initial stages of coastal evolution. It is evident that once the sediment plume enters

Hollendarbukta, basin processes such as wave action, tidal range, and wind energy influences dispersal of the sediment plume, as indicated by the varied trajectory of the sediment plume in both an easterly and westerly direction (Figure 43 and 45). Having identified the Early Holocene deltaic system occurred in an embayed coastal setting, it is probable that wave reworking and redistribution occurred to a lesser extent than is observed in the present-day linear shoreline. A considerable difference that likely exists between the modern braided system at Hollendarelva and the Early Holocene system is glaciers margin and ice extent. This would play a crucial role in the volume, delivery and turbidity of melt water supplied to the shallow marine and thus influence the extent and concentration of the sediment plume. As a result, the modern fluvial system at Hollendarelva is concluded as acting as a reasonable modern analogue to the Early Holocene system.

#### **4.5.2 Characteristics of Bogebecken shoreline**

The modern beach at Bogebecken is characterised by a linear sand and gravel shoreline affected by oblique waves and a *c.* 1.5 m tidal range (The Norwegian Mapping Authority 2014). Two morphological ridges run parallel to the shoreline and are classified as a high tide and storm berm (Figure 47). The two berms are steep faced with an amplitude of *c.* 20-30 cm and are separated by a *c.* 10 m distance from each other. Coarse pebble clasts were observed on the upper surface of the high tide berm and driftwood is evident on the storm berm. Cutting the beachface is the fluvial channel of Bogebecken and a *c.* 30 m wide mouthbar that becomes partially sub-aerial during low spring tides. Behind the beachface is the *c.* 8 m high raised marine terrace that has permafrost polygons on its surface.

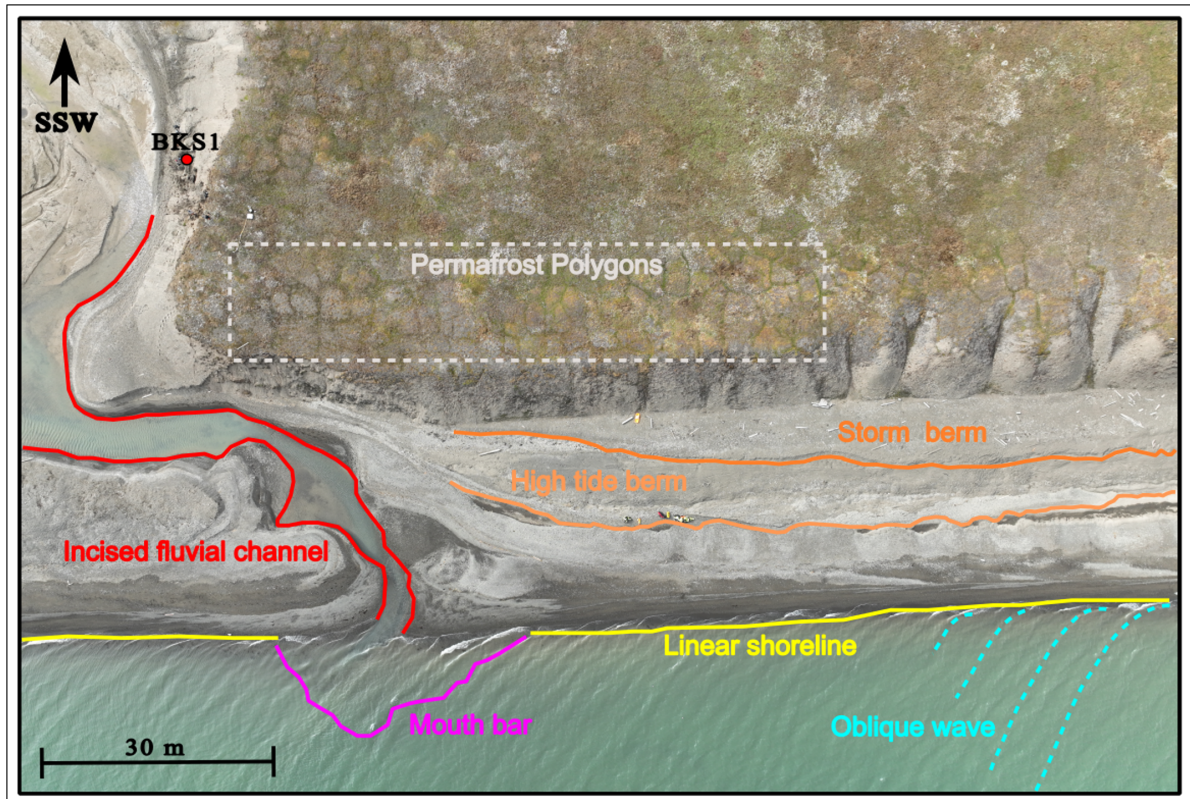


Figure 47: Annotated drone image of the modern shoreline at Bogebecken indicating the morphology of the linear gravel beach that is affected by oblique waves hitting the beachface. High tide and storm berms are highlighted on the beachface with a narrow-incised channel breaching the beach. Permafrost polygons are present on the raised marine terrace.

#### 4.5.2.1 Analogue interpretation: wave dominated shoreline

The morphology of the modern linear shoreline at Bogebecken is shaped by wave action with the presence of a storm berm indicating the beachface is subject to periods of high energies induced by storms. Morphological features with a similar sediment character to the beachface berms on the modern beach are recognised in the sedimentary record of the *Arctica islandica* Section at Bogebecken (Figure 40). This supports the depositional processes and resulting morphologies as forming within a high energy, wave dominated, beachface environment. The present-day shoreline at Bogebecken therefore holds a reasonable potential to be considered as a modern analogue to the Middle Holocene, gravel beach deposits.

## 5 Discussion

### 5.1 Assigning a relative sea level curve

To understand the evolution of the coastal environment within Bogebeekken in response to deglaciation, association of the landforms and elevation of the base of sections with a relative sea level (RSL) curve is necessary. As no curve has been directly established for the study site, and this study does not provide adequate data for the construction of a curve, adopting one that is suitable is required. As Figure 8 illustrates, the marine limit as well as glacio-isostatic uplift rates around Svalbard are highly variable (Forman et al., 2004; Farnsworth et al., 2020). This ultimately results from variations in glacial history and behaviour which is controlled by ice-cover thickness, duration, and the timing of deglaciation (Ingólfsson & Landvik, 2013; Fjeldskaar et al., 2018; Farnsworth et al., 2020). Considerable differences in marine limit and rates of glacio-isostatic uplift emphasise the significance of selecting an appropriate RSL curve for the study site that is most comparable with respects to marine limit and rate of uplift.

Previously, Sharin et al. (2014) established the marine limit within Hollendarbukta to be 70 m a.s.l., based on the elevation of the highest observable beach ridges on the coastline. This is similar to sites in close proximity to Hollendarbukta, for example Grønfjorden, the neighbouring fjord to the west, where Mangerund and Svendsen (1990) identified the marine limit to also be 70 m a.s.l. Furthermore, at Kapp Linné, *c.* 16 km west of Hollendarbukta, a marine limit of 70 m a.s.l. was established (Johnson, 2020). Geomorphic mapping conducted in this study identifies the marine limit to be *c.* 65 m a.s.l. Discrepancy between the results may come from differences in observations conducted by field versus remote mapping techniques and/or the precision of elevation data. Additionally, slope processes such as solifluction may have altered the highest elevated beach ridges making them more difficult to identify through remote mapping. As this study identifies a broad *c.* 10-20 m wide band of colluvium above the highest elevated beach ridges this is probable (Figure 13). Johnson (2020) produced a RSL curve for Kapp Linné that is not only in close proximity to Hollendarbukta on the western shore of Isfjorden, but also with a similarly identified marine limit. As a result, this RSL curve holds potential to be applicable to Hollendarbukta, and so the dates were recalibrated accordingly and the RSL curve is presented in Figure 48. To add comparison to the RSL curve by Johnson (2020) and validate its suitability in this study, two other RSL curves in close proximity to Hollendarbukta are analysed.



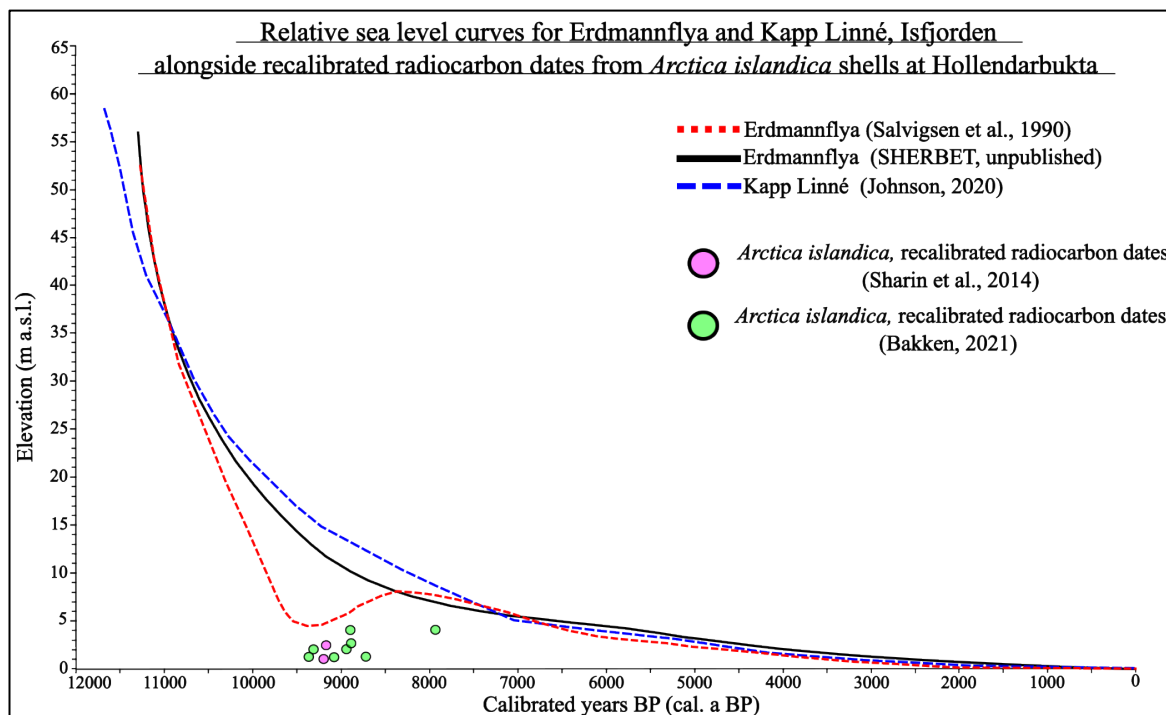


Figure 48: Recalibrated relative sea level curves for Erdmannflya, Isfjorden from Salvigsen et al., 1990 (red dashed line) and SHERBET, unpublished project (Mark Furze pers comm.). Kapp Linné relative sea level curve from Johnson (2020). All dates used in construction of the RSL curve have been recalibrated with the Marine20 calibration curve (Heaton et al., 2020) using the online calibration programme Calib 8.20 (<http://calib.org/calib/calib.html>) provided by (Stuiver & Reimer, 1993) with a  $\Delta R$  correction age of  $-61 \pm 37$   $^{14}\text{C}$  applied (Pieńkowski et al., 2022). Recalibrated *Arctica islandica* ages from the *Arctica islandica* Section at Bogebeekken (BKS1) from Bakken (2021) in green and Sharin et al. (2014) in purple.

At Bohemanflya, across Isfjorden and opposite to Hollendarbukta (Figure 1), Salvigsen et al. (1990) established a marine limit of *c.* 65.5 m a.s.l., through evidence of wave wash on the slopes of ‘Cairnhill’. Several kilometres to the west, Salvigsen et al. (1990) identified marine sediments at *c.* 53 m a.s.l. on Erdmannflya, east of Esmarkbreen, and concluded that this was likely the marine limit there. With these findings, they constructed a RSL curve for Erdmannflya (Figure 48). Recent unpublished work conducted at Erdmannflya as part of the Svalbard Holocene Elucidation of Raised Beach Emergence and Timing project (SHERBET) identified a new marine limit at 56 m a.s.l. (Mark Furze pers. comm.). Additionally, the project recalibrated the original dates from Salvigsen et al. (1990) and with the addition of new dates, constructed a revised RSL curve for the site (Figure 48). The addition of new dates and recalibration of Salvigsen et al. (1990) old dates results in a RSL curve that is more robust. This includes the removal of the proposed marine transgression at *c.* 9.5 cal. ka BP put forward by Salvigsen et al. (1990) due to a well constrained, in both time and elevation, whale cranium at 13.5 m a.s.l. that dates to 9.4 cal. ka BP (Mark Furze pers comm.). This new finding leaves no room in the RSL curve for the proposed marine transgression at Erdmannflya (Figure 48) and as a result, the transgression is dismissed. The revised marine

limit is also more comparable to the marine limit at Hollendarbukta, which increases the revised RSL curves suitability for use in this investigation. Furthermore, the close proximity of the two sites means they likely lie on the same glacio-isostatic isobase and so have been affected by a comparable degree of crustal loading during the LGM of the SBIS (Forman et al., 2004). This further validates the use of the sea level curve for application in the study.

Despite slight differences, the revised RSL curve for Erdmannflya and Kapp Linné are relatively comparable considering marine limit, and proximity to Hollendarbukta. Therefore, they are deemed most suitable for use in this investigation as no direct RSL curve for Hollendarbukta is available.

## 5.2 Constraining ages of undated sections

The lack of dates for the sections in Hollendardalen (HDS3 and HDS4) and the *Mya truncata* Section at Bogebecken (BKS2) means their ages are tentatively based on their stratigraphic position up-valley, the correlation of elevation data with the assigned RSL curve and extrapolation of other published work regarding the first occurrence of mollusc shells.

The Hollendardalen sections, contain no molluscs and so their stratigraphic position up-valley along with the elevation data for the base of the sections is used to determine their relative age compared to the two sections at Bogebecken. As the outcrops at Hollendardalen are positioned furthest from the present-day shoreline and have the highest elevation at their surface, through applying basic principles of sequence stratigraphy, it is possible to determine that they have been deposited before the sections in Bogebecken. To assign an age to the section is more problematic, although correlating elevation data with the assigned sea level curve is to some extent useful. Mollusc shells were not present within the outcrop and so water depth at the time of deposition cannot be well constrained. However, the marine terrace directly above the sections at Hollendardalen is elevated at *c.* 30.5 m a.s.l., which when correlated with the RSL curve (including several meters adjustment for the beach ridge/sea level relationship) indicates an age of *c.* 11.0 cal. ka BP. This age of deposition for the backshore and beachface at Hollendardalen aligns with the section being the oldest of the deposits studied within this investigation and is assigned whilst recognising its uncertainty. Validating this method of age constraint is the close association that the dated *Arctica islandica* and observed *Mytilus* sp. shells show with the two RSL curves in Figure 48, once the proposed correction for 10-25 m water depth discussed in §4.4.3 has been applied

(Peacock, 1993). In this case, the dated *Arctica islandica* shells align more closely with the RSL established by Johnson (2020), which strengthens its suitability and application in this investigation.

The *Mya truncata* Section in Bogebecken is assigned the tentative age of <11-10.8 cal. ka BP determined by the presence of a *Mytilus* sp. shell within the section. This age assumes that for the *Mytilus* sp. to be present, the deposit must be younger than the age of its first occurrence in Svalbard during the Holocene. *Mytilus* sp. were first observed on the west coast of Spitsbergen at Kaffiøyra at c. 11-10.8 cal. ka BP (Goslar & Pazdur, 1985; Mangerud & Svendsen, 2018) and no later than 10.6 cal. ka BP they had rapidly spread, reaching Kapp Ekholm at the head of Isfjorden (Mangerud & Svendsen, 2018). Kaffiøyra is c. 80 km north of Isfjorden (Figure 1) and considering the rapid migration of *Mytilus* sp. after their first occurrence on the west coast of Spitsbergen (Mangerud & Svendsen, 2018), it seems probable that they would have arrived shortly after their first occurrence on the west coast. It is recognised that neither author studied the sites at Bogebecken and so the assigned date has a large amount of uncertainty.

### **5.3 Coastal evolution**

Using the presented results from the three investigated sites at Hollendardalen and Bogebecken as well as other published and unpublished literature, a timeline for the coastal evolution of the study area is proposed. This is discussed in relation to processes, products, and environmental controls such as climate, sediment supply and glacial state that may have influenced the shallow marine environment during its evolution.

#### **5.3.1 Deglaciation**

The mouth of Isfjorden was deglaciated at c. 14.1 cal. ka BP with the final glacial retreat into the inner parts of its tributaries approximately 11.3 cal. ka BP (Mangerud et al., 1992; Elverhøi et al., 1995; Svendsen et al., 1996; Mangerud et al., 1998; Lønne, 2005).

Recently, two *Hiatella arctica* shells from a diamict-terrace elevated at 52 m a.s.l. at Heftyevatnet, Grønfjorden have been dated to c. 12.9-12.8 cal. ka BP (Farnsworth et al., 2022) which indicates open marine conditions and suggests deglaciation of Grønfjorden occurred c. 1.5 ka earlier than Mangerud et al. (1992) proposed. Grønfjorden is c. 7 km west of the study sites at Hollendarbukta and so in light of the new dates provided by Farnsworth

et al. (2022) it is reasonable to associate the deglaciation and open marine conditions within Hollendabrukta to approximately the same time at *c.* 12.9-12.8 cal. ka BP. Concurrent with deglaciation was transgression of the marine environment onto the coastal plain marked in Hollendardalen by shorelines cut into the coastline to an elevation of *c.* 65 m a.s.l. (Figure 13). The highest elevated beach ridges on the western edge of the valley are orientated with their strike perpendicular to the present-day shoreline (Figure 13). This indicates that, as expected, under the marine high-stand, Hollendarbukta was an embayed fjord side coastline. Following this marine transgression, was rapid glacio-isostatic uplift with an emergence rate of 2-3 m per 100 years (Forman et al., 2004; Farnsworth et al., 2020) and in light of the recent findings up to 4.5 m per 100 years in close proximity to the study site (Farnsworth et al., 2022). Rapid glacio-isostatic uplift would have resulted in a rapidly falling relative sea level.

### **5.3.2 Early Holocene**

#### **5.3.2.1 >9.4 to 7.9 cal. ka BP**

Despite the uncertainty in ages, the sedimentary record indicates that during the early stages of coastal evolution of Hollendarbukta, the shallow marine environment was characterised by a fjord side deltaic environment. Stratigraphic investigation of the outcrops in Hollendardalen reveal the segregation of this coarsening sequence into five sub-environments that include a prodelta, lower delta slope, upper delta slope, delta-front beach, and backshore. In the context of rapid (10-25 m per 1.0 ka) glacio-isostatic uplift during the Early Holocene (Salvigsen, 1981; Salvigsen & Österholm, 1982; Forman et al., 2004) the regime controls dominating valley evolution at this time would be basin depth and relative sea level. As relative sea level fell rapidly, the accommodation space available for sediment to accumulate within would have drastically reduced, causing the infilling of the shallow marine and progradation of the shoreline during this time interval (Corner, 2006).

Likely also contributing to this rapidly prograding shoreline, is the equally significant regime control of sediment supply that is interpreted to be high for the following reasons. The catchment area for Hollendarelva is 87.78 km<sup>2</sup> (NVE, 2024) and at present contains five valley glaciers (Figure 4). The catchment area is sizeable and thus supply of sediment from fluvial and glaciofluvial cannibalisation of the landscape post glaciation would facilitate a high sediment yield to the shallow marine environment, promoting rapid shoreline

progradation. During this time interval (prior to 8.8 cal. ka BP) the highest sedimentation rates throughout the Holocene are observed in central Isfjorden (Forwick & Vorren, 2009).

Furthermore, glacial lake records from Linnévatnet in close proximity to the study site and along the Western Spitsbergen coast, indicate that glaciers were absent from the valley catchment during the Early Holocene (Svendsen & Mangerud, 1997; Snyder et al., 2000). However, more recent findings based on relative sea level modelling from Fjeldskaar et al. (2018) indicate that glaciers on Svalbard did survive the HTM, although these were predominantly confined to the Nordaustlandet and Eastern Spitsbergen. This is in accordance with the findings of Forwick and Vorren (2009) that suggest similarly to present-day, a strong E-W temperature gradient existed across Svalbard (cooler east and relatively warmer west). As this investigation focusses on a site on the west coast, it seems more reasonable to align with the findings of Svendsen and Mangerud (1997) and Snyder et al. (2000), and assume that the five glaciers in their valley were drastically reduced in size or even absent during the Early Holocene. Further lines of evidence that support this include the findings of Birks (1991) that suggest mean July temperatures on the western coast of Spitsbergen were *c.* 2 °C higher than present. Mangerud and Svendsen (2018) suggest summer surface water temperatures as much as 6 °C warmer than present between *c.* 10.2-9.7 cal. ka BP based on the presence of the thermophilous mollusc *Zirfaea crispata* in raised marine sediments at Kapp Ekholm. In line with this, temperature is alkenone records from lakes in Northern Svalbard that have been used to reconstruct peak Early Holocene temperatures as high as 7° C warmer than present due to enhanced radiative forcing and intensified warm Atlantic Water inflow (van der Bilt et al., 2019). The melting of these glaciers within the catchment area of Hollendarelva would undoubtedly contribute towards a considerable sediment supply to the shallow marine environment promoting shoreline progradation.

The deltaic sedimentary succession at Hollendardalen is interpreted to reflect highly seasonal sediment supplies that are largely modulated by fluvial activity. A strong seasonality reflected within the early stages of coastal evolution of Hollendarbukta may reflect higher summer and lower winter insolation than present during this time interval (Berger & Loutre, 1991; Renssen et al., 2012; Zhang et al., 2016). Indeed, it is not only the sedimentary record of the shallow marine environment that records a highly seasonal Early Holocene. Offsets in  $\delta^{18}\text{O}$  values of benthic foraminifera *Nonionellina labradorica* and *Cibicides lobatulus* used to interpret bottom water temperatures reveal seasonal contrasts in Atlantic bottom water within

Isfjorden prior to c. 8.2 cal. ka BP (Rasmussen et al., 2012). Drawing this seasonality back to the terrestrial realm, the glacial lake records of van der Bilt et al. (2019) indicate Early Holocene temperatures fluctuating between the coldest and warmest of the past 12 cal. ka BP. Under these climatic and marine environmental conditions, it is unsurprising that a strong seasonality is recorded within the early stages of coastal evolution of the shallow marine sedimentary succession in Hollendarbukta.

As the deltaic system progressed throughout the side entry fjord during the Early Holocene, the *Mya truncata* Section at Bogebeekken indicates that the shallow marine environment at Bogebeekken was at least to some extent influenced by glacial activity within Isfjorden. Whilst the outcrop provides only a glimpse into conditions prior to 8.9-7.9 cal. ka BP, it holds significance not least in acting as a distinct comparison to the *Arctica islandica* section. Characteristics of the glacimarine deltaic bottomset indicate that a high sediment supply was a governing regime control during the deposition of this unit. Strengthening this interpretation is the frequent occurrence of *Mya truncata* specimens that were observed in a growth position with their siphons out and preserved in the sediment. Sedimentation up-valley at the Hollendardalen outcrops is argued to reflect catchment area size, paraglacial landscape readjustment in response to glacial ablation and enhanced fluvial activity relating to a prominent seasonality. In the glacimarine deltaic bottomset, sedimentation is likely to reflect a high sedimentation from the above, but also ice-rafting processes that reflect glacial state both within the catchment area and Isfjorden system. The poor time constraint on the glacimarine unit in Bogebeekken broadly being younger than the first occurrence of *Mytilus* sp. in Svalbard <11.0-10.8 cal. ka BP (Goslar & Pazdur, 1985; Mangerud & Svendsen, 2018) means correlations with periods of ice rafting within Isfjorden is limited. However, deposition of the section likely occurred just before, or even during the Holocene Thermal Maximum on the Western Spitsbergen continental margin 10.0-9.0/8.8 cal. ka BP (Birks, 1991; Salvigsen et al., 1992; Sarnthein et al., 2003; Hald et al., 2004; Rasmussen et al., 2007). Within Isfjorden, this time corresponds with a period of significantly reduced ice-rafting (Forwick & Vorren, 2009). This makes it unlikely that ice-rafting played a dominant role on sedimentation during the deposition of the unit, however, it certainly left a signature.

Ensuing the Holocene Thermal Maximum, it is interpreted that ice-rafting in Isfjorden after 10.2 cal. ka BP occurred exclusively from icebergs, most likely produced by tidewater glaciers on East Spitsbergen and transported west due to a strong temperature gradient at the

time (Forwick & Vorren, 2009). The presence of ice-rafted material within this section that fits in grain size and shape with iceberg rafted material, aligns with these findings and provides a degree of evidence supporting the work of Forwick and Vorren (2009). On this note, it would be interesting to hypothesise to what extent Hollendarbukta's position close to the mouth of Isfjorden may have favoured the accumulation of icebergs transported into the fjord system. Conversely, given the outcrops association with an embayed deltaic coastal environment, to what extent the input of freshwater from the fluvial system had on the formation of shore-fast ice and seasonal sea ice within Hollendarbukta during the time of deposition. Enhanced meltwater, fluvial runoff (Swingedouw et al., 2008) and increased precipitation (Marsland & Wolff, 2001; Liu & Curry, 2010) resulting in increased stratification of marine environments are all mechanisms which have been attributed to potentially contribute towards increase sea ice and shore-fast ice concentrations in polar regions (Brendryen et al., 2015). Under the circumstances of a highly seasonal Early Holocene climate, it seems probable that such mechanisms may to some extents have influenced the hydrological system within Hollendarbukta at the time of deposition of the glacial marine bottomset deposit. As a result, enhanced shore-fast ice and seasonal sea ice within the fjord side environment may have controlled the influence of ice-rafted material within the deposit. On one hand, enhancing it through beach plucking of material from the littoral zone, which could have provided the mechanism for transport of the *Mytilus* sp. shell. Alternatively, acting as a seasonal barrier preventing icebergs from being transported into fjord side environments (Forwick & Vorren, 2009).

Recognition of deltaic deposits with distinct characteristics indicating relative influences of regime control such as basin depth, sediment supply, climatic forcing and glacial state have altogether provided an insight into the Early Holocene coastal and environmental evolution of Hollendarbukta during the interval >9.4-7.9 cal. ka BP.

#### **5.3.2.2 9.4-7.9 cal. ka BP**

The lower and middle shoreface deposits in the *Arctica islandica* Section at Bogebecken (BKS1) were deposited between *c.* 9.4-7.9 cal. ka BP (Sharin et al., 2014; Bakken, 2021) (Figure 48). This broadly coincides with the timing of the Holocene Thermal Maximum on the Western Spitsbergen continental margin 10.0-9.0/8.8 cal. ka BP (Birks, 1991; Salvigsen et al., 1992; Sarnthein et al., 2003; Hald et al., 2004; Rasmussen et al., 2007). Over this period, there was an increased influence of Atlantic Water along the Svalbard shelf and slope

(Ślubowska et al., 2005; Rasmussen et al., 2007; Ślubowska-Woldengen et al., 2007; Skirbekk et al., 2010). Additionally, sediment cores from inner-Isfjorden reveal a dominance of *Nonionellina labradorica* that correlates with maximum Atlantic Water intrusion at the bottom of Isfjorden over the summer months (Rasmussen et al., 2012). The lower and middle shoreface deposits at Bogebekken were therefore deposited during a time when Atlantic Water was present throughout Isfjorden, with the capability of influencing the shallow marine environment.

The oldest of the sediments in the lower shoreface at 1-1.3 m a.s.l. date to *c.* 9.4 cal. ka BP (Bakken, 2021) and so fall in line with what Mangerud and Svendsen (2018) defined as “the peak warmth of the thermal maximum, 10.2-9.2 cal. ka BP”. Additionally, three *Arctica islandica* shells between 1-2.5 m a.s.l. date to *c.* 9.2-9.3 cal. ka BP (Sharin et al., 2014; Bakken, 2021) and thus fall somewhat in line with the proposed peak warmth in the shallow marine during the Holocene Thermal Maximum (Mangerud & Svendsen, 2018). At this time, Mangerud and Svendsen (2018) suggest that summer surface water temperatures around Isfjorden were 6 °C warmer than present predominantly based on the occurrence of the thermophilous mollusc *Zirfaea crispata* at Kapp Ekholm. Their findings are to a large extent concurrent with Beierlein et al. (2015) who demonstrate through measuring  $\delta^{18}\text{O}$  profiles of *Arctica islandica* shells from Dicksonfjorden, Isfjorden that water temperatures at *c.* 30 m water depth were 6 °C warmer than present at *c.* 10.0 cal. ka BP.

Bogebekken contained no *Zirfaea crispata* and the dates of the *Arctica islandica* are considerably younger than the those that indicate 6 °C warmer than present water temperatures at 10.0 cal. ka BP (Beierlein et al., 2015). Furthermore, temperature reconstructions conducted on *Arctica islandica* from Bogebekken at *c.* 9.4 cal. ka BP suggest sea surface temperatures ranged between 6-8 °C (Christman, 2022), which is warmer than present, although not as warm as reconstructed by Beierlein et al. (2015) for Dicksonfjorden. This suggests that whilst the lower shoreface deposits and *Arctica islandica* at Bogebekken fall in line with this period of peak warmth, towards the end of this period, a cooling of sea surface temperatures in the shallow marine may have been experienced. Despite this, the four recalibrated dates of *Arctica islandica* between *c.* 9.4-9.2 cal. ka BP (Sharin et al., 2014; Bakken, 2021) provide a degree of support to strengthen the suggestion that considerably warmer than present conditions occurred between 10.2-9.2 cal. ka BP in the shallow marine environment of Isfjorden.



On the other hand, this investigation identifies *Arctica islandica* shells regularly throughout the lower and middle shoreface deposits (Figure 35). The youngest date (*c.* 7.9 cal. ka BP) at the highest elevation above sea level (4-4.1 m a.s.l.) disagrees with the suggestion of Mangerud and Svendsen (2018), that following 8.2 cal. ka BP, the waters in the shallow marine environment were not as warm as during the thermal maximum. Whilst this may be true, another date at the same elevation recalibrated from Bakken (2021) reveals an age of *c.* 8.7 cal. ka BP. This highlights a large discrepancy between the age ranges of the dates from similar heights above sea level that are used in this investigation. As a result, the dates hold little insight in to constraining the timing of peak warmth in the shallow marine environment of Isfjorden that is at present determined as *c.* 10.2-9.2 cal. ka BP (Mangerud & Svendsen, 2018). Despite this, using the oldest age of *c.* 8.7 cal. ka BP at 4-4.1 m a.s.l. (Bakken, 2021), it can be concluded that the lower to middle shoreface sediments fall in line deposition during the timing of the Holocene Thermal Maximum on the Western Spitsbergen continental margin 10.0-9.0/8.8 cal. ka BP (Birks, 1991; Salvigsen et al., 1992; Sarnthein et al., 2003; Hald et al., 2004; Rasmussen et al., 2007). Despite a broad time constraint and age zonation on the *Arctica islandica* shells within BKS1 (Table 1), their presence infers that climate and oceanic forcing through Atlantic Water intrusion, were largely influential in the environmental evolution of the shallow marine setting at the time of deposition.

Aside from climatic and oceanographic forcing influencing the evolution of the shallow marine environment between *c.* 9.4-7.9 cal. ka BP, the RSL curve in Figure 48 indicates that relative sea level fall was still a considerable regime control. Following the rapid uplift at the onset of the Holocene, RSL was falling more gradually during this time interval with an emergence of *c.* 5 m per 1.0 ka (Bondevik et al., 1995; Forman et al., 2004; Johnson, 2020). The sedimentation rate during deposition of the lower and middle shoreface deposits was still evidently high as indicated by molluscs buried in growth position (Figure 37, A). This can again be correlated to the findings of Forwick and Vorren (2009) who establish the highest sedimentation rates throughout the Holocene in Isfjorden prior to 8.8 cal. ka BP. With RSL falling moderately, and a high sedimentation rate evident, the accommodation space within the basin would be considerably reducing, promoting conditions for shallow marine progradation. This continued shoreline progradation throughout the Early Holocene would have resulted in a transition from the interpreted embayed fjord side deltaic environment recorded at Hollendardalen to a shallower and more linear coastline as observed at BKS1. The sediment character, sedimentary structures and molluscs within the lower to middle

shoreface deposits of BKS1 are in accordance with this and indicate a shallow (*c.* 10-25 m), wave dominated and high energy shoreface with nearshore currents and suspension fallout facies dominating (Brenchley & Newall, 1977; Mills, 1983; Mackiewicz et al., 1984; Peacock, 1993; Dahlgren et al., 2000).

### **5.3.3 Early Middle Holocene**

#### **5.3.3.1 <7.9 cal. ka BP**

The Middle Holocene is defined as 8.2-4.2 ka BP (Cohen et al., 2013; Walker et al., 2014). The coastal evolution of Hollendarbukta during the early stage of the Middle Holocene is recorded in BKS1 by a period of upper shoreface and beachface progradation and the penultimate stage of infilling of the shallow marine environment. The youngest date (*c.* 7.9 cal. ka BP) of the *Arctica islandica* collected by Bakken (2021) at 4-4.1 m a.s.l., correlates in this investigation with the boundary between the middle to upper shoreface deposits (Figure 34). Therefore, the upper shoreface, beachface and backshore deposits identified within this investigation are proposed to have been deposited later than this period, and hence, classified into <7.9 cal. ka BP and defined as the Early Middle Holocene.

During this period, the RSL curve smooths and glacio-isostatic uplift decreases to *c.* 5 m per 1.0 ka (Bondevik et al., 1995; Forman et al., 2004). The evidence presented in the geomorphic investigation in Figure 13 correlates with this as the gradient of the beach ridges that cap BKS1 and the associated coastal plain is low. This is especially noticeable when compared with the gradient of the beach ridges that mark the marine limit at *c.* 65 m a.s.l. up valley, adjacent to the Hollendardalen sections (Figure 13). This indicates that during the penultimate stage of coastal evolution, changes in RSL was to a lesser extent a regime control on the progradation of the shoreline. Furthermore, the beach ridges adjacent to BKS1 are orientated strike parallel to the present shoreline. This contrasts to the highest elevated beach ridges at *c.* 65 m a.s.l. that mark the marine limit in the Early Holocene and are orientated with their strike perpendicular to the present shoreline. This confirms that during the infilling of the valley and evolution of the coastal environment at Hollendarbukta a transition from an embayed fjord side deltaic environment to a more linear coastline occurred.

As this transition progressed, evidence from the modern environment analysis conducted on Bogebecken shoreline holds an insight into the processes and products that may have been affecting development of the linear shoreline. With the valley filling, and a linear shoreline

becoming more prominent it is likely that Hollendarbukta became increasingly more exposed to storm waves that were fetching through Isfjorden. As a result, the storm berm morphologies observed on the modern beach at Bogebecken were likely prominent features along the transitioning shoreline. Furthermore, the modern environment analysis identifies oblique waves intersecting the coastline and thus, it is probable that longshore drift and sediment transport along the beachface were similarly influencing the transitioning embayed to linear system in the Early Middle Holocene.

#### **5.3.4 Late Middle Holocene to present**

The Late Middle Holocene to present is identified in this investigation as a period where final uplift of the raised marine terraces within Hollendarbukta occurred. The elevation of the terrace at Bogebecken is *c.* 8 m a.s.l. (Figure 33, C). No surface date is available for the top of the section, although when the elevation is correlated with the RSL curves in Figure 48, an uplift of *c.* 8 m following the period of *c.* 7.9 cal. ka BP fits reasonably well and aligns with an emergence rate of *c.* 1 m per 1.0 ka (Forman et al., 2004; Johnson, 2020).

Accompanying this final uplift and shoreline regression was the development of the wave cut scarp that is highlighted in the geomorphic map (Figure 13) and exposes the raised marine terraces along the modern shoreline of Hollendarbukta. The development of the *c.* 8 m erosional feature indicates that as the Middle Holocene progressed, sediment supply was reducing, and basin redistribution processes such as wave and tidal action were outpacing shoreline progradation. This suitably correlates with the transition to a linear shoreface, that is becoming increasingly more exposed to both fair weather and storm waves within Isfjorden. Additionally, the recognition of both high tide and storm morphologies on the present shoreline identified in the modern environment analysis support that beachface erosion in such a system is a prominent influence on environmental character.

Following the formation of the wave cut scarp, downcutting through fluvial incision by the braided system of Hollendarelva and Bogebecken, exposed the *c.* 2.5 km stretch of raised marine terraces present within Hollendarbukta (Figure 4 and 9). During the Late Holocene, RSL was approaching its present-day state. At this time, the braided river systems of Hollendarelva and Bogebecken were likely well-established throughout the entire of the valley. The identification of active and inactive braid plains adjacent to the main distributary channel at Hollendarelva indicates lateral migration of the system (Figure 13 and 41).

Association of this stage of costal evolution at Hollendarbukta with the late Holocene seems fitting and can be supported through the identification of the *c.* 1-2 m eroded fluvial banks that separate the active and inactive braid plains at Hollendarelva (Figure 41). Correlating this degree of fluvial incision with the RSL curve in Figure 48 provides a plausible match when attributing the final stage of uplift during the Late Holocene with most recent incision of Hollendarelva.

As RSL approached its present-day state, the linear, wave dominated and microtidal coarse grained beach system became fully established developed (Figure 41 and 47). Sediment supply to the system evidently takes place through the distribution of fine sediment through the buoyant plumes identified during the modern environment analysis at the mouth of Hollendarelva and Bogebekken. Additionally, cannibalisation of the raised marine terraces by storm events responsible for the construction of the storm berms present in the modern beach of Bogebekken provide coarse clasts to the sediment composition (Figure 47).

#### **5.4 Assessment of grain size analysis**

There are three key points to discuss regarding the assessment of the grain size analysis: the sample selection, sample analysis and generation of the results using Gradistat v 8.0.

The focus of sediment sampling in the field was to target fine grained sediment that may contain foraminifera. As a result, any sediment that was coarser than fine sand was avoided. This led to an underrepresentation of the coarser size fractions when conducting detailed grain size analysis. This is significant for the deltaic sections in Hollendardalen and the *Arctica islandica* Section at Bogebekken, as considerable amounts of the outcrop were coarser than fine sand and so were not sampled. On the other hand, the *Mya truncata* Section at Bogebekken consisted almost entirely of clay, silt and sand which meant a representative selection of samples from the entire outcrop were taken.

During analysis using the Laser Particle Size Analyser, only 0.15-0.2 g of sediment was selected for analysis in the instrument. This was randomly selected from each prepared sample to increase the validity of the results. Although it is debatable how well 0.15-0.2 g of sediment reflects the sample as a whole, especially considering all the samples are classified as very poorly sorted. It is important to state that all methods of particle size analysis are to some extent influenced by particle shape, density and optical properties (Blott & Pye, 2001).

An example of this regarding the Laser Particle Size Analyser is where large, platy grains are measured as smaller particles due to orientation in suspension when the laser is deflected off their surface (Ingvild Hald pers. comm. 2023). To account for this, tests were repeated three times, and an average was calculated. Furthermore, samples with grains larger than 2 mm were avoided which again leads to an underrepresentation of coarser size fractions.

Lastly, when describing and interpreting the results generated through Gradistat v8.0, the Folk and Ward (1957) graphical method was used instead of the method of moments. This was largely due to the graphical method being relatively insensitive to sediments that contain a large particle size range in the tails of the distribution (Blott & Pye, 2001). The grain size distribution curves for the sediments analysed in this investigation to some extent fell into this classification and contained a long tail with low frequencies. As a result, the method of moments can overemphasize the importance of these tails (Blott & Pye, 2001). Whereas the Folk and Ward (1957) graphical method is more likely to accurately describe the general characteristics of the bulk sample (Blott & Pye, 2001).

## **5.5 Absence of foraminifera**

As mentioned in the aims of this thesis, the initial purpose of this investigation was to sample the raised marine terraces within Hollendarbukta, in the hope that they would contain foraminifera to use as a biogenic proxy for a paleoenvironmental reconstruction. It is unfortunate that an initial analysis of the 100 µm size fraction showed the samples were devoid of foraminifera, although it is necessary to conclude with a discussion of why this may be. Two propositions are put forward, firstly, the idea of ‘non-deposition’ and secondly, ‘deposition and dissolution’ is discussed.

The overarching interpretation supporting ‘non-deposition’ of foraminifera within the investigated environments is that they were too shallow and/or the depositional energy was too high. An investigation into the modern distribution of benthic foraminifera within the fjord delta setting at Tana fjord in Northern Norway, revealed an absence or low abundance (dominated by calcareous species) of foraminifera on the wave influenced delta platform deposits at <25 m water (Corner et al., 1996). This wave influenced fjord delta setting and corresponding water depth align with the depositional environment at BKS1 where nearshore currents dominate and a water depth of 15-30 m is probable based on the preferred water depth of *Arctica islandica* (Dahlgren et al., 2000). In turn, these findings to some extent

support each other and strengthen the depositional environment interpretation at BKS1 being <30 m water depth and a high energy shoreface that was inhospitable to benthic foraminifera.

Conversely, in the High Arctic fjord side setting of Kongsfjorden, surface samples of prodeltaic sediment from a glacial sandur delta (Bourriquen et al., 2018) retrieved from *c.* 35-38 m water depth revealed a faunal composition of *Nonionellina labradorica*, *Globobulimina auriculata*, *Stainforthia feylingi* and *Reophax fusiformis* (Fossile et al., 2022). These findings indicate the potential benthic foraminifera have for inhabiting fjord deltaic environments in a High Arctic setting, albeit at a slightly deeper water depth, and interpreted lower energy environment. In which case, it is surprising for the glacimarine deltaic bottomset at BKS2 to contain no foraminifera as there is a high degree of similarity in sediment character and depositional environment between this setting and the one described in Kongsfjorden (Fossile et al., 2022).

There is of course the possibility that foraminifera did inhabit the shallow and high energy coastal environments of Hollendarbukta. In which case, one possibility for their absence when examining the sediment samples is that they were subsequently dissolved by post depositional processes such as ground water leaching. Whilst this is noted, it seems unlikely, due to the high degree of preservation that characterises the molluscan fauna. In almost all cases, the periostracum was preserved and thus if a thin organic lining can withstand dissolution, then it is likely that this process did not contribute towards the dissolution of the foraminifera. The conclusion of this investigation is that the primary reason for a lack of foraminifera within the raised marine deposits is that the environments were too shallow and/or too high energy.

This aspect of the investigation may be poetically concluded with wise words of the English biologist, Thomas Henry Huxley “The great tragedy of science - the slaying of a beautiful hypothesis by an ugly fact” (Huxley, 1870).

## 6 Conclusions

Through sedimentological and geomorphic investigation of the Hollendardalen and Bogebekken Sections, this study has provided an insight in to the coastal and environmental evolution of the fjord side environment of Hollendarbukta throughout the Early Holocene to present. The results reveal three phases of coastal evolution that have contributed towards the valley fill of Hollendarbukta over the investigated period.

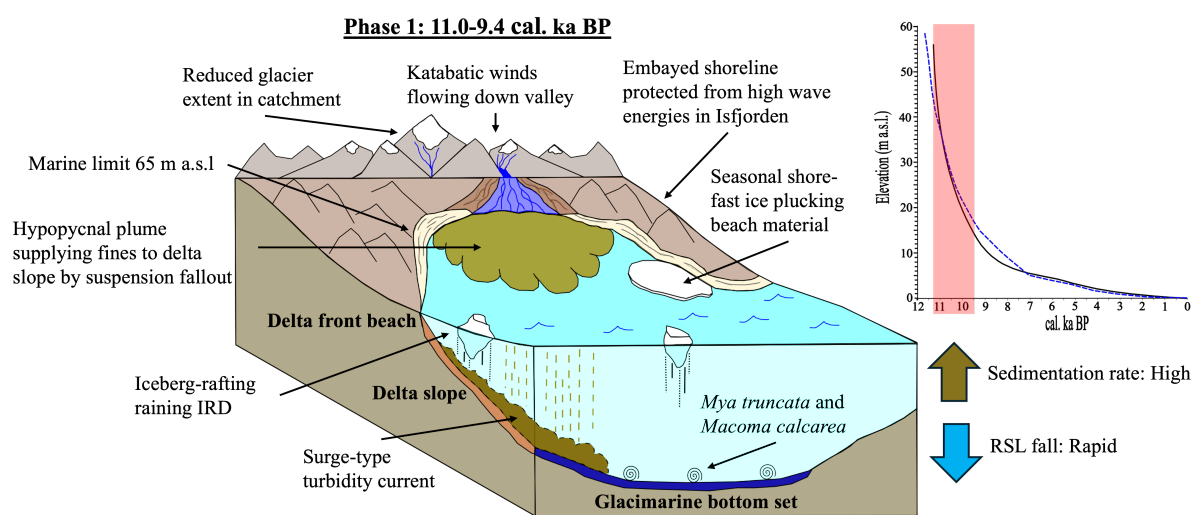


Figure 49: Conceptual model of 'Phase 1: 11.0-9.4 cal. ka BP' of the coastal and environmental evolution of Hollendarbukta, highlighting key depositional environments, sedimentary processes, and regime controls. Relative sea level curve adapted from §5.1 and highlighting the time frame of this stage of evolution in red. Inspiration for aspects of this model provided by Hogan et al. (2016).

Initially over the period of *c.* 11.0-9.4 cal. ka BP, infill of the valley occurred through the progradation of an embayed fjord side deltaic system. A coarsening upwards sequence of sediments are recorded within the outcrops at Hollendardalen and include five sub-environments: prodelta, lower delta slope, upper delta slope, delta front beach and backshore. Sediment character and sedimentary structures indicate that the depositional processes governing these sedimentary environments were sediment fallout from hypopycnal plumes, surge-type turbidity currents, wave traction and ultimately katabatic winds. In a distal setting of the embayed fjord side delta, a glacimarine bottomset environment is evident and outcrops within the raised marine terrace in Bogebekken. Depositional processes controlling sedimentation in the environment were suspension fallout from hypopycnal flows, surge-type turbidity currents and to some extent ice-rafting. The molluscan fauna is dominated by *Mya truncata* and to a lesser extent *Macoma calcarea* with a single *Mytilus* sp. observed. The evolution of Hollendarbukta during this time interval was largely controlled by a rapidly

falling sea level and a considerably seasonal climate. Together these regime controls influenced the shallow marine through inducing a high sediment flux governed by a prominent fluvial regime and periods of ice-rafting. Identification of sediment plumes dispersed *c.* 4-7 km from the shoreline of the modern fluvial system and covering an area *c.* 11 km<sup>2</sup>, suggests hypopycnal plumes dispersed from the fluvial system during the Early Holocene would have the potential to influence sedimentation in both nearshore, and shore-distal settings.

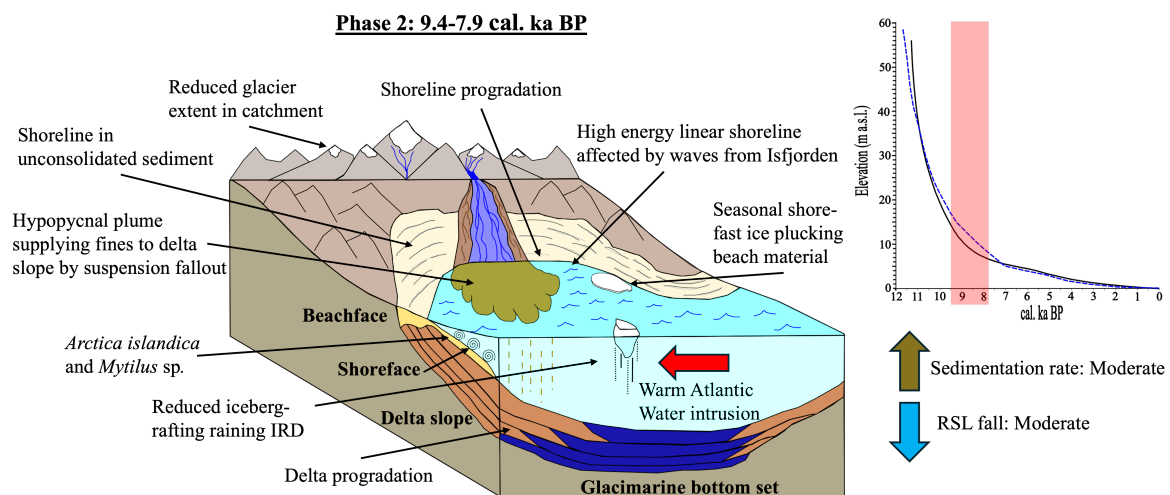


Figure 50: Conceptual model of 'Phase 2: 9.4-7.9 cal. ka BP' of the coastal and environmental evolution of Hollendarbukta, highlighting key depositional environments, sedimentary processes, and regime controls. Relative sea level curve adapted from §5.1 and highlighting the time frame of this stage of evolution in red. Inspiration for aspects of this model provided by Hogan et al. (2016).

The *Arctica islandica* Section at Bogebecken records the stage of coastal evolution between 9.4-7.9 cal. ka BP. The coarsening upwards sequence provides an insight into shallow marine environment of Bogebecken during the Holocene Thermal Maximum. Two sub-environments are identified with this period: the lower and middle shoreface. The sediment character and mollusc content indicate processes governing the deposition of these environments are suspension fallout and nearshore currents. The molluscan fauna is diverse and dominated by the thermophilous *Arctica islandica*. Deposition of this sequence occurred during a time when relative sea level was falling less rapidly but the sedimentation rate within the shallow marine environment was considerable. The sedimentological and geomorphic investigation reveal that during the Holocene Thermal Maximum, the shallow marine environment had evolved to a high energy, wave dominated and linear shoreline that was subject to warm Atlantic Water intrusion. The occurrence of beach face morphologies observed in the present-day shoreline system at Bogebecken, such as high tide and storm



berms are also present within the palaeo-sedimentary record which strengthens the interpreted evolution to an increasingly wave and storm influenced shoreline. This leads to the conclusion that climate and oceanographic forcing were the most significant regime controls on the evolution of the coastal environment during this period and to a lesser extent relative sea level fall and high sediment influx.

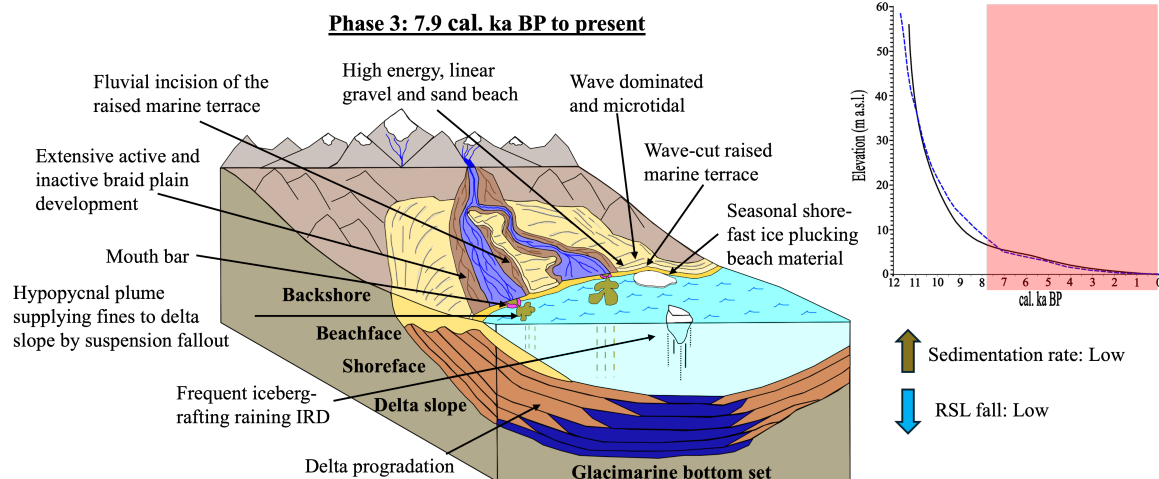


Figure 51: Conceptual model of 'Phase 3: 7.9 cal. ka BP to present' of the coastal and environmental evolution of Hollendarbukta, highlighting key depositional environments, sedimentary processes, and regime controls. Relative sea level curve adapted from §5.1 and highlighting the time frame of this stage of evolution in red. Inspiration for aspects of this model provided by Hogan et al. (2016).

The last stage of coastal evolution identified in this investigation is determined as <7.9 cal. ka BP to present. At the beginning of the Middle Holocene, progradation of the upper shoreface, beachface and backshore environments at the *Arctica islandica* Section in Bogebecken took place. The sedimentary processes governing deposition are related to wave traction and katabatic winds. Throughout the Middle to Late Holocene, sediment dispersal by basin processes such as waves, wind and tides out-paced sediment supply and a wave cut scarp along the marine terrace south of the modern shoreline was established. Glacio-isostatic uplift was slowing but was still significant enough to cause the c. 13-8 m of fluvial incision of the raised marine terraces throughout Hollendarbukta. At this time, the braided system of Hollendarelva and Bogebecken had developed and migrated throughout the entire valley, downcutting and transitioning to its present-day state where it breaches the modern, linear and wave dominated gravel shoreline in Hollendarbukta.

## 7 Future work

This investigation highlights that there is a suite of possibilities for future work to be conducted at the study site in Hollendarbukta, and just a few will be outlined below.

Firstly, establishing a well-constrained relative sea curve for Hollendarbukta would be beneficial. This could be achieved through further dating the *Mya truncata* shells collected from Bogebecken Section 2 where firm elevation data has been established in this investigation. Furthermore, the observation of whale cranium up valley within Hollendardalen, that has clearly been eroded from within the raised beach sediments it is adjacent to, would broaden this relative sea level curve. It would also remove the considerable uncertainty that is highlighted through correlating surface elevations with relative sea level curves from locations nearby, as discussed in §5.1. From a geomorphic point of view, there is a lot more work to be done. This investigation maps only a small section of the valley with a focus on the raised marine terraces. Detailed and expansive geomorphic mapping up valley could identify marginal ice landforms and assess whether there are any signs of glacier re-advance during the late deglacial or even Early Holocene as is recorded at Heftyebreen, Grønfjorden (Farnsworth et al., 2022) and Bolterdalen, Isfjorden (Lønne, 2005)

Additionally, future that would enhance the findings of this study may come from conducting geochemical analysis on the sediment samples that were collected. In this way, the grain size analysis of the results would be complimented with a further investigation into the inorganic sediment fraction. X-Ray Fluorescence (XRF) could be used to analyse major elements (Al, Ca, Fe, K, Mg, Mn, Na, P, Si and Ti). Al, Fe, Si and Ti are frequently used as indicators of terrestrial sediment supply to the marine environment in sediment core studies (Zabel et al., 2001; Bertrand et al., 2012; Faust, 2014; Wehrmann et al., 2014; Brendryen et al., 2015; Faust et al., 2017). Conversely, Ca and calcite shows a strong relationship with marine productivity and therefore, water temperature, salinity, nutrient supply and ice cover, which makes it a suitable proxy to reconstruct climate and environmental changes (Schneider et al., 2006; Faust et al., 2017). Indeed, Faust et al. (2017) successfully demonstrated that Ca/Al is a suitable proxy for investigating changes in marine carbonate productivity versus terrestrial sediment supply in fjords in Northern Norway. Their conclusions therefore strengthening its potential to serve as an indicator for changes in Atlantic Water inflow when compared to

river discharge, nutrient supply, and sea surface temperature changes. In which case, these elemental ratios may similarly assist with deciphering such changes within the shallow marine environment of Bogebecken throughout the Early Holocene and over the course of the Holocene Thermal Maximum.

Furthermore, it is generally understood that changes in temperature and precipitation control the fluvial sediment flux generated through the weathering and erosion of bedrock, glacial deposits and soils from land to ocean basins (White & Blum, 1995; Lamy et al., 2001; Govin et al., 2012). Therefore, geochemical analysis of the sediment samples within the raised marine terraces may lead to greater insights into the provenance, weathering, transport of terrigenous material entering the shallow marine through freshwater runoff. As Early Holocene warming undoubtedly impacted precipitation patterns and the hydrological system around Svalbard (Kjellman et al., 2020), investigating how these changes may have been reflected and recorded within the shallow marine realm would be fascinating. As well as providing a new insight into land-ocean interactions in the High Arctic, it may help to elucidate nutrient pathways into the fjord and provide an aspect of the answer as to what the molluscs were feeding on if no foraminifera were found.

# 8 Appendix

## 8.1 Hollendardalen: (HDS3/4)

### 8.1.1 Grain size analysis (Prodelta)

#### 8.1.1.1 Grain size distribution charts

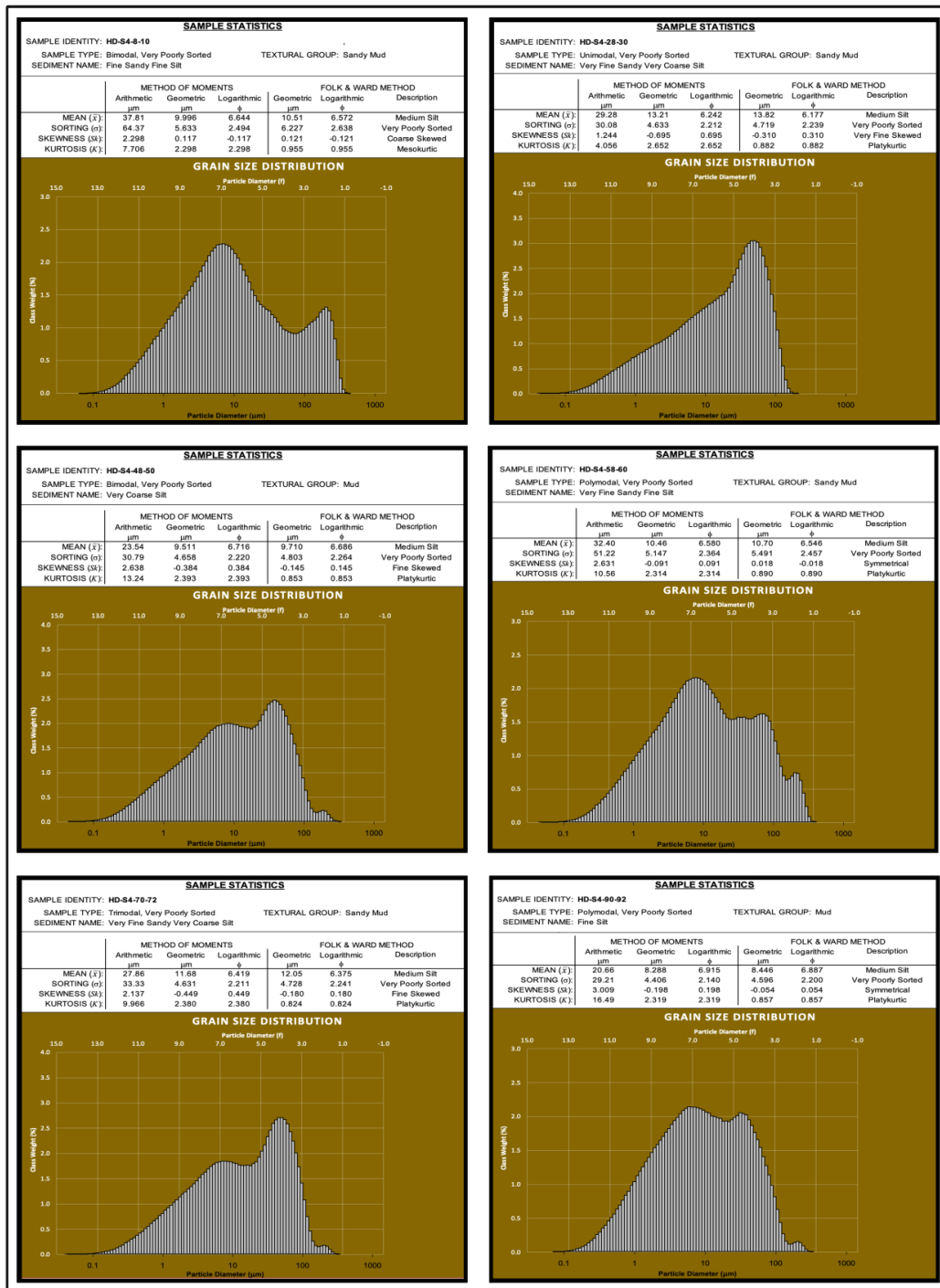


Figure 52: Grain size distribution charts for sediment samples from the prodeltaic deposits in Section 4 at Hollendardalen. Generated with GRADISTAT v8 (Blott, 2010).

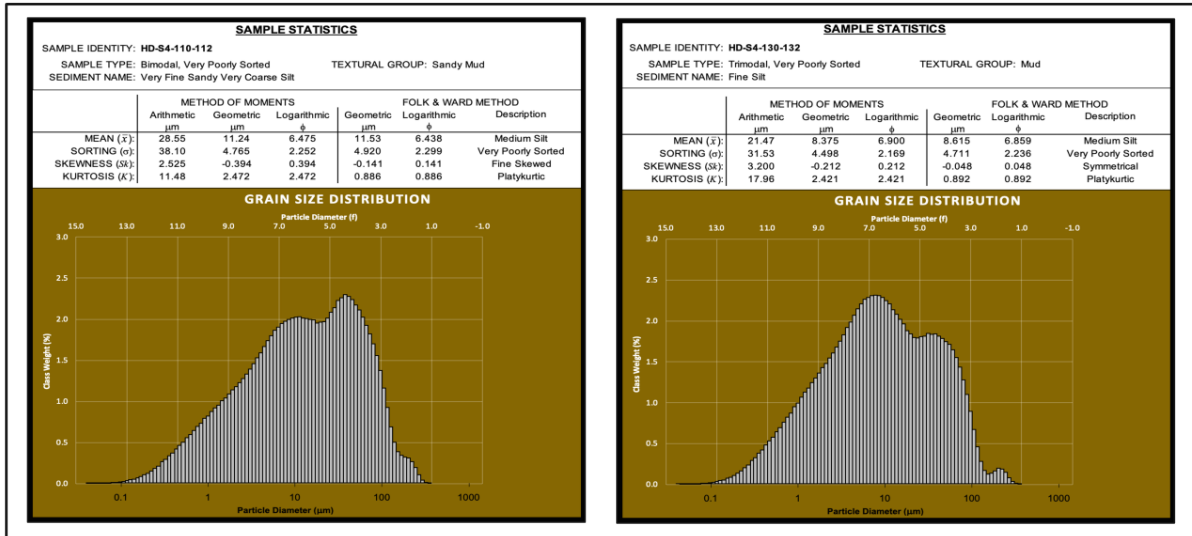


Figure 53: Grain size distribution charts for sediment samples from the prodeltaic deposits in Section 4 at Hollendardalen. Generated with GRADISTAT v8 (Blott, 2010).

### 8.1.1.2 Grain size statistics table

SAMPLE STATISTICS		Hollendardalen Section 4			
		HD-S4-8-10	HD-S4-28-30	HD-S4-48-50	HD-S4-58-60
SAMPLE TYPE:		Bimodal, Very Poorly Sorted	Unimodal, Very Poorly Sorted	Bimodal, Very Poorly Sorted	Polymodal, Very Poorly Sorted
TEXTURAL GROUP:		Sandy Silt	Sandy Silt	Silt	Sandy Silt
SEDIMENT NAME:		Fine Sandy Fine Silt	Very Fine Sandy Very Coarse Silt	Very Coarse Silt	Very Fine Sandy Fine Silt
METHOD OF MOMENTS Arithmetic (µm)	MEAN ( $\bar{x}_n$ ):	37.81	29.28	23.54	32.40
	SORTING ( $\sigma_n$ ):	64.37	30.08	30.79	51.22
	SKEWNESS ( $Sk_n$ ):	2.298	1.244	2.638	2.631
	KURTOSIS ( $K_n$ ):	7.706	4.056	13.24	10.56
METHOD OF MOMENTS Geometric (µm)	MEAN ( $\bar{x}_g$ ):	9.996	13.21	9.511	10.46
	SORTING ( $\sigma_g$ ):	5.633	4.633	4.658	5.147
	SKEWNESS ( $Sk_g$ ):	0.117	-0.695	-0.384	-0.091
	KURTOSIS ( $K_g$ ):	2.298	2.652	2.393	2.314
METHOD OF MOMENTS Logarithmic (φ)	MEAN ( $\bar{x}_l$ ):	6.644	6.242	6.716	6.580
	SORTING ( $\sigma_l$ ):	2.494	2.212	2.220	2.364
	SKEWNESS ( $Sk_l$ ):	-0.117	0.695	0.384	0.091
	KURTOSIS ( $K_l$ ):	2.298	2.652	2.393	2.314
FOLK AND WARD METHOD (µm)	MEAN ( $M_n$ ):	10.51	13.82	9.710	10.70
	SORTING ( $\sigma_n$ ):	6.227	4.719	4.803	5.491
	SKEWNESS ( $Sk_n$ ):	0.121	-0.310	-0.145	0.018
	KURTOSIS ( $K_n$ ):	0.955	0.882	0.853	0.890
FOLK AND WARD METHOD (φ)	MEAN ( $M_n$ ):	6.572	6.177	6.686	6.546
	SORTING ( $\sigma_n$ ):	2.638	2.239	2.264	2.457
	SKEWNESS ( $Sk_n$ ):	-0.121	0.310	0.145	-0.018
	KURTOSIS ( $K_n$ ):	0.955	0.882	0.853	0.890
FOLK AND WARD METHOD (Description)	MEAN:	Medium Silt	Medium Silt	Medium Silt	Medium Silt
	SORTING:	Very Poorly Sorted	Very Poorly Sorted	Very Poorly Sorted	Very Poorly Sorted
	SKEWNESS:	Coarse Skewed	Very Fine Skewed	Fine Skewed	Symmetrical
	KURTOSIS:	Mesokurtic	Platykurtic	Platykurtic	Platykurtic
MODE 1 (µm):		7.091	45.80	38.01	7.784
MODE 2 (µm):		203.7		8.546	73.03
MODE 3 (µm):					31.54
MODE 1 (φ):		7.141	4.450	4.719	7.007
MODE 2 (φ):		2.297		6.872	3.777
MODE 3 (φ):					4.988
D <sub>10</sub> (µm):		1.076	1.310	1.058	1.155
D <sub>50</sub> (µm):		8.671	18.52	10.93	10.12
D <sub>90</sub> (µm):		136.4	73.97	61.58	92.48
(D <sub>90</sub> - D <sub>10</sub> ) (µm):		126.8	56.45	58.22	80.07
(D <sub>90</sub> / D <sub>10</sub> ) (µm):		135.3	72.66	60.53	91.33
(D <sub>75</sub> - D <sub>25</sub> ) (µm):		11.80	9.693	10.57	11.85
(D <sub>75</sub> / D <sub>25</sub> ) (µm):		31.50	41.18	30.70	35.18
D <sub>10</sub> (φ):		2.874	3.757	4.021	3.435
D <sub>50</sub> (φ):		6.850	5.754	6.515	6.627
D <sub>90</sub> (φ):		9.860	9.576	9.885	9.758
(D <sub>90</sub> / D <sub>10</sub> ) (φ):		3.431	2.549	2.458	2.841
(D <sub>90</sub> - D <sub>10</sub> ) (φ):		6.986	5.819	5.864	6.323
(D <sub>75</sub> / D <sub>25</sub> ) (φ):		1.732	1.737	1.697	1.759
(D <sub>75</sub> - D <sub>25</sub> ) (φ):		3.560	3.277	3.403	3.567
% GRAVEL:		0.0%	0.0%	0.0%	0.0%
% SAND:		18.3%	14.9%	9.7%	16.7%
% MUD:		81.7%	85.1%	90.3%	83.3%
% V COARSE GRAVEL:		0.0%	0.0%	0.0%	0.0%
% COARSE GRAVEL:		0.0%	0.0%	0.0%	0.0%
% MEDIUM GRAVEL:		0.0%	0.0%	0.0%	0.0%
% FINE GRAVEL:		0.0%	0.0%	0.0%	0.0%
% V FINE GRAVEL:		0.0%	0.0%	0.0%	0.0%
% V COARSE SAND:		0.0%	0.0%	0.0%	0.0%
% COARSE SAND:		0.0%	0.0%	0.0%	0.0%
% MEDIUM SAND:		2.0%	0.0%	0.0%	0.9%
% FINE SAND:		9.0%	0.8%	1.4%	5.2%
% V FINE SAND:		7.2%	14.1%	8.3%	10.6%
% V COARSE SILT:		8.0%	22.2%	17.4%	11.8%
% COARSE SILT:		10.8%	16.5%	15.4%	12.1%
% MEDIUM SILT:		15.5%	13.3%	14.7%	15.4%
% FINE SILT:		16.5%	10.8%	14.2%	15.4%
% V FINE SILT:		12.8%	8.3%	11.1%	11.8%
% CLAY:		18.1%	13.9%	17.4%	16.7%

Figure 54: Grain size statistics table for 4 sediment samples (HD-S4-8-10 cm to HD-S4-58-60 cm) from the prodeltaic deposits in Section 4 at Hollendardalen. Generated with GRADISTAT v8 (Blott, 2010).

		BK-S4-70-72	HD-S4-90-92	HD-S4-110-112	HD-S4-130-132
SAMPLE TYPE:		Trimodal, Very Poorly Sorted	Polymodal, Very Poorly Sorted	Bimodal, Very Poorly Sorted	Trimodal, Very Poorly Sorted
TEXTURAL GROUP:		Sandy Silt	Silt	Sandy Silt	Silt
SEDIMENT NAME:		Very Fine Sandy Very Coarse Silt	Fine Silt	Very Fine Sandy Very Coarse Silt	Fine Silt
METHOD OF MOMENTS Arithmetic (µm)	MEAN ( $\bar{x}$ ):	27.86	20.66	28.55	21.47
	SORTING ( $\sigma_x$ ):	33.33	29.21	38.10	31.53
	SKEWNESS ( $Sk_x$ ):	2.137	3.009	2.525	3.200
	KURTOSIS ( $K_x$ ):	9.966	16.49	11.48	17.96
METHOD OF MOMENTS Geometric (µm)	MEAN ( $\bar{x}_g$ ):	11.68	8.288	11.24	8.375
	SORTING ( $\sigma_{xg}$ ):	4.631	4.406	4.765	4.498
	SKEWNESS ( $Sk_{xg}$ ):	-0.449	-0.198	-0.394	-0.212
	KURTOSIS ( $K_{xg}$ ):	2.380	2.319	2.472	2.421
METHOD OF MOMENTS Logarithmic (φ)	MEAN ( $\bar{x}_l$ ):	6.419	6.915	6.475	6.900
	SORTING ( $\sigma_{xl}$ ):	2.211	2.140	2.252	2.169
	SKEWNESS ( $Sk_{xl}$ ):	0.449	0.198	0.394	0.212
	KURTOSIS ( $K_{xl}$ ):	2.380	2.319	2.472	2.421
FOLK AND WARD METHOD (µm)	MEAN ( $M_z$ ):	12.05	8.446	11.53	8.615
	SORTING ( $\sigma_z$ ):	4.728	4.596	4.920	4.711
	SKEWNESS ( $Sk_z$ ):	-0.180	-0.054	-0.141	-0.048
	KURTOSIS ( $K_z$ ):	0.824	0.857	0.886	0.892
FOLK AND WARD METHOD (φ)	MEAN ( $M_z$ ):	6.375	6.887	6.438	6.859
	SORTING ( $\sigma_z$ ):	2.241	2.200	2.299	2.236
	SKEWNESS ( $Sk_z$ ):	0.180	0.054	0.141	0.048
	KURTOSIS ( $K_z$ ):	0.824	0.857	0.886	0.892
FOLK AND WARD METHOD (Description)	MEAN:	Medium Silt	Medium Silt	Medium Silt	Medium Silt
	SORTING:	Very Poorly Sorted	Very Poorly Sorted	Very Poorly Sorted	Very Poorly Sorted
	SKEWNESS:	Fine Skewed	Symmetrical	Fine Skewed	Symmetrical
	KURTOSIS:	Platykurtic	Platykurtic	Platykurtic	Platykurtic
MODE 1 (µm):	45.80	5.885	38.01	7.784	
MODE 2 (µm):	7.091	7.091	11.31	31.54	
MODE 3 (µm):	16.41	31.54		38.01	
MODE 1 (φ):	4.450	7.410	4.719	7.007	
MODE 2 (φ):	7.141	7.141	6.468	4.958	
MODE 3 (φ):	5.931	4.988		4.719	
D <sub>10</sub> (µm):	1.309	1.086	1.216	1.061	
D <sub>50</sub> (µm):	14.02	8.688	12.96	8.723	
D <sub>90</sub> (µm):	72.46	56.20	76.20	59.59	
(D <sub>90</sub> / D <sub>10</sub> ) (µm):	55.34	51.77	62.69	56.14	
(D <sub>90</sub> - D <sub>10</sub> ) (µm):	71.15	55.12	74.99	58.53	
(D <sub>75</sub> / D <sub>25</sub> ) (µm):	11.02	9.815	10.28	9.404	
(D <sub>75</sub> - D <sub>25</sub> ) (µm):	38.70	24.71	35.50	24.57	
D <sub>10</sub> (φ):	3.787	4.153	3.714	4.069	
D <sub>50</sub> (φ):	6.156	6.847	6.270	6.841	
D <sub>90</sub> (φ):	9.577	9.847	9.684	9.880	
(D <sub>90</sub> / D <sub>10</sub> ) (φ):	2.529	2.371	2.608	2.428	
(D <sub>90</sub> - D <sub>10</sub> ) (φ):	5.790	5.694	5.970	5.811	
(D <sub>75</sub> / D <sub>25</sub> ) (φ):	1.760	1.636	1.720	1.624	
(D <sub>75</sub> - D <sub>25</sub> ) (φ):	3.463	3.295	3.361	3.233	
% GRAVEL:	0.0%	0.0%	0.0%	0.0%	
% SAND:	13.8%	8.2%	14.1%	9.2%	
% MUD:	86.2%	91.8%	85.9%	90.8%	
% V COARSE GRAVEL:	0.0%	0.0%	0.0%	0.0%	
% COARSE GRAVEL:	0.0%	0.0%	0.0%	0.0%	
% MEDIUM GRAVEL:	0.0%	0.0%	0.0%	0.0%	
% FINE GRAVEL:	0.0%	0.0%	0.0%	0.0%	
% V FINE GRAVEL:	0.0%	0.0%	0.0%	0.0%	
% V COARSE SAND:	0.0%	0.0%	0.0%	0.0%	
% COARSE SAND:	0.0%	0.0%	0.0%	0.0%	
% MEDIUM SAND:	0.1%	0.1%	0.2%	0.1%	
% FINE SAND:	1.4%	1.1%	2.8%	1.2%	
% V FINE SAND:	12.3%	7.1%	11.1%	7.8%	
% V COARSE SILT:	19.6%	14.0%	16.6%	13.3%	
% COARSE SILT:	14.5%	14.8%	15.3%	13.8%	
% MEDIUM SILT:	13.5%	15.4%	15.1%	16.5%	
% FINE SILT:	13.3%	15.8%	13.6%	16.5%	
% V FINE SILT:	10.5%	13.2%	10.1%	12.6%	
% CLAY:	14.7%	18.5%	15.3%	18.2%	

Figure 55: Grain size statistics table for 4 sediment samples (HD-S4-70-72 cm to HD-S4-130-132 cm) from the prodeltaic deposits in Section 4 at Hollendardalen. Generated with GRADISTAT v8 (Blott, 2010).

## 8.1.2 Grain size analysis (Lower delta slope)

### 8.1.2.1 Grain size distribution charts

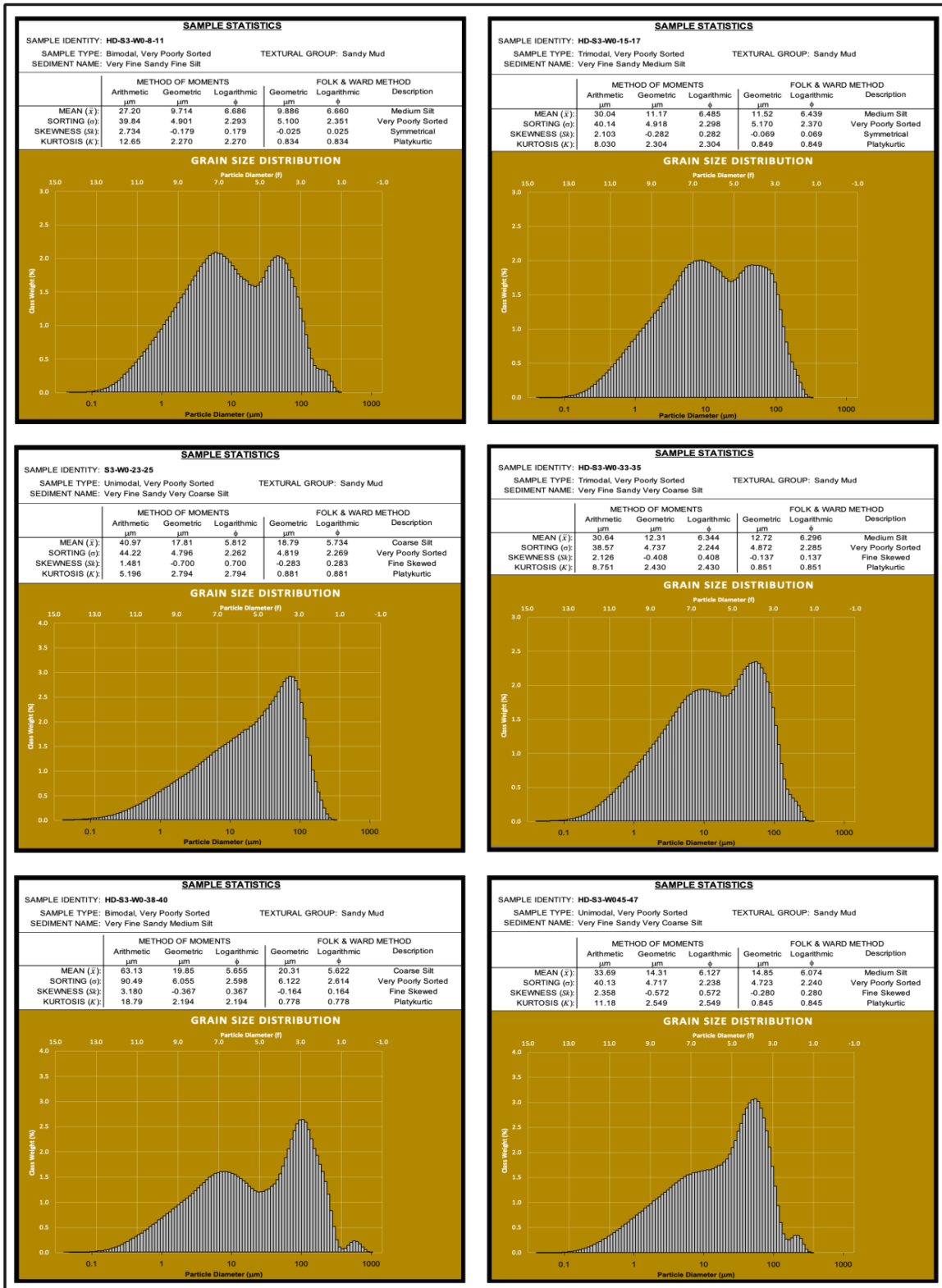


Figure 56: Grain size distribution charts for sediment samples from Window 0 within Section 3 at Hollendardalen. Generated with GRADISTAT v8 (Blott, 2010).



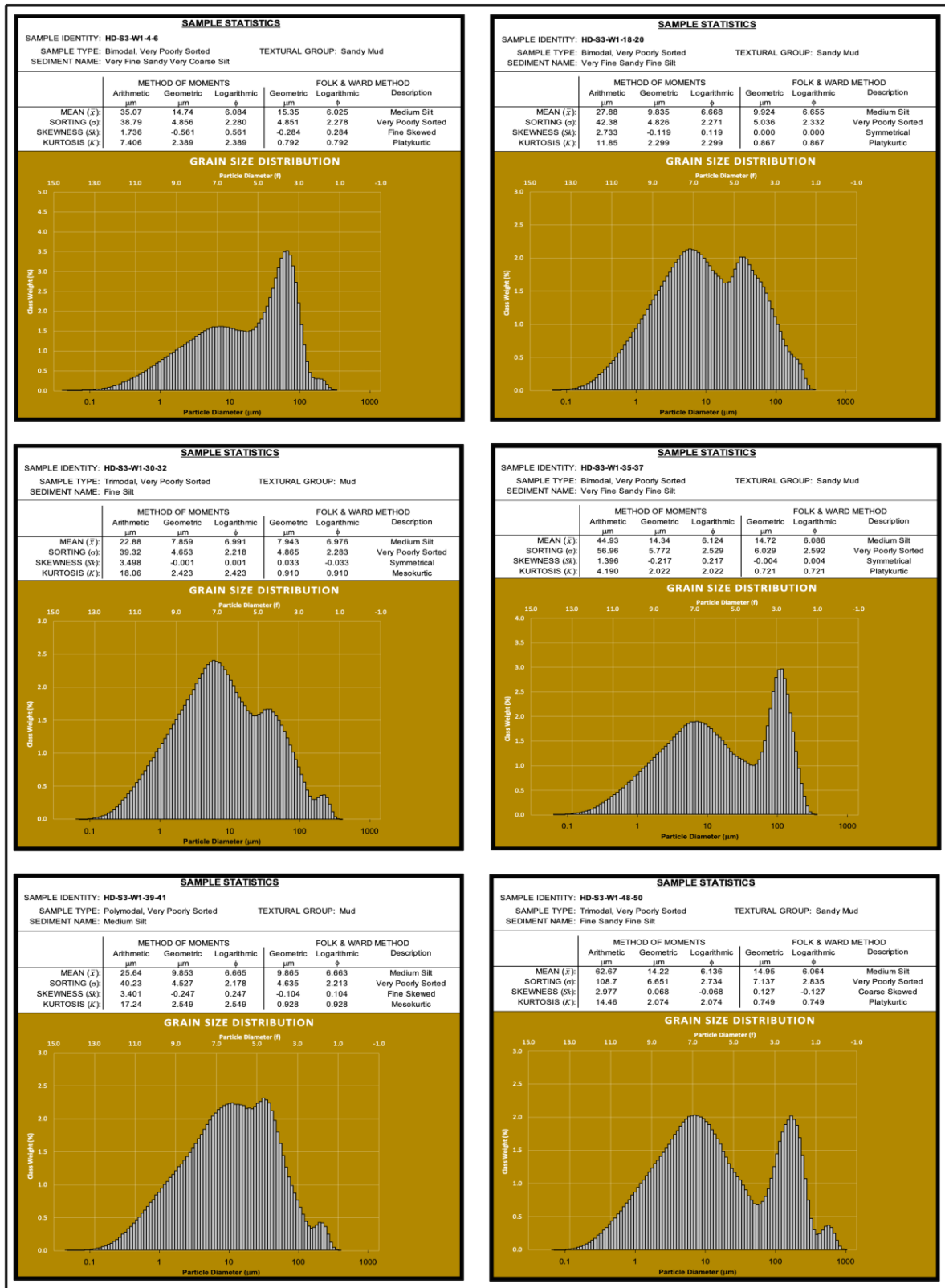


Figure 57: Grain size distribution charts for sediment samples from Window 1 within Section 3 at Hollendardalen. Generated with GRADISTAT v8 (Blott, 2010).

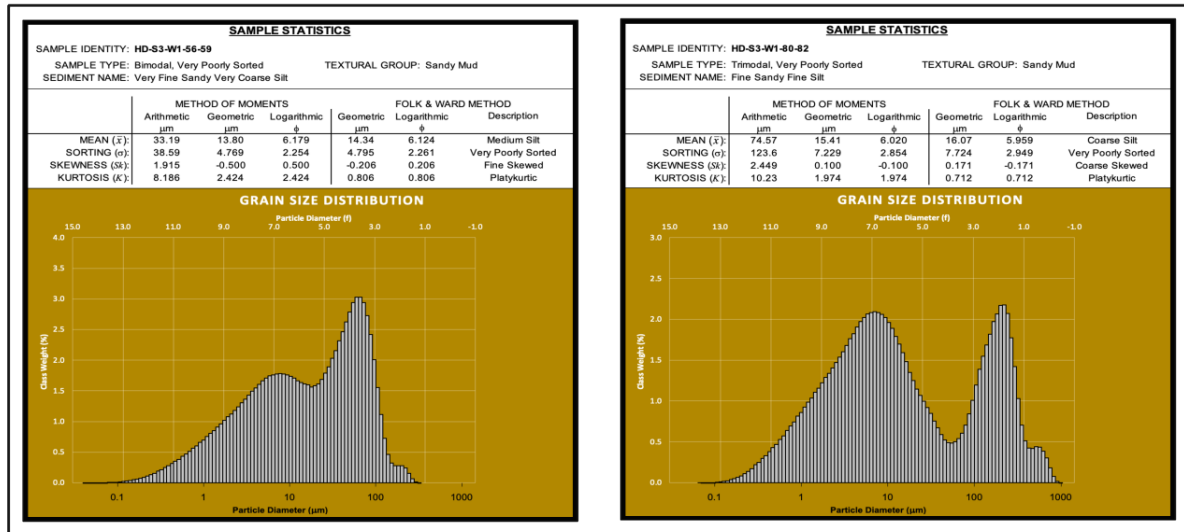


Figure 58: Grain size distribution charts for sediment samples from Window 1 within Section 3 at Hollendardalen. Generated with GRADISTAT v8 (Blott, 2010).



SEDIMENT NAME:		HD-S3-W1-18-20	HD-S3-W1-30-32	HD-S3-W1-35-37	HD-S3-W1-38-41	HD-S3-W1-48-50	HD-S3-W1-56-58	HD-S3-W1-80
METHOD OF MOMENTS Arithmetic (um)	MEAN (x̄): SKRTING (s <sub>x</sub> ): KURTOSIS (k <sub>x</sub> ):	Bimodal, Very Poorly Sorted Sandy Silt 27.88 42.38 27.88	Trimodal, Very Poorly Sorted Silt 22.88 39.32 22.88	Bimodal, Very Poorly Sorted Sandy Silt 44.93 56.96 44.93	Polymodal, Very Poorly Sorted Silt 25.64 40.23 25.64	Trimodal, Very Poorly Sorted Sandy Silt 62.67 108.7 62.67	Bimodal, Very Poorly Sorted Sandy Silt 33.19 38.59 33.19	Trimodal, Very Poorly Sorted Sandy Silt 74.57 123.6 74.57
METHOD OF MOMENTS Geometric (um)	MEAN (x̄): SKRTING (c <sub>x</sub> ): KURTOSIS (k <sub>x</sub> ):	27.33 11.85 9.835	3.998 18.06 7.859	1.396 14.34 5.772	3.401 17.24 9.853	2.977 14.46 14.22	2.449 8.186 13.30	2.449 10.23 15.41
METHOD OF MOMENTS Logarithmic (μ)	MEAN (x̄): SKRTING (c <sub>x</sub> ): KURTOSIS (k <sub>x</sub> ):	-0.119 2.289 6.668	-0.001 2.423 2.218	-0.217 2.529 2.218	-0.247 2.549 2.178	0.068 2.074 2.334	-0.500 2.424 2.254	0.100 1.974 2.854
FOLK AND WARD METHOD (um)	MEAN (M <sub>z</sub> ): SKRTING (s <sub>z</sub> ): KURTOSIS (K <sub>z</sub> ):	0.119 9.924 5.036	0.001 2.423 4.865	0.217 14.72 6.029	0.247 9.865 4.635	-0.068 14.95 7.137	0.500 14.34 4.795	-0.100 16.07 7.724
FOLK AND WARD METHOD (μ)	MEAN (M <sub>z</sub> ): SKRTING (s <sub>z</sub> ): KURTOSIS (K <sub>z</sub> ):	0.000 0.867 6.655	0.033 0.910 2.833	-0.004 0.721 6.086	-0.104 0.928 6.663	0.127 0.749 6.064	-0.206 6.124 5.959	0.171 0.712 2.949
FOLK AND WARD METHOD (Description)	MEAN: SKRTING: KURTOSIS:	0.000 0.867 0.910	0.033 0.910 0.910	0.004 0.721 0.928	0.104 0.928 0.928	-0.127 0.749 0.749	0.206 6.124 6.124	-0.171 0.712 0.712
MODE 1 (um):	MODE 1 (um):	7.410	7.410	16.4	31.54	7.091	60.59	223.7
MODE 2 (um):	MODE 2 (um):	4.988	2.492	1.164	18.78	1.141	7.784	57.8
MODE 3 (um):	MODE 3 (um):	1.193	1.026	1.326	1.203	0.817	4.046	2.162
D <sub>10</sub> (um):	D <sub>10</sub> (um):	9.649	7.468	13.53	10.89	1.244	1.492	1.261
D <sub>20</sub> (um):	D <sub>20</sub> (um):	77.23	61.42	132.8	62.36	11.36	17.09	11.16
D <sub>30</sub> (um):	D <sub>30</sub> (um):	64.76	59.87	100.1	51.85	156.5	84.14	237.8
D <sub>40</sub> (um):	D <sub>40</sub> (um):	76.04	60.40	131.5	61.16	193.4	56.40	188.6
D <sub>50</sub> (um):	D <sub>50</sub> (um):	11.17	9.841	21.21	8.903	24.84	82.84	286.5
D <sub>60</sub> (um):	D <sub>60</sub> (um):	31.71	22.82	76.46	27.47	82.67	11.81	32.53
D <sub>70</sub> (um):	D <sub>70</sub> (um):	3.695	4.025	2.913	4.003	2.961	48.15	110.5
D <sub>80</sub> (um):	D <sub>80</sub> (um):	6.695	7.065	6.208	6.521	6.460	5.871	6.485
D <sub>90</sub> (um):	D <sub>90</sub> (um):	9.711	9.929	9.588	9.700	9.651	9.389	9.632
D <sub>100</sub> (um):	D <sub>100</sub> (um):	2.628	2.467	3.281	2.423	4.087	2.629	4.648
D <sub>100</sub> - D <sub>50</sub> (um):	D <sub>100</sub> - D <sub>50</sub> (um):	6.017	5.904	6.646	6.646	7.290	5.817	7.559
% GRAVEL:	% GRAVEL:	1.719	1.817	4.407	1.829	2.310	1.838	2.602
% SAND:	% SAND:	3.481	3.669	4.407	3.154	4.635	3.582	5.024
% MUD:	% MUD:	0.0%	0.0%	0.0%	0.0%	0.0%	0.0%	0.0%
% V COARSE GRAVEL:	% V COARSE GRAVEL:	13.5%	9.7%	29.7%	10.0%	27.9%	19.4%	30.5%
% COARSE GRAVEL:	% COARSE GRAVEL:	88.5%	90.3%	70.3%	90.0%	72.1%	80.5%	69.5%
% MEDIUM GRAVEL:	% MEDIUM GRAVEL:	0.0%	0.0%	0.0%	0.0%	0.0%	0.0%	0.0%
% FINE GRAVEL:	% FINE GRAVEL:	0.0%	0.0%	0.0%	0.0%	0.0%	0.0%	0.0%
% V FINE GRAVEL:	% V FINE GRAVEL:	0.0%	0.0%	0.0%	0.0%	0.0%	0.0%	0.0%
% COARSE SAND:	% COARSE SAND:	0.0%	0.0%	0.0%	0.0%	0.0%	0.0%	0.0%
% MEDIUM SAND:	% MEDIUM SAND:	0.0%	0.0%	0.0%	0.0%	0.0%	0.0%	0.0%
% FINE SAND:	% FINE SAND:	0.0%	0.0%	0.0%	0.0%	1.3%	0.0%	0.0%
% V FINE SAND:	% V FINE SAND:	0.3%	0.5%	0.3%	0.5%	13.9%	0.1%	7.1%
% COARSE SILT:	% COARSE SILT:	9.2%	17.8%	6.7%	6.6%	6.1%	16.7%	6.9%
% MEDIUM SILT:	% MEDIUM SILT:	13.9%	11.7%	8.1%	14.8%	6.1%	19.4%	4.5%
% FINE SILT:	% FINE SILT:	14.2%	12.1%	9.7%	16.5%	14.1%	12.8%	8.7%
% CLAY:	% CLAY:	15.7%	17.6%	13.1%	14.9%	14.7%	12.8%	15.1%

Figure 60: Grain size statistics table for 7 sediment samples (HD-S3-W1-18-20 cm to HD-S3-W1-80 cm) from Section 3 at Hollendardalen. Generated with GRADISTAT v8 (Blott, 2010).

## 8.1.3 Grain size analysis (Upper delta slope)

### 8.1.3.1 Grain size distribution charts

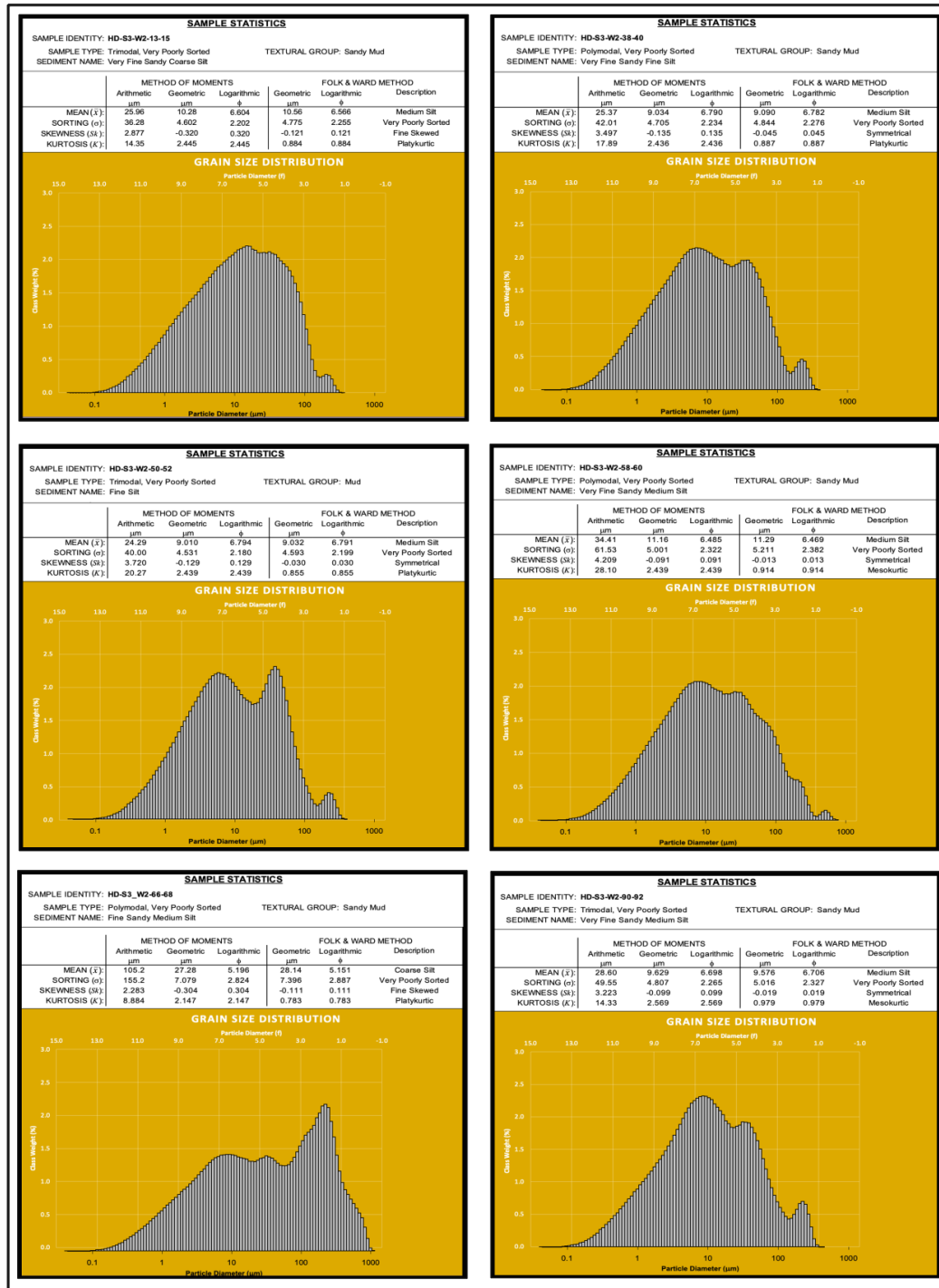


Figure 61: Grain size distribution charts for sediment samples from Window 2 within Section 3 at Hollendardalen. Generated with GRADISTAT v8 (Blott, 2010).

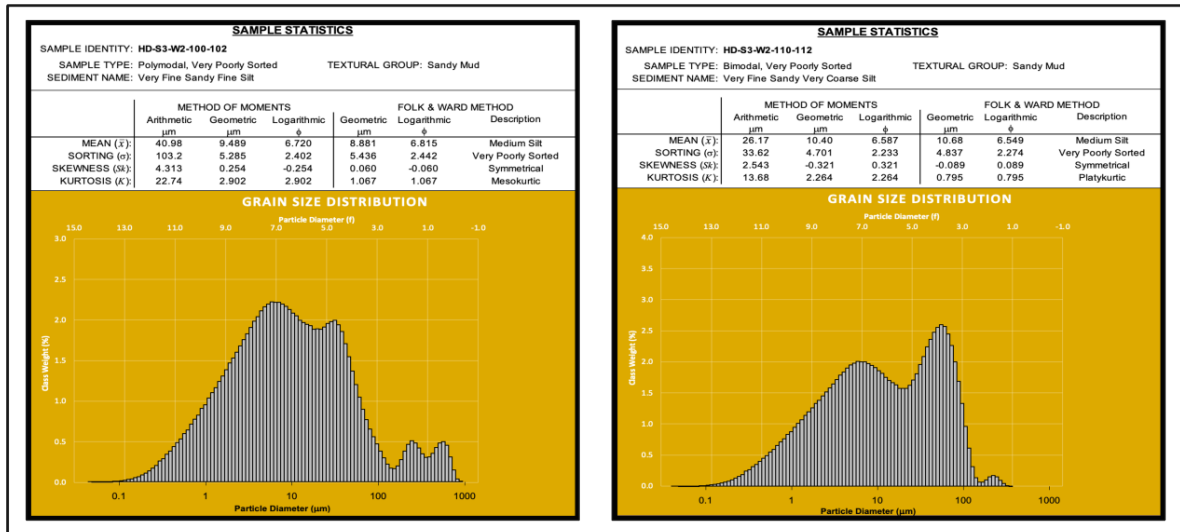


Figure 62: Grain size distribution charts for sediment samples from Window 2 within Section 3 at Hollendardalen. Generated with GRADISTAT v8 (Blott, 2010).

### 8.1.3.2 Grain size statistics table

SAMPLE STATISTICS		Hollendardalen Section 3				
		HD-S3-W2-13-15	HD-S3-W2-38-40	HD-S3-W2-50-52	HD-S3-W2-58-60	
SAMPLE TYPE:		Trimodal, Very Poorly Sorted	Polymodal, Very Poorly Sorted	Trimodal, Very Poorly Sorted	Polymodal, Very Poorly Sorted	
TEXTURAL GROUP:		Sandy Silt	Sandy Silt	Silt	Sandy Silt	
SEDIMENT NAME:		Very Fine Sandy Coarse Silt	Very Fine Sandy Fine Silt	Fine Silt	Very Fine Sandy Medium Silt	
METHOD OF MOMENTS		MEAN ( $\bar{x}_n$ ):	25.95	25.37	24.29	34.41
Arithmetic ( $\mu\text{m}$ )		MEAN ( $\bar{x}_g$ ):	36.23	42.01	40.00	61.53
		SKETCHING ( $\sigma_x$ ):	2.868	3.497	3.720	4.209
		SKETCHING ( $3\bar{x}_n$ ):	14.29	17.89	20.27	28.10
		KURTOSIS ( $K_n$ ):	10.28	9.034	9.010	11.16
METHOD OF MOMENTS		MEAN ( $\bar{x}_g$ ):	4.603	4.705	4.531	5.001
Geometric ( $\mu\text{m}$ )		SKETCHING ( $\sigma_g$ ):	-0.321	-0.135	-0.129	-0.091
		SKETCHING ( $3\bar{x}_g$ ):	2.443	2.436	2.439	2.439
		KURTOSIS ( $K_g$ ):	6.605	6.790	6.794	6.485
METHOD OF MOMENTS		MEAN ( $\bar{x}_p$ ):	2.203	2.234	2.180	2.322
Logarithmic ( $\phi$ )		SKETCHING ( $\sigma_p$ ):	0.321	0.135	0.129	0.091
		SKETCHING ( $3\bar{x}_p$ ):	2.443	2.436	2.439	2.439
		KURTOSIS ( $K_p$ ):	10.56	9.090	9.032	11.29
FOLK AND WARD METHOD		MEAN ( $M_z$ ):	4.777	4.844	4.593	5.211
(um)		SKETCHING ( $\sigma_z$ ):	-0.122	-0.045	-0.030	-0.013
		SKETCHING ( $3\bar{x}_z$ ):	0.884	0.887	0.855	0.914
		KURTOSIS ( $K_z$ ):	6.566	6.782	6.791	6.469
FOLK AND WARD METHOD		MEAN ( $M_\phi$ ):	2.256	2.276	2.199	2.382
(phi)		SKETCHING ( $\sigma_\phi$ ):	0.122	0.045	0.030	0.013
		SKETCHING ( $3\bar{x}_\phi$ ):	0.884	0.887	0.855	0.914
		KURTOSIS ( $K_\phi$ ):	Medium Silt	Medium Silt	Medium Silt	Medium Silt
FOLK AND WARD METHOD		MEAN:	Very Poorly Sorted	Very Poorly Sorted	Very Poorly Sorted	Very Poorly Sorted
(Description)		SKETCHING:	Fine Skewed	Symmetrical	Symmetrical	Symmetrical
		SKETCHING:	Platykurtic	Platykurtic	Platykurtic	Mesokurtic
		KURTOSIS:	16.41	7.091	38.01	7.784
		MODE 1 ( $\mu\text{m}$ ):	31.54	38.01	5.885	26.17
		MODE 2 ( $\mu\text{m}$ ):	26.17	31.54	223.7	31.54
		MODE 3 ( $\mu\text{m}$ ):	5.931	7.141	4.719	7.007
		MODE 1 ( $\phi$ ):	4.988	4.719	7.410	5.258
		MODE 2 ( $\phi$ ):	5.258	4.988	2.162	4.988
		MODE 3 ( $\phi$ ):	1.204	1.100	1.189	1.294
		$D_{10}$ ( $\mu\text{m}$ ):	11.69	9.336	9.033	11.25
		$D_{50}$ ( $\mu\text{m}$ ):	69.52	64.18	58.69	91.65
		$(D_{90} / D_{10})$ ( $\mu\text{m}$ ):	57.74	58.35	49.34	70.82
		$(D_{90} - D_{10})$ ( $\mu\text{m}$ ):	68.32	63.08	57.50	90.36
		$(D_{75} / D_{25})$ ( $\mu\text{m}$ ):	9.808	10.08	10.08	10.63
		$(D_{75} - D_{25})$ ( $\mu\text{m}$ ):	30.70	27.15	27.63	33.97
		$D_{10}$ ( $\phi$ ):	3.846	3.962	4.091	3.448
		$D_{50}$ ( $\phi$ ):	6.419	6.743	6.791	6.474
		$D_{90}$ ( $\phi$ ):	9.698	9.828	9.716	9.594
		$(D_{90} / D_{10})$ ( $\phi$ ):	2.521	2.481	2.375	2.783
		$(D_{90} - D_{10})$ ( $\phi$ ):	5.852	5.867	5.625	6.146
		$(D_{75} / D_{25})$ ( $\phi$ ):	1.676	1.660	1.663	1.720
		$(D_{75} - D_{25})$ ( $\phi$ ):	3.294	3.334	3.334	3.410
		% GRAVEL:	0.0%	0.0%	0.0%	0.0%
		% SAND:	12.0%	10.4%	8.9%	15.9%
		% MUD:	88.0%	89.6%	91.1%	84.1%
		% V COARSE GRAVEL:	0.0%	0.0%	0.0%	0.0%
		% COARSE GRAVEL:	0.0%	0.0%	0.0%	0.0%
		% MEDIUM GRAVEL:	0.0%	0.0%	0.0%	0.0%
		% FINE GRAVEL:	0.0%	0.0%	0.0%	0.0%
		% V FINE GRAVEL:	0.0%	0.0%	0.0%	0.0%
		% V COARSE SAND:	0.0%	0.0%	0.0%	0.0%
		% COARSE SAND:	0.0%	0.0%	0.0%	0.3%
		% MEDIUM SAND:	0.2%	0.7%	0.7%	1.2%
		% FINE SAND:	2.1%	2.6%	2.2%	4.8%
		% V FINE SAND:	9.7%	7.1%	6.0%	9.6%
		% V COARSE SILT:	15.0%	13.8%	15.6%	12.8%
		% COARSE SILT:	16.1%	14.3%	14.0%	14.3%
		% MEDIUM SILT:	16.0%	15.6%	14.8%	15.2%
		% FINE SILT:	13.9%	15.6%	16.3%	14.9%
		% V FINE SILT:	11.0%	12.5%	13.4%	11.7%
		% CLAY:	16.0%	17.7%	16.9%	15.3%

Figure 63: Grain size statistics table for 4 sediment samples (HD-S3-W2-13-15 cm to HD-S3-W2-58-60 cm) from Section 3 at Hollendardalen. Generated with GRADISTAT v8 (Blott, 2010).

		HD-S3-W2-66-68	HD-S3-W2-90-92	HD-S3-W2-100-102	HD-S3-W2-110-112
	SAMPLE TYPE:	Polymodal, Very Poorly Sorted	Polymodal, Very Poorly Sorted	Polymodal, Very Poorly Sorted	Bimodal, Very Poorly Sorted
	TEXTURAL GROUP:	Sandy Silt	Sandy Silt	Sandy Silt	Sandy Silt
	SEDIMENT NAME:	Fine Sandy Medium Silt	Very Fine Sandy Medium Silt	Very Fine Sandy Fine Silt	Very Fine Sandy Very Coarse Silt
METHOD OF MOMENTS Arithmetic (µm)	MEAN ( $\bar{x}_n$ ):	105.2	30.61	40.98	26.17
	SORTING ( $\sigma_n$ ):	155.2	56.98	103.2	33.62
	SKEWNESS ( $Sk_n^*$ ):	2.283	3.754	4.313	2.543
	KURTOSIS ( $K_n$ ):	8.884	19.94	22.74	13.68
METHOD OF MOMENTS Geometric (µm)	MEAN ( $\bar{x}_g$ ):	27.28	9.814	9.489	10.40
	SORTING ( $\sigma_g$ ):	7.079	4.898	5.285	4.701
	SKEWNESS ( $Sk_g^*$ ):	-0.304	-0.063	0.254	-0.321
	KURTOSIS ( $K_g$ ):	2.147	2.602	2.902	2.264
METHOD OF MOMENTS Logarithmic (φ)	MEAN ( $\bar{x}_l$ ):	5.196	6.671	6.720	6.587
	SORTING ( $\sigma_l$ ):	2.824	2.292	2.402	2.233
	SKEWNESS ( $Sk_l^*$ ):	0.304	0.063	-0.254	0.321
	KURTOSIS ( $K_l$ ):	2.147	2.602	2.902	2.264
FOLK AND WARD METHOD (µm)	MEAN ( $M_w$ ):	28.14	9.702	8.881	10.68
	SORTING ( $\sigma_w$ ):	7.396	5.115	5.436	4.837
	SKEWNESS ( $Sk_w^*$ ):	-0.111	-0.009	0.060	-0.089
	KURTOSIS ( $K_w$ ):	0.783	0.993	1.067	0.795
FOLK AND WARD METHOD (φ)	MEAN ( $M_w$ ):	5.151	6.688	6.815	6.549
	SORTING ( $\sigma_w$ ):	2.887	2.355	2.442	2.274
	SKEWNESS ( $Sk_w^*$ ):	0.111	0.009	-0.060	0.089
	KURTOSIS ( $K_w$ ):	0.783	0.993	1.067	0.795
FOLK AND WARD METHOD (Description)	MEAN:	Coarse Silt	Medium Silt	Medium Silt	Medium Silt
	SORTING:	Very Poorly Sorted	Very Poorly Sorted	Very Poorly Sorted	Very Poorly Sorted
	SKEWNESS:	Fine Skewed	Symmetrical	Symmetrical	Symmetrical
	KURTOSIS:	Platykurtic	Mesokurtic	Mesokurtic	Platykurtic
	MODE 1 (µm):	223.7	8.546	5.885	55.20
	MODE 2 (µm):	8.546	31.54	31.54	5.885
	MODE 3 (µm):	31.54	223.7	19.78	
	MODE 1 (φ):	2.162	6.872	7.410	4.181
	MODE 2 (φ):	6.872	4.988	4.988	7.410
	MODE 3 (φ):	4.988	2.162	5.661	
	D <sub>10</sub> (µm):	1.777	1.158	1.136	1.211
	D <sub>50</sub> (µm):	31.43	9.891	8.877	11.10
	D <sub>90</sub> (µm):	298.2	73.05	70.43	70.43
	(D <sub>90</sub> / D <sub>10</sub> ) (µm):	167.8	63.06	62.01	58.13
	(D <sub>90</sub> - D <sub>10</sub> ) (µm):	296.4	71.89	69.30	69.21
	(D <sub>75</sub> / D <sub>25</sub> ) (µm):	25.01	9.350	9.541	12.13
	(D <sub>75</sub> - D <sub>25</sub> ) (µm):	145.2	27.78	25.51	37.24
	D <sub>10</sub> (φ):	1.746	3.775	3.828	3.828
	D <sub>50</sub> (φ):	4.992	6.660	6.816	6.493
	D <sub>90</sub> (φ):	9.136	9.754	9.782	9.689
	(D <sub>90</sub> / D <sub>10</sub> ) (φ):	5.234	2.584	2.556	2.531
	(D <sub>90</sub> - D <sub>10</sub> ) (φ):	7.391	5.979	5.955	5.861
	(D <sub>75</sub> / D <sub>25</sub> ) (φ):	2.704	1.644	1.634	1.779
	(D <sub>75</sub> - D <sub>25</sub> ) (φ):	4.644	3.225	3.254	3.600
	% GRAVEL:	0.0%	0.0%	0.0%	0.0%
	% SAND:	40.0%	12.0%	11.2%	13.2%
	% MUD:	60.0%	88.0%	88.8%	86.8%
	% V COARSE GRAVEL:	0.0%	0.0%	0.0%	0.0%
	% COARSE GRAVEL:	0.0%	0.0%	0.0%	0.0%
	% MEDIUM GRAVEL:	0.0%	0.0%	0.0%	0.0%
	% FINE GRAVEL:	0.0%	0.0%	0.0%	0.0%
	% V FINE GRAVEL:	0.0%	0.0%	0.0%	0.0%
	% V COARSE SAND:	0.0%	0.0%	0.0%	0.0%
	% COARSE SAND:	3.7%	0.0%	1.9%	0.0%
	% MEDIUM SAND:	9.9%	1.7%	2.9%	0.2%
	% FINE SAND:	15.1%	4.1%	2.2%	1.0%
	% V FINE SAND:	11.3%	6.2%	4.3%	12.0%
	% V COARSE SILT:	10.1%	12.9%	11.8%	17.9%
	% COARSE SILT:	10.3%	14.2%	14.5%	12.5%
	% MEDIUM SILT:	10.7%	16.8%	15.5%	13.7%
	% FINE SILT:	10.2%	16.0%	16.4%	14.8%
	% V FINE SILT:	7.9%	11.7%	13.2%	11.8%
	% CLAY:	10.9%	16.4%	17.4%	16.1%

Figure 64: Grain size statistics table for 4 sediment samples (HD-S3-W2-66-68 cm to HD-S3-W2-110-112 cm) from Section 3 at Hollendardalen. Generated with GRADISTAT v8 (Blott, 2010).



# 8.2 Bogebecken: Mya truncata Telegraph Section (BKS2)

## 8.2.1 Grain size analysis

### 8.2.1.1 Grain size statistics table

SAMPLE STATISTICS		Bogebecken Section 2											
METHOD OF MOMENTS	TEXTURAL GROUP:	BK-S2-24-41		BK-S2-24-46		BK-S2-30-32		BK-S2-43-45		BK-S2-56-58		BK-S2-75-78	
		Bimodal, Very Poorly Sorted Sandy Silt	Very Fine Sandy Medium Silt	Bimodal, Very Poorly Sorted Sandy Silt	Very Fine Sandy Very Coarse Silt	Bimodal, Very Poorly Sorted Sandy Silt	Very Fine Sandy Medium Silt	Polymodal, Very Poorly Sorted Sandy Silt	Very Fine Sandy Very Coarse Silt	Unimodal, Very Poorly Sorted Sandy Silt	Very Fine Sandy Very Coarse Silt	Polymodal, Very Poorly Sorted Sandy Silt	Very Fine Sandy Very Coarse Silt
METHOD OF MOMENTS	MEAN (G.):	31.66	53.07	44.36	47.99	50.28	49.60	85.77	85.77	85.77	85.77	85.77	85.77
Arithmetic (um)	SKENNESS (K <sub>s</sub> ):	2.248	1.314	1.533	1.232	1.088	1.088	2.813	2.813	2.813	2.813	2.813	2.813
	KURTOSIS (K <sub>k</sub> ):	8.506	4.352	4.964	4.273	3.792	3.792	14.46	14.46	14.46	14.46	14.46	14.46
METHOD OF MOMENTS	MEAN (G.):	10.84	5.499	5.913	5.172	20.23	20.23	6.056	6.056	6.056	6.056	6.056	6.056
Geometric (um)	SKENNESS (K <sub>s</sub> ):	-0.156	-0.568	-0.288	-0.633	-0.835	-0.835	5.495	5.495	5.495	5.495	5.495	5.495
	KURTOSIS (K <sub>k</sub> ):	2.314	2.340	2.113	2.485	2.214	2.214	5.627	5.627	5.627	5.627	5.627	5.627
METHOD OF MOMENTS	MEAN (G.):	6.527	5.696	6.045	5.664	2.371	2.371	2.599	2.599	2.599	2.599	2.599	2.599
Logarithmic (um)	SKENNESS (K <sub>s</sub> ):	2.334	2.463	2.463	2.371	2.599	2.599	2.334	2.334	2.334	2.334	2.334	2.334
	KURTOSIS (K <sub>k</sub> ):	2.314	2.340	2.113	2.485	2.214	2.214	2.875	2.875	2.875	2.875	2.875	2.875
FOLK AND WARD METHOD	MEAN (G.):	11.44	20.92	15.38	20.72	15.66	20.72	4.853	4.853	4.853	4.853	4.853	4.853
(um)	SKENNESS (K <sub>s</sub> ):	0.001	-0.272	0.048	-0.334	0.601	-0.404	0.601	0.601	0.601	0.601	0.601	0.601
	KURTOSIS (K <sub>k</sub> ):	6.450	5.979	6.022	5.993	5.993	5.993	5.993	5.993	5.993	5.993	5.993	5.993
FOLK AND WARD METHOD	MEAN (G.):	2.443	2.467	2.515	2.369	2.279	2.279	2.638	2.638	2.638	2.638	2.638	2.638
(um)	SKENNESS (K <sub>s</sub> ):	0.801	0.712	0.946	0.784	0.784	0.784	0.784	0.784	0.784	0.784	0.784	0.784
	KURTOSIS (K <sub>k</sub> ):	0.383	0.179	0.152	0.152	0.152	0.152	0.152	0.152	0.152	0.152	0.152	0.152
FOLK AND WARD METHOD	MODE 1 (um):	88.00	9.382	96.60	16.41	3.508	88.00	3.508	3.508	3.508	3.508	3.508	3.508
(Description)	MODE 2 (um):	6.738	6.738	6.738	5.931	4.988	6.738	6.738	6.738	6.738	6.738	6.738	6.738
	MODE 3 (um):	3.508	1.663	1.434	1.728	1.615	1.889	1.615	1.615	1.615	1.615	1.615	1.615
	D <sub>10</sub> (um):	10.776	27.84	15.15	29.33	35.29	117.8	23.84	23.84	23.84	23.84	23.84	23.84
	D <sub>16</sub> (um):	80.57	136.2	81.90	87.82	116.7	116.7	116.7	116.7	116.7	116.7	116.7	116.7
	D <sub>25</sub> (um):	95.38	134.6	124.5	132.5	145.8	145.8	145.8	145.8	145.8	145.8	145.8	145.8
	D <sub>50</sub> (um):	11.34	15.40	17.83	13.52	10.67	10.67	10.67	10.67	10.67	10.67	10.67	10.67
	D <sub>60</sub> (um):	35.94	81.84	70.92	73.86	72.95	88.41	88.41	88.41	88.41	88.41	88.41	88.41
	D <sub>75</sub> (um):	3.372	2.876	2.990	3.078	3.085	2.439	2.439	2.439	2.439	2.439	2.439	2.439
	D <sub>80</sub> (um):	6.539	5.167	6.045	5.091	5.391	5.391	5.391	5.391	5.391	5.391	5.391	5.391
	D <sub>85</sub> (um):	9.704	9.232	9.446	9.177	8.974	8.974	8.974	8.974	8.974	8.974	8.974	8.974
	D <sub>90</sub> (um):	2.878	3.210	3.160	2.982	2.989	2.989	2.989	2.989	2.989	2.989	2.989	2.989
	D <sub>95</sub> (um):	6.332	6.366	6.457	6.099	5.889	5.889	5.889	5.889	5.889	5.889	5.889	5.889
	D <sub>98</sub> (um):	1.751	2.122	2.113	2.050	1.940	1.940	1.940	1.940	1.940	1.940	1.940	1.940
	D <sub>99</sub> (um):	3.503	3.945	4.157	3.757	3.416	3.416	3.416	3.416	3.416	3.416	3.416	3.416
	% SAND:	0.0%	0.0%	0.0%	0.0%	0.0%	0.0%	34.2%	34.2%	34.2%	34.2%	34.2%	34.2%
	% GRAVEL:	18.3%	35.7%	29.3%	33.4%	34.5%	65.5%	65.5%	65.5%	65.5%	65.5%	65.5%	65.5%
	% MUD:	81.7%	64.3%	70.7%	66.6%	65.5%	34.5%	34.5%	34.5%	34.5%	34.5%	34.5%	34.5%
	% V COARSE GRAVEL:	0.0%	0.0%	0.0%	0.0%	0.0%	0.0%	0.0%	0.0%	0.0%	0.0%	0.0%	0.0%
	% MEDIUM GRAVEL:	0.0%	0.0%	0.0%	0.0%	0.0%	0.0%	0.0%	0.0%	0.0%	0.0%	0.0%	0.0%
	% FINE GRAVEL:	0.0%	0.0%	0.0%	0.0%	0.0%	0.0%	0.0%	0.0%	0.0%	0.0%	0.0%	0.0%
	% V COARSE SAND:	0.0%	0.0%	0.0%	0.0%	0.0%	0.0%	0.0%	0.0%	0.0%	0.0%	0.0%	0.0%
	% MEDIUM SAND:	0.0%	0.0%	0.0%	0.0%	0.0%	0.0%	0.0%	0.0%	0.0%	0.0%	0.0%	0.0%
	% FINE SAND:	0.3%	0.0%	0.0%	0.2%	0.0%	0.0%	0.0%	0.0%	0.0%	0.0%	0.0%	0.0%
	% V COARSE SILT:	12.8%	23.3%	19.1%	25.0%	18.1%	26.3%	18.1%	18.1%	18.1%	18.1%	18.1%	18.1%
	% MEDIUM SILT:	10.2%	12.6%	10.2%	11.4%	11.5%	11.4%	11.5%	11.5%	11.5%	11.5%	11.5%	11.5%
	% FINE SILT:	15.1%	11.4%	13.7%	10.0%	11.4%	10.0%	11.4%	11.4%	11.4%	11.4%	11.4%	11.4%
	% V FINE SILT:	11.1%	8.0%	10.1%	8.0%	8.8%	8.8%	8.8%	8.8%	8.8%	8.8%	8.8%	8.8%
	% CLAY:	16.0%	11.6%	13.6%	11.2%	12.0%	12.0%	12.0%	12.0%	12.0%	12.0%	12.0%	12.0%

Figure 65: Grain size statistics table for 6 sediment samples (9-11 cm to 75-78 cm) from Section 2 at Bogebecken. Generated with GRADISTAT v8 (Blott, 2010).



## 8.2.1.2 Grain size distribution charts

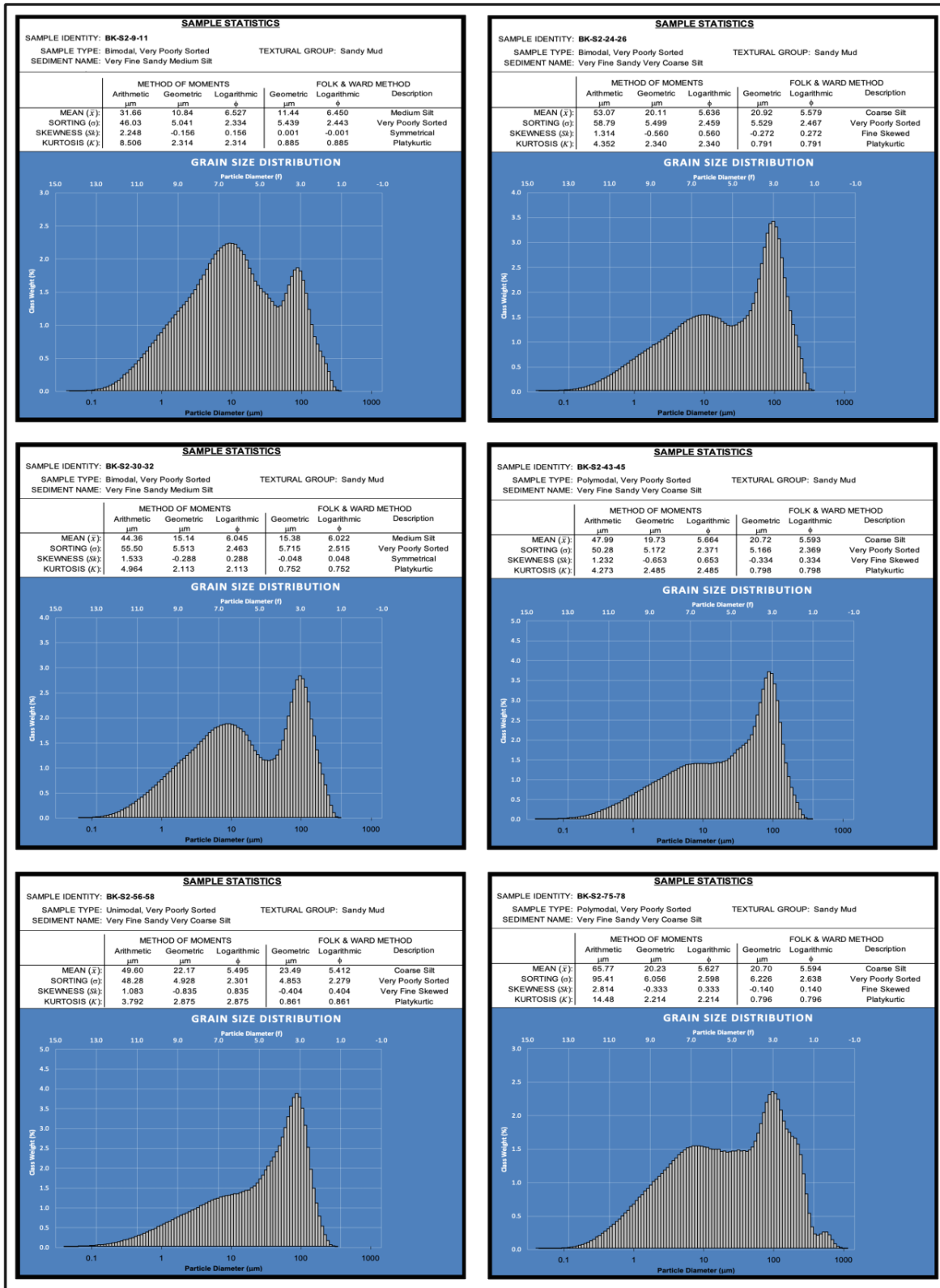


Figure 67: Grain size distribution charts for sediment samples from Section 2 at Bogebecken. Generated with GRADISTAT v8 (Blott, 2010).

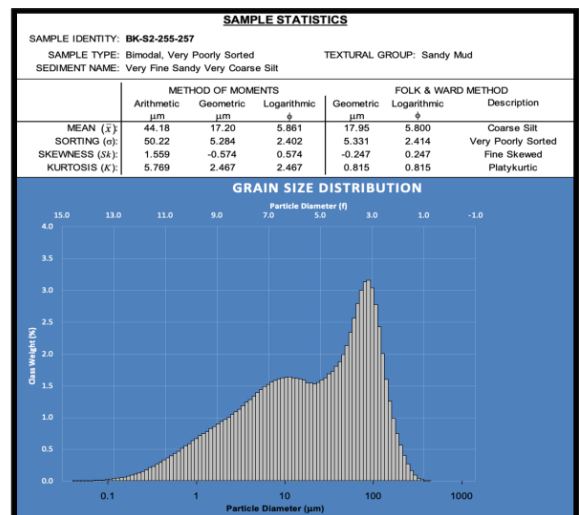
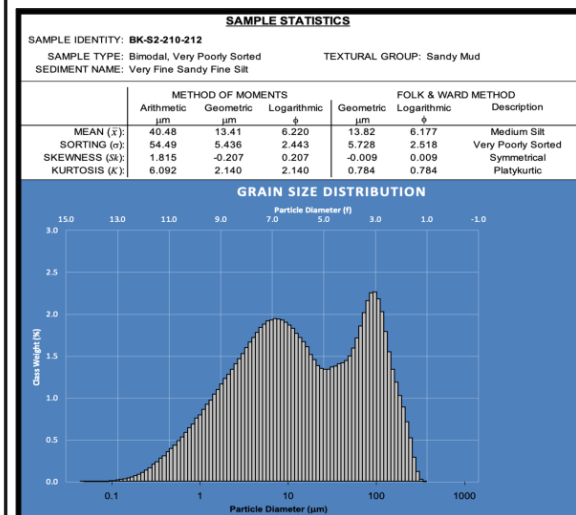
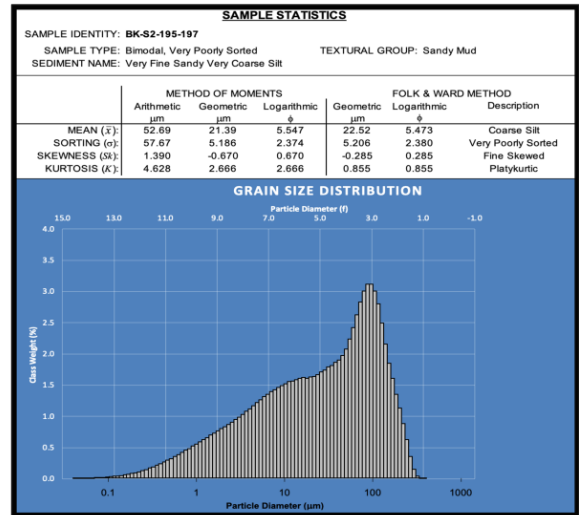
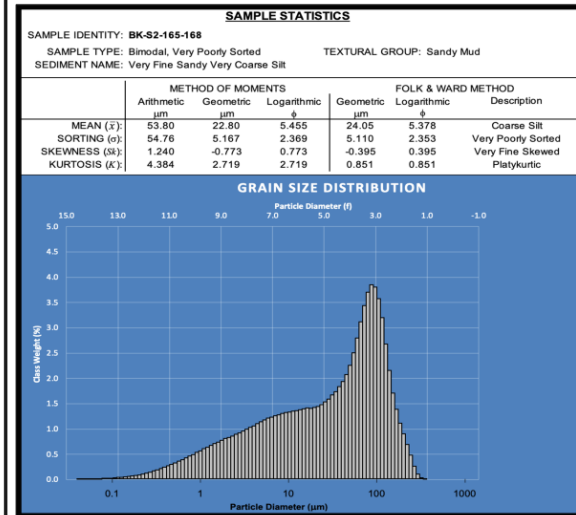
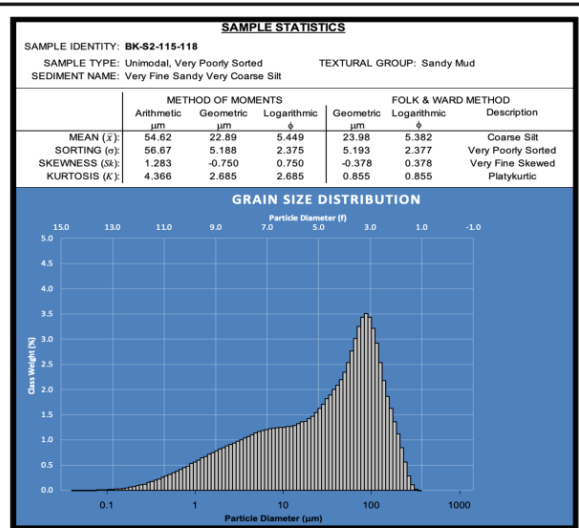
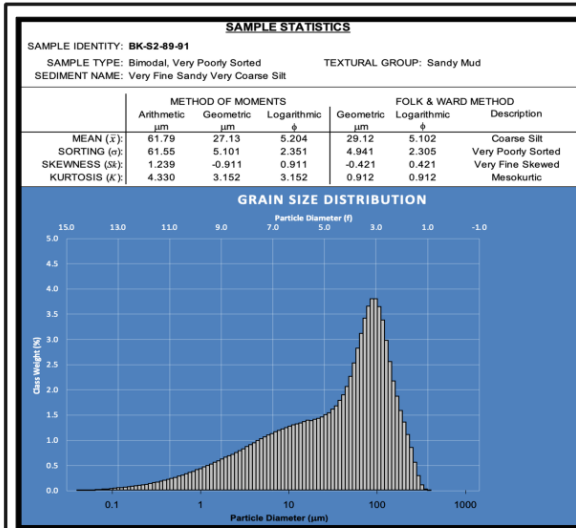


Figure 68: Grain size distribution charts for sediment samples from Section 2 at Bogebecken. Generated with GRADISTAT v8 (Blott, 2010).

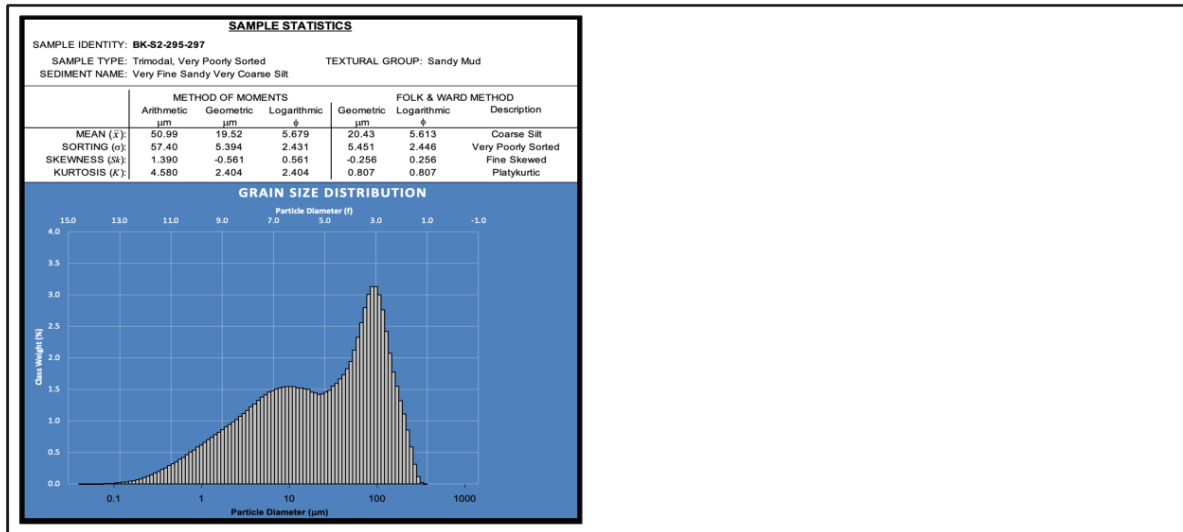


Figure 69: Grain size distribution charts for sediment samples from Section 2 at Bogebecken. Generated with GRADISTAT v8 (Blott, 2010).

## 8.3 Bogebecken: Arctica islandica Section (BKS1)

### 8.3.1 Grain size analysis

#### 8.3.1.1 Grain size distribution charts

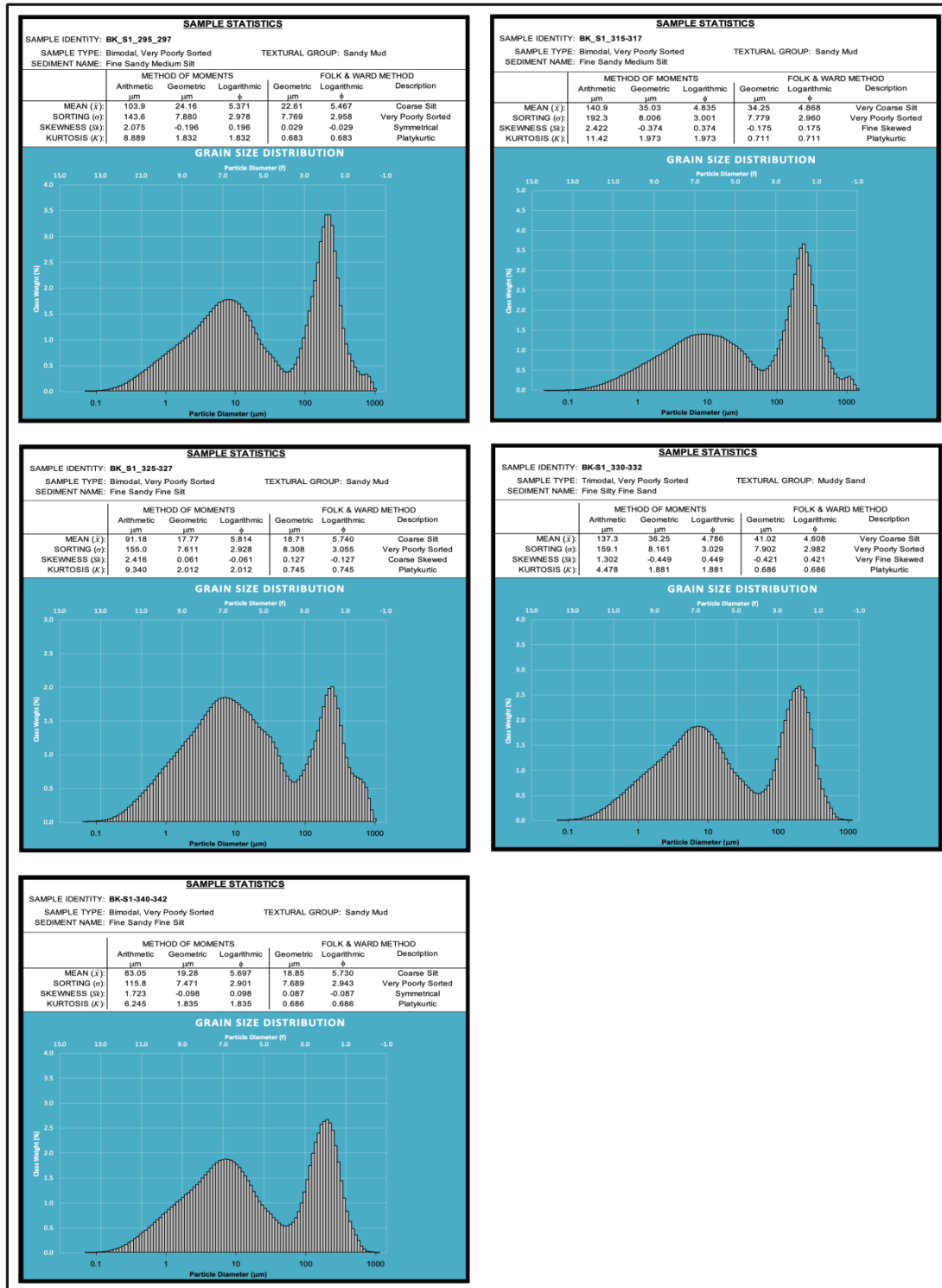


Figure 70: Grain size distribution charts for sediment samples from Section 1 at Bogebecken. Generated with GRADISTAT v8 (Blott, 2010).

### 8.3.1.2 Grain size statistics table

SAMPLE STATISTICS		Bogebekken Section 1				
SAMPLE TYPE:		BK-S1-295-297	BK-S1-315-317	BK-S1-325-327	BK-S1-330-332	BK-S1-340-342
TEXTURAL GROUP:		Bimodal, Very Poorly Sorted	Bimodal, Very Poorly Sorted	Bimodal, Very Poorly Sorted	Trimodal, Very Poorly Sorted	Bimodal, Very Poorly Sorted
SEDIMENT NAME:		Fine Sandy Medium Silt	Fine Sandy Medium Silt	Fine Sandy Fine Silt	Fine Silty Sand	Fine Sandy Fine Silt
METHOD OF MOMENTS	MEAN (x̄):	103.9	141.0	91.22	137.3	83.95
Arithmetic (um)	SKWESS (s <sub>k</sub> <sup>2</sup> ):	143.6	192.5	135.1	139.1	115.8
	KURTOSIS (k <sub>k</sub> ):	2.075	2.429	2.420	1.723	1.723
METHOD OF MOMENTS	MEAN (x̄):	8.889	11.48	9.376	4.478	6.245
Geometric (um)	SKWESS (s <sub>k</sub> <sup>2</sup> ):	24.16	35.04	17.78	36.25	19.28
	KURTOSIS (k <sub>k</sub> ):	7.880	8.006	0.061	-0.449	-0.449
METHOD OF MOMENTS	MEAN (x̄):	-0.196	-0.374	0.061	0.061	0.098
Logarithmic (μ)	SKWESS (s <sub>k</sub> <sup>2</sup> ):	1.832	1.973	2.012	1.881	1.835
	KURTOSIS (k <sub>k</sub> ):	5.371	4.835	5.814	4.786	5.697
METHOD OF MOMENTS	MEAN (x̄):	2.978	3.001	2.928	3.029	2.901
Logarithmic (μ)	SKWESS (s <sub>k</sub> <sup>2</sup> ):	0.196	0.374	-0.061	-0.449	0.098
	KURTOSIS (k <sub>k</sub> ):	1.832	1.973	2.012	1.881	1.835
FOLK AND WARD METHOD	MEAN (μ <sub>w</sub> ):	22.61	34.25	18.71	41.02	18.85
(um)	SKWESS (s <sub>w</sub> <sup>2</sup> ):	0.029	-0.175	0.127	-0.421	0.087
	KURTOSIS (k <sub>w</sub> ):	0.883	0.711	0.745	0.686	0.686
FOLK AND WARD METHOD	MEAN (μ <sub>w</sub> ):	5.467	4.868	5.740	4.608	5.730
(um)	SKWESS (s <sub>w</sub> <sup>2</sup> ):	2.958	2.960	3.055	2.982	2.943
	KURTOSIS (k <sub>w</sub> ):	-0.029	0.175	-0.127	0.421	-0.087
FOLK AND WARD METHOD	MEAN (μ <sub>w</sub> ):	0.683	0.711	0.745	0.686	0.686
(μ)	SKWESS (s <sub>w</sub> <sup>2</sup> ):	0.883	0.711	0.745	0.686	0.686
	KURTOSIS (k <sub>w</sub> ):	0.883	0.711	0.745	0.686	0.686
FOLK AND WARD METHOD	MEAN (μ <sub>w</sub> ):	203.7	245.5	245.5	203.7	203.7
(Description)	SKWESS (s <sub>w</sub> <sup>2</sup> ):	8.546	7.091	5.885	7.091	7.091
	KURTOSIS (k <sub>w</sub> ):	2.297	2.028	2.028	2.297	2.297
	MODE 1 (μ):	6.872	6.872	7.141	7.141	7.141
	MODE 2 (μ):	1.494	1.888	1.296	1.794	1.348
	D <sub>10</sub> (um):	19.48	41.89	14.08	77.32	14.86
	D <sub>20</sub> (um):	27.91	32.25	28.9	349.8	250.7
	D <sub>30</sub> (um):	186.8	186.7	223.7	195.0	186.0
	D <sub>40</sub> / D <sub>60</sub> (um):	277.6	350.6	288.6	348.0	249.4
	D <sub>50</sub> - D <sub>10</sub> (um):	38.61	35.39	32.72	39.46	36.56
	D <sub>75</sub> - D <sub>25</sub> (um):	176.6	221.1	121.6	226.3	142.2
	D <sub>85</sub> (μ):	1.441	1.504	1.786	1.515	1.996
	D <sub>90</sub> (μ):	5.882	4.577	6.150	3.693	6.072
	D <sub>95</sub> / D <sub>50</sub> (μ):	9.387	9.049	9.591	9.123	9.535
	(D <sub>95</sub> - D <sub>50</sub> ) (μ):	5.098	6.015	5.370	6.020	4.778
	(D <sub>90</sub> - D <sub>10</sub> ) (μ):	7.545	7.545	7.805	7.607	7.539
	(D <sub>75</sub> - D <sub>25</sub> ) (μ):	3.140	3.409	2.680	3.517	2.832
	(D <sub>75</sub> - D <sub>25</sub> ) (μ):	3.271	5.145	5.032	5.302	5.182
	% SAND:	0.0%	0.0%	0.0%	0.0%	0.0%
	% GRAVEL:	41.8%	47.5%	30.6%	51.3%	36.9%
	% MUD:	58.2%	52.5%	69.4%	48.7%	63.1%
	% V COARSE GRAVEL:	0.0%	0.0%	0.0%	0.0%	0.0%
	% COARSE GRAVEL:	0.0%	0.0%	0.0%	0.0%	0.0%
	% MEDIUM GRAVEL:	0.0%	0.0%	0.0%	0.0%	0.0%
	% FINE GRAVEL:	0.0%	0.0%	0.0%	0.0%	0.0%
	% V FINE GRAVEL:	0.0%	0.0%	0.0%	0.0%	0.0%
	% COARSE SAND:	0.0%	1.0%	0.0%	0.0%	0.0%
	% MEDIUM SAND:	2.2%	3.9%	3.5%	3.8%	0.8%
	% FINE SAND:	11.1%	16.8%	9.4%	18.1%	9.3%
	% V FINE SAND:	6.9%	6.1%	12.0%	22.0%	18.5%
	% V COARSE SILT:	3.7%	5.2%	6.9%	4.2%	8.3%
	% COARSE SILT:	7.6%	8.9%	10.7%	5.9%	7.8%
	% MEDIUM SILT:	12.5%	10.4%	13.1%	9.3%	12.7%
	% FINE SILT:	9.2%	7.7%	10.5%	8.2%	10.3%
	% V FINE SILT:	12.8%	10.3%	14.8%	10.9%	14.3%
	% CLAY:					

Figure 71: Grain size statistics table for sediment samples from Section 1 at Bogebekken. Generated with GRADISTAT v8 (Blott, 2010).

## References

- Aagaard, K., Foldvik, A., & Hillman, S. (1987). The West Spitsbergen Current: disposition and water mass transformation. *Journal of Geophysical Research: Oceans*, 92(C4), 3778-3784.
- Aagaard, T., Greenwood, B., & Hughes, M. (2013). Sediment transport on dissipative, intermediate and reflective beaches. *Earth-Science Reviews*, 124, 32-50.
- Aagaard-Sørensen, S., Husum, K., Hald, M., & Knies, J. (2010). Paleooceanographic development in the SW Barents Sea during the late Weichselian–Early Holocene transition. *Quaternary Science Reviews*, 29(25-26), 3442-3456.
- Alexanderson, H., & Bernhardson, M. (2019). Late glacial and Holocene sand drift in northern Götaland and Värmland, Sweden: sediments and ages. *GFF*, 141(2), 84-105.
- Allen, J. R. L., & Thornley, D. (2004). Laser granulometry of Holocene estuarine silts: effects of hydrogen peroxide treatment. *The Holocene*, 14(2), 290-295.
- Bakken, J. M. (2021). *Early and Mid-Holocene environments in Isfjorden, Svalbard-what does the foraminifera and molluscs tell?* NTNU]. <https://ntnuopen.ntnu.no/ntnu-xmlui/handle/11250/2976501>. <https://hdl.handle.net/11250/2976501>
- Barnes, P. W., Reimnitz, E., & Fox, D. (1982). Ice rafting of fine-grained sediment, a sorting and transport mechanism, Beaufort Sea, Alaska. *Journal of Sedimentary Research*, 52(2), 493-502.
- Batchelor, C., & Dowdeswell, J. (2014). The physiography of High Arctic cross-shelf troughs. *Quaternary Science Reviews*, 92, 68-96.
- Bates, C. C. (1953). Rational theory of delta formation. *Aapg Bulletin*, 37(9), 2119-2162.
- Beierlein, L., Salvigsen, O., Schöne, B. R., Mackensen, A., & Brey, T. (2015). The seasonal water temperature cycle in the Arctic Dicksonfjord (Svalbard) during the Holocene Climate Optimum derived from subfossil *Arctica islandica* shells. *The Holocene*, 25(8), 1197-1207.
- Berge, J., Johnsen, G., Nilsen, F., Gulliksen, B., & Slagstad, D. (2005). Ocean temperature oscillations enable reappearance of blue mussels *Mytilus edulis* in Svalbard after a 1000 year absence. *Marine Ecology Progress Series*, 303, 167-175.
- Berger, A. (1978). Long-term variations of daily insolation and Quaternary climatic changes. *Journal of Atmospheric Sciences*, 35(12), 2362-2367.
- Berger, A., & Loutre, M.-F. (1991). Insolation values for the climate of the last 10 million years. *Quaternary Science Reviews*, 10(4), 297-317.
- Bergstrøm, B., Reite, A., Sveian, H., & Olsen, L. (2001). Feltrutiner, kartleggingsprinsipper og standarder for kvartærgeologisk kartlegging/løsmassekartlegging ved NGU. *Norges geologiske undersøkelse. Intern rapport 2001.018*.



- Bertrand, S., Huguen, K. A., Sepulveda, J., & Pantoja, S. (2012). Geochemistry of surface sediments from the fjords of Northern Chilean Patagonia (44–47 S): Spatial variability and implications for paleoclimate reconstructions. *Geochimica et Cosmochimica Acta*, 76, 125-146.
- Bintanja, R., & Selten, F. (2014). Future increases in Arctic precipitation linked to local evaporation and sea-ice retreat. *Nature*, 509(7501), 479-482.
- Birks, H. H. (1991). Holocene vegetational history and climatic change in west Spitsbergen—plant macrofossils from Skardtjørna, an Arctic lake. *The Holocene*, 1(3), 209-218.
- Blake, W. (1961). *Radiocarbon Dating of Raised Beaches in Nordaustlandet, Spitsbergen*. Weston Blake. University of Toronto Press.
- Blott, S. J., & Pye, K. (2001). GRADISTAT: a grain size distribution and statistics package for the analysis of unconsolidated sediments. *Earth surface processes and Landforms*, 26(11), 1237-1248.
- Bluck, B. (1998). Clast assembling, bed-forms and structure in gravel beaches. *Earth and Environmental Science Transactions of the Royal Society of Edinburgh*, 89(4), 291-323.
- Bluck, B. J. (1967). Sedimentation of beach gravels; examples from South Wales. *Journal of Sedimentary Research*, 37(1), 128-156.
- Bluck, B. J. (2011). Structure of gravel beaches and their relationship to tidal range. *Sedimentology*, 58(4), 994-1006.
- Bondevik, S., Mangerud, J., Ronnert, L., & Salvigsen, O. (1995). Postglacial sea-level history of Edgeøya and Barentsøya, eastern Svalbard. *Polar Research*, 14(2), 153-180.
- Böse, M., Lüthgens, C., Lee, J. R., & Rose, J. (2012). Quaternary glaciations of northern Europe. *Quaternary Science Reviews*, 44, 1-25.
- Bouma, A. (1964). Turbidites. In *Developments in sedimentology* (Vol. 3, pp. 247-256). Elsevier.
- Bourgeois, J., & Leithold, E. L. (1984). Wave-worked conglomerates—depositional processes and criteria for recognition. *Sedimentology of Gravels and Conglomerates, Memoir 10, 1984*, Pages 331-343.  
[https://archives.datapages.com/data/cspg\\_sp/data/010/010001/331\\_cspgsp0100331.htm](https://archives.datapages.com/data/cspg_sp/data/010/010001/331_cspgsp0100331.htm)
- Bourriquen, M., Mercier, D., Baltzer, A., Fournier, J., Costa, S., & Roussel, E. (2018). Paraglacial coasts responses to glacier retreat and associated shifts in river floodplains over decadal timescales (1966–2016), Kongsfjorden, Svalbard. *Land Degradation & Development*, 29(11), 4173-4185.
- Brenchley, P. J., & Newall, G. (1977). The significance of contorted bedding in upper Ordovician sediments of the Oslo region, Norway. *Journal of Sedimentary Research*, 47(2), 819-833.

- Brendryen, J., Haflidason, H., Rise, L., Chand, S., Vanneste, M., Longva, O., L'Heureux, J. S., & Forsberg, C. F. (2015). Ice sheet dynamics on the Lofoten–Vesterålen shelf, north Norway, from Late MIS-3 to Heinrich Stadial 1. *Quaternary Science Reviews*, *119*, 136-156.
- Brückner, H., Schellmann, G., & van der Borg, K. (2002). Uplifted Beach Ridges in Northern Spitsbergen as Indicators for Glacio-Isostasy and Palaeo-Oceanography; Uplifted Beach Ridges in Northern Spitsbergen as Indicators for Glacio-Isostasy and Palaeo-Oceanography. *Zeitschrift für Geomorphologie*, *46*(3), 309-336.
- Caldwell, N., & Williams, A. (1985). The role of beach profile configuration in the discrimination between differing depositional environments affecting coarse clastic beaches. *Journal of Coastal Research*, 129-139.
- Christiansen, H. H., Etzelmüller, B., Isaksen, K., Juliussen, H., Farbrot, H., Humlum, O., Johansson, M., Ingeman - Nielsen, T., Kristensen, L., & Hjort, J. (2010). The thermal state of permafrost in the nordic area during the international polar year 2007–2009. *Permafrost and Periglacial Processes*, *21*(2), 156-181.
- Christman, E. I. (2022). *Reconstructing early Holocene warmth in outer Isfjorden, Svalbard using stable isotope analysis on the ocean quahog, Arctica islandica* [Bates College, Maine, USA].
- Church, M., & Gilbert, R. (1975). Proglacial fluvial and lacustrine environments.
- Church, M., & Ryder, J. M. (1972). Paraglacial sedimentation: a consideration of fluvial processes conditioned by glaciation. *Geological Society of America Bulletin*, *83*(10), 3059-3072.
- Clark, C. D., Hughes, A. L., Greenwood, S. L., Jordan, C., & Sejrup, H. P. (2012). Pattern and timing of retreat of the last British-Irish Ice Sheet. *Quaternary Science Reviews*, *44*, 112-146.
- Cohen, K. M., Finney, S. C., Gibbard, P. L., & Fan, J.-X. (2013). The ICS international chronostratigraphic chart. *Episodes Journal of International Geoscience*, *36*(3), 199-204.
- Copernicus Data Space Ecosystem Hub (2023). *Copernicus Browser*. <https://dataspace.copernicus.eu/browser>
- Corner, G. D. (2006). A transgressive-regressive model of fjord-valley fill: stratigraphy, facies and depositional controls. *Incised Valleys in Time and Space*. <https://doi.org/https://doi.org/10.2110/pec.06.85.0161>
- Corner, G. D., Steinsund, P. I., & Aspeli, R. (1996). Distribution of recent benthic foraminifera in a subarctic fjord-delta: Tana, Norway. *Marine Geology*, *134*(1-2), 113-125.

- Cottier, F., Tverberg, V., Inall, M., Svendsen, H., Nilsen, F., & Griffiths, C. (2005). Water mass modification in an Arctic fjord through cross - shelf exchange: The seasonal hydrography of Kongsfjorden, Svalbard. *Journal of Geophysical Research: Oceans*, 110(C12).
- Cottier, F. R., Nilsen, F., Inall, M., Gerland, S., Tverberg, V., & Svendsen, H. (2007). Wintertime warming of an Arctic shelf in response to large - scale atmospheric circulation. *Geophysical Research Letters*, 34(10).
- Dahlgren, K. T., Vorren, T. O., Stoker, M. S., Nielsen, T., Nygård, A., & Sejrup, H. P. (2005). Late Cenozoic prograding wedges on the NW European continental margin: their formation and relationship to tectonics and climate. *Marine and Petroleum Geology*, 22(9-10), 1089-1110.
- Dahlgren, T., Weinberg, J., & Halanych, K. (2000). Phylogeography of the ocean quahog (*Arctica islandica*): influences of paleoclimate on genetic diversity and species range. *Marine Biology*, 137, 487-495.
- Dallmann, W. (2002). Bedrock map of Svalbard and Jan Mayen. *Norsk Polarinstitutt Temakart*, 33.
- Dallmann, W. K. (2015). *Geoscience atlas of Svalbard*. Norsk Polarinstitutt. <http://hdl.handle.net/11250/2580810>
- Dansgaard, W., Johnsen, S. J., Clausen, H. B., Dahl-Jensen, D., Gundestrup, N. S., Hammer, C. U., Hvidberg, C. S., Steffensen, J. P., Sveinbjörnsdóttir, A., & Jouzel, J. (1993). Evidence for general instability of past climate from a 250-kyr ice-core record. *Nature*, 364(6434), 218-220.
- De Giorgio, V., Sabato, L., & Tropeano, M. (2023). Gravelly Beach Deposits as a Proxy for Relative Sea-Level Changes in Microtidal Wave-Dominated Shoreline Systems: Examples from the Hinterland of the Taranto Gulf (Middle Pleistocene, Basilicata, Southern Italy). *Water*, 15(20), 3631.
- De Raaf, J., Boersma, J., & Van Gelder, s. (1977). Wave - generated structures and sequences from a shallow marine succession, Lower Carboniferous, County Cork, Ireland. *Sedimentology*, 24(4), 451-483.
- Dickson, R., Osborn, T., Hurrell, J., Meincke, J., Blindheim, J., Adlandsvik, B., Vinje, T., Alekseev, G., & Maslowski, W. (2000). The Arctic ocean response to the North Atlantic oscillation. *Journal of Climate*, 13(15), 2671-2696.
- Dowdeswell, J. A., Hogan, K., Evans, J., Noormets, R., Ó Cofaigh, C., & Ottesen, D. (2010). Past ice-sheet flow east of Svalbard inferred from streamlined subglacial landforms. *Geology*, 38(2), 163-166.
- Duarte, P., Sundfjord, A., Meyer, A., Hudson, S. R., Spreen, G., & Smedsrud, L. H. (2020). Warm Atlantic water explains observed sea ice melt rates north of Svalbard. *Journal of Geophysical Research: Oceans*, 125(8), e2019JC015662.

- Ehlers, J., & Gibbard, P. L. (2007). The extent and chronology of Cenozoic global glaciation. *Quaternary International*, 164, 6-20.
- Eilertsen, R., Corner, G., Kvale, E., & Jensen, M. (2005). Quaternary tidal rhythmites as a proxy for paleoprecipitation. Geological Society of America Abstracts with Programs,
- Eilertsen, R. S., Corner, G. D., Aasheim, O., & Hansen, L. (2011). Facies characteristics and architecture related to palaeodepth of Holocene fjord–delta sediments. *Sedimentology*, 58(7), 1784-1809.
- El bani Altuna, N., Rasmussen, T. L., Ezat, M. M., Vadakkepuliambatta, S., Groeneveld, J., & Greaves, M. (2021). Deglacial bottom water warming intensified Arctic methane seepage in the NW Barents Sea. *Communications Earth & Environment*, 2(1), 188.
- Elverhøi, A., Svendsen, J. I., Solheim, A., Andersen, E. S., Milliman, J., Mangerud, J., & Hooke, R. L. (1995). Late Quaternary sediment yield from the high Arctic Svalbard area. *The journal of geology*, 103(1), 1-17.
- Elvevold, S., Dallmann, W., & Blomeier, D. (2007). *Geology of Svalbard*.
- Farnsworth, W. R., Allaart, L., Ingólfsson, Ó., Alexanderson, H., Forwick, M., Noormets, R., Retelle, M., & Schomacker, A. (2020). Holocene glacial history of Svalbard: Status, perspectives and challenges. *Earth-Science Reviews*, 208, 103249.
- Farnsworth, W. R., Ingólfsson, Ó., Mannerfelt, E. S., Kalliokoski, M. H., Guðmundsdóttir, E. R., Retelle, M., Allaart, L., Brynjólfsson, S., Furze, M. F., & Hancock, H. J. (2022). Vedde Ash constrains Younger Dryas glacier re-advance and rapid glacio-isostatic rebound on Svalbard. *Quaternary Science Advances*, 5, 100041.
- Faust, J. C. (2014). Environmental response to past and recent climate variability in the Trondheimsfjord region, central Norway-A multiproxy geochemical approach.
- Faust, J. C., Scheiber, T., Fabian, K., Vogt, C., & Knies, J. (2017). Geochemical characterisation of northern Norwegian fjord surface sediments: A baseline for further paleo-environmental investigations. *Continental Shelf Research*, 148, 104-115.
- Feyling-Hanssen, R. W. (1955). Stratigraphy of the marine late-Pleistocene of Billefjorden, Vestspitsbergen.
- Fjeldskaar, W., Bondevik, S., & Amantov, A. (2018). Glaciers on Svalbard survived the Holocene thermal optimum. *Quaternary Science Reviews*, 199, 18-29.
- Folk, R. L. (1954). The distinction between grain size and mineral composition in sedimentary-rock nomenclature. *The journal of geology*, 62(4), 344-359.
- Folk, R. L. (1980). *Petrology of sedimentary rocks*. Hemphill publishing company.
- Folk, R. L., & Ward, W. C. (1957). Brazos River bar [Texas]; a study in the significance of grain size parameters. *Journal of Sedimentary Research*, 27(1), 3-26.

- Forman, S., Lubinski, D., Ingólfsson, Ó., Zeeberg, J., Snyder, J., Siegert, M., & Matishov, G. (2004). A review of postglacial emergence on Svalbard, Franz Josef Land and Novaya Zemlya, northern Eurasia. *Quaternary Science Reviews*, 23(11-13), 1391-1434.
- Forman, S. L. (1989). Late Weichselian glaciation and deglaciation of Forlandsundet area, western Spitsbergen, Svalbard. *Boreas*, 18(1), 51-60.
- Forman, S. L. (1990). Post-glacial relative sea-level history of northwestern Spitsbergen, Svalbard. *Geological Society of America Bulletin*, 102(11), 1580-1590.
- Forman, S. L., Mann, D. H., & Miller, G. H. (1987). Late Weichselian and Holocene relative sea-level history of Bröggerhalvöya, Spitsbergen. *Quaternary Research*, 27(1), 41-50.
- Forwick, M., & Vorren, T. O. (2009). Late Weichselian and Holocene sedimentary environments and ice rafting in Isfjorden, Spitsbergen. *Palaeogeography, Palaeoclimatology, Palaeoecology*, 280(1-2), 258-274.
- Fossile, E., Nardelli, M. P., Howa, H., Baltzer, A., Poprawski, Y., Baneschi, I., Doveri, M., & Mojtahid, M. (2022). Influence of modern environmental gradients on foraminiferal faunas in the inner Kongsfjorden (Svalbard). *Marine Micropaleontology*, 173, 102117.
- Fraser, N. J., Skogseth, R., Nilsen, F., & Inall, M. E. (2018). Circulation and exchange in a broad Arctic fjord using glider-based observations. *Polar Research*, 37(1), 1485417.
- French, H. M. (2017). *The periglacial environment*. John Wiley & Sons.
- Funder, S., Kjeldsen, K. K., Kjær, K. H., & Cofaigh, C. Ó. (2011). The Greenland Ice Sheet during the past 300,000 years: A review. *Developments in Quaternary Sciences*, 15, 699-713.
- Gilbert, R. (1983). Sedimentary processes of Canadian Arctic fjords. *Sedimentary Geology*, 36(2-4), 147-175.
- Gilbert, R. (1990). Rafting in glacial marine environments. *Geological Society, London, Special Publications*, 53(1), 105-120.
- Goldschmidt, P., Pfirman, S., Wollenburg, I., & Henrich, R. (1992). Origin of sediment pellets from the Arctic seafloor: sea ice or icebergs? *Deep Sea Research Part A. Oceanographic Research Papers*, 39(2), S539-S565.
- Goslar, T., & Pazdur, M. F. (1985). Datowanie muszli mięczaków metodą <sup>14</sup>C. *Geological Quarterly*, 29(2), 459-472.
- Govin, A., Holzwarth, U., Heslop, D., Ford Keeling, L., Zabel, M., Mulitza, S., Collins, J. A., & Chiessi, C. M. (2012). Distribution of major elements in Atlantic surface sediments (36 N–49 S): Imprint of terrigenous input and continental weathering. *Geochemistry, Geophysics, Geosystems*, 13(1).

- Gray, A. B., Pasternack, G. B., & Watson, E. B. (2010). Hydrogen peroxide treatment effects on the particle size distribution of alluvial and marsh sediments. *The Holocene*, 20(2), 293-301.
- Hagen, J. O., Liestøl, O., Roland, E., & Jørgensen, T. (1993). *Glacier atlas of Svalbard and Jan mayen*.
- Hald, M., Ebbesen, H., Forwick, M., Godtlielsen, F., Khomenko, L., Korsun, S., Olsen, L. R., & Vorren, T. O. (2004). Holocene paleoceanography and glacial history of the West Spitsbergen area, Euro-Arctic margin. *Quaternary Science Reviews*, 23(20-22), 2075-2088.
- Hansen, J., Hanken, N. M., Nielsen, J. K., Nielsen, J. K., & Thomsen, E. (2011). Late Pleistocene and Holocene distribution of *Mytilus edulis* in the Barents Sea region and its palaeoclimatic implications. *Journal of Biogeography*, 38(6), 1197-1212.
- Hansen, L. (2004). Deltaic infill of a deglaciated arctic fjord, East Greenland: sedimentary facies and sequence stratigraphy. *Journal of Sedimentary Research*, 74(3), 422-437.
- Hanssen-Bauer, I., Førland, E., Hisdal, H., Mayer, S., Sandø, A., & Sorteberg, A. (2019). Climate in Svalbard 2100. *A knowledge base for climate adaptation*.
- Hanssen-Bauer, M. (1990). The climate of Spitsbergen. *Klima, Den Norske Meteorologiske Institutt Rapport*, 39, 1-40.
- Harrison, S. P., Prentice, I. C., & Bartlein, P. J. (1992). Influence of insolation and glaciation on atmospheric circulation in the North Atlantic sector: implications of general circulation model experiments for the Late Quaternary climatology of Europe. *Quaternary Science Reviews*, 11(3), 283-299.
- Hart, B., & Plint, A. (1989). Gravelly shoreface deposits: a comparison of modern and ancient facies sequences. *Sedimentology*, 36(4), 551-557.
- Heaton, T. J., Köhler, P., Butzin, M., Bard, E., Reimer, R. W., Austin, W. E., Ramsey, C. B., Grootes, P. M., Hughen, K. A., & Kromer, B. (2020). Marine20—the marine radiocarbon age calibration curve (0–55,000 cal BP). *Radiocarbon*, 62(4), 779-820.
- Hill, P. R., Lewis, C. P., Desmarais, S., Kauppaymuthoo, V., & Rais, H. (2001). The Mackenzie Delta: Sedimentary processes and facies of a high - latitude, fine - grained delta. *Sedimentology*, 48(5), 1047-1078.
- Hjort, C., Mangerud, J., Adrielsson, L., Bondevik, S., Landvik, J. Y., & Salvigsen, O. (1995). Radiocarbon dated common mussels *Mytilus edulis* from eastern Svalbard and the Holocene marine climatic optimum. *Polar Research*, 14(2), 239-243.
- Hogan, K. A., Cofaigh, C. Ó., Jennings, A. E., Dowdeswell, J. A., & Hiemstra, J. F. (2016). Deglaciation of a major palaeo-ice stream in Disko Trough, West Greenland. *Quaternary Science Reviews*, 147, 5-26.

- Hogan, K. A., Dowdeswell, J. A., Hillenbrand, C. D., Ehrmann, W., Noormets, R., & Wacker, L. (2017). Subglacial sediment pathways and deglacial chronology of the northern Barents Sea Ice Sheet. *Boreas*, 46(4), 750-771.
- Holtedahl, H. (1975). The geology of the Hardangerfjord, West Norway.
- Hopkins, T. S. (1991). The GIN Sea—A synthesis of its physical oceanography and literature review 1972–1985. *Earth-Science Reviews*, 30(3-4), 175-318.
- Hormes, A., Akcar, N., & Kubik, P. W. (2011). Cosmogenic radionuclide dating indicates ice - sheet configuration during MIS 2 on Nordaustlandet, Svalbard. *Boreas*, 40(4), 636-649.
- Hoskin, C. M., & Burrell, D. C. (1972). Sediment transport and accumulation in a fjord basin, Glacier Bay, Alaska. *The journal of geology*, 80(5), 539-551.
- Hughes, A. L., Gyllencreutz, R., Lohne, Ø. S., Mangerud, J., & Svendsen, J. I. (2016). The last Eurasian ice sheets—a chronological database and time - slice reconstruction, DATED - 1. *Boreas*, 45(1), 1-45.
- Huxley, T. H. (1870). The British Association - Liverpool Meeting. *Nature*, 402.  
[https://books.google.no/books?id=8YUCAAAAIAAJ&q=%22ugly+fact%22&redir\\_esc=y#v=snippet&q=%22ugly%20fact%22&f=false](https://books.google.no/books?id=8YUCAAAAIAAJ&q=%22ugly+fact%22&redir_esc=y#v=snippet&q=%22ugly%20fact%22&f=false)
- Ingólfsson, Ó., & Landvik, J. Y. (2013). The Svalbard–Barents Sea ice-sheet—Historical, current and future perspectives. *Quaternary Science Reviews*, 64, 33-60.
- Ingólfsson, Ó., Rögnvaldsson, F., Bergsten, H., Hedenäs, L., Lemdahl, G., Lirio, J. M., & Sejrup, H. P. (1995). Late Quaternary glacial and environmental history of Kongsøya, Svalbard. *Polar Research*, 14(2), 123-139.
- Ingvaldsen, R. B., Asplin, L., & Loeng, H. (2004). The seasonal cycle in the Atlantic transport to the Barents Sea during the years 1997–2001. *Continental Shelf Research*, 24(9), 1015-1032.
- Jakobsson, M., Long, A., Ingólfsson, Ó., Kjær, K. H., & Spielhagen, R. F. (2010). New insights on Arctic Quaternary climate variability from palaeo-records and numerical modelling. *Quaternary Science Reviews*, 29(25-26), 3349-3358.
- Jensen, A. S. (1942). *Two new West Greenland localities for deposits from the ice age and the post-glacial warm period*. Munksgaard.
- Jerram, D. A. (2001). Visual comparators for degree of grain-size sorting in two and three-dimensions. *Computers & geosciences*, 27(4), 485-492.
- Johnson, H. B. (2020). *Late Glacial to Holocene Sea Level History of Kapp Linné, Svalbard, Norwegian High Arctic* Bates College, Maine, USA].  
<https://scarab.bates.edu/honorstheses/320/>.
- Kaplan, M. R., & Wolfe, A. P. (2006). Spatial and temporal variability of Holocene temperature in the North Atlantic region. *Quaternary Research*, 65(02), 223-231.

- Kaufman, D. S., Ager, T. A., Anderson, N. J., Anderson, P. M., Andrews, J. T., Bartlein, P. J., Brubaker, L. B., Coats, L. L., Cwynar, L. C., & Duvall, M. L. (2004). Holocene thermal maximum in the western Arctic (0–180 W). *Quaternary Science Reviews*, 23(5-6), 529-560.
- Kauppaymuthoo, V. (1997). *Étude de la dynamique sédimentaire hivernale du Delta du Mackenzie au niveau de Kugmallit Bay* Université du Québec à Rimouski].
- Kjellman, S. E., Schomacker, A., Thomas, E. K., Håkansson, L., Duboscq, S., Cluett, A. A., Farnsworth, W. R., Allaart, L., Cowling, O. C., & McKay, N. P. (2020). Holocene precipitation seasonality in northern Svalbard: Influence of sea ice and regional ocean surface conditions. *Quaternary Science Reviews*, 240, 106388.
- Kneller, B. (1995). Beyond the turbidite paradigm: physical models for deposition of turbidites and their implications for reservoir prediction. *Geological Society, London, Special Publications*, 94(1), 31-49.
- Kneller, B., & Buckee, C. (2000). The structure and fluid mechanics of turbidity currents: a review of some recent studies and their geological implications. *Sedimentology*, 47, 62-94.
- Knies, J., Kleiber, H.-P., Matthiessen, J., Müller, C., & Nowaczyk, N. (2001). Marine ice-rafted debris records constrain maximum extent of Saalian and Weichselian ice-sheets along the northern Eurasian margin. *Global and Planetary Change*, 31(1-4), 45-64.
- Kolås, E., & Fer, I. (2018). Hydrography, transport and mixing of the West Spitsbergen Current: the Svalbard Branch in summer 2015. *Ocean Science*, 14(6), 1603-1618.
- Kopec, B. G., Feng, X., Michel, F. A., & Posmentier, E. S. (2016). Influence of sea ice on Arctic precipitation. *Proceedings of the National Academy of Sciences*, 113(1), 46-51.
- Koster, E. H., & Steel, R. J. (1984). *Sedimentology of gravels and conglomerates* (Vol. 10). Canadian Society of Petroleum Geologists Calgary.
- Kranck, K. (1973). Flocculation of suspended sediment in the sea. *Nature*, 246(5432), 348-350.
- Kristensen, D. K., Rasmussen, T. L., & Koç, N. (2013). Palaeoceanographic changes in the northern Barents Sea during the last 16 000 years—new constraints on the last deglaciation of the Svalbard–Barents Sea Ice Sheet. *Boreas*, 42(3), 798-813.
- Krüger, J., & Kjær, K. H. (1999). A data chart for field description and genetic interpretation of glacial diamicts and associated sediments... with examples from Greenland, Iceland, and Denmark. *Boreas*, 28(3), 386-402.
- Krumbein, W., & Pettijohn, F. (1938). *Manual of sedimentary petrology*. Appleton-Century Co., Nueva York, Nueva York, EEUU.
- Kuenen, P. H. (1953). Graded Bedding with Observations on Lower Palaeozoic Rocks in Great Britain. *Uerh. Kon. Ned. Ak. V. Wetenschappen*, 20(3).



- Lambeck, K. (1996). Limits on the areal extent of the Barents Sea ice sheet in Late Weichselian time. *Global and Planetary Change*, 12(1-4), 41-51.
- Lamy, F., Hebbeln, D., Röhl, U., & Wefer, G. (2001). Holocene rainfall variability in southern Chile: a marine record of latitudinal shifts of the Southern Westerlies. *Earth and Planetary Science Letters*, 185(3-4), 369-382.
- Landvik, J. Y., Bondevik, S., Elverhøi, A., Fjeldskaar, W., Mangerud, J., Salvigsen, O., Siegert, M. J., Svendsen, J.-I., & Vorren, T. O. (1998). The last glacial maximum of Svalbard and the Barents Sea area: ice sheet extent and configuration. *Quaternary Science Reviews*, 17(1-3), 43-75.
- Landvik, J. Y., Ingólfsson, Ó., Mienert, J., Lehman, S. J., Solheim, A., Elverhøi, A., & Ottesen, D. (2005). Rethinking Late Weichselian ice - sheet dynamics in coastal NW Svalbard. *Boreas*, 34(1), 7-24.
- Landvik, J. Y., Landvik, J. Y., & Salvigsen, O. (1987). The Late Weichselian and Holocene shoreline displacement on the west - central coast of Svalbard. *Polar Research*, 5(1), 29-44.
- Landvik, J. Y., & Salvigsen, O. (1985). Glaciation development and interstadial sea-level on central Spitsbergen, Svalbard. *Polar Research*, 3(1), 1-10.
- Lantuit, H., Overduin, P. P., Couture, N., Wetterich, S., Aré, F., Atkinson, D., Brown, J., Cherkashov, G., Drozdov, D., & Forbes, D. L. (2012). The Arctic coastal dynamics database: A new classification scheme and statistics on Arctic permafrost coastlines. *Estuaries and Coasts*, 35, 383-400.
- Lee, H., Calvin, K., Dasgupta, D., Krinner, G., Mukherji, A., Thorne, P., Trisos, C., Romero, J., Aldunce, P., & Barret, K. (2023). IPCC, 2023: Climate Change 2023: Synthesis Report, Summary for Policymakers. Contribution of Working Groups I, II and III to the Sixth Assessment Report of the Intergovernmental Panel on Climate Change [Core Writing Team, H. Lee and J. Romero (eds.)]. IPCC, Geneva, Switzerland.
- Lee, J. (2018). Glacial lithofacies and stratigraphy. In *Past glacial environments* (pp. 377-429). Elsevier.
- Linnaeus, C. v. (1767). *Systema naturae per regna tria naturae, secundum classes, ordines genera, species cum characteribus, differentiis, synonymis, locis, Tomus I. Editio duodecima, reformata*.
- Linné, C. v. (1758). *Caroli Linnæi... Systema naturæ per regna tria naturæ, secundum classes, ordines, genera, species, cum characteribus, differentiis, synonymis, locis*.
- Lisitzin, A. P. (2002). *Sea-ice and iceberg sedimentation in the ocean: recent and past*. Springer Science & Business Media.
- Liu, J., & Curry, J. A. (2010). Accelerated warming of the Southern Ocean and its impacts on the hydrological cycle and sea ice. *Proceedings of the National Academy of Sciences*, 107(34), 14987-14992.

- Lønne, I. (2005). Faint traces of high Arctic glaciations: an early Holocene ice - front fluctuation in Bolterdalen, Svalbard. *Boreas*, 34(3), 308-323.
- Lønne, I., & Nemeč, W. (2004). High - arctic fan delta recording deglaciation and environment disequilibrium. *Sedimentology*, 51(3), 553-589.
- Mackiewicz, N. E., Powell, R. D., Carlson, P. R., & Molnia, B. F. (1984). Interlaminated ice-proximal glacial marine sediments in Muir Inlet, Alaska. *Marine Geology*, 57(1-4), 113-147.
- Maejima, W. (1982). Texture and Stratification of Gravelly Beach Sediments, Enju Beach. *Journal of geosciences Osaka City University*, 25, 35-51.
- Mangerud, J., Bolstad, M., Elgersma, A., Helliksen, D., Landvik, J. Y., Lønne, I., Lycke, A. K., Salvigsen, O., Sandahl, T., & Svendsen, J. I. (1992). The last glacial maximum on Spitsbergen, Svalbard. *Quaternary Research*, 38(1), 1-31.
- Mangerud, J., Dokken, T., Hebbeln, D., Heggen, B., Ingólfsson, Ó., Landvik, J. Y., Mejdahl, V., Svendsen, J. I., & Vorren, T. O. (1998). Fluctuations of the Svalbard–Barents Sea Ice Sheet during the last 150 000 years. *Quaternary Science Reviews*, 17(1-3), 11-42.
- Mangerud, J., Gosse, J., Matiouchkov, A., & Dolvik, T. (2008). Glaciers in the Polar Urals, Russia, were not much larger during the Last Global Glacial Maximum than today. *Quaternary Science Reviews*, 27(9-10), 1047-1057.
- Mangerud, J., & Svendsen, J. I. (2018). The Holocene thermal maximum around Svalbard, Arctic North Atlantic; molluscs show early and exceptional warmth. *The Holocene*, 28(1), 65-83.
- Mangerud, J., & Svendsen, J. I. (1990). Deglaciation chronology inferred from marine sediments in a proglacial lake basin, western Spitsbergen, Svalbard. *Boreas*, 19(3), 249-272.
- Marsland, S., & Wolff, J. O. (2001). On the sensitivity of Southern Ocean sea ice to the surface freshwater flux: A model study. *Journal of Geophysical Research: Oceans*, 106(C2), 2723-2741.
- Massari, F. (1984). Resedimented conglomerates of a Miocene fan-delta complex, Southern Alps, Italy.
- Massari, F., & Parea, G. (1988). Progradational gravel beach sequences in a moderate - to high - energy, microtidal marine environment. *Sedimentology*, 35(6), 881-913.
- Maxwell, B. (1980). *The climate of the Canadian Arctic Islands and adjacent waters*. Environment Canada, Atmospheric Environment Service.
- Mikutta, R., Kleber, M., Kaiser, K., & Jahn, R. (2005). Organic matter removal from soils using hydrogen peroxide, sodium hypochlorite, and disodium peroxodisulfate. *Soil science society of America journal*, 69(1), 120-135.

- Miller, G. H., Alley, R. B., Brigham-Grette, J., Fitzpatrick, J. J., Polyak, L., Serreze, M. C., & White, J. W. (2010). Arctic amplification: can the past constrain the future? *Quaternary Science Reviews*, 29(15-16), 1779-1790.
- Mills, P. C. (1983). Genesis and diagnostic value of soft-sediment deformation structures—a review. *Sedimentary Geology*, 35(2), 83-104.
- Nemec, W. (1990). Aspects of sediment movement on steep delta slopes. *Coarse-grained deltas*, 10(2), 29-73.
- Nielsen, T., & Rasmussen, T. L. (2018). Reconstruction of ice sheet retreat after the Last Glacial maximum in Storfjorden, southern Svalbard. *Marine Geology*, 402, 228-243.
- Nilsen, F., Cottier, F., Skogseth, R., & Mattsson, S. (2008). Fjord–shelf exchanges controlled by ice and brine production: the interannual variation of Atlantic Water in Isfjorden, Svalbard. *Continental Shelf Research*, 28(14), 1838-1853.
- Nilsen, F., Skogseth, R., Vaardal-Lunde, J., & Inall, M. (2016). A simple shelf circulation model: intrusion of Atlantic Water on the West Spitsbergen Shelf. *Journal of Physical Oceanography*, 46(4), 1209-1230.
- Nordli, Ø., Wyszynski, P., Gjelten, H., Isaksen, K., Łupikasza, E., Niedźwiedz, T., & Przybylak, R. (2020). Revisiting the extended Svalbard Airport monthly temperature series, and the compiled corresponding daily series 1898–2018.
- Norwegian Centre for Climate services. (2023). *Monthly precipitation values for Isfjord radio station*. Norwegian Meteorological Institute. Retrieved 1st January 2024 from <https://seklima.met.no/>
- Norwegian Polar Institute. (2009a). *NP\_Basiskart\_Svalbard\_WMTS\_25833* [Topographic map, Svalbard]. <https://geodata.npolar.no/>
- Norwegian Polar Institute. (2009b). *NP\_Ortofoto\_Svalbard\_WMTS\_25833* [Orthophoto, Svalbard]. <https://geodata.npolar.no/>
- Norwegian Polar Institute. (2014). *Digital Terrain Model, Svalbard*. <https://doi.org/https://doi.org/10.21334/npolar.2014.dce53a47>
- Norwegian Polar Institute / USGS Landsat (2009). *NP\_Satellitt\_Svalbard\_WMTS\_25833* [Satellite imagery, Svalbard]. <https://geodata.npolar.no/>
- Nuth, C., Kohler, J., König, M., Von Deschwenden, A., Hagen, J., Käab, A., Moholdt, G., & Pettersson, R. (2013). Decadal changes from a multi-temporal glacier inventory of Svalbard. *The Cryosphere*, 7(5), 1603-1621.
- NVE. (2024). *Catchment area and fluvial regime of Hollendarelva*. The Norwegian Mapping Authority. Retrieved 1st January, 2024 from <https://temakart.nve.no/tema/faresoner>.
- Olsson, I., & Feyling-Hanssen, R. W. (1959). *Five Radiocarbon Datings of Post Glacial Shorelines in Central Spitsbergen*. Universitetsforlaget.

- Onarheim, I. H., Smedsrud, L. H., Ingvaldsen, R. B., & Nilsen, F. (2014). Loss of sea ice during winter north of Svalbard. *Tellus A: Dynamic Meteorology and Oceanography*, 66(1), 23933.
- Orford, J. D. (1977). A proposed mechanism for storm beach sedimentation. *Earth Surface Processes*, 2(4), 381-400.
- Orford, J. D. (1978). *Methods of identifying, and interpreting the dynamics of littoral zone facies using particle size and form, with special reference to beach gravel sedimentation* [University of Reading].
- Østby, T. I., Schuler, T. V., Hagen, J. O., Hock, R., Kohler, J., & Reijmer, C. H. (2017). Diagnosing the decline in climatic mass balance of glaciers in Svalbard over 1957–2014. *The Cryosphere*, 11(1), 191-215.
- Ottesen, D., Dowdeswell, J., & Rise, L. (2005). Submarine landforms and the reconstruction of fast-flowing ice streams within a large Quaternary ice sheet: The 2500-km-long Norwegian-Svalbard margin (57–80 N). *Geological Society of America Bulletin*, 117(7-8), 1033-1050.
- Ottesen, D., & Dowdeswell, J. A. (2009). An inter-ice-stream glaciated margin: Submarine landforms and a geomorphic model based on marine-geophysical data from Svalbard. *Geological Society of America Bulletin*, 121(11-12), 1647-1665.
- Ottesen, D., Dowdeswell, J. A., Landvik, J. Y., & Mienert, J. (2007). Dynamics of the Late Weichselian ice sheet on Svalbard inferred from high - resolution sea - floor morphology. *Boreas*, 36(3), 286-306.
- Patton, H., Andreassen, K., Bjarnadóttir, L. R., Dowdeswell, J. A., Winsborrow, M. C., Noormets, R., Polyak, L., Auriac, A., & Hubbard, A. (2015). Geophysical constraints on the dynamics and retreat of the Barents Sea ice sheet as a paleobenchmark for models of marine ice sheet deglaciation. *Reviews of Geophysics*, 53(4), 1051-1098.
- Patton, H., Hubbard, A., Andreassen, K., Auriac, A., Whitehouse, P. L., Stroeven, A. P., Shackleton, C., Winsborrow, M., Heyman, J., & Hall, A. M. (2017). Deglaciation of the Eurasian ice sheet complex. *Quaternary Science Reviews*, 169, 148-172.
- Patton, H., Hubbard, A., Andreassen, K., Winsborrow, M., & Stroeven, A. P. (2016). The build-up, configuration, and dynamical sensitivity of the Eurasian ice-sheet complex to Late Weichselian climatic and oceanic forcing. *Quaternary Science Reviews*, 153, 97-121.
- Peacock, J. (1993). Late Quaternary marine mollusca as palaeoenvironmental proxies: a compilation and assessment of basic numerical data for NE Atlantic species found in shallow water. *Quaternary Science Reviews*, 12(4), 263-275.
- Pieńkowski, A. J., Husum, K., Belt, S. T., Ninnemann, U., Köseoğlu, D., Divine, D. V., Smik, L., Knies, J., Hogan, K., & Noormets, R. (2021). Seasonal sea ice persisted through the Holocene Thermal Maximum at 80 N. *Communications Earth & Environment*, 2(1), 124.

- Pieńkowski, A. J., Husum, K., Furze, M. F., Missana, A. F., Irvali, N., Divine, D. V., & Eilertsen, V. T. (2022). Revised  $\Delta R$  values for the Barents Sea and its archipelagos as a pre-requisite for accurate and robust marine-based  $^{14}\text{C}$  chronologies. *Quaternary Geochronology*, 68, 101244.
- Polyakov, I. V., Pnyushkov, A. V., Alkire, M. B., Ashik, I. M., Baumann, T. M., Carmack, E. C., Goszczko, I., Guthrie, J., Ivanov, V. V., & Kanzow, T. (2017). Greater role for Atlantic inflows on sea-ice loss in the Eurasian Basin of the Arctic Ocean. *Science*, 356(6335), 285-291.
- Postma, G., & Nemec, W. (1990). Regressive and transgressive sequences in a raised Holocene gravelly beach, southwestern Crete. *Sedimentology*, 37(5), 907-920.
- Powell, R. D. (1981). A model for sedimentation by tidewater glaciers. *Annals of Glaciology*, 2, 129-134.
- Powell, R. D. (1984). Glacimarine processes and inductive lithofacies modelling of ice shelf and tidewater glacier sediments based on Quaternary examples. *Marine Geology*, 57(1-4), 1-52.
- Powell, R. D., & Molnia, B. F. (1989). Glacimarine sedimentary processes, facies and morphology of the south-southeast Alaska shelf and fjords. *Marine Geology*, 85(2-4), 359-390.
- Powers, M. C. (1953). A new roundness scale for sedimentary particles. *Journal of Sedimentary Research*, 23(2), 117-119.
- Rasmussen, C. F., Christiansen, H. H., Buylaert, J.-P., Cunningham, A., Schneider, R., Knudsen, M. F., & Stevens, T. (2023). High-resolution OSL dating of loess in Adventdalen, Svalbard: Late Holocene dust activity and permafrost development. *Quaternary Science Reviews*, 310, 108137.
- Rasmussen, T. L., Forwick, M., & Mackensen, A. (2012). Reconstruction of inflow of Atlantic Water to Isfjorden, Svalbard during the Holocene: Correlation to climate and seasonality. *Marine Micropaleontology*, 94, 80-90.
- Rasmussen, T. L., & Thomsen, E. (2021). Climate and ocean forcing of ice-sheet dynamics along the Svalbard-Barents Sea ice sheet during the deglaciation ~ 20,000–10,000 years BP. *Quaternary Science Advances*, 3, 100019.
- Rasmussen, T. L., Thomsen, E., Skirbekk, K., Ślubowska-Woldengen, M., Kristensen, D. K., & Koç, N. (2014). Spatial and temporal distribution of Holocene temperature maxima in the northern Nordic seas: interplay of Atlantic-, Arctic-and polar water masses. *Quaternary Science Reviews*, 92, 280-291.
- Rasmussen, T. L., Thomsen, E., Ślubowska, M. A., Jessen, S., Solheim, A., & Koç, N. (2007). Paleoceanographic evolution of the SW Svalbard margin (76 N) since 20,000  $^{14}\text{C}$  yr BP. *Quaternary Research*, 67(1), 100-114.

- Renssen, H., Seppä, H., Crosta, X., Goosse, H., & Roche, D. M. (2012). Global characterization of the Holocene thermal maximum. *Quaternary Science Reviews*, 48, 7-19.
- Rinke, A., Maturilli, M., Graham, R. M., Matthes, H., Handorf, D., Cohen, L., Hudson, S. R., & Moore, J. C. (2017). Extreme cyclone events in the Arctic: Wintertime variability and trends. *Environmental Research Letters*, 12(9), 094006.
- Rogers, J. C., Yang, L., & Li, L. (2005). The role of Fram Strait winter cyclones on sea ice flux and on Spitsbergen air temperatures. *Geophysical Research Letters*, 32(6).
- Rosen, P. S. (1979). Boulder barricades in central Labrador. *Journal of Sedimentary Research*, 49(4), 1113-1123.
- Rubensdotter, L., Sandøy, G., Sletten, K., & Stalsberg, K. (2018). High resolution quaternary geological map, assisting hazard evaluations in Norway. In *Landslides and Engineered Slopes. Experience, Theory and Practice* (pp. 1751-1758). CRC Press.
- Russell, C. E., Pohl, F., & Fernández, R. (2023). Plastic as a Sediment—A Universal and Objective practical solution to growing ambiguity in plastic litter classification schemes.
- Saloranta, T. M., & Svendsen, H. (2001). Across the Arctic front west of Spitsbergen: high-resolution CTD sections from 1998–2000. *Polar Research*, 20(2), 177-184.
- Salvigsen, O. (1978). Holocene emergence and finds of pumice, whalebones and driftwood at Svartknausflya, Nordaustlandet. *Norsk Polarinstitutt Årbok, 1977*, 217-228.
- Salvigsen, O. (1981). Radiocarbon dated raised beaches in Kong Karls Land, Svalbard, and their consequences for the glacial history of the Barents Sea area. *Geografiska Annaler: Series A, Physical Geography*, 63(3-4), 283-291.
- Salvigsen, O. (2002). Radiocarbon-dated *Mytilus edulis* and *Modiolus modiolus* from northern Svalbard: climatic implications. *Norsk Geografisk Tidsskrift-Norwegian Journal of Geography*, 56(2), 56-61.
- Salvigsen, O., Elgersma, A., Hjort, C., Lagerlund, E., Liestøl, O., & Svensson, N.-O. (1990). Glacial history and shoreline displacement on Erdmannflya and Bohemanflya, Spitsbergen, Svalbard. *Polar Research*, 8(2), 261-273.
- Salvigsen, O., Forman, S. L., & Miller, G. H. (1992). Thermophilous molluscs on Svalbard during the Holocene and their paleoclimatic implications. *Polar Research*, 11(1), 1-10.
- Salvigsen, O., & Nydal, R. (1981). The Weichselian glaciation in Svalbard before 15,000 BP. *Boreas*, 10(4), 433-446.
- Salvigsen, O., & Österholm, H. (1982). Radiocarbon dated raised beaches and glacial history of the northern coast of Spitsbergen, Svalbard. *Polar Research*, 1982(1), 97-115.

- Sarnthein, M., Van Kreveld, S., Erlenkeuser, H., Grootes, P. M., Kucera, M., Pflaumann, U., & Schulz, M. (2003). Centennial - to - millennial - scale periodicities of Holocene climate and sediment injections off the western Barents shelf, 75 N. *Boreas*, 32(3), 447-461.
- Schneider, R. R., Schulz, H. D., & Hensen, C. (2006). Marine carbonates: their formation and destruction. *Marine geochemistry*, 311-337.
- Schomacker, A., Farnsworth, W. R., Ingólfsson, Ó., Allaart, L., Håkansson, L., Retelle, M., Siggaard-Andersen, M.-L., Korsgaard, N. J., Rouillard, A., & Kjellman, S. E. (2019). Postglacial relative sea level change and glacier activity in the early and late Holocene: Wahlenbergfjorden, Nordaustlandet, Svalbard. *Scientific reports*, 9(1), 6799.
- Sejrup, H. P., Hjelstuen, B. O., Dahlgren, K. T., Haflidason, H., Kuijpers, A., Nygård, A., Praeg, D., Stoker, M. S., & Vorren, T. O. (2005). Pleistocene glacial history of the NW European continental margin. *Marine and Petroleum Geology*, 22(9-10), 1111-1129.
- Sejrup, H. P., Hjelstuen, B. O., Patton, H., Esteves, M., Winsborrow, M., Rasmussen, T. L., Andreassen, K., & Hubbard, A. (2022). The role of ocean and atmospheric dynamics in the marine-based collapse of the last Eurasian Ice Sheet. *Communications Earth & Environment*, 3(1), 119.
- Sessford, E. G., Strzelecki, M. C., & Hormes, A. (2015). Reconstruction of Holocene patterns of change in a High Arctic coastal landscape, Southern Sassenfjorden, Svalbard. *Geomorphology*, 234, 98-107.
- Sharin, V., Kokin, O., & Gusev, E. (2014). New geochronological data from Quaternary sediments of the Nordenskiöld Land area (the Spitsbergen Archipelago). *Vestnik St. Petersburg State University Series*, 7(1), 159-168.
- Shukla, S. (2011). Freeze drying process: A review. *International journal of pharmaceutical sciences and research*, 2(12), 3061.
- Skei, J. (1983). Why sedimentologists are interested in fjords. *Sedimentary Geology*, 36(2-4), 75-80.
- Skirbekk, K., Kristensen, D. K., Rasmussen, T. L., Koç, N., & Forwick, M. (2010). Holocene climate variations at the entrance to a warm Arctic fjord: evidence from Kongsfjorden trough, Svalbard. *Geological Society, London, Special Publications*, 344(1), 289-304.
- Skogseth, R., Haugan, P., & Jakobsson, M. (2005). Watermass transformations in Storfjorden. *Continental Shelf Research*, 25(5-6), 667-695.
- Ślubowska, M. A., Koç, N., Rasmussen, T. L., & Klitgaard - Kristensen, D. (2005). Changes in the flow of Atlantic water into the Arctic Ocean since the last deglaciation: evidence from the northern Svalbard continental margin, 80 N. *Paleoceanography*, 20(4).

- Ślubowska-Woldengen, M., Rasmussen, T. L., Koç, N., Klitgaard-Kristensen, D., Nilsen, F., & Solheim, A. (2007). Advection of Atlantic Water to the western and northern Svalbard shelf since 17,500 cal yr BP. *Quaternary Science Reviews*, 26(3-4), 463-478.
- Snyder, J., Werner, A., & Miller, G. (2000). Holocene cirque glacier activity in western Spitsbergen, Svalbard: sediment records from proglacial Linnévatnet. *The Holocene*, 10(5), 555-563.
- Sternal, B., Junntila, J., Hegstad, S. K., Dahl, T. M., & Hald, I. (2017). Tests for establishing a procedure of marine sediments pretreatment for grain-size analysis – oxidation using hydrogen peroxide (H<sub>2</sub>O<sub>2</sub>) [Report].
- Stroeven, A. P., Hättestrand, C., Kleman, J., Heyman, J., Fabel, D., Fredin, O., Goodfellow, B. W., Harbor, J. M., Jansen, J. D., & Olsen, L. (2016). Deglaciation of fennoscandia. *Quaternary Science Reviews*, 147, 91-121.
- Stuiver, M., & Reimer, P. J. (1993). Extended 14C data base and revised CALIB 3.0 14C age calibration program. *Radiocarbon*, 35(1), 215-230.
- Svendsen, H., Beszczynska-Møller, A., Hagen, J. O., Lefauconnier, B., Tverberg, V., Gerland, S., Børre Ørbæk, J., Bischof, K., Papucci, C., & Zajaczkowski, M. (2002). The physical environment of Kongsfjorden–Krossfjorden, an Arctic fjord system in Svalbard. *Polar Research*, 21(1), 133-166.
- Svendsen, J. I., Alexanderson, H., Astakhov, V. I., Demidov, I., Dowdeswell, J. A., Funder, S., Gataullin, V., Henriksen, M., Hjort, C., & Houmark-Nielsen, M. (2004). Late Quaternary ice sheet history of northern Eurasia. *Quaternary Science Reviews*, 23(11-13), 1229-1271.
- Svendsen, J. I., Elverhmi, A., & Mangerud, J. (1996). The retreat of the Barents Sea Ice Sheet on the western Svalbard margin. *Boreas*, 25(4), 244-256.
- Svendsen, J. I., & Mangerud, J. (1997). Holocene glacial and climatic variations on Spitsbergen, Svalbard. *The Holocene*, 7(1), 45-57.
- Swift, J. H. (1986). The arctic waters. In *The Nordic Seas* (pp. 129-154). Springer.
- Swingedouw, D., Fichefet, T., Huybrechts, P., Goosse, H., Driesschaert, E., & Loutre, M. F. (2008). Antarctic ice - sheet melting provides negative feedbacks on future climate warming. *Geophysical Research Letters*, 35(17).
- Syvitski, J. P., & Farrow, G. E. (1989). Fjord sedimentation as an analogue for small hydrocarbon-bearing fan deltas. *Geological Society, London, Special Publications*, 41(1), 21-43.
- Syvitski, J. P., & Shaw, J. (1995). Sedimentology and geomorphology of fjords. *Developments in sedimentology*, 53, 113-178.
- The Norwegian Mapping Authority (2014). *Sea level results from Ny-Ålesund water level gauge*. The Norwegian Mapping Authority. Retrieved 1st January, 2024 from



<https://www.kartverket.no/til-sjos/se-havniva/resultat?id=1082348&location=Ny-%C3%85lesund%20vannstandsm%C3%A5ler>

- Udden, J. A. (1914). Mechanical composition of clastic sediments. *Bulletin of the geological society of America*, 25(1), 655-744.
- van der Bilt, W. G., Bakke, J., Vasskog, K., D'Andrea, W. J., Bradley, R. S., & Ólafsdóttir, S. (2015). Reconstruction of glacier variability from lake sediments reveals dynamic Holocene climate in Svalbard. *Quaternary Science Reviews*, 126, 201-218.
- van der Bilt, W. G., D'Andrea, W. J., Werner, J. P., & Bakke, J. (2019). Early Holocene temperature oscillations exceed amplitude of observed and projected warming in Svalbard lakes. *Geophysical Research Letters*, 46(24), 14732-14741.
- Walczowski, W., & Piechura, J. (2011). Influence of the West Spitsbergen Current on the local climate. *International journal of climatology*, 31(7), 1088-1093.
- Walker, M., Gibbard, P., Berkelhammer, M., Bjorck, S., Cwynar, L., Fisher, D., Long, A., Lowe, J., Newnham, R., & Rasmussen, S. (2014). Formal subdivision of the Holocene series/epoch. STRATI 2013: First International Congress on Stratigraphy At the Cutting Edge of Stratigraphy,
- Ward, K. R., & Matejtschuk, P. (2021). The principles of freeze-drying and application of analytical technologies. *Cryopreservation and freeze-drying protocols*, 99-127.
- Wehrmann, L. M., Formolo, M. J., Owens, J. D., Raiswell, R., Ferdelman, T. G., Riedinger, N., & Lyons, T. W. (2014). Iron and manganese speciation and cycling in glacially influenced high-latitude fjord sediments (West Spitsbergen, Svalbard): evidence for a benthic recycling-transport mechanism. *Geochimica et Cosmochimica Acta*, 141, 628-655.
- Wentworth, C. K. (1922). A scale of grade and class terms for clastic sediments. *The journal of geology*, 30(5), 377-392.
- Węśławski, J. M., Koszteyn, J., Zajączkowski, M., Wiktor, J., & Kwaśniewski, S. (1995). Fresh water in Svalbard fjord ecosystems. *Ecology of fjords and coastal waters. Elsevier Sci. BV*, 229-241.
- White, A. F., & Blum, A. E. (1995). Effects of climate on chemical weathering in watersheds. *Geochimica et Cosmochimica Acta*, 59(9), 1729-1747.
- Williams, A., & Caldwell, N. (1988). Particle size and shape in pebble-beach sedimentation. *Marine Geology*, 82(3-4), 199-215.
- Wright, L. D., & Short, A. D. (1984). Morphodynamic variability of surf zones and beaches: a synthesis. *Marine Geology*, 56(1-4), 93-118.
- Zabel, M., Schneider, R. R., Wagner, T., Adegbie, A. T., de Vries, U., & Kolonic, S. (2001). Late Quaternary climate changes in Central Africa as inferred from terrigenous input to the Niger Fan. *Quaternary Research*, 56(2), 207-217.

- Zavala, C. (2020a). Hyperpycnal (over density) flows and deposits. *Journal of Palaeogeography*, 9(1), 1-21.
- Zavala, C. (2020b). Hyperpycnal (over density) flows and deposits. *Journal of Palaeogeography*, 9(1), 17.
- Zhang, X., He, J., Zhang, J., Polyakov, I., Gerdes, R., Inoue, J., & Wu, P. (2013). Enhanced poleward moisture transport and amplified northern high-latitude wetting trend. *Nature Climate Change*, 3(1), 47-51.
- Zhang, Y., Renssen, H., & Seppä, H. (2016). Effects of melting ice sheets and orbital forcing on the early Holocene warming in the extratropical Northern Hemisphere. *Climate of the Past*, 12(5), 1119-1135.
- Zingg, T. (1935). *Beitrag zur schotteranalyse* ETH Zurich].